A HIGH RESOLUTION SEISMIC REFLECTION STUDY OF THE CARBONIFEROUS BAY ST. GEORGE SUBBASIN, WESTERN NEWFOUNDLAND

TERESIA KANYIVA NGUURI

A HIGH RESOLUTION SEISMIC REFLECTION STUDY OF THE CARBONIFEROUS BAY ST. GEORGE SUBBASIN, WESTERN NEWFOUNDLAND.

BY

© TERESIA KANYIVA NGUURI, B.ED (SCIENCE) (HONS)

A thesis submitted to the School of Graduate

Studies in partial fulfilment of the

requirements for the degree of

Master of Science.

Department of Earth Sciences

Memorial University of Newfoundland

November 1992

St. John's Newfoundland

ISBN 0-315-82671-1

ABSTRACT

A seismic reflection profile from onshore Bay St. George Subbasin in western Newfoundland was reprocessed and reinterpreted to determine the structure and extent of the Carboniferous rocks. The main emphasis of reprocessing was placed on velocity analyses and dip move-out (DMO). The quality of the data was improved significantly by the reprocessing. A few features which had not been discovered before became evident. An example of this is an unconformity at a depth of 3.0 km to 5.0 km.

The basin has the configuration of a half graben dipping to the east. The maximum thickness of the Carboniferous sediments is about 5 km in individual depocentres. The basin appears to be bounded downwards by unconformity "U", which separates the Carboniferous rocks from either Lower Palaeozoic rocks or Precambrian rocks.

The fault system is very complex. A few faults correspond to the surface geology. The pattern of faults suggest that the basin was opened by strike slip movements and later deformed by compressional forces.

ACKNOWLEDGEMENT

I would wish to express my gratitude to the following for the support and resources they gave me during my study in Memorial University of Newfoundland:

My thesis supervisor, Dr. Jeremy Hall for his guidance, advice, stimulation, encouragement and freedom of thought necessary for producing this piece of work;

Dr. Hugh Miller for allowing me to use his computer for potential fields data processing. I also appreciate his ideas on the interpretation of gravity and magnetic data;

Drs. James Wright, Garry Quinlan, Cedric Wright, Joe Hodych, E.R. Deutsch, Mike Rochester, Henry Williams and G.S. Murthy for teaching me and for any advice they gave me during my stay in Memorial University;

George Langdon for his guidance on the geology and the tectonics of the Bay St. George Subbasin;

Tony Kocurko for attending to all the technical problems of the CONVEX C1 XL mini-supercomputer in the geophysics unit;

Brian Roberts for his assistance on the processing, especially for making some of the original processing jobs available to me;

The entire technical and supporting staff of department of Earth Sciences for their support and any help they gave me;

Texaco Limited for giving me permission to cite material directly from STARPAK processing and reference manuals;

Canadian International Development Agency (CIDA) for awarding me a scholarship to study in Canada;

The Kenya High Commission at Ottawa for managing efficiently my finances and the programme on behalf of CIDA;

My fellow graduate colleagues, Bill Nickerson, Khalid, Satria Bijakana, Peng, Ron Wiseman, Seyed Mohamoud, Sue Webb, Estelle Blais, for their daily help in one way or another especially with the computers;

Last but not least my entire family back in Kenya for their daily support, prayers and encouragement in one way or another.

DEDICATION

This piece of work is dedicated to my mother, Helenia Mũthoni Njagĩ and my beautiful daughter, Christine Mũmbi, without whom this would not have been possible.

In loving memory of my father, Njagĩ Ngũũri.

TABLE OF CONTENTS

LIST OF TABLES

LIST OF FIGURES

Chapter 1: Introduction

The main objective of this project was to reprocess and interpret a seismic profile across Robinson's river, Bay St. George subbasin of western Newfoundland. This study was undertaken to try and define the structure and the extent of the Carboniferous rocks. The processed data had indicated that the basin could be as deep as 4 km (Hall et al., 1992). However, this was not clear due to the complex structure of the profile. It was felt that reprocessing the profile especially with special emphasis on pre-stack migration i.e. dip moveout correction (DMO) would improve the data quality and hopefully the interpretation.

The basin, which forms the eastern portion of the Magdalen basin (figure 2.1), has been a target of many geophysical and geological studies dating as early as the 1950's. Vernall (1954) compiled a gravity report of the St. George's Bay lowlands onshore. Spector (1969) reported and interpreted an aeromagnetic survey conducted in 1969 by Lockwood Geophysical. Knight (1983) mapped the geology of the Carboniferous rocks onshore. Peavy (1985) compiled a potential fields study on the area. This study suggested that the basin could attain a depth of up to 4 km. The study was not well constrained by other geophysical data. Kilfoil (1988) attempted an integrated geophysical study on the basin onshore using all available geophysical data at that time. The conclusion was that the basin could be a half graben about 2 to 4 km depth. Miller et al. (1990) combined both the studies of Peavy (1985) and Kilfoil (1988) and found that the basin could be as deep as 3 km.

The data for the current project were acquired in October 1989 for Memorial University of Newfoundland and the Government of Newfoundland and Labrador through a contract with Capilano Geophysical Limited of Calgary Alberta. The aim of conducting this seismic survey was to try and image the structure of the basin onshore using seismic reflection. The offshore section of basin had been covered by a seismic reflection survey of Mobil Oil in 1971 and 1973. These seismic sections are generally poor in quality, though the structures they reveal are similar to those of the current seismic profile. The Cabot Strait area, 75 km southeast of the study area, had been covered by a reflection survey of Petro-Canada, between 1981 and 1983. Very little seismic data covered the onshore section of the basin. Therefore, the seismic survey was deemed necessary. These data were of very high quality, but needed careful processing because of the complexity of the structure.

Data were processed using the STARPAK software centred around a CONVEX C1 XL mini-supercomputer. Apart from DMO, careful front muting, field statics based on refraction picks and more velocity analyses, most of the other processors are as mentioned by Hall et al. (1992). DMO is considered a powerful tool in cleaning up the data and helping image complex structures.

The interpreted seismic profile favours the hypothesis that the basin is a half graben of depths up to 5 km. Most of the structural features and stratigraphy of the basin are discussed in the text and 3 models are produced.

Chapter 2: Regional geology of the Bay St.George Carboniferous Subbasin

2.1 Introduction

The Bay St. George Subbasin forms part of the Maritimes Carboniferous basin of Atlantic Canada (see Fig. 2.1). The basin formed as a pull-apart basin within a post-Acadian dextral strike-slip system (Wilson, 1962). In this project most of the geological discussion is derived from the work of Knight (1983), unless otherwise stated. The geology here will only be outlined; for a detailed geology the reader is referred to Knight (1983). Figure 2.2 is a general geology map of the study area.

2.2 Pre-Late Devonian/Carboniferous geology

The pre-Carboniferous basement, where not exposed, is likely composed of Precambrian age rocks (Williams, 1978), similar to those of the Indian Head Complex. Knight's (1983) interpretation indicates that the basement to the immediate northwest of the onshore Anguille outcrop was reduced to a peneplain of Grenville rocks during the Tournaisian, prior to deposition of the uppermost Anguille Group.

At the hinge of the Flat Bay anticline, conglomerates assigned to the Anguille Group rest unconformably on Grenvillian basement, probably similar to that of the Indian Head complex (Knight 1982). This means that the lower Palaeozoic carbonate sequence may be limited in its southward extent from the Port au Port peninsula (Knight 1983; Williams, 1985) toward the Bay St. George Subbasin, and may not underlie the Carboniferous, as is interpreted by Watts (1972) in the East Magdalen

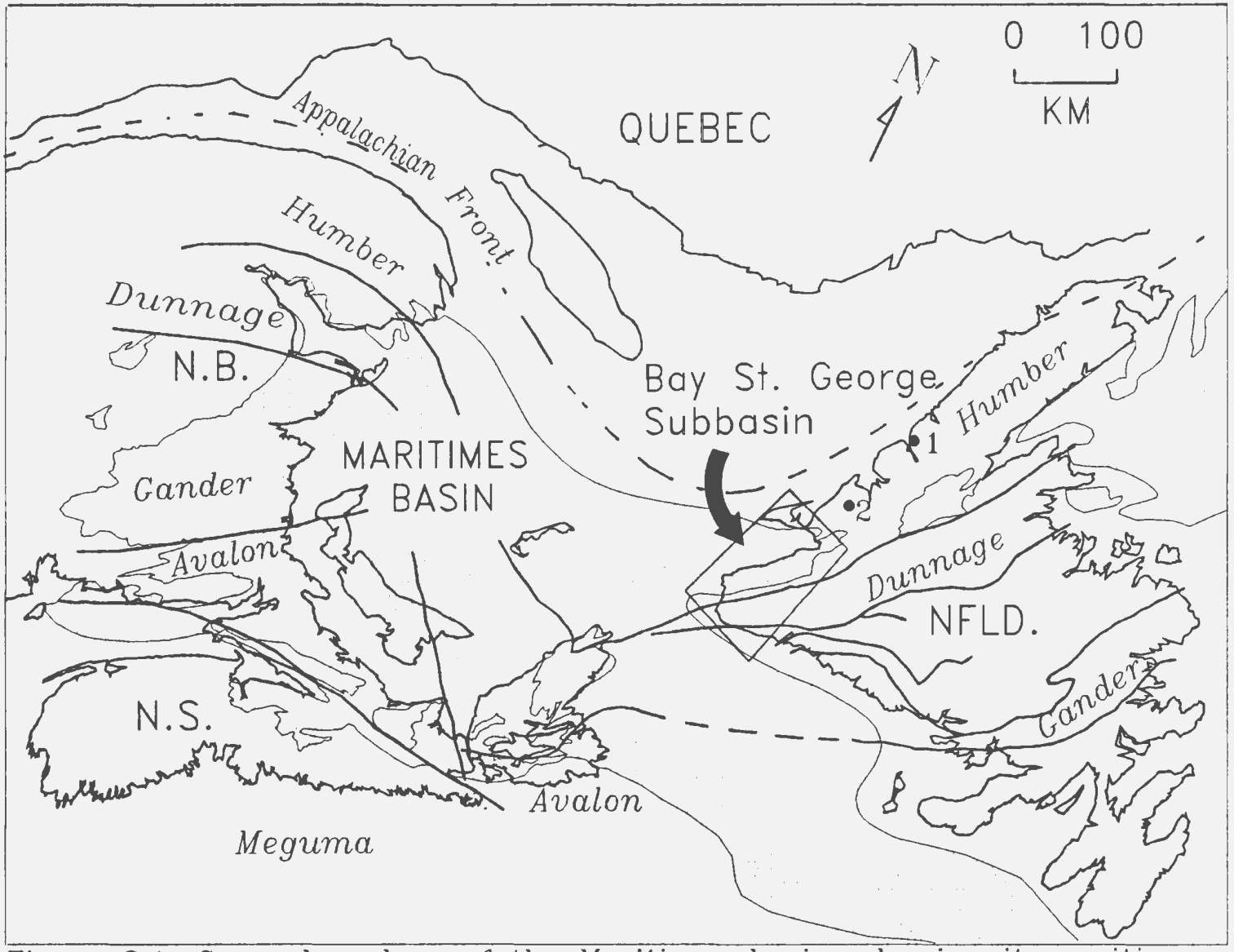

Figure 2.1. General geology of the Maritimes basin, showing its position relative to the Appalachian mobile belt and the location of the Bay St. George subbasin (modified from Hall et al., 1992).

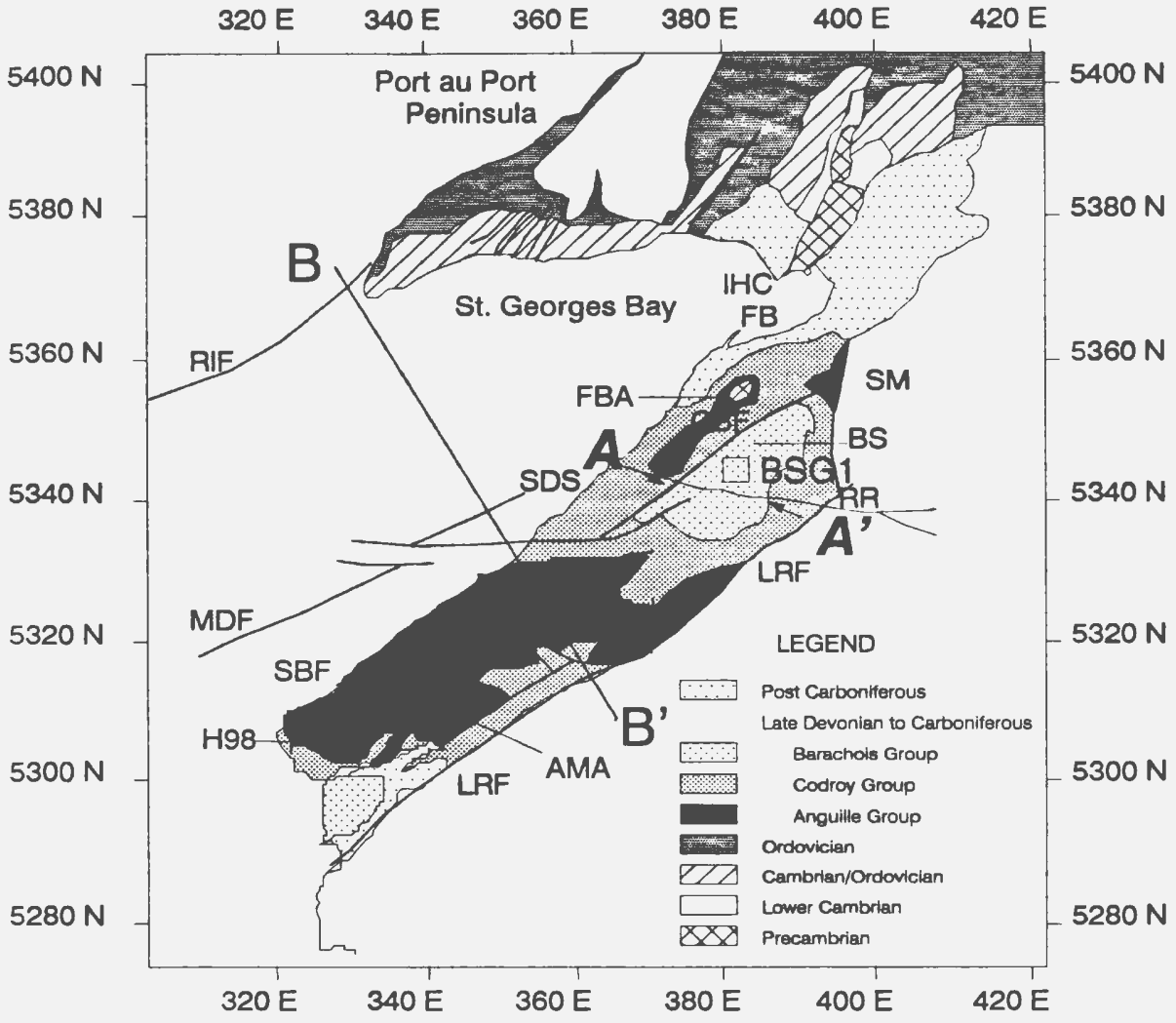

Fig.2.2. The Bay St. George subbasin: outcrop geology in the vicinity of the seismic line (modified from Schillereff and Williams (1979), Knight (1983) and Williams (1985)).

Abbrevations: AMA = Anguille Mountains Anticline, BS = Barachois Synclinorium, FB = Flat Bay, FBA = Flat Bay Anticline, IHC = Indian Head Complex, LRF = Long Range Fault, SBF = Snakes Bight Fault, SDS = St. David's Synclinorium, SM = Steel Mountain Complex, BSG1 = Memorial University drillhole, H98 = Union Brinex H-98 well CBF = Crabbes Brook Fault, MDF = Mid-Bay Fault, RIF = Red Island Fault, RR = Robison's River.

Heavy lines are the major faults mapped by Knight (1983) and Schilleriff and Williams (1979).

Arrows A and A' indicate the two ends of the seismic profile presented in this study. The potential field profile shown in Figure 2.7 is close to and parallel to the seismic line.

B-B' is one of the gravity profiles interpreted by Kilfoil (1988) and quoted in this paper.

basin. Onshore, exposures of the Indian Head Complex consist of foliated dioritic to granodioritic gneisses which become more massive toward the south, with outcrops of anorthosites and layered gabbroic rocks cut by foliated rocks of granitic composition (Williams, 1985). Lenses and bands of magnetite occur within the foliated gabbros, and are the probable cause of the magnetic anomalies observed over the complex (Peavy, 1985).

2.3 Late Devonian to Carboniferous Rocks

2.3.1 Introduction

A succession of late Devonian to Carboniferous age strata overlie Precambrian basement in the Bay St. George subbasin. These sediments have been subdivided into three groups, each distinguishable by its character and mode of deposition.

1. The Anguille Group (late Devonian to Early Mississippian), consists of nonmarine sequences of mostly red to grey fluviodeltaic shale to coarse sandstones, with local conglomerates.

2. The Codroy Group (Upper Mississippian) consists of both marine and nonmarine sequences of siliciclastics, evaporites and calcareous sediments.

3. The Barachois Group (lower Pennsylvanian) is made up of red to grey siltstone-sandstone sequences of fluvial origin with minor mudstones and coals.

The stratigraphy and sedimentology is further summarised in table 2.1 and figure 2.3.

Table 2.1. List of abbreviations

cg - conglomerate	peb - pebbly(es)
ss - sandstone	mic- micaceous
slst - siltstone	ark - arkosic
sh - shale	arg - argillaceous
mdst - mudstone	fluv - fluvial
lut - lucite	x-b - cross-bedded
carb - carbonate	plan - planer
ls - limestone	lam - laminated
dol - dolomite	c - coarse
evap - evaporites	rd - red
gyp - gypsum	gn - green
anh - anhydrite	gy - grey
hal - halite	brn - brown
pot - potash salts	bk - black
clch - caliche	seq(s) - sequence(s)

Table 2.1. Summary of the geology of Bay St. George Subbasin (modified from Knight, 1983)

Group	Formation/ Member	Lithology	Dipositional enviroment	Thickness(m)	Age	Correlation
Barachois	Undivided Barachois	gy peb ss;gy-bk mdst, sh, coal	Meandering river channels; floodplain.	1500-1600	Latest Westphalian	Pictouan
	Searston Formation	rd slst;gn-rd peb ss; minor bk sh mdst; minor brn cg		2500	Namurian	Canso Fm. of Nova Scotia
Codroy	Woody Cape Fm.	gy-gn-bk slst with mic ss, gy-bk carb, rd beds.	Deltaic	690	Visean	Windsor C D E
	Robinson's Riv. Fm. — Overfall Brook Mbr. (Brow Pond Lentil)	rd-brn massive to x-b ark to arg ss; minor cg, slst, mdst.	Northwest progradation of alluvium; salt formation in depressions;	>345		
	Robinson's Riv. Fm. — Mollichignick Member	rd slst, mic ss, ark to arg peb ss near margins; coarse up seqs marine carb near middle.	inland sea with small deltas;	2275		
	Robinson's Riv. Fm. — Highlands Member	rd-gy ss to slst;cg to N and E; fining up seqs x-b and plan ss; minor clch, lam ls.	Arid but large perenial river from distant source; wide rivers and associated meanderbelts;	884		
	Robinson's Riv. Fm. — Jefferies Village Member	rd-gy sh, mdst, slst, ss, minor cg interbed with carb and eva: gyp, anh, hal, pot; coarsens up near top.	semiarid in Mollichignick Mbr. to humid in Overfall Brook Member.	1400-2000		
	Codroy Road Fm.	Rd slst to ss, lam ss;near top gy sh, evap: gyp anh; minor carb and gy-bk slst.	Central lagoonal area; Progradation of alluvium from Long Range	120-300		Windsor B
	Ship Cove Fm.	lam ls; minor gyp nodules, rd-gy sh mdst.	Tidal and subtidal conditions; north to south transgression.	18-20		Windsor A
Anguille	Spout Falls Fm.	rd-gy fluv. ss, slst, calc-ark-mic ss; well-bedded; minor cg near margins.	Gravelly, fluvial; semi-arid conditions.	780-2250	Tournaisian	Upper Horton
	Friars Cove Fm.	Cg to ss; gy ss-cg-sh; x-b c ss at top: minor thick bk sh seqs; ss peb of Cam-Ord Origin.	Fluvio-deltaic; shallow lacustrine setting.	500-1300		NB Albert Fm.
	Snake's Bight Fm.	bk lut, gy ss, sh; thin slst to thick ark ss (flysch); minor dol, mdst, concretions.	Turbidites; deep narrow perenial lake.	785-1000		NB Albert Fm.
	Kennels Brook Fm.	Gn-gy peb ss to cg; rd ss to rd-gn slate; fining up seqs; minor brn mdst, ls	Fluviatile, fanglomerate and shallow lacustrine.	>3200	Famennian	Pre-Horton

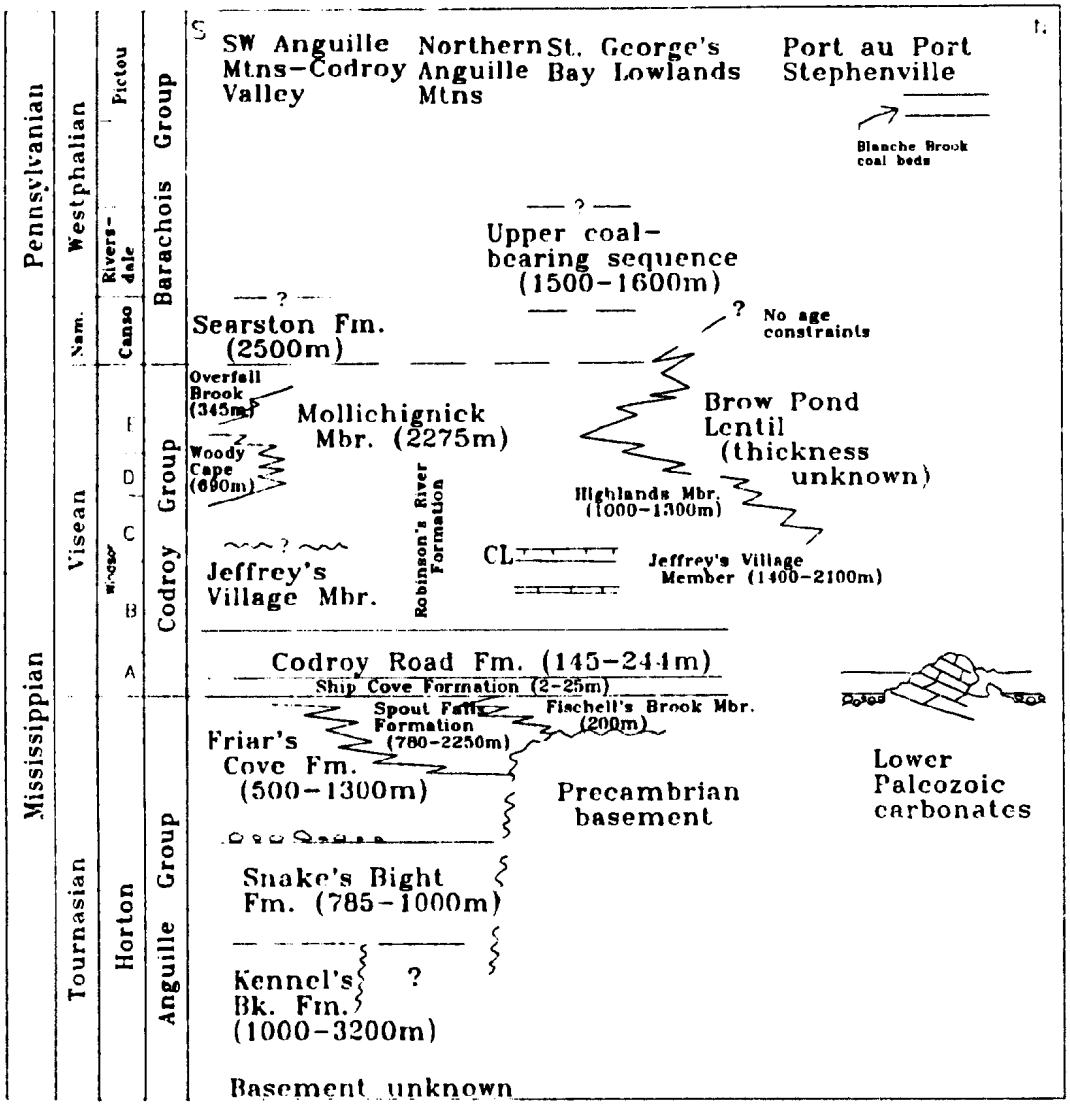

Figure 2.3. Stratigraphy of the Bay St. George subbasin, showing correlations with other rock units in the Maritimes Basin. CL = Crabbe's limestone (after Hall et al., 1992).

2.3.2 The Anguille Group

The Anguille Group, which is the oldest and thickest of the sedimentary groups, is exposed in anticlinal structures. It shows rapid changes of facies. Knight (1983) interpreted that the Anguille records the creation and infill of a deep lake measuring about 30 km by 100 km. The detritus for the infill was mainly derived from the southeast of the Long Range Fault. A northwest trending marginal fault, parallel to the Snakes Bight Fault onshore, is assumed to lie concealed beneath Codroy strata just offshore at the present day coastline. The early subbasin may be viewed as a graben type feature, though its evolution is complicated by lateral strike-slip movements along the faults defining its margins to the southeast and northwest.

The Kennels Brook Formation, the lowest in the Group, consists of a thick molassic sequence, comprising fluvial redbeds with minor lacustrine sediments that may have extended beyond the margins of the early subbasin. The strata are correlated with lower Horton or pre-Horton in other parts of the Maritimes Basin. The thickness of this formation is not known because the basal contact is nowhere exposed in the Anguille region; a drill hole (H98, see Figure 2.2) which penetrated 2200 m may not have drilled the true stratigraphic thickness. The conformably overlying Snakes Bight Formation, which is correlated with the Albert formation of New Brunswick, is composed of deep water clastic sediments typically deposited in alluvial fan-delta and submarine fan (turbidite) environments. The Friars Cove Formation consists of grey sandstones to black shales, and represents the transition

from a lacustrine through fluvio-deltaic to fluvial plain setting. This formation is equivalent to the well-known, petroliferous Albert Formation of the Horton Group in New Brunswick. The overlying Spout Falls Formation is correlated with the uppermost Horton in the Maritimes and consists of fluviatile rock sequences localized in three areas: (1) red and grey sandstones, minor siltstones and conglomerate, with abundant scouring and well-bedded sheet geometry, are found mainly in the south; (2) grey and minor red conglomerates and sandstones overly the Grenvillian basement in the Flat Bay anticline (Fischell's Brook Mbr.); (3) a thick sequence of fault-bound, red arkosic rocks (Brow Pond Lentil) may also be partly equivalent to upper Codroy rocks. This unit is approximately 780-2250 metres thick and is thought to represent an exhumed fault scarp (Knight 1983).

2.3.3 The Codroy Group

This Group is similar to the Windsor Group of the Maritimes. It represents a regional transgression and shift to marine and marginal marine conditions in early Visean time.

The lowest Ship Cove Formation, which on average has a thickness of 18-20 metres, is mostly composed of well-laminated, grey limestones, becoming shalier and containing gypsum and marls upward. This formation is correlated with the Macumber Formation of the early Visean of Nova Scotia and New Brunswick (Windsor Subzone A, in part).

The overlying Codroy Road Formation is made up of fine grained, red and grey siliciclastics, evaporites and minor carbonate. Redbeds in the south give way to evaporites in the north. The thickness varies from 120 metres at Ship Cove to about 300 metres in the Codroy Valley. This formation is roughly equivalent to Windsor subzone B (early Visean).

The Robinson's River Formation is composed of four more or less equivalent members: the Jeffrey's Village Member of about 1400-2100 metres thickness, the Highlands Member (884+ m) in the St George's lowlands, and the Mollichignick (2275+ m) and Overfall Brook (345+ m) in the Codroy lowlands. The formation is a complex succession of terrigenous clastic rocks with lesser amounts of carbonates and evaporites and is correlated with the upper half of the Visean; that is, it is roughly equivalent to subzones C, D, and E of the Windsor in the other parts of the Maritimes.

The Woody Cape Formation, consisting of predominantly grey, green and black fine grained siliciclastics, intercalated with micaceous sandstones, grey and black carbonates, and minor redbeds, has a thickness of about 690 metres. The Formation is placed in Windsor subzones D and E, which makes it partly equivalent to Overfall Brook and Mollichignick members earlier described.

3.3.4 The Barachois Group

Rocks of this Group occur in two outcrop areas and represent two different periods

of deposition. In the south, the early Namurian Searston Formation represents the Canso strata of the Maritimes Basin, while deposits in the St. George's Bay lowlands in the north are probably Westphalian in age, although neither the top nor the base is well defined in age. Lithologies include buff-weathering, grey sandstone intercalated with grey siltstone and/or grey to black mudstones, shales and occasional coal beds. Conglomerates and sandstones lying unconformably on the basement in the southeast are included but may belong to the Codroy Group. The thickness is not known exactly, but may be about 2500 metres for the Searston beds in the Codroy lowlands and about 1600 metres in the St. George's Coalfield.

The Searston Formation is equivalent to the Canso Formation of Nova Scotia, but the uppermost Barachois beds near Stephenville may be Pictouan (latest Westphalian) in age. The coal-bearing beds are Westphalian A to C in age but it is not clear whether the Namurian B and C are represented.

2.4 Structural History

The strata are principally deformed by north easterly trending folds and faults produced during the Hercynian Orogeny in post or late Pennsylvanian times (Knight, 1983). Major structures trend parallel or subparallel to the Long Range Fault and associated faults within the subbasin (see Figure 2.2). Folds vary from open and upright to tight and overturned. Fault types include high angle faults (dips of 60-90 degrees), thrust faults and decollement zones (Knight, 1983). The structural style is

generally simple in the north where Precambrian basement gneisses underlie Carboniferous strata at shallow depth (Riley, 1962, Belt, 1969). In the south, particularly beneath the southern Anguille Mountains, the structure is complex and reflects the great thickness of the succession and the relative degrees of competence of the different lithologies.

Major folds that show a northeasterly trend include the Anguille Anticline, Flat Bay Anticline and the Barachois Synclinorium. The Anguille Anticline is a large anticlinorium which exposes the Anguille Group strata in the Anguille Mountains, and is modified by numerous subsidiary folds. It is also cut by the Snake's Bight Fault close to its axial plane. At its northern limits it varies from moderately dipping to overturned. In the south, folds are arranged en echelon to the faults which strike generally in a northeasterly direction; in the north the Anguille Anticline swings to 068 degrees. The Flat Bay Anticline, which is a harmonic folding of both Anguille and Codroy strata around a core of Grenville basement, trends 037 degrees. The Barachois Synclinorium is a broad open feature and trends 027 degrees.

There are few structures of northwesterly trend. The St David's Syncline, which is situated between the Anguille and the Flat Bay anticlines, is peculiar because it trends at right angles to other regional structures.

Knight (1983) mapped various thrust faults and decollement zones. Many of these developed locally within relatively incompetent evaporites and shales of the Snake's Bight and Codroy Road Formation respectively. Thrust faults of local extent occur

where there is competency contrast, for example where the thick black sandstone units overlie thick black shale units in the Snake's Bight Formation (Knight, 1983). A decollement zone is developed at the base of the Codroy Road Formation in the central and northern areas where fine siliciclastics and evaporites of the Formation overlie the Ship Cove Formation.

High angle faults of northeasterly, northwesterly and easterly orientation are mapped by Knight (1983). The major ones of these are the northeasterly faults which include the Long Range Fault (Cabot Fault), the Snake's Bight and the Crabbes Brook Faults. En echelon fold trends are associated with several of these faults which show right-lateral strike slip motion. Some faults show slickensides. The Long Range Fault, the most prominent of these faults, extends as a general straight feature along the full extent of the southern margin of the subbasin. This fault, though rarely exposed, is confirmed by aeromagnetic data (Miller et al., 1990). In the Codroy area, the fault is exposed twice on the Branch river and poorly on Stephen Brook. In the north the fault is not exposed at all. Field observations indicate two periods of movement, firstly strike-slip and secondly oblique-slip which have occurred most recently. South of the basin the fault dips generally southward at high angles, but locally is vertical or dips at high angles into the basin. Sediments within the basin adjacent to the fault generally dip steeply away from it, or are deformed in overturned synclines.

The Snake's Bight Fault which transects the Anguille Anticline is represented by a prominent northwestward facing fault scarp. This fault trends parallel to the Long

Range Fault in the southwest but further northeast it swings eastward. The angle of intersection between the Snake's Bight and the Long Range Faults is approximately 25 degrees. In a manner similar to that of the Snake's Bight Fault, the Crabbes Brook and the Ryan's Hill Faults trend subparallel to the Long Range Fault. These two show a downthrow to the southeast of several thousand metres and evidence of significant right-lateral movement, and show compression in an associated array of en echelon faults.

2.5 Previous Geophysical Studies

2.5.1 Introduction

The Bay St.George's basin has been studied using most of the common geophysical methods, including potential field surveys with concomitant measurement of rock density and magnetic susceptibilities, and reflection seismic.

In 1984 an underwater gravity survey was conducted from the CSS Dawson. In the summers of 1983 and 1984 gravity surveys were carried out in the areas onshore by personnel from Memorial University of Newfoundland. The Bouguer anomaly map (Fig. 2.4) in the current project combines data from all surveys that have been carried out to date.

The magnetic data (Fig.2.7) is digitized from the existing aeromagnetic maps of the government of Canada (Kilfoil and Bruce, 1991). The data area covers onshore

part of the basin only.

Mobil Oil obtained seismic data in 1971 and 1973 covering the central offshore region. The Lithoprobe East seismic reflection line 86-4 traverses the outer limits of the basin. Between 1981 and 1983, Petro Canada conducted a major seismic reflection survey in the Cabot Strait which is 75 km southeast of the study area.

2.5.2 Physical Parameters

Densities and magnetic susceptibilities for the samples of pre-Carboniferous basement and Carboniferous sediment rocks collected or obtained from drill cores were studied by Peavy (1985) and Kilfoil (1988). The results of their study are summarised in Table 2.2.

2.5.2.1 Density

Each sample was identified with respect to group, formation and or member and general lithology. The overall density of each member or formation was calculated by weighting the average density obtained for each rock type within the unit by its percent composition. To get an estimate of the density for a particular group, the thickness contribution of the members of the group were used as weighting factors.

Halite, gypsum and anhydrite from drill cores were sampled to obtain representative densities for the evaporite sequences. Average density of the evaporites is close to that of the Codroy Group, in which most of the evaporites are found. It

should be noted, however, that the known evaporite deposits contain significantly more gypsum and salt than anhydrite, thus the average density of an evaporite deposit is significantly lower than that of the Codroy rocks (Miller et al., 1990).

Table 2.2. Rock Densities (Miller et al., 1990).

Group	Geological Unit (Fm/Mbr)	Density±SD (g/cm^3)
Anguille	Kennels Brook	2.58±0.11
	snakes Bight	2.67±0.10
	Friars Cove	2.67±0.04
	Spout Falls	2.59±0.04
	Fischell's Cong.	2.32±0.03
	Average	**2.63±0.06**
Codroy	Ship Cove	2.72±0.03
	Codroy Road	2.48±0.14
	Robinson's River/ Jeffrey's Village	2.40±0.09
	Highlands	2.53±0.13
	Brow Pond Lentil	2.58±0.03
	Robinson's River/ Overfall Brook	2.44±0.08
	Mollichignick	2.55±0.12
	Average	**2.47±0.09**
Barachois	Searston	2.51±0.08
	Upper Series	2.56±0.08
	Average	**2.54±0.08**
Evaporites	Anhydrite	2.97±0.03
		2.28±0.03
		2.18±0.03

Representative densities of 2.63, 2.47 and 2.54 g/cm^3 were obtained by Peavy and

Kilfoil (1988) from thickness-averaged samples from the Anguille, Codroy and Barachois groups respectively. Anguille units show higher densities and hence density contrasts (relative to 2.67 g/cm^3) lower in magnitude than the overlying Codroy and Barachois Groups. This is consistent with Knight's (1983) observation that competent, well cemented, Anguille clastics contrast sharply with the more friable, younger Carboniferous clastics. Consistent results were obtained for samples from the Indian Head basement. These samples of anorthositic to granitic compositions are locally gneissic (Williams, 1985) and have densities averaging 2.68 ± 0.07 g/cm^3. This is in contrast to the measured densities of rock samples from the more anorthositic Steel Mountain Complex which averaged 2.83 ± 0.034 g/cm^3 with 10 samples giving values above 2.70 g/cm^3 (Peavy, 1985).

The greater variability in density of Steel Mountain samples is caused by a few samples of high density, two of which are greater than 3.20 g/cm^3.

There were no samples available for measurement from offshore. Knight (1983) considers that the offshore Carboniferous sediments most likely belong to the Codroy Group. Thus, these sediments are considered to have densities similar to those of the Codroy Group (Table 2.2).

2.5.2.2 Magnetic Susceptibilities

The sediments have such low susceptibility that they can be considered transparent to an external inducing field (Peavy, 1985). In comparison, samples of basement

rocks show susceptibilities that vary from near zero to 6000 x 10^{-6} cgs units (Peavy, 1985). Samples from the Indian Head Complex show consistently low susceptibilities, i.e., < 100 x 10^{-6} cgs units, but gabbroic lenses or layers rich in titaniferous magnetite within the complex (Williams, 1985) would be expected to have higher values. Samples from the Steel Mountain anorthosite were responsible for most of the variability in magnetic content of the basement samples measured, because they contained magnetite rich lenses or zones (Murthy and Rao, 1976).

2.5.3 Potential fields data

2.5.3.1 Qualitative Study

In order to separate the effects of the basement from those of the underlying sediments the gravity and magnetic data were subjected to a regional-residual separation procedure consisting of fitting third-order polynomial surfaces to the data sets. These maps are especially useful in discerning basement trends since removal of a low-order regional field eliminates the long wavelength portion of the field arising from general basement geometry (Miller et al., 1990). Figure 2.5 is the residual anomaly map after a residual-regional separation by fitting a third-order polynomial (Figure 2.6) to the Bouguer anomaly data (Figure 2.4). The polynomial surface was capable of discerning the main features in the region. This kind of polynomial fitting is similar to strike sensitive filtering as can be observed in Figure 2.6. The lows and highs can be seen clearer after the polynomial fitting (c.f. Figure 2.4 with Figure 2.5).

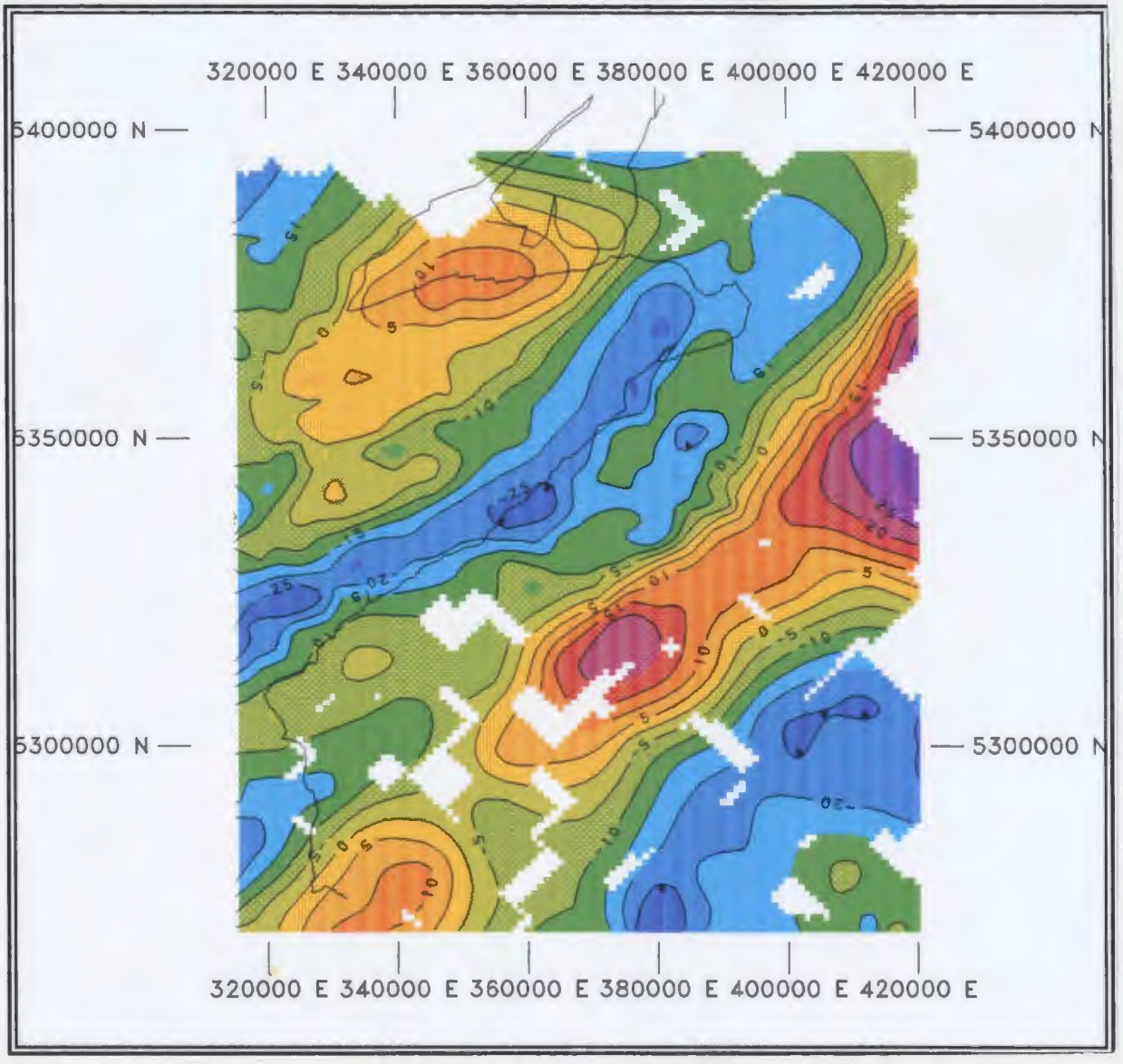

Figure 2.4. Bouguer anomaly map of the St. George subbasin. Contour intervals at 5 mgals. Empty spaces are areas with no data.

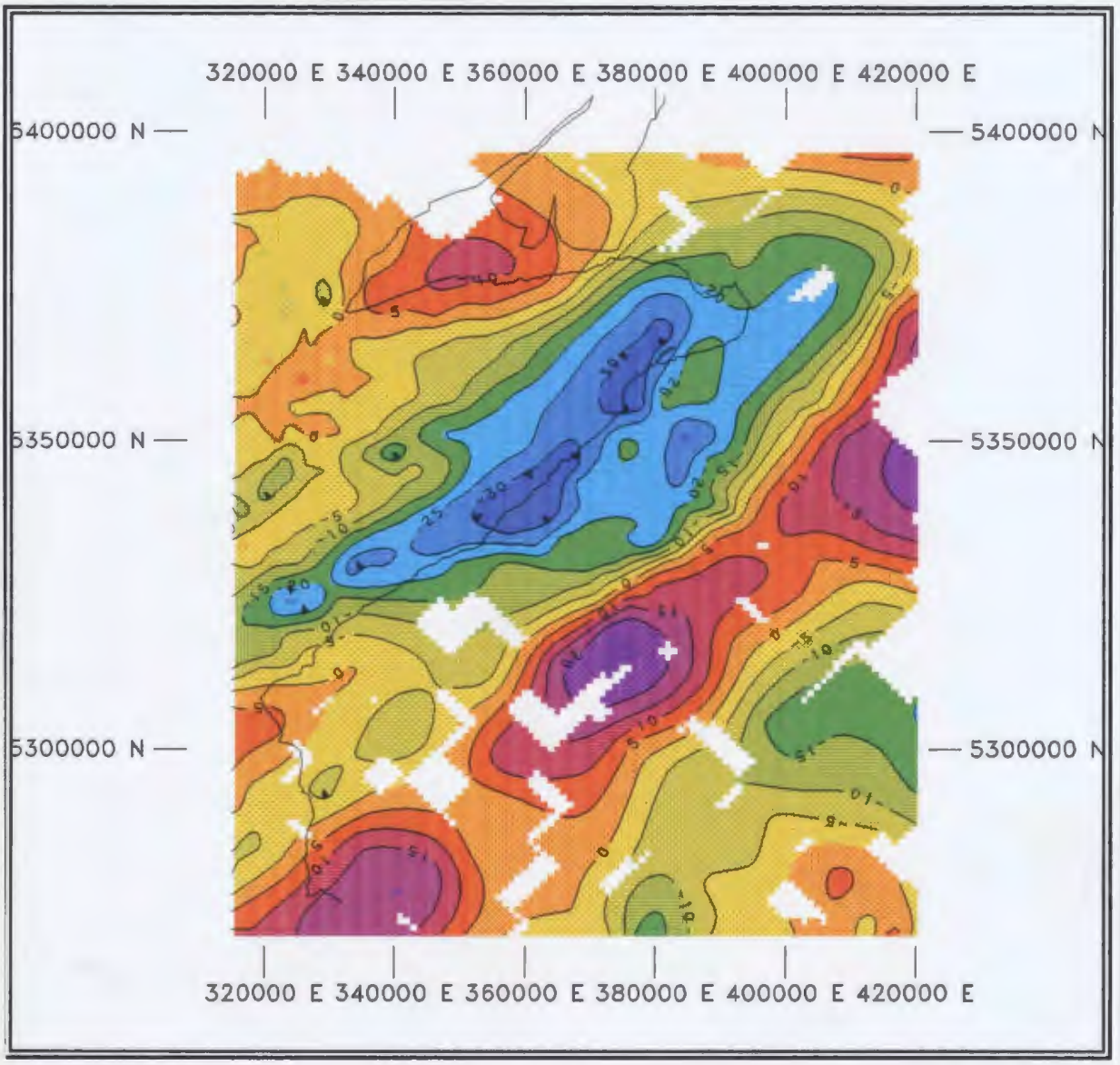

Figure 2.5. Residual anomaly map of the St. George subbasin after fitting a third order polynomial surface to the Bouguer anomaly map of figure 2.4.

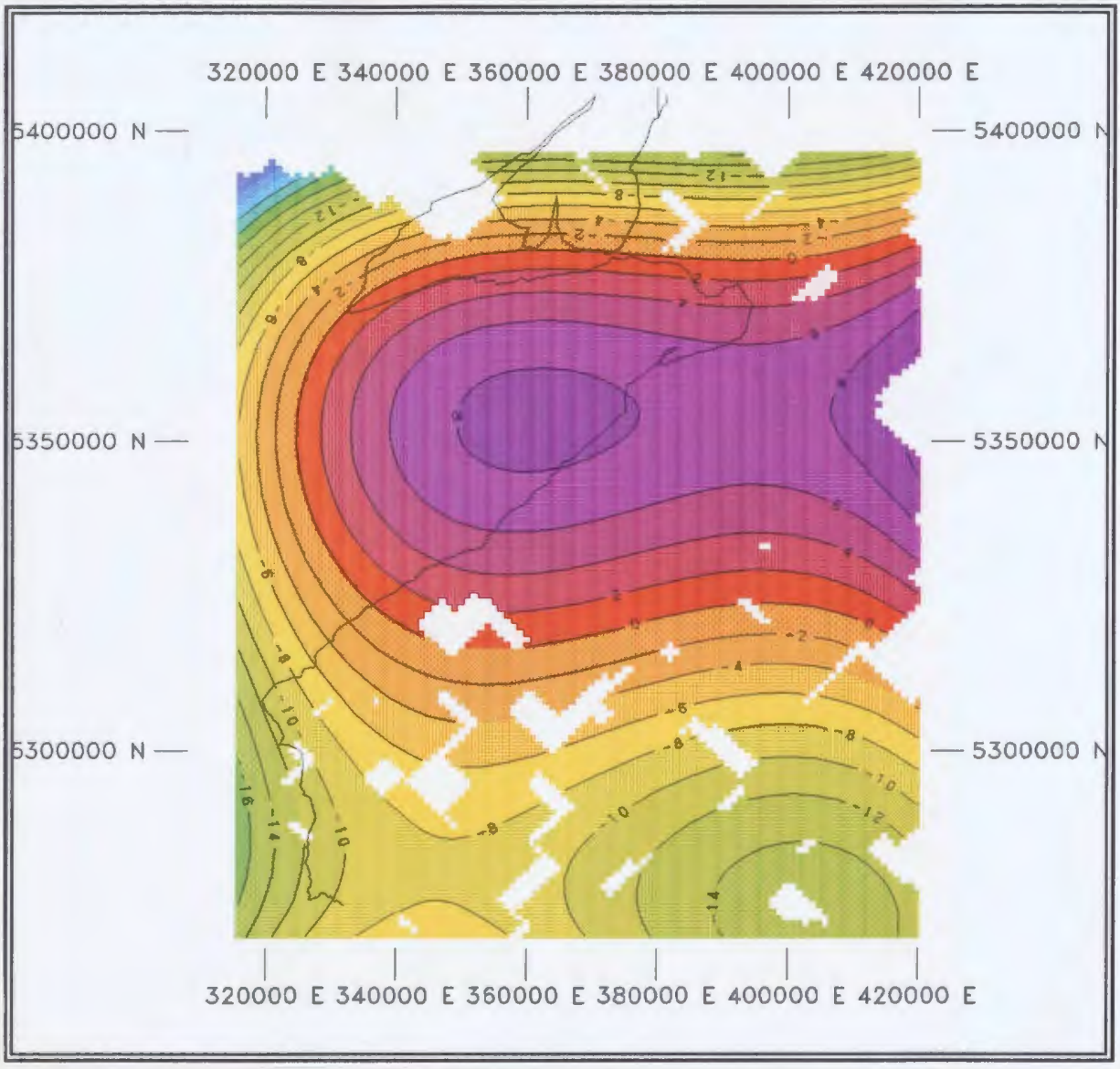

Figure 2.6. Plot of polynomial surface fitted to the Bouguer anomaly map.

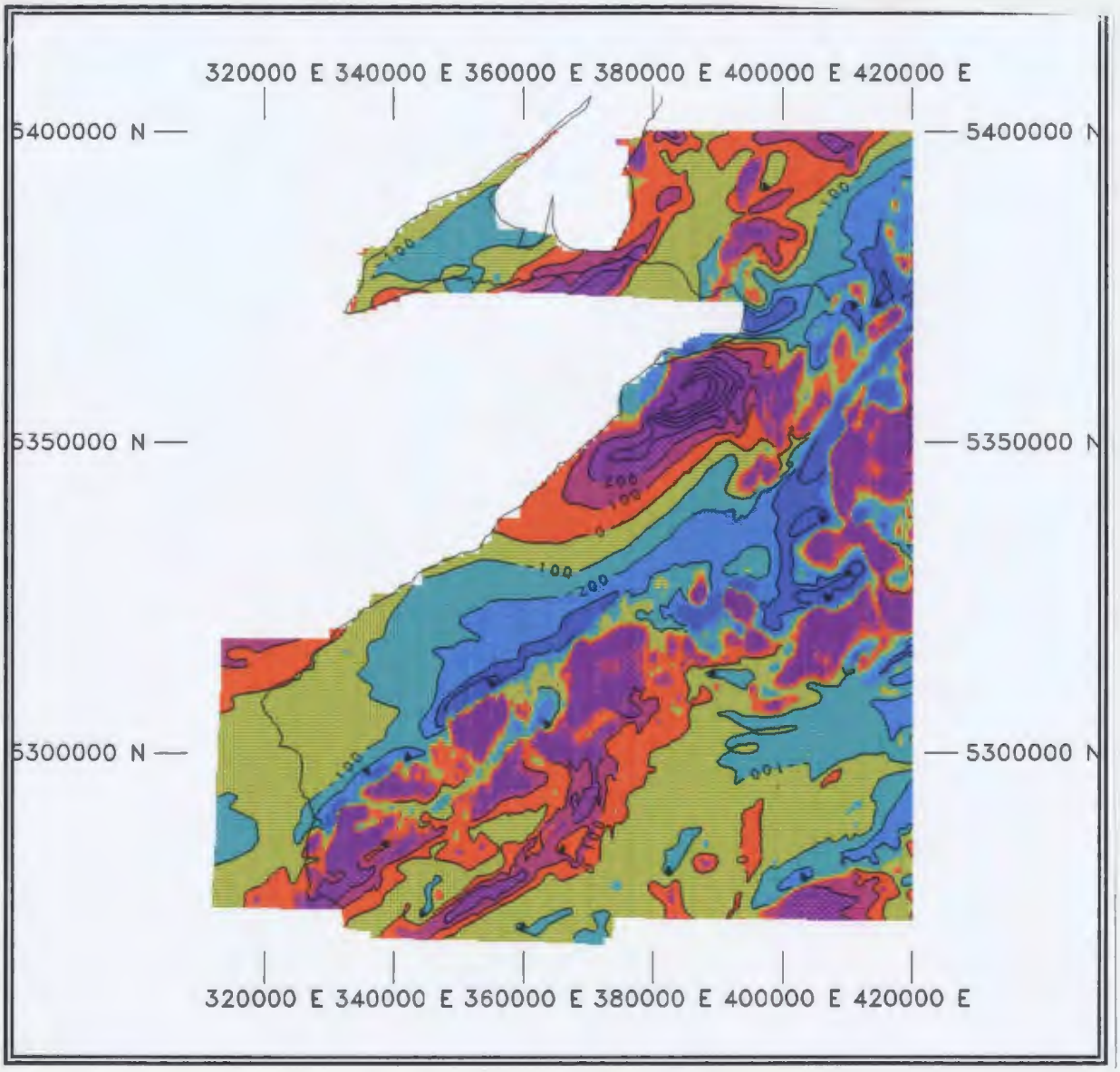

Figure 2.7. Magnetic data after fitting a third order polynomial surface to the original data. Contour intervals 100 nanoT.

Positive residual gravity anomalies correspond to small dimension basement topographic highs, and negative residuals indicate local thicker sedimentary accumulations, or even the presence of evaporites (Miller et al., 1990). The residual maps indicate that the sediments occur on both gravity and magnetic low (see Figures 2.5 and 2.7). There are some areas within the sedimentary basin with magnetic highs, especially the Flat Bay anticline. This is assumed to be floored by the Indian Head Complex. Other magnetic highs could be related to the basement which is assumed to have lenses of magnetite (Peavy, 1985). More negative gravity anomalies in the offshore correlate with the thickening of the Carboniferous sediments there. The strong northeast trending gradient with a positive step to the southeast corresponds to the Long Range Fault that defines the boundary of the basin (Miller et al., 1990). The Anguille and Flat Bay anticlines are expressed as relative gravity highs paralleling the general trend of the Long Range Fault. The general pattern of closely spaced gravity contours associated with these features suggests that both are fault-bounded to the west, with westward downthrow and thickening of the sedimentary wedge.

In addition to the strong northeasterly trends, secondary east-west trends are also significant. East-west lineations formed by the truncation and apparent dextral offset of residual gravity features indicate the presence of the east-west trends. Strike sensitive filtering also discerns these features.

Legend of figure 2.7

1	Pre-Carboniferous Basement
5	Spout Falls Formation
5A	Fischell's Conglomerate
6	Ship Cove Formation
7	Codroy Road Formation
8	Robinson's River Formation (undivided)
8A	Jeffrey's Village Member
8B	Highlands Member
11	Undivided Barachois Group

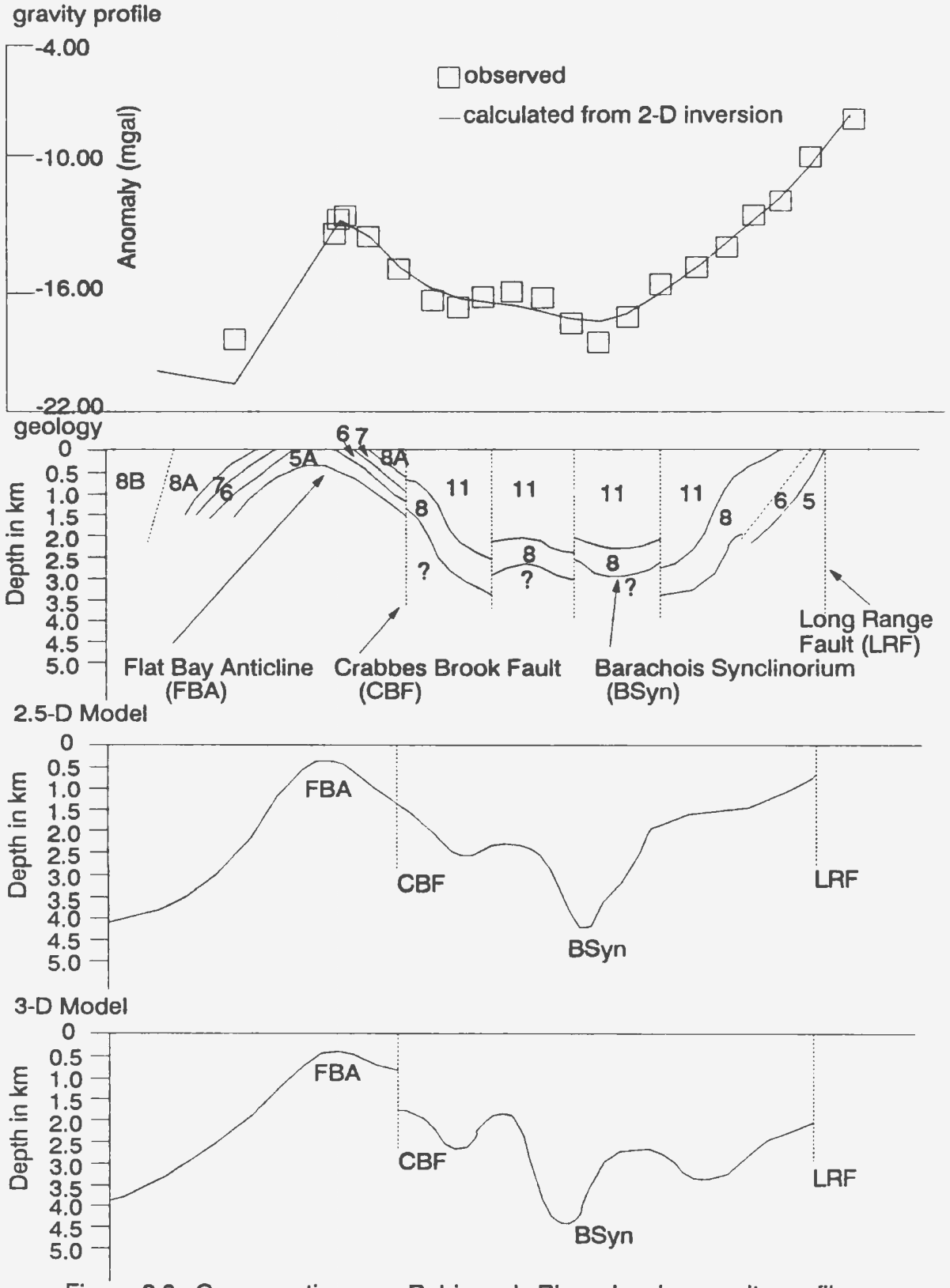

Figure 2.8. Cross-section near Robinson's River showing gravity profile, geology, 2-D and 3-D gravity models (after Peavy, 1985).

2.5.3.2 Quantitative Analysis

Peavy (1985) used a 2.5-D gravity inversion and 3-D forward modelling on profiles across the subbasin in order to determine the basement topography and the thickness of the sediments. Before undertaking the inversion qualitative interpretation of the gravity and magnetic data was made similar to that discussed above. In all the profiles a density contrast of -0.18 g/cm^3 between the average sediments and basement was used. All stations with positive anomalies were removed from the profiles because the density contrast is negative. A strike length of 60 km, determined from a geology map, was used in all of the 16 profiles.

From the 2.5-D inversion model, the Crabbes Brook Fault was interpreted to have an apparent downthrow to the west of 1.5-2.0 km at the northern end, reduced to 0.5 km near the Anguille Anticline. The average depth of the Barachois Synclinorium determined from this study was ~4 km. The average thickness of the sediments in the Brow Pond area was about 1.5 km. The thickness of the Anguille strata in the southern part of the area was not well defined owing to the limited number of data points in this area.

The results of the 3-D modelling were in good agreement with the 2.5-D inversion. Figure 2.8 is a cross-section close to and parallel with the Robinson's River seismic line showing the geology and 2.5-D and 3-D models. The only difference between the two models was a 2 mgal discrepancy in the Barachois area.

Potential fields solutions are non-unique. All the above results need to be

constrained with other geophysical data. Kilfoil (1988) tried to use some of the available offshore seismic data in the area to constrain his models. Four profiles were modelled. One of the models (Figure 2.9) is shown here alongside the interpretation of a seismic line across the same section. The modelling process was one of interactive forward modelling after inversion techniques had been developed and used to determine the configuration of the evaporite deposits (Kilfoil, 1988). The model shown here demonstrates that the Carboniferous sediments fill a half-graben structure with the thickest sediments just offshore. In contrast the sediments are thinner onshore. Offshore sediments are up to 6 km thick, while onshore sediments attain thicknesses up to 3 km (Miller et al., 1990).

2.5.4 Seismic data

Kilfoil (1988) used the offshore data acquired by Mobil Oil in the early 1970's to do an integrated gravity, magnetic and seismic interpretation of Bay St. George.

The most prominent reflector, identified on most of the seismic sections and denoted by the thick line in Figure 2.8, is interpreted as the pre-Carboniferous basement. From this section it is obvious that the basin thickens, in general monoclinally, to the southeast. The southeastward dip of the strong reflector is interrupted locally by at least one basement fault downthrown to the northwest. Basement reflector picks on the seismic lines trending east-northeast have very little dip, indicating that these lines are oriented nearly parallel to basin strike, as is

expected from trends observed on the gravity maps (Miller et al., 1990).

The seismic data support the interpretation that the basin is an asymmetrical half-graben with the basement dipping toward the Bay St. George southeastern coastline and striking subparallel to the Long Range Fault, which defines the basin margin.

The Mid-Bay and Red Island strike-slip faults have also been mapped in Bay St.George (Langdon, pers. comm., 1992). These two faults trend parallel or subparallel to the Long Range Fault and take up some of the dextral offset associated with the regional strike-slip system.

Salt structures that have been mapped offshore trend parallel to the regional fault system and probably are oriented according to stress conditions at the time of faulting. These salt structures are offset by subsidiary east-west faults discussed earlier.

The Cabot Strait seismic data displays features similar to the Robinson's River data; this particularly applies to the structural style of the detachment within the salt at the base of the Codroy (see Figure 2.10). The basin in this area, bounded by the Long Range Fault and the southward extension of the St. George's Bay "Coastal Fault", is similar in shape and dimension to that observed in the Robinson's River area (Langdon, pers. comm., 1992).

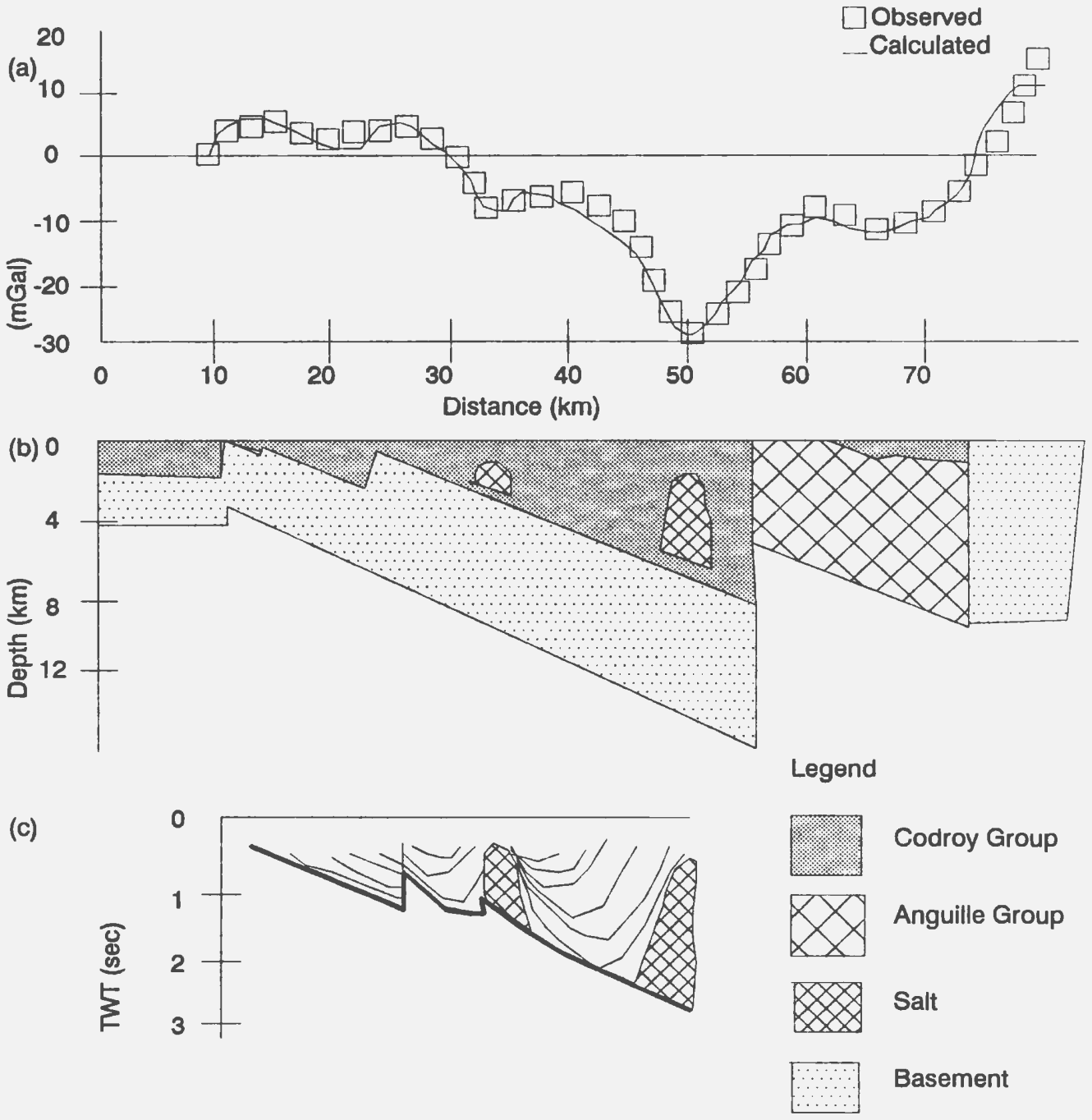

Figure 2.9. Modelled interpretation for profile B-B' oriented NW-SE (fig. 2.2) from Kilfoil (1988). a. Distance along profile in km indicated below gravity profile. b. Geological model inferred from gravity and seismic data along B-B'. c. Two-way travel time line drawing of significant reflectors along the seismic line (E-20). Thick, dark line represents basement, thin lines are intra-carboniferous reflectors. Salt indicated by hatched pattern. Line is shown in correct lateral position relative to the longer gravity profile in (b). Vertical scale is two-way travel time in seconds. Horizontal scale is the same as in (a).

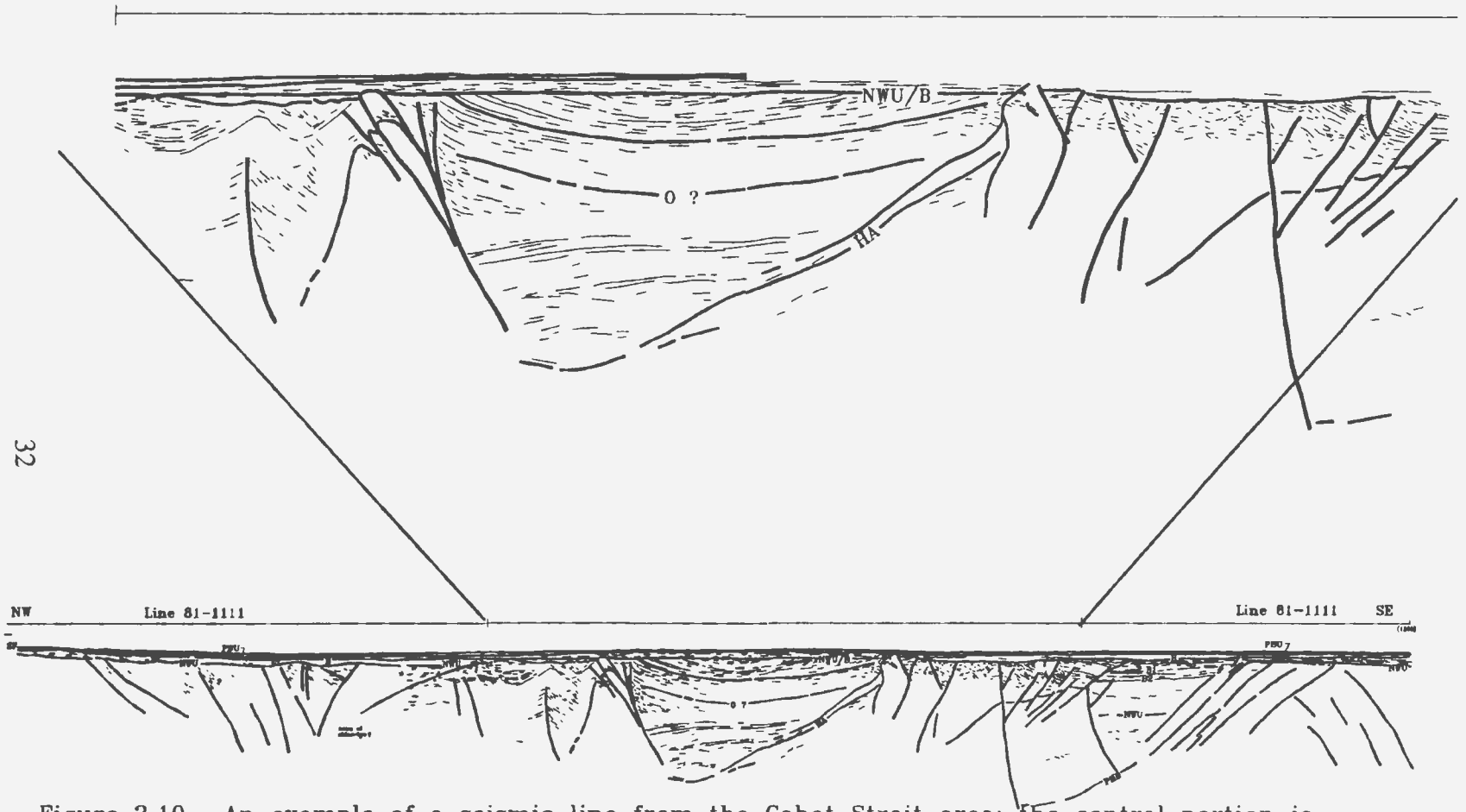

Figure 2.10. An example of a seismic line from the Cabot Strait area; the central portion is similar to the graben shown on the Robinson's data (modified from Langdon and Hall, in prep.).

Chapter 3: Seismic Reflection Profile

3.1 Introduction

The aim of the seismic survey was to image, by the seismic reflection method, the subsurface structure of the Carboniferous and older age rocks occupying an area of land in the vicinity of Robinson's River in the Bay St. George sub-basin of western Newfoundland (see Figure 2.2). Surface mapping and shallow borings had indicated a complex structure in the Carboniferous rocks in the area, but the overall structure appeared to be basinal (i.e. synclinal) with a possible thickness of 4 km of Carboniferous rocks in the area east of the Trans-Canada Highway (Knight, 1983). Thus, the seismic line was designed to test this structure.

12.68 km of seismic data were acquired and processed. The processed data show several sets of reflecting geological boundaries, some as deep as the base of the recorded section. A strong reflector at shallow depth, i.e. less than 2 km, appears to limit the downward extension of the complex structure mapped at the surface. Below the strong reflector are bands of reflectivity with apparently simpler structure.

After inspecting the processed data, it was felt that reprocessing of this line would possibly improve the events and hopefully the interpretation.

Therefore, the processing in this project was carried out more carefully than previously done. A few procedures were included that had not been carried out originally. Examples of these include field statics based on refraction picks, prestack migration i.e. dip moveout correction (DMO) and more velocity analyses.

3.2 Acquisition

The seismic profile was acquired for Memorial University of Newfoundland and the Government of Newfoundland and Labrador through a contract with Capilano Geophysical Limited of Calgary, Alberta. The field parameters and their tolerance for discretionary choice at the start of the survey, were agreed upon before the survey with staff of the Provincial Department of Mines and Energy. The parameters were as follows :

Recording instruments:	240 channel DFS V with Calder FS, recorded on digital magnetic tape in SEG Y format;
geophone group interval	20 m;
spread	symmetrical split, 26 station gap at v.p.;
geophones	12 per group, spaced at 1.5 m, 14 Hz;
source type	Vibroseis: 4 mertz vibrators (max. peak force 44000 lbs each)over 30 m;
vibration point (v.p) interval	40 m;
common depth point coverage	6000 percent (60 fold stack);
vibrator sweeps	4 per v.p. with 8 m move-up, each 8 s, non-linear 20-90 Hz;
record length	4 s (correlated data); data also recorded uncorrelated (12 s length);
sample rate	2 ms;
noise rejection	diversity stack plus alternating sweep anti-phase for 60 Hz rejection.

A gap of 13 stations (260 m) each side of the v.p. was chosen as a compromise of retaining data at short offset and avoiding high amplitude vibrator-generated noise

based on tests conducted at the beginning of the acquisition.

A 20-90 Hz non-linear (2 db/octave pre-emphasis) sweep ensured that ground-roll was avoided and the recording of high frequencies retained.

Because the spread length including the gap at the v.p. exceeded 5 km, and the total length was only 12-13 km, it was decided to roll in to the spread from the first geophone station using the same v.p. interval, and to roll off the end of the final spread. There was no gap employed during the roll-on and roll-off. The roll-on and -off was to ensure that the reflection point coverage extended the full length of the line and that the fold of the coverage near the line ends built up rapidly to the standard 60-fold.

Data were recorded using DFS instruments and a Calder Field System, with paper monitors of all shots produced on a Seistronix camera, and data recorded on digital magnetic tape in both correlated and uncorrelated form in SEG Y demultiplexed format at 6250 bpi.

3.3 Processing

3.3.1 Introduction

These field data were processed using the STARPAK software running on a CONVEX C1 XL mini-supercomputer.

The processing included crooked line binning, field statics based on refraction picks, dip moveout correction, CMP gather, notching of 60 Hz, NMO correction

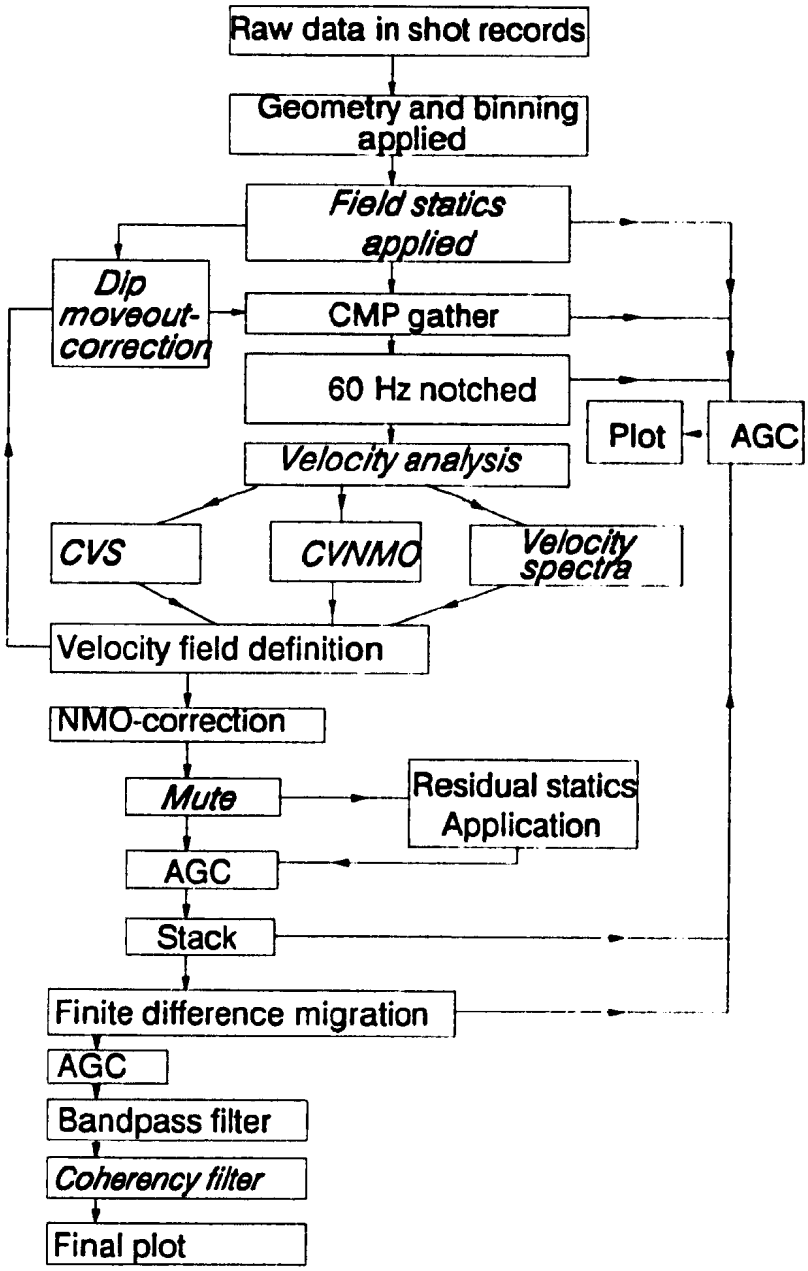

Figure 3.1. Data processing sequence. The processes in italics are either new or those done throughly in this project compared to previous processing of Hall et al. (1992).

based on velocity analyses and constant velocity stacks, front mute, gain equalization, CMP stack, residual statics, time-varying bandpass filter, trace sum, finite difference time migration, coherency filtering and display. The order of the processing procedure is summarized in Figure 3.1.

3.3.2 Pre-stack processing

3.3.2.1 Geometry and Binning

The binning strategy in this project was as determined previously in the original processing.

The binning that was applied was a crooked line that was based on a processing line that gave a best fit to the midpoint distribution along the line. Owing to the surface gradients and line bends, the distribution of 635 stations at a surface-taped interval of 20 m corresponds to a total horizontal crooked line length of 12.05 km as opposed to 12.68, the taped surface distance. Thus, on the final sections, every 10th station number was annotated for every 19th CMP rather than every 20th, so as to compensate for the difference in surface and crooked line geometries. The geometry of the job was set in the original data processing. The binning procedure included setting up of the bins of width and length of 10 and 20 m respectively and applying them to the shot records.

After binning only 72316 traces out of a total of 76320 (240 traces for each of the 318 shot records) traces fell into 1251 bins because 4875 traces did not fall into any

Figure 3.3. Shot record 250 from TWT 0.0 to 0.2 s showing example of section used to estimate refraction picks.

Figure 3.4. Shot record 1 from TWT 0.0 to 0.2 showing portion used to estimate velocity of the weathered layer.

bin. There were 70574 traces in at most one bin, 871 traces in at most 2 bins and no traces falling in at most 3 bins. The maximum fold of any bin was 104 traces. The binning chart, Figure 3.2, is in folder. The binning width and length was 10 m and 20 m respectively.

3.3.2.2 Field static corrections

The aim of field statics corrections is to correct for the irregularities in the topography and in the thickness of the weathered layer in the subsurface.

The field statics corrections were based on velocities estimated from the first breaks of the shot records. All the shots were plotted using vertical and horizontal scales of 100 cm/s and 5 traces/cm respectively (see Figure 3.3). Only the first 0.2 seconds of the shot records were analyzed because this was the only region of the data with reasonably good refractions. The vertical scale ensured time picking a resolution of 1 ms, thus quite accurate velocities and time intercepts could be picked. From each shot record, time intercept (t_i) and velocity of the bedrock (v_b) could be determined. The velocity of the weathered layer (v_w) was determined from the direct arrivals of the non-gapped records (see Figure 3.4). The assumption made at this point was that the direct seismic wave travelled at the top of the weathered layer. Thus, the slope of the direct wave is the reciprocal of the velocity of this layer. The following two equations were used to get the thickness of the weathered layer (z_w) and the static correction (Yilmaz, 1987) (t_D) respectively;

$$Z_w = \frac{v_b v_w t_i}{2(v_b^2 - v_w^2)^{\frac{1}{2}}} \qquad (3.1)$$

$$t_D = \frac{-Z_w}{v_w} + \frac{(E_D - E_s + Z_w)}{v_b} \qquad (3.2)$$

where E_D and E_s are the datum plane and the elevation in metres respectively. The datum plane was chosen as 150 m, to keep the statics as close to zero as possible. This was to ensure that the data were not shifted too much for further processing ; this is especially important for velocity analyses.

From the results obtained it was observed that v_b varied from 2.8 km/s to approximately 5.0 km/s and the lowest value of t_D was -39 ms while the highest value was +6 ms (see Appendix A). The velocity of the weathered layer (v_w) was estimated to be about 2.0 km/s. This value is high but is the best estimate from the non-gapped shot records (see Figure 3.4).

The values for the elevation were measured during the data collection.

The values of statics calculated were applied to the shot records after binning and geometry had been applied. The time, t_D, was simply added to each shot and the appropriate receiver traces respectively.

Figure 3.5 displays the results of field static corrections. From Figure 3.5b it can

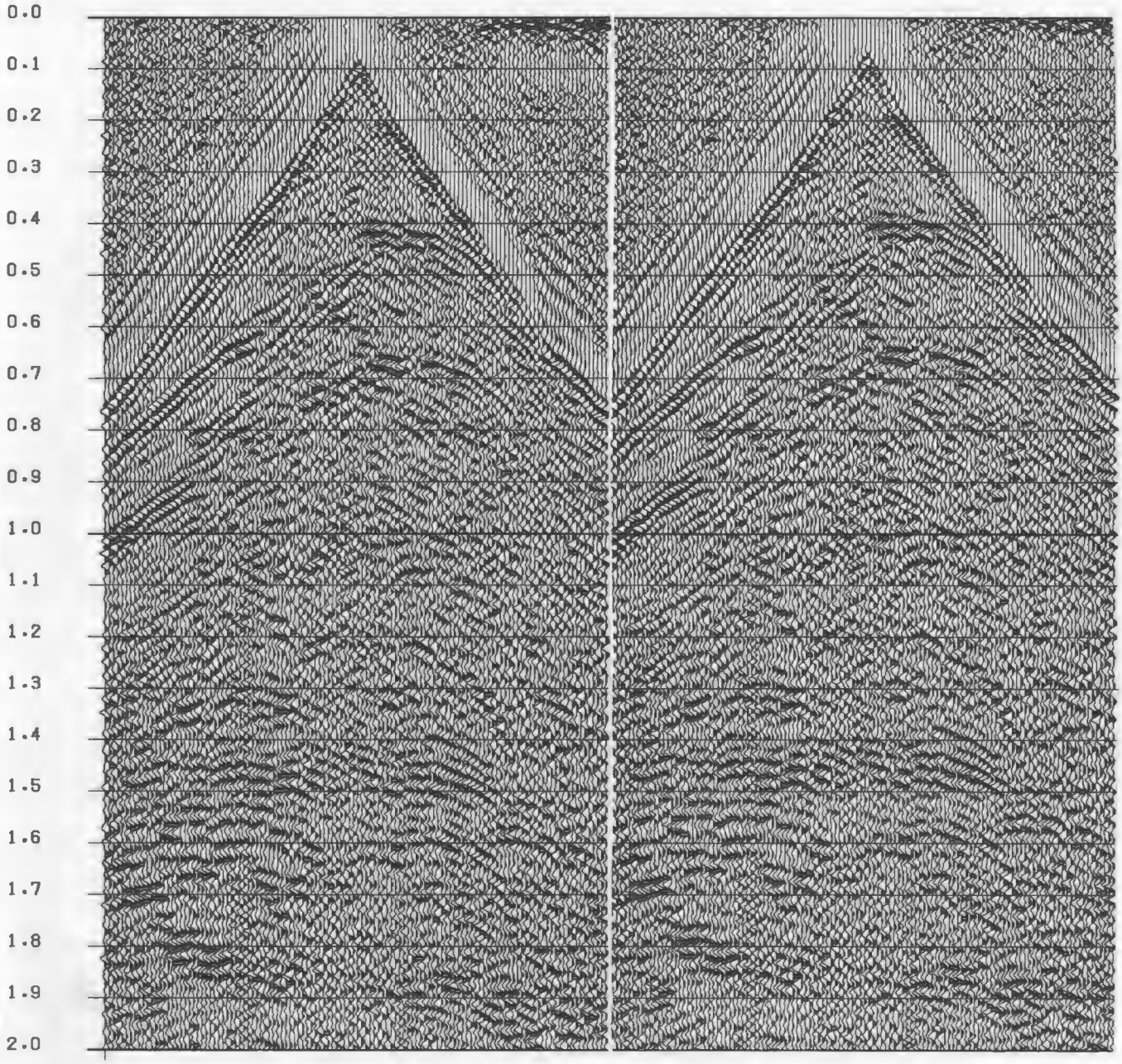

Figure 3.5. Shot record 250 from twt 0.0 to 2.0 sec. (a) Before applying field statics. (b) After field statics corrections. There is not much difference between the two records, except that the events are shifted in (b) slightly upwards.

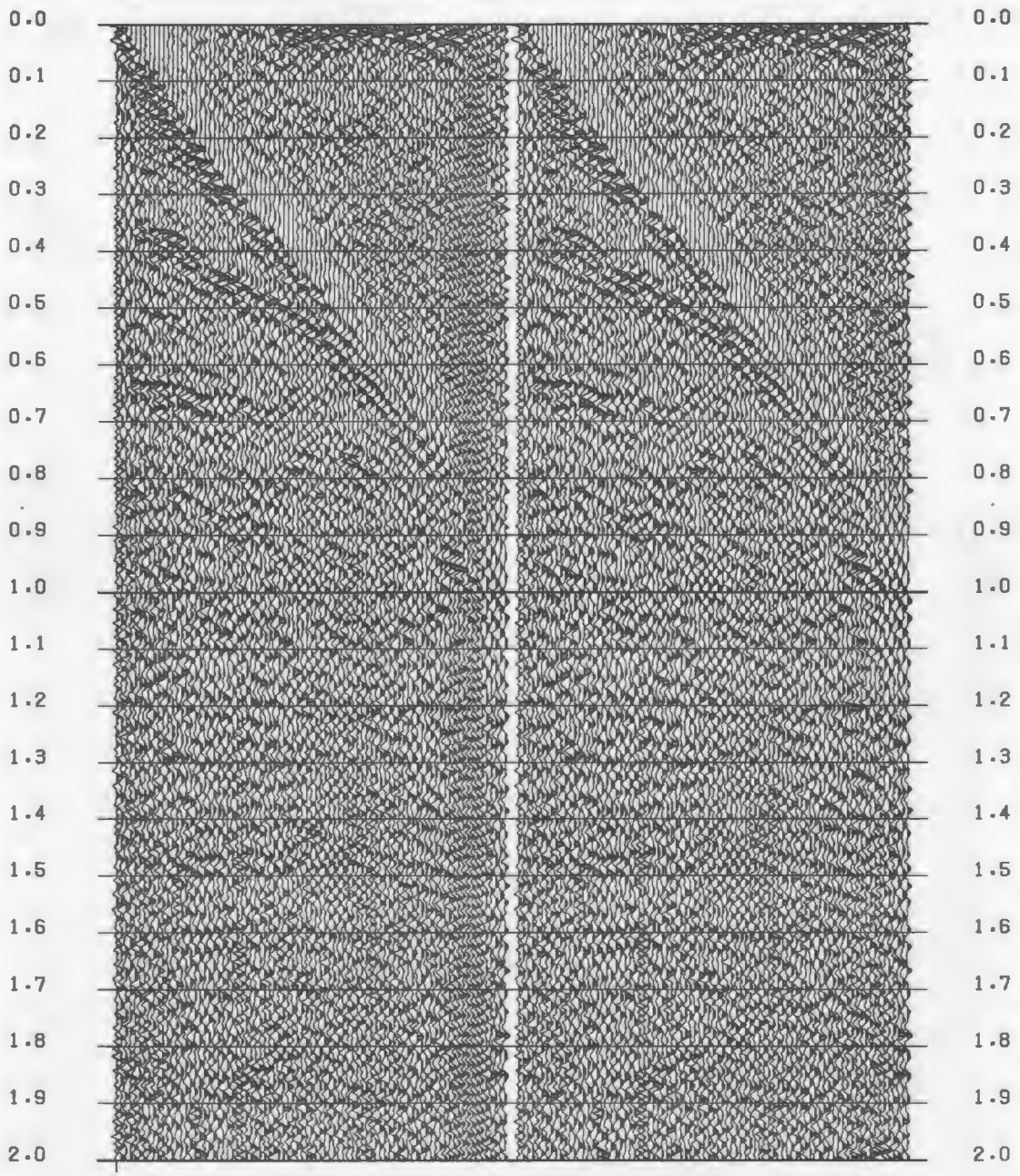

(a) (b)

Figure 3.6. CMP 1000. (a) Before notching 60 Hz. (b) After applying a notch filter to reject 60 Hz, 120 Hz, 180 Hz etc i.e. multiples of 60 Hz noise.

be observed that there is not much difference between the two shot records. This was expected because of the modest values of t_D.

3.3.2.3 CMP gather

After binning and geometry were established, the data which had been either corrected for field statics or corrected for both field statics and dip moveout was sorted into CMP records. All the CMPs were saved on tape ready for further processing. Every 20 th CMP was plotted to check for any kind of noise inherent in the data. Though 60 Hz noise was minimized during data acquisition, this noise was still present in the CMP gathers. To eliminate this noise, a notch filter, which rejected 60 Hz, 120 Hz, 180 Hz, i.e. multiples of 60 Hz, was used (see Figure 3.6). This filter was applied in the time domain.

3.3.2.4 Velocity analysis

3.3.2.4.1 Constant-Velocity Stacks (CVS)

The whole set of data was NMO-corrected at constant velocities and stacked. The velocities ranged from 2500 m/s to 5500 m/s. The choice of these velocities was based on refraction picks (Table A1) and previous processing by Hall et al. (1992). At low velocities (2500 m/s to 3300 m/s) an increment of 100 m/s was used, otherwise at high velocities (3500 m/s to 5500 m/s) the increment was 200 m/s. At lower velocities the normal moveout, defined by the following equation (Robinson,

1983):

$$\Delta t_{NMO} \approx \frac{x^2}{2 t_0 V_{NMO}^2} \qquad (3.3)$$

is large, thus it was felt that small increments of velocity would retain more information, i.e. events would not come into, and fall out of, focus between velocities. At larger velocities the increment was increased, since the likelihood of losing data between velocities is less.

The CVS were done for only the first 2 seconds of the data and all stacks (see Figures 3.7a to 3.7t, in folder) were plotted on paper for visual analysis. This is because most of the reflectors for which velocity estimation is critical are in this section. Figures 3.7a to 3.7t display all the velocities which were analyzed. The velocity picks on figures 3.7a to 3.7t were made after a comparison between these figures and the velocity spectra, and at the same time trying to discriminate against possible multiples. The data in this project image a complex structure, so CVS were particularly useful in choosing the stack with the best possible event continuity (Yilmaz, 1987).

The CVS were used to compare velocity picks from CVNMO and velocity spectra.

3.3.2.4.2 Constant velocity normal moveout (CVNMO)

Every 50 th CMP was NMO-corrected at constant velocities that ranged from 2500

to 5500 m/s at increments of 200 m/s. The results were displayed on paper for velocity picks (see Figure 3.8, in folder). This type of velocity analysis was important in determining velocities at T (TWT)=0. Otherwise, it was difficult to pick velocities from this analysis owing to the complex structure of this seismic line. Nonetheless, CVNMO gave a good velocity check to the velocity spectra and CVS.

3.3.2.4.3 Velocity spectra

Velocity analysis using contours (semblance plots) were performed on every 50 th CMP. The contours plotted were normalised semblance, which implies that the highest possible value is unity. For clarity, only values 0.3-1.0 at intervals of 0.1 were contoured. This ensured that the effects of noise were minimized. Velocity spectra display stacking velocity analyses from CMP gathered records.

Let us say we have traces a_1, a_2,-------,a_N and we want to find semblance at a certain time 'T'. This is found for a set of velocities (V_1, V_2,------,V_m). The move-out time using a hyperbolic normal move-out velocity v_j for a trace with range 'r_i' is (STARPAK Reference Manual, 1989):

$$T_I\ (V_j) = \sqrt{T^2 + \frac{r_i^2}{V_j^2}} \qquad (3.4)$$

The move-out times are rounded to the nearest sample point:

$$w_{ij} = (T_i(V_j) + \frac{SR}{2}) \qquad (3.5)$$

where T_i is the time at velocity v_j and r_i is the range while SR is the sample rate. For a window length 'u' and a single velocity V_j, we have a grid of move-out data;

$a_1(w_{1j})$, $a_1(w_{1j} + SR)$,-----, $a_1(w_{1j} + u)$,

$a_2(w_{2j})$, $a_2(w_{2j} + SR)$,-----, $a_2(w_{2j} + u)$,

$a_N(w_{Nj})$, $a_N(w_{Nj} + SR)$,-----, $a_N(w_{Nj} + u)$. One of the ways of measuring the goodness of the move-out velocity is by finding the semblance, defined as:

$$Semblance = \frac{(\sum x_i)^2}{\sum x_i^2} \qquad (3.6)$$

for a set of numbers. Semblance is unity when all the numbers are equal and as low as zero when the summed value is zero. In the case of multiple time samples in the window, the multichannel semblance is defined to be (Neidell and Taner, 1971):

$$SEM_j = \frac{\sum_{u=0}^{U} (\sum_{i=1}^{N} a_i(W_{ij} + u))^2}{N \times \sum_{u=0}^{U} \sum_{i=1}^{N} a_i(W_{ij} + u)^2} \qquad (3.7)$$

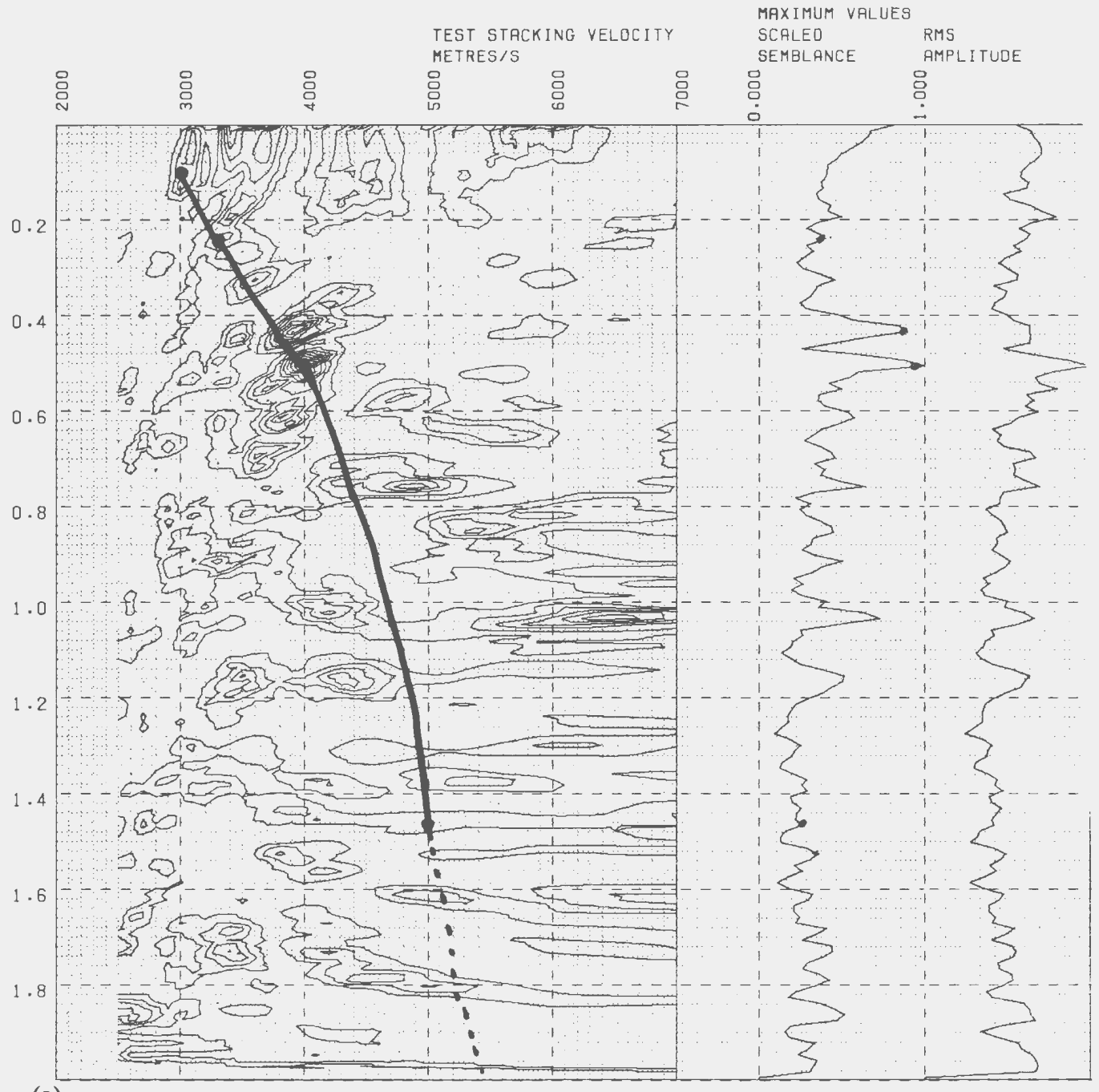

(a)

Figure 3.9. Velocity spectrum of CMP 950. (a) Velocity spectrum before DMO correction. (b) velocity spectrum after DMO correction. Notice the increase in magnitude of both semblance and amplitude after DMO correction. Black dots are possible velocity picks. The question marks indicate probable multiples.

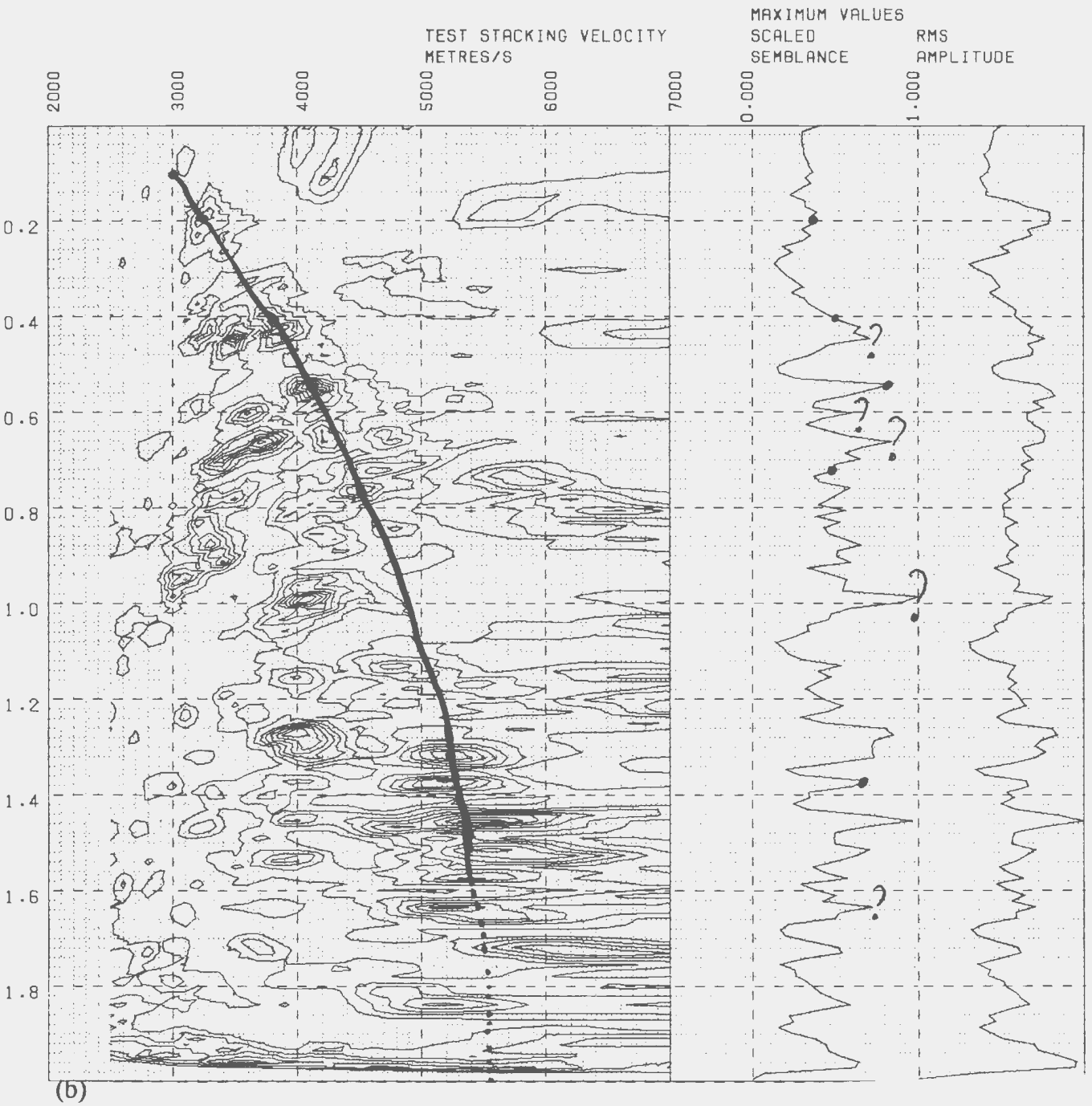

(b)

Figure 3.9 (cont.)

It should be noted that semblance includes cross-terms between traces and also terms of the overall energy of the traces.

To calculate the semblance, interpolation was done between the highest and thelowest velocities, which were 2500 and 5500 m/s, using a velocity increment of 100 m/s.

Let an input trace be divided in fixed time gates t_1.....t_n. Then the amplitude is defined as ;

$$A = \sqrt{ReX(f)^2 + ImX(f)^2}$$

where x(f) is the Fourier transform of the input trace in time series. The RMS amplitude plotted in Figure 3.9 is defined as (Yilmaz, 1987) ;

$$A_{RMS} = \sqrt{A_{t1}^2 + A_{t2}^2 + \ldots\ldots A_{tn}^2}$$

In most instances only a single CMP was analyzed at a time, though in some cases the average semblance of about 10 to 12 CMPs were contoured. This was to check for continuity of real events and to discriminate against false events. Only the first 2 seconds of the data were analyzed because most of the reflectors are in this region. Velocity spectra were measured on CMPs both before and after DMO correction (see Figure 3.9). From a comparison of Figures 3.9a and 3.9b, it can be observed that the

Table 3.1. Velocity defintion before DMO–correction.

CMP	T	V	T	V	T	V	T	V	T	V	T	V
50	100	3050	220	3200	3500	5500						
100	100	3000	260	3300	3500	5500						
150	140	3500	220	3700	3500	5500						
160	0	3300	200	3700	520	4000	3500	5500				
270	0	3300	200	3700	520	4000	3500	5500				
300	0	2700	300	2800	560	4000	3500	5500				
350	0	2700	300	2800	580	4100	3500	5500				
400			200	2800	300	3100	1300	4500	3500	5500		
450			200	3100	360	3300	440	3800	1300	4500	3500	5500
500					400	3450	840	4200	3500	5500		
550	80	2900	240	3300	460	3700	1020	4700	1640	5000	3550	5500
600	0	2700	140	3400	480	3900	1440	5000	3500	5500		
650	0	2900	240	3200	460	4100	1280	4500	1500	5000	3500	5500
700	0	3300	200	3600	520	4400	1500	5000	3500	5500		
750	140	3400	560	4400	1400	5000	3500	5500				
800	120	2900	600	4100	1220	4400	1600	5000	3500	5500		
850	140	3000	260	3400	600	4000	1380	4600	1800	5000	3500	5500
900	200	2900	300	3500	520	3750	600	4100	1800	5000	3500	5500
950	100	3000	220	3400	500	4000	1460	5000	3500	5500		
1000	200	3200	380	3900	640	4300	1460	5000	3500	5500		
1050	200	3200	300	3400	600	4200	1500	4900	3500	5500		
1100	0	3300	220	3600	600	4000	1440	5100	3500	5500		

T is two way time in ms and V is velocity in m/s.

Table 3.2. Velocity definition after DMO–correction.

CMP	T	V	T	V	T	V	T	V	T	V	T	V	T	V
50	120	3000	220	3200									3500	5500
100	40	3000	100	3100	260	3300	380	3700	440	4000	500	4400	3500	5500
150	0	3300	210	3500	440	4200	3500	5500						
200	80	3600	500	4000	3500	5500								
250	0	3300	80	3700	600	4100	1100	4600	3500	5500				
300	210	2600	500	3600	940	4400	3500	5500						
350	0	2800	560	3400	820	3900	940	4300	1740	4800	3500	5500		
400	0	2700	300	3100	660	3300	860	3800	1600	4700	3500	5500		
450	0	2700	380	3400	440	3700	660	4000	1300	4600	3500	5500		
500	0	2800	220	3100	400	3400	600	3800	1080	4700	3500	5500		
550	80	2900	460	3900	840	4600	1080	4700	1640	5000	3500	5500		
600	100	2900	220	3200	460	4000	1180	4600	1440	5000	3500	5500		
650	0	3300	340	3600	460	4100	800	4500	1300	4800	1500	5000	3500	5500
700	0	3300	300	3700	500	4000	960	4600	1080	4800	1540	5000	3500	5500
750	100	3400	600	4400	1000	4800	1560	5000	3500	5500				
800	60	3000	580	4200	1260	4600	1380	5000	3500	5500				
850	160	3000	600	4000	1300	4600	1580	5000	3500	5500				
900	100	2900	520	3700	600	4100	1440	5000	3500	5500				
950	100	3000	200	3200	400	3800	540	4100	760	4500	1380	5200	3500	5500
1000	0	3000	160	3100	380	3700	600	3900	740	4400	1380	5200	3500	5500
1050	0	3000	280	3400	600	4100	1360	5200	3500	5500				
1100	0	3300	320	3500	400	4200	600	4500	1720	5000	3500	5500		
1150	140	2800	300	3500	440	4200	980	4800	1600	5000	3500	5500		
1200	100	2700	400	4000	3500	5500								

T is two way time in ms and V is velocity in m/s.

Table 3.3. Mute specifications.

CMP	W	T	W	T	W	T	W	T	W	T
50	20	100	500	230	861	420	1558	600	1989	700
145	180	100	510	300	2385	760				
165	23	100	529	200	1500	530	2300	700	4336	950
265	19	100	500	300	4424	1060				
305	352	100	509	360	1538	800	3588	1100		
425	252	100	500	350	1700	700	2474	1060		
505	352	100	509	290	2486	900				
525	257	100	500	260	2200	780	2400	860		
565	232	100	540	220	2538	850				
625	280	100	590	290	2000	680	2500	770		
705	233	100	550	270	1770	600	2459	730		
745	654	100	809	350	2000	620				
765	635	100	960	340	2100	630				
785	630	100	950	360	2400	710				
805	342	100	513	260	1540	520	2350	720		
845	280	100	485	220	1540	640	2450	780		
885	336	100	500	240	1500	600	2100	650		
1005	60	100	500	210	1500	550	3400	950		
1085	38	100	500	200	1300	600	2500	860		
1125	75	100	500	190	1200	450	1900	580		
1145	19	100	500	230	1600	500				

T is two way time in ms and w is range in metres.

DMO corrected CMP has more picks than the CMP not DMO corrected. The magnitudes of the velocities did not vary much after DMO, (see Tables 3.1 and 3.2) but the amplitudes and the semblance of the events increased, as can be observed from Figure 3.9. The velocity picks on Figure 3.9 were based on high semblance and increase in velocity with increase in time. This was aimed at discriminating against possible multiples.

The velocity field specification was based primarily on velocity spectra with checks with CVS and CVNMO (cf. Figure 3.9 with Figure 3.10 in folder).

3.3.2.4.4 Velocity field definition

After all the velocity picks, the velocities were plotted as a function of CMPs. This was important in checking for typing errors and final adjustment of the velocities. The final results of velocity picks are displayed in tables 3.1, 3.2, Figures 3.11 and 3.12 (both Figures in folder).

3.3.2.5 Mute

Muting is used to alter portions of a trace to zero (mute). The aim of muting in this project was to remove refractions and wavelets distorted by normal moveout i.e. "stretch". A front mute, which sets amplitudes of all samples between the start of the trace and the given mute value to zero, was used as defined in table 3.3. A front taper of 40 ms was used to prevent sharp data edges (STARPAK Processing manual, 1989).

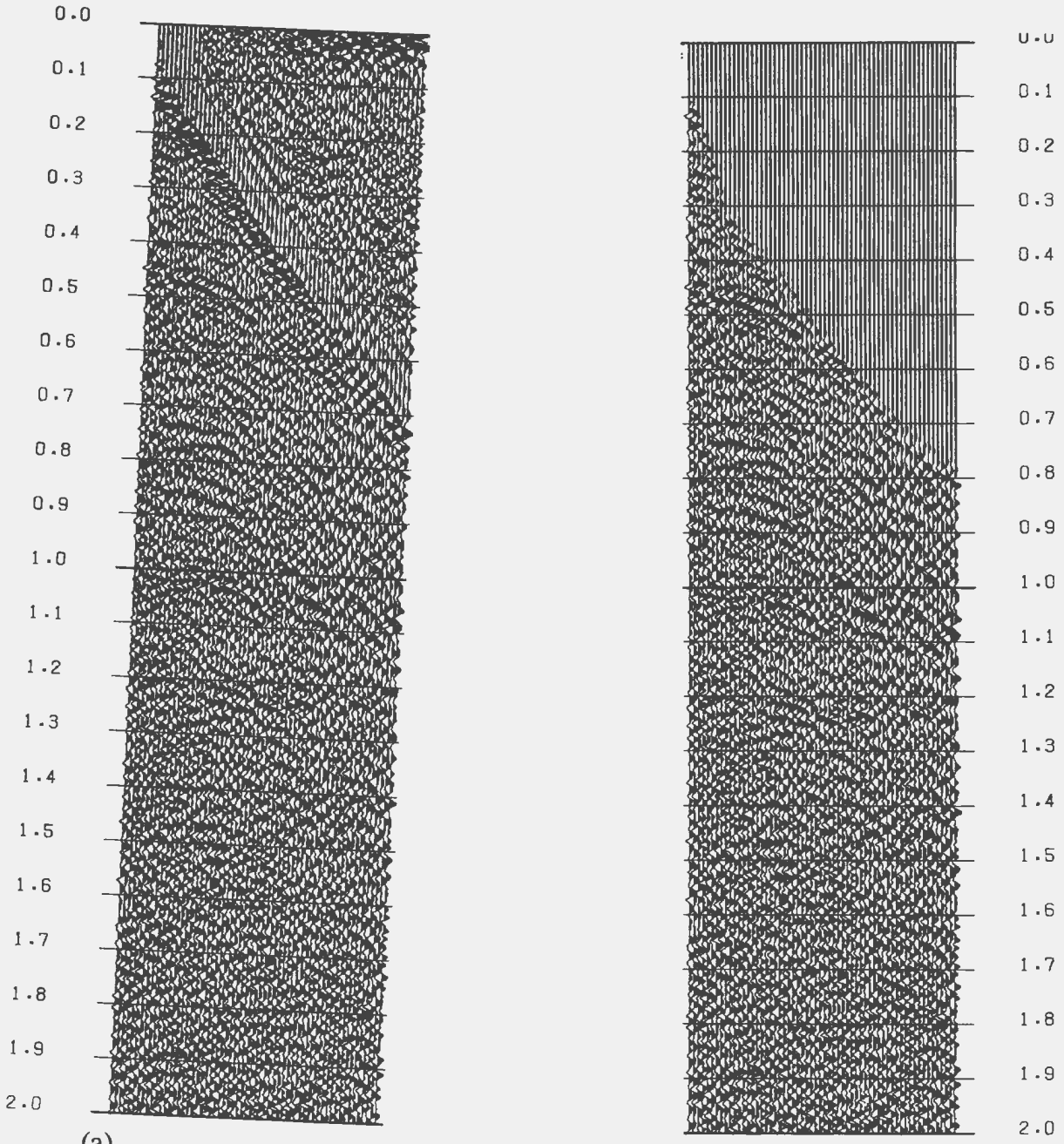

Figure 3.13. CMP 630. (a) Before front muting. (b) After muting. (c) With NMO stretch. (d) With NMO stretch muted.

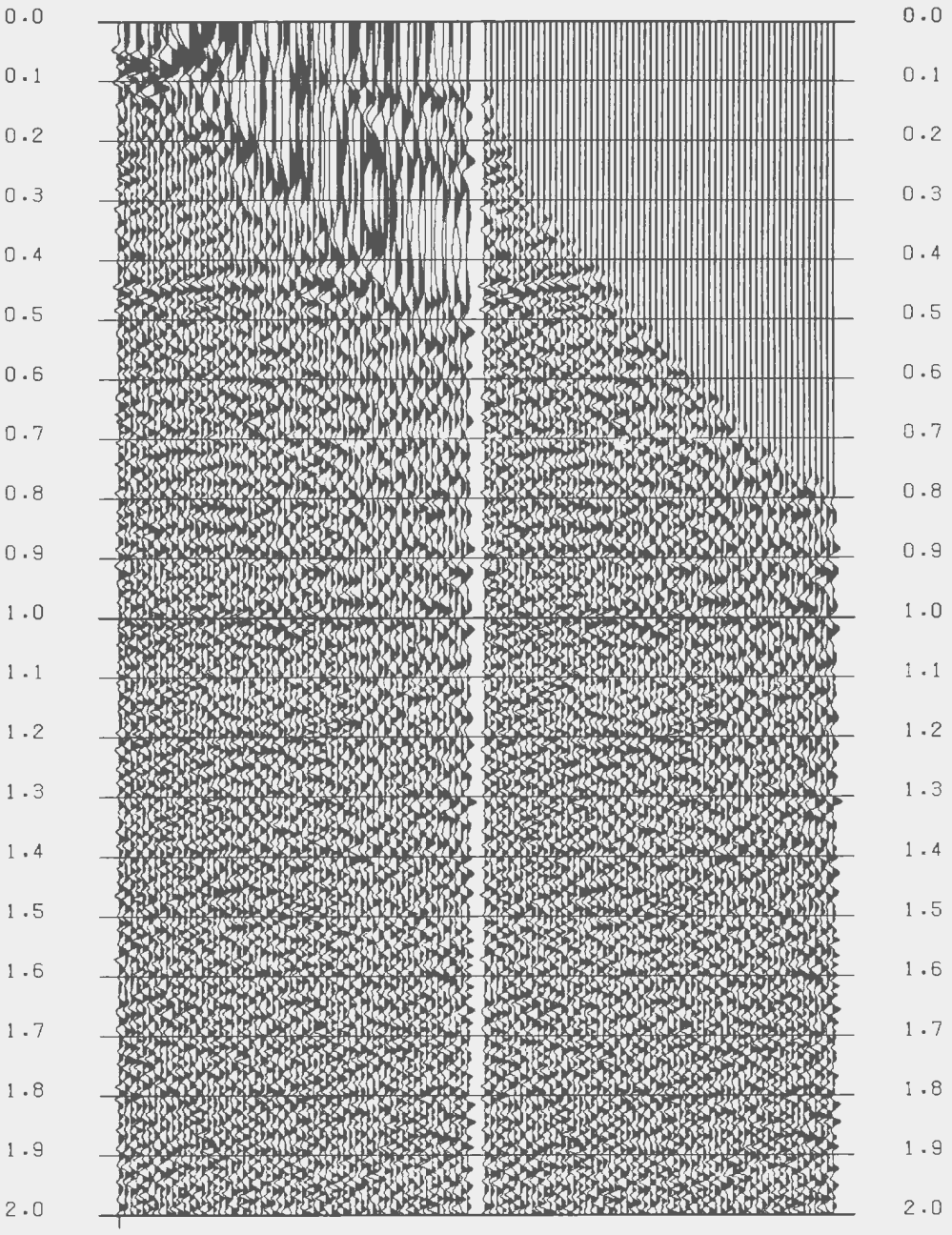

(d)

(c)

Figure 3.13 (Cont.)

The mute values (Table 3.3) were determined by inspecting every 20 th CMP. A transparency was passed along the CMPs, such that every time the alignment of first arrivals on the CMP changed, the mute specifications were changed. Figure 3.13 illustrates the effects of front muting CMP 630 to remove refractions and NMO stretch.

3.3.2.6 Dip Moveout correction (DMO)

The aim of dip moveout-correction (DMO) is to remove the effects of a dipping layer on the moveout velocity in a CMP gather. A dipping reflector increases the moveout velocity, compared to a non-dipping reflector, by a factor of $1/\cos\theta$, where θ is angle of dip relative to horizontal. The assumption made in NMO-correction is that the ground is horizontally layered, which is not always the case. DMO is the process which corrects the effect of dip in the data after normal moveout (NMO) and transforms it to zero-offset data (Biondi and Ronen, 1987).

3.3.2.6.1 DMO Theory

The impulse response in time-space coordinates of the DMO operator derived by Biondi and Ronen (1987) is an ellipse:

$$\left(\frac{t}{t_1}\right)^2 + \left(\frac{x - x_1}{x_1}\right)^2 = 1 \qquad (3.8)$$

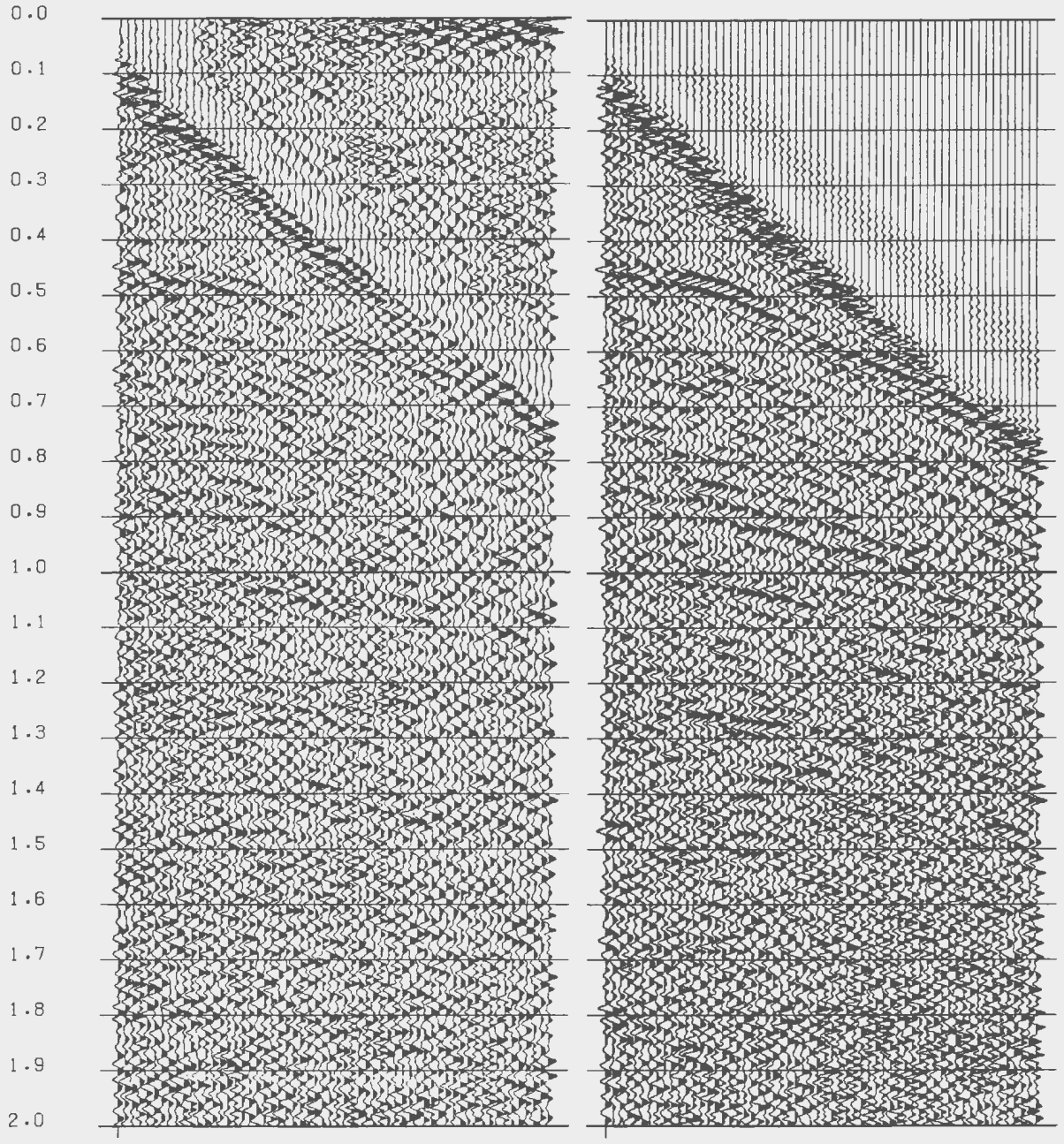

(a) (b)

Figure 3.14. CMP 630. 9 (a) Before DMO correction. (b) After DMO correction. Note the improvement in the focus of events in (b). The muting in (b) was automatic in the process of DMO correction, but was reasonable.

where t_i is the location of the impulse and x represents full offset. The above equation is only part of the operator, no amplitude information is included in it. Amplitude information is ignored at this point due to its uncertainty. The final result after all the analytical computations is:

$$g(m\Delta t, k) = \sum_{n=m}^{\infty} f(n\Delta t, k) \left[e^{jkln\left[1 - \sqrt{1 - \left(\frac{m}{n} + 1\right)^2}\right]} \right.$$

$$- e^{jkln\left[1 - \sqrt{1 - \left(\frac{m}{n}\right)^2}\right]} - e^{jkln\left[1 + \sqrt{1 - \left(\frac{m}{n+1}\right)^2}\right]}$$

$$\left. + e^{jkln\left[1 + \sqrt{1 - \frac{m^2}{n}}\right]} \right] \qquad (3.9)$$

where t = m * dt and s = n * dt. The complete derivation of equation 3.9 is contained in Appendix B. The above expression is the DMO operator used in this project. It is implemented by stretching the space axis of an NMO-corrected shot gather, Fourier transforming the space axis, multiplying and integrating according to equation B.9, inverse transforming the space axis and then finally unstretching the space axis.

3.3.2.6.2 Application of DMO

DMO has to be applied in shot records whose geometry and binning have been established. Since this information is stored in the trace headers, velocity specification

can be defined in terms of CMP numbers. Therefore, velocities defined in section 3.3.2.4 were used to NMO correct the shot records, because DMO is only applied in STARPAK to data which have been NMO corrected. After DMO correction, NMO correction was removed from the shot gathers. The shot records were subsequently sorted to CMP records for further processing. DMO improves the events and removes a lot of noise from the data, as can be observed in Figure 3.14.

3.3.2.7 Automatic Gain Control (AGC)

This is a trace-wise amplitude balancing process and so does not preserve spatial relative amplitudes. The equalization of amplitudes by AGC for structural mapping and conventional plotting defeats attempts to discern amplitude variations associated with changes in gas/water saturation or lithology (Dobrin and Savit, 1988).

A fixed or variable length window slides down the trace one sample at a time. Within this window of the original unbalanced trace, the average of the absolute amplitudes is calculated (STARPAK processing manual, 1989);

$$A = \sum_{i=1}^{N} \frac{|a_i|}{N} \qquad (3.10)$$

The ratio of the desired output average amplitude (AVGAMP) to the average amplitude calculated within the window is the gain scalar applied to the central sample point in the window:

$$S = \frac{AVGAMP}{A} \qquad (3.11)$$

where AVGAMP is the average amplitude normalization level.

AGC was applied mainly before plotting (see Figure 3.1), except before stack, to suppress anomalous amplitudes.

The final plot was gained using a window of 500 ms, otherwise a window of 1000 ms was used always.

3.3.2.8 Stack

The aim of stacking is to sum together all NMO corrected traces in a CMP record and output one stacked trace for each record. It is a very powerful tool for improving the signal-to-noise ratio of the data (Rietsch, 1980). The data were not weighted, only a direct summation being applied to the traces. Before stacking the data, all CMPs were NMO-corrected using the velocities defined in section 3.3.2.4. Subsequently the data were muted to remove refraction arrivals and NMO stretch. The mutes are as specified in table 3.3.

Let a trace be represented as (Rietsch, 1980):

$$a_{ij} = s_j + n_{ij} \qquad (3.12)$$

where a_{ij} is the j th sample of the first trace in the record, s_j is the j th sample of the signal, the same on all traces. n_{ij} is the noise at the j th sample of the i th trace. The stacked trace A_j is simply the sum of the 'L' traces in the record:

$$A_j = \sum_i a_{ij} \quad (3.22)$$

$$= \sum_i (s_j + n_{ij})$$

$$= L \times s_j + \sum_i n_{ij} \quad (3.13)$$

The signal-to-noise ratio on a single trace is the ratio of the signal energy to the noise energy:

$$\left(\frac{S}{n_i}\right)^2 = \frac{\sum_j s_j^2}{\sum_j n_{ij}^2} = \frac{S^2}{n_i^2} \quad (3.14)$$

The signal-to-noise ratio of the stacked trace is:

$$\left(\frac{S}{N}\right)^2 = \frac{\sum_j (L \times S_j)^2}{\sum_j ((\sum n_{ij})^2)}$$

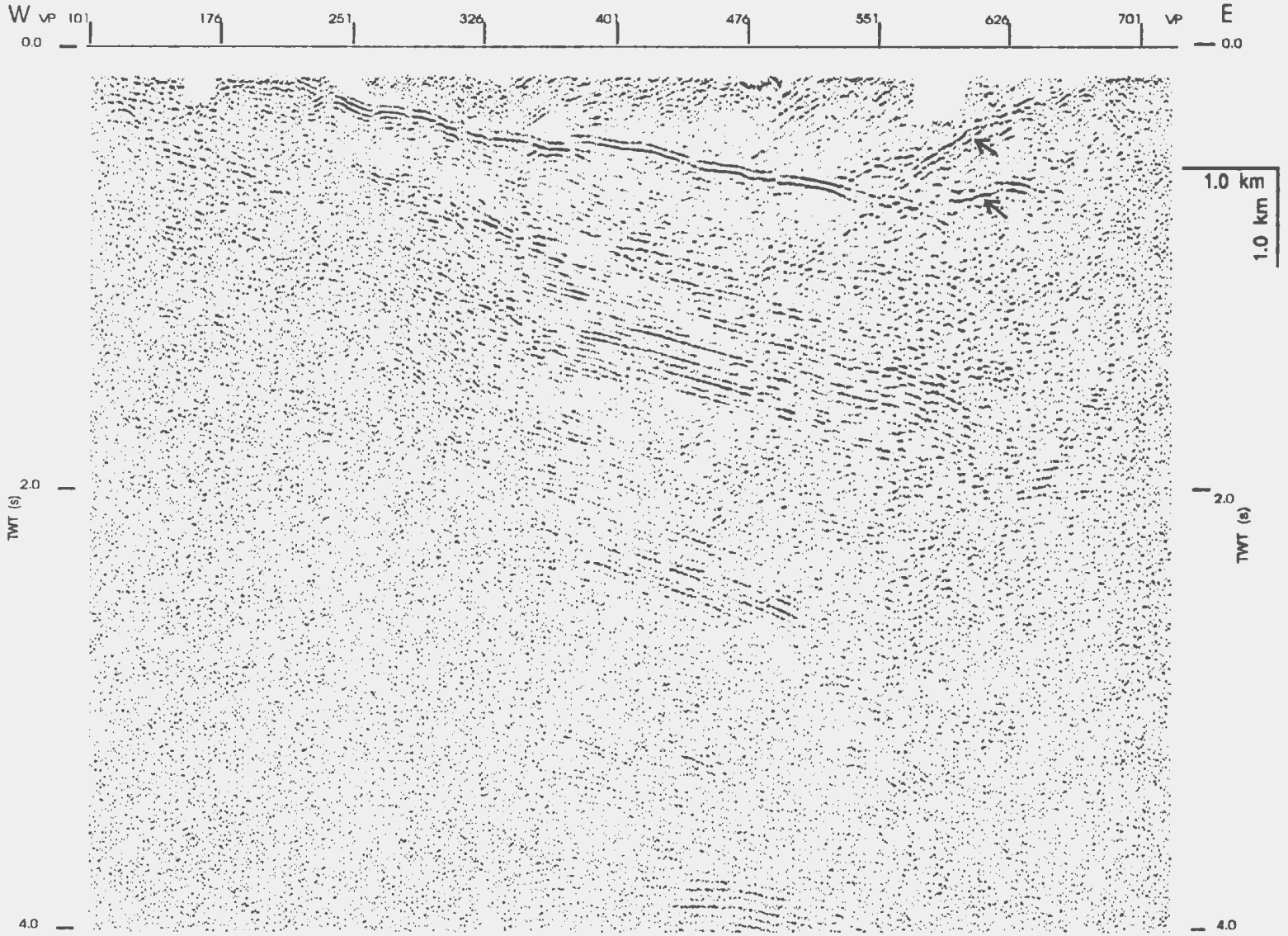

Figure 3.15. Stacked section without DMO and no post stack processing.

This was a direct summation, no weighting was employed.

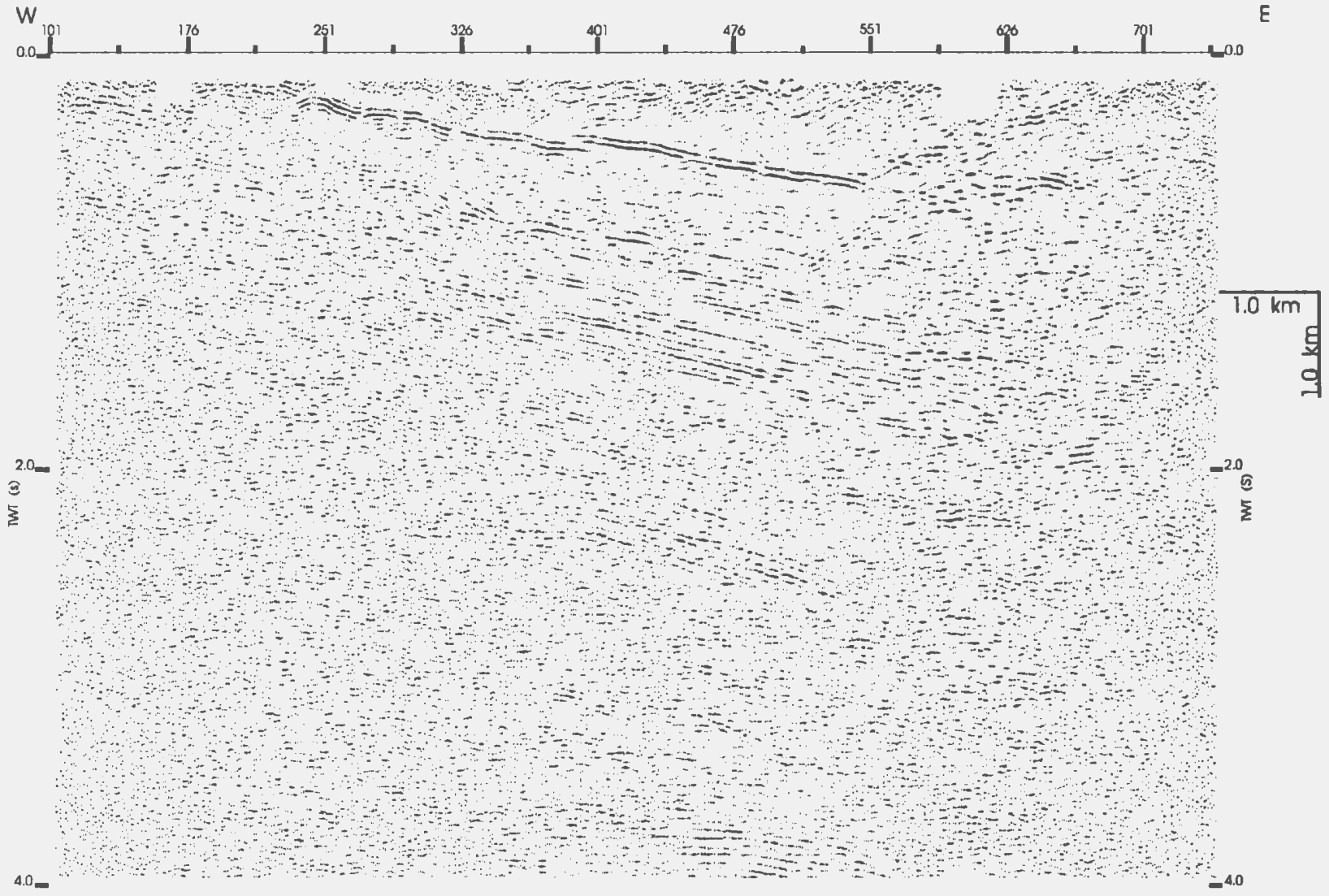

Figure 3.16. Stacked section with DMO and no post stack processing. Note the difference between this figure and Figure 3.15, especially the focusing of events and removal of artifacts (marked by arrows in Figure 3.15) in the vicinty od VP 551 to 626, TWT 0.3 to 0.6 seconds.

$$= \frac{L^2 \times s^2}{\sum_i \sum_k n_i n_k}$$

$$= \frac{L^2 \times s^2}{\sum_i \sum_k (n_i \times n_k)} \qquad (3.15)$$

It can be assumed that the noise is uncorrelated from trace to trace. This is reasonable for very long traces, so that $n_i \times n_k = 0$, for all cases where $i = k$. Furthermore, it can be assumed that the noise energy is about the same on all traces:

$$(\frac{S}{N})^2 = \frac{L^2 \times s^2}{\sum_i (n_i \times n_i)}$$

$$= \frac{L^2 \times s^2}{L \times n_i^2}$$

$$= L \times (\frac{s}{n_i})^2$$

$$\frac{S}{N} = \frac{s}{n_i} \times \sqrt{L}$$

$$\frac{S}{N} = \frac{s}{n_1} \times \sqrt{L} \qquad (3.16)$$

From the above expression, it can be concluded that the stacking process increases the signal-to-noise ratio by a factor equal to the square root of the number of traces in a record. Therefore, the higher the fold of the data, the better the signal-to-noise ratio after stack. This seismic profile has an average fold of 60 traces per record, therefore stacking would theoretically be expected to improve the signal-to-noise ratio by approximately 7.7. Figure 3.15 displays the stacked data with no post stack processing.

After DMO correction, the CMPs were stacked after NMO correction using the velocity defined in table 3.2. This section, as seen in Figure 3.16 (also in folder) has better events than the section of Fig. 3.15, which was not DMO-corrected. For example the artifact at 0.2 to 0.6 s TWT in the vicinity of VP 570 to 611 has been removed by DMO-correction.

3.3.3 Post Stack Processing

Post stack processing consisted of residual static correction, finite-difference migration, time varying bandpass filter, coherency filtering, and final display.

3.3.3.1 Residual static correction

Residual statics corrects for deviations from proper hyperbolic trends. Field statics

corrections remove a significant part of these travel time distortions from the data. Nonetheless, these corrections usually do not account for rapid changes in elevation, the base weathering and weathering velocity (Yilmaz, 1987). From Figure 3.5, it can

Table 3.4. Horizon and window length used to define reference trace.

CMP	TWT	Window length
50	220	200
100	260	"
200	500	600
250	600	"
300	210	300
400	300	400
500	400	600
550	450	"
600	420	"
650	450	"
700	500	"
800	600	"
850	620	"
900	520	"
950	450	"
1000	600	"
1050	600	"
1100	600	"

be seen that the events do not define a good hyperbola even after field static corrections. Therefore, it was necessary to apply residual statics.

Building of a reference trace and determination of midpoint consistent statics is the

first step in residual static correction procedure. This reference trace is picked from the stacked data, where signal-to-noise ratio is high. Therefore, the DMO-corrected stack was used to pick the reference trace. Table 3.4 shows the horizon and the length of the window used, to define the reference trace.

The detailed composite static equation which is used to resolve the midpoint consistent statics into surface consistent statics for a trace is given by (STARPAK reference manual, 1989):

$$T_{ij} = S_i + R_j + C_k + N_k x_{ij}^2 + D_{k,} {}_{ij} \qquad (3.17)$$

where

T = total static applied

S = shot consistent shift

R = receiver consistent shift

C = cdp consistent shift

N = residual NMO coefficient (CMP consistent)

x = trace offset

D = cross dip coefficient (CMP consistent)

y = cross dip distance

and subscripts

i = shot index

j = receiver index

k = cdp index

The residual NMO term in eq. 3.17 arises in case of incorrect (but not too incorrect) moveout velocity has been applied to a hyperbolic event. The term N is constant for the gather k. The crossdip term in eq. 3.17 may be important if the dip of the subsurface geology is not in the direction of the processing line (Larner et. al., 1979). The angle between the dominant dip direction and the processing line direction leads to a time delay which is proportional to the crossdip distance. This distance is the distance of the trace midpoint perpendicular to the line of dominant dip direction which passes through the trace centroid. If g is defined as the subsurface dip, the time error is found to be:

$$dt = \frac{2 \sin g}{v} y = D y \qquad (3.18)$$

where D is constant for CMP k.

Equation 3.17 can be expressed in matrix form as:

$$A x = b \qquad (3.19)$$

where A is a matrix whose ij th component gives the contribution of j-th component

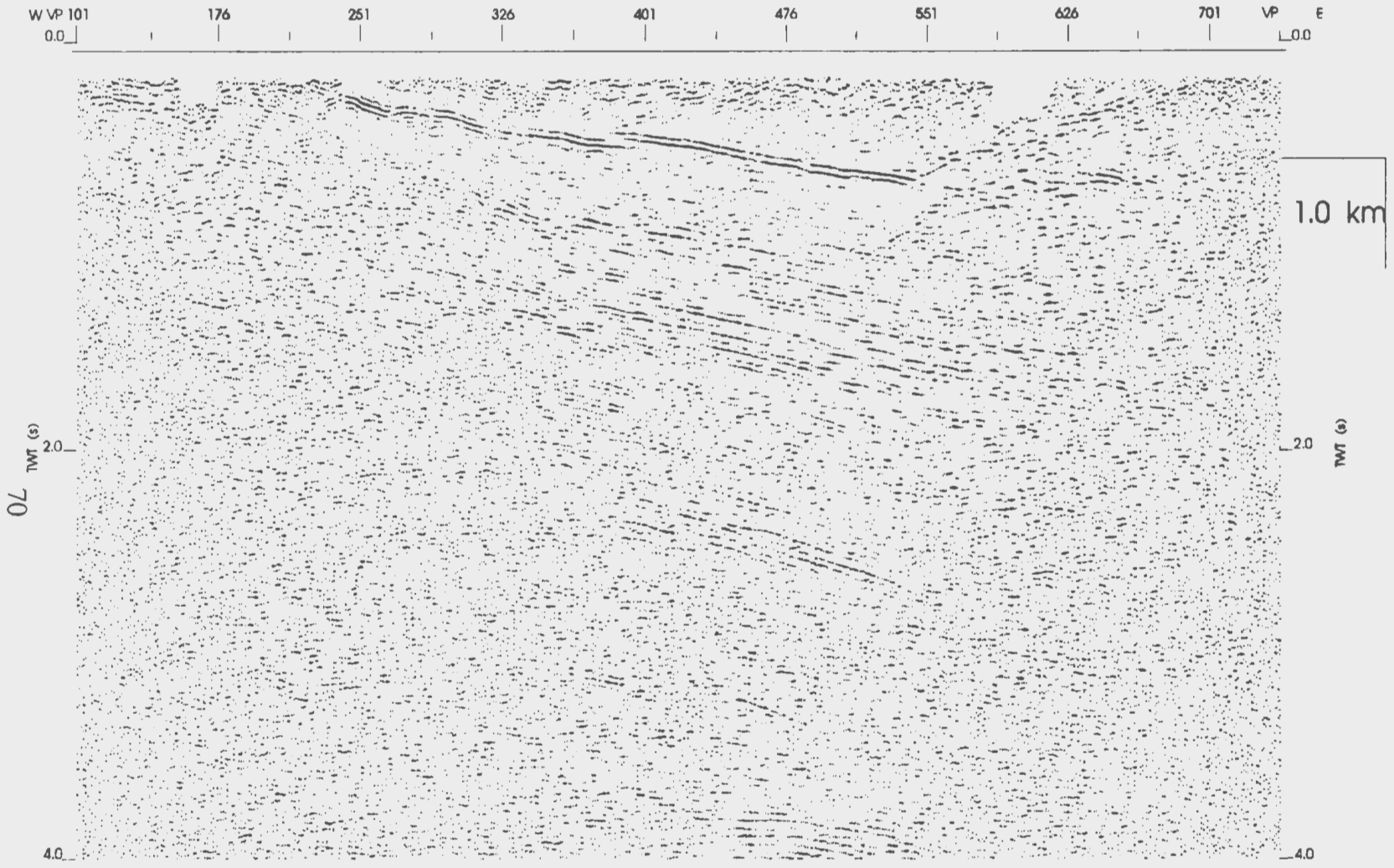

Figure 3.17. Stack section after residual statics corrections. Note that there is not much difference between this section and the section in Figure 3.16 i.e. before statics correction.

of x to the i-th equation, and is based on the geometry of experiment; x is the vector of the consistent shifts to be determined; and b is the vector measured shifts (T_{ij}).If n_e is the number of equations and n_x is the number of unknown components, then the matrix A has the size n_e by n_x, the solution vector x is n_x by 1 and the measured vector b is n_e by 1.

The matrix A has very few non-zero components, i.e. it is sparse. The above equations are either underdetermined or over determined, therefore, they are solved by iterations, specifically the Gauss-Seidel method. In this approach the values of x recently found are used instead of values from previous iteration. For details of this method, the reader should refer to Wiggins et al. (1976). There are several additional steps which are used to make the Gauss-Seidel solution robust;

(a) The residual NMO and cross-dip terms are not allowed to exceed a user specified threshold value.

(b) The equations are weighted with a power of the normalised cross correlation.

(c) Picks which are too large are down weighted.

(d) Equations which produce large errors in the averaging technique are eliminated.

Before applying the statics calculated, the surface consistent statics were plotted. This was a checking procedure to get a feel of how the statics varied from one CMP to the other. From this plot, the maximum and minimum values of statics as a function of CMP values was +12 and -12 ms respectively. These values are significantly small and not much change is expected to the data after applying them.

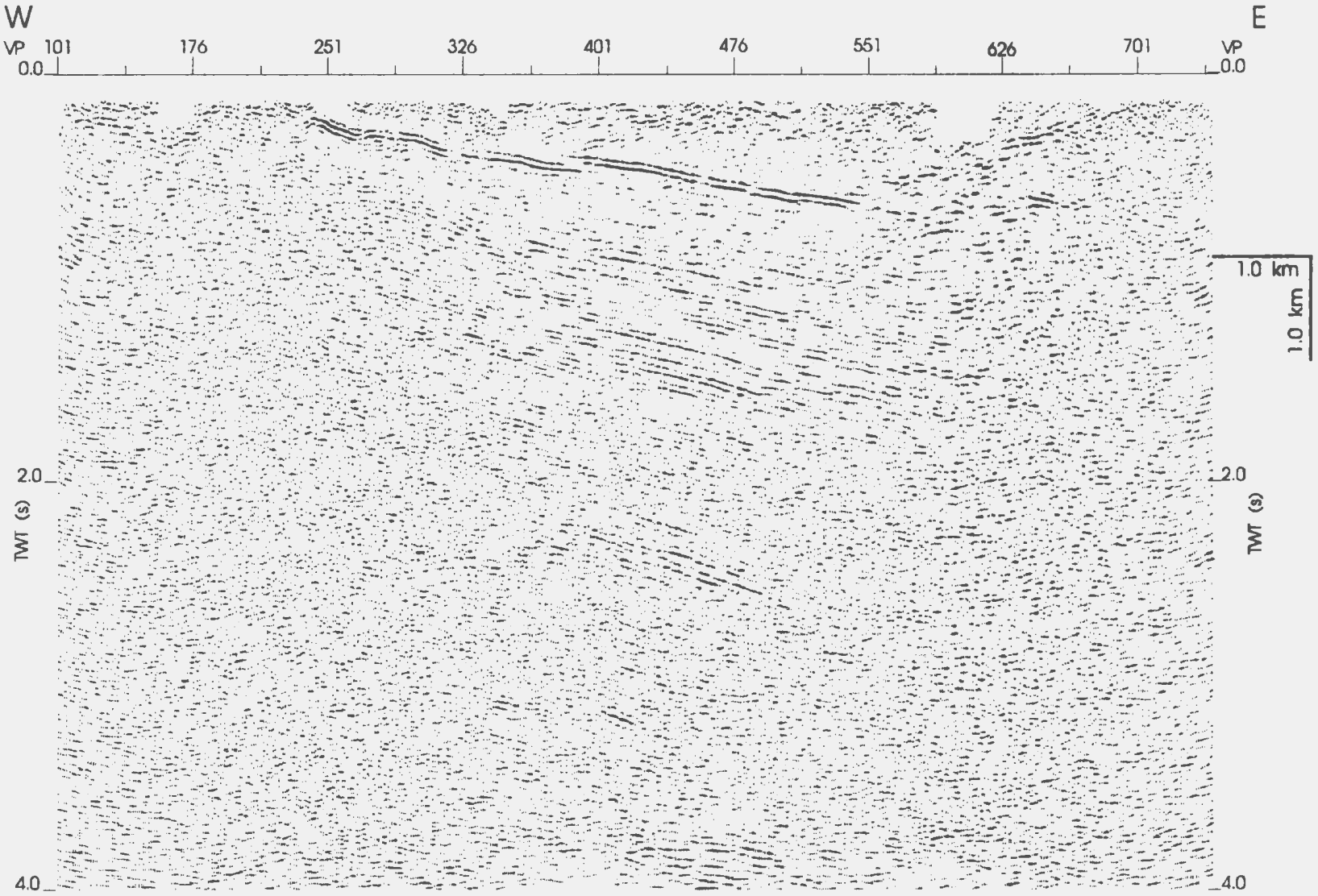

Figure 3.18 Migrated section. Notice the edge effects in this section as compared compared to Figure 3.17. To see clearly the results of migration look in Figure 3.22 in folder.

The surface consistent statics were finally applied to the CMPs which had been DMO corrected. The surface consistent static is the sum of receiver and shot static. This application finds the surface consistent static shift and applies it to the input trace.

After residual statics correction, the NMO corrected CMPs were stacked. From this stacked section (Figure 3.17) there is not much change as compared to figure 3.16, the section with no residual statics applied.

3.3.3.2 Finite-difference migration

The aim of migration is to move dipping reflectors to their true subsurface positions and collapse diffractions, thereby delineating detailed subsurface features such as fault planes (Yilmaz, 1987). A 45-degree finite-difference migration was applied to the stacked section after residual statics corrections. To minimize edge effects the data were padded at the edges with 100 dead traces. The traces were also weighted at the edges to reduce their amplitudes because the traces at the edges had such high amplitudes that they were causing a lot of edge effects. Only 40 traces on either side of data were weighted as follows: CMP 23 which was the first trace in the data was given a weight of 0.00001 whereas CMP 62, the 40 th, was given a weight of 1.0. In between the weighting factors were interpolated using the CMPs. Similarly the last 40 traces (CMPs) were weighted in the reverse order so as to give the last CMP (1220) a weight of 0.00001 and CMP 1181 a weight of 1.0. After migration,

the CMPs were weighted back to normal.

The mathematics for finite-difference migration are very complex, therefore, in this project only the final equation will be quoted. The basis for the 15-degree finite-difference migration is (Yilamz, 1987):

$$\frac{\partial^2 Q}{\partial \tau \partial t} = \frac{v^2 \partial^2 Q}{8 \partial y^2} \qquad (3.20)$$

where Q is the retarded wave field, t is the input time, τ is the output time, and y is the midpoint coordinate. The above equation is derived from the dispersion relation, assuming that velocity varies vertically. Nonetheless, in practice, the velocity function in the equation can be varied laterally, provided it is smooth.

For 45-degree finite-difference, the above equation is modified to (Yilmaz, 1987):

$$\frac{i\beta_1}{\alpha_1 m}\frac{\partial^2 Q}{\partial z \partial y} - \frac{\partial^2 Q}{\partial y^2} + i\frac{m}{\alpha_1}\frac{\partial Q}{\partial z} = 0 \qquad (3.21)$$

where m is equal to $2\omega/v$, β_1 and α_1 are coefficients such that for the 15-degree algorithm $\alpha_1 = 0.5$ and $\beta_1 = 0$ whereas for the 45-degree $\alpha_1 = 0.5$ and $\beta_1 = 0.25$.

After residual statics application, the section was migrated using the velocities of Table 3.2. Figure 3.18 displays the results of migration. From this figure it can be observed that diffractions are collapsed and fault planes are revealed (cf. Figure 3.16 with Figure 3.22, both figures also in folder).

3.3.3.3 Filtering

The data were filtered after migration using a bandpass filter and a coherency filter.

3.3.3.3.1 Bandpass filter

A bandpass filter, which varies with time, based on test panels (see Figure 3.19), was applied to the data after migration. In the region 0 to 2000 msec, a bandpass of 20 to 90 Hz was applied, while in the section 2500 to 4000 ms a bandpass of 20 to 60 Hz was used. The merge zone was 500 ms. Data between the two windows were merged from the end of the top window (2000 ms) to the beginning of the next lower window (2500 ms). All data were filtered. Filtering was done in time domain as shown below (STARPAK processing manual, 1989):

$$F(t) = \sum_{u} T(t - u) * O(u) \qquad (3.22)$$

where T is the input trace, o is the filter operator, F is the filtered trace and * indicates convolution.

3.3.3.3.2 Coherency filtering

The aim of coherency filtering is to enhance reflectors for interpretation purposes. The filter that was used for this kind of processing is one that attenuates incoherent energy within a specified slope. For each input trace and time sample, the processor

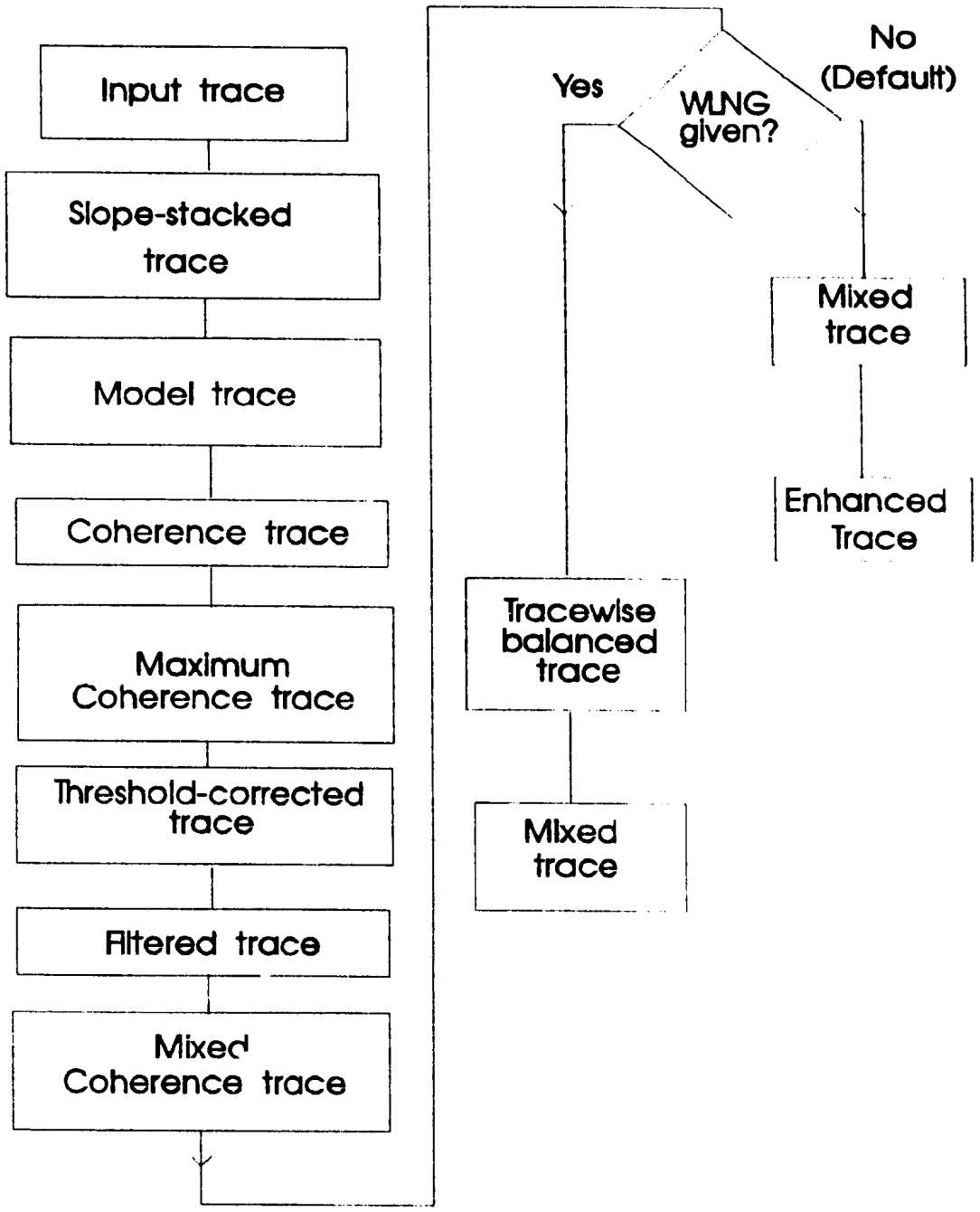

Figure 3.20. Calculation steps in the coherency filter (STARPAK reference manual, 1989).

checks the neighbouring traces for waveform alignment along several different time slopes (STARPAK Processing Manual, 1989). The degree of alignment is a measure of coherency. After finding coherences, data with low coherency are attenuated. Therefore, seismic events aligning with at least one of the slopes, generate large coherences and are preserved. The slope (FAN) used for the data was -6 to +6 ms/trace. The value of the slope determines the number of slopes to be generated for finding alignment. For example for a slope (FAN) of -6 to +6 ms/trace, 7 traces were generated at -6, -4, -2, 0, 2, 4, 6 ms/trace for sample rate of 2 ms. These generated slopes are used to find alignment for the input trace. A slope-stacked trace is formed by stacking the number of traces (i.e. 9 , the number used in filtering this profile) along each slope thus generated. To the input trace a certain percentage of the slope-stacked trace is added to generate a model trace (see Figure 3.20). A coherence trace is formed by determining degree of alignment between the slope-stacked trace and the model trace at each slope within the user defined slope (FAN), using a user defined window. The maximum coherence trace is determined by finding the maximum coherence at each sample of the set of coherence traces. A threshold-coherence trace is formed by attenuating the model trace using (coherence ^{POWER}) times (amplitude) for values of coherence below a certain value say THRESH (the values of POWER and THRESH for this project were 1 and 65 % respectively). A filtered trace is achieved by taking the amplitude of the threshold-coherence trace corresponding to the maximum coherence trace. For every input trace a corresponding

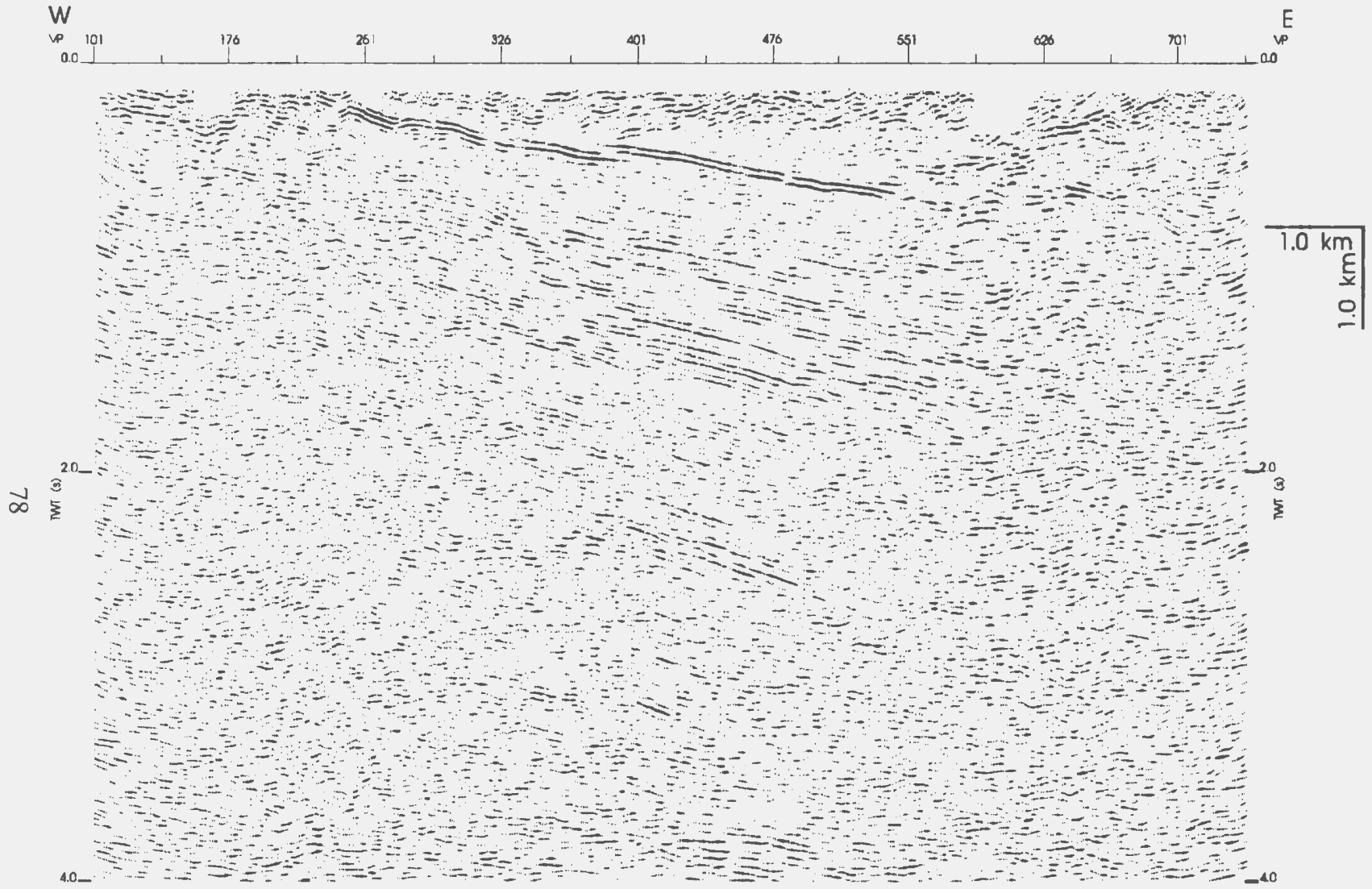

Figure 3.21. Migrated section after applying both bandpass and coherency filters. In this section the events are more focused than in Figure 3.18. The edge effects have been reduced.

output filtered trace is made. A mixed coherence trace is formed by adding (filtered trace) times (max. coh.^{COHMIX}) to (input trace) times (1 - max.coh.^{COHMIX}). The value of COHMIX is user defined, and for filtering these data its value was set to 0. If window (WLNG) is not given a certain percentage (PERCMIX) (100 % was used to filter these data) of the input trace is added to the filtered trace to get a mixed trace. A suite normalization is applied to the amplitudes of all mixed traces, such that the average absolute amplitudes of the output is equal to that of input. Otherwise, if window (WLNG) is given, the amplitudes of the filtered trace is balanced using the window WLNG to get tracewise balanced trace. To get the mixed trace, percentage (PERCMIX) of the tracewise balanced trace is added to (100 - PERCMIX) % of the input trace. In filtering these data, WLNG was not used, therefore, an enhanced trace was achieved by the former method. The choice of the parameters was based on the recomended values in STAPARK manual (1989).

Figure 3.21 displays the results of bandpass and coherency filtering. The events are better focused in Figure 3.21 than in Figure 3.18.

3.3.3.4 Final display

The final section (in folder, Figure 3.22) was plotted using a horizontal and a vertical scale of 14 traces/cm and 8 cm/s respectively. Two traces were summed to produce one trace. This is a 1:1 section if an average velocity of 4 km/s is assumed for the whole section.

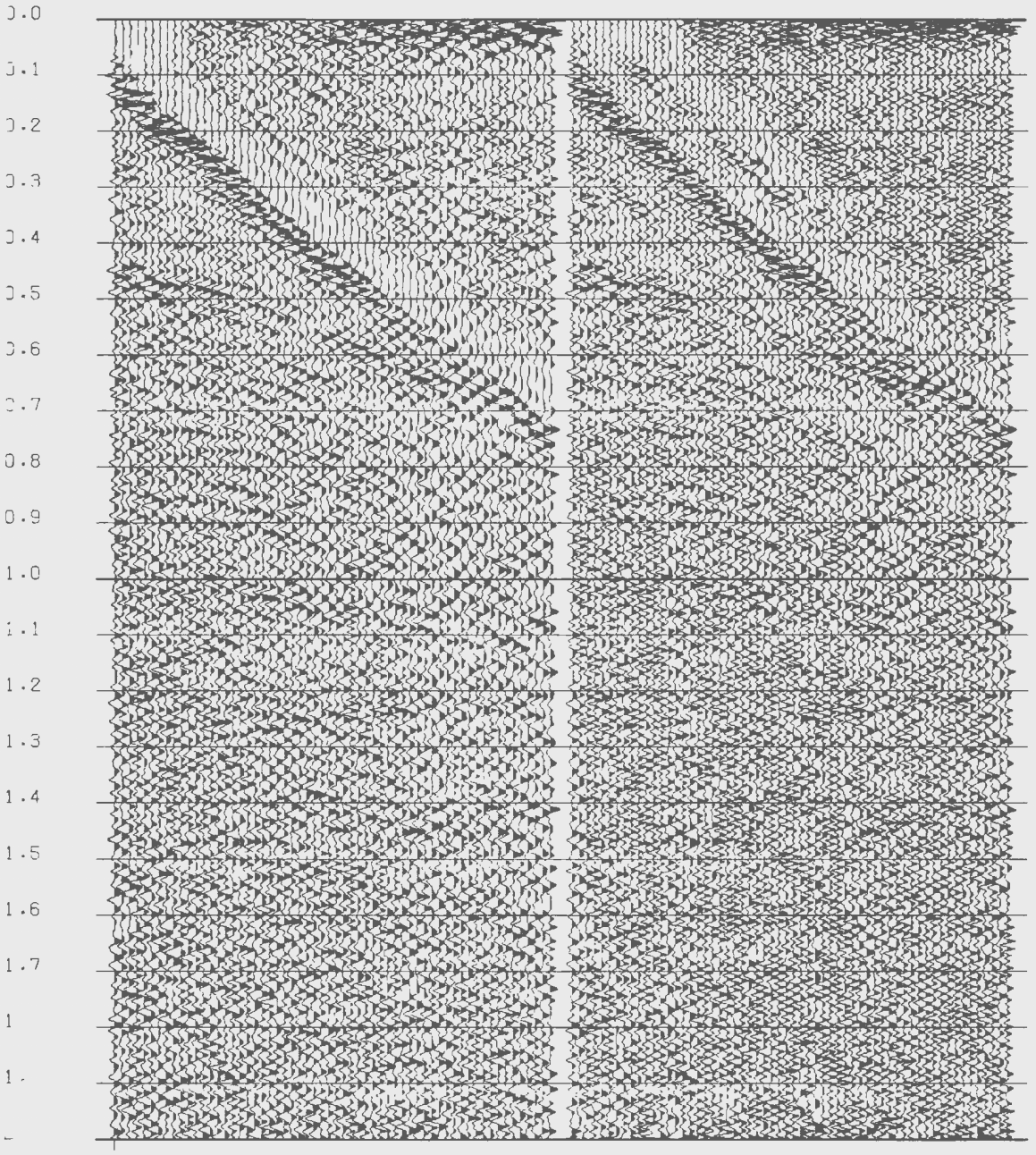

(a) (b)

Figure 3.23. Deconvolution of CMP 630. (a) Before spiking deconvolution. (b) After spiking deconvolution. The lag and operator length were 2 ms and 250 ms respectively. Notice the noise in (b).

3.3.4. Other processing

An attempt was made to apply spiking deconvolution to the data (see Figure 3.23). From this figure, it can be oberved that deconvolution introduces a lot of ringing noise to the data. Therefore, deconvolution was not applied to the data.

The data was quite clean, thus there was no need for such proce.sing as F-K filtering, inner trace muting etc.

Chapter 4: Interpretation

4.1. Introduction

There are no deep boreholes in this part of the subbasin, therefore, the geologic interpretation will be based on seismic character and surface geology as mapped by Knight (1982). The nearest borehole (BSG1, see Figures 2.2 and 4.3) is located about 500 m north of the centre of the seismic line; it was drilled to a depth of 300 m and encountered only Barachois Group (Solomon, 1986).

Data quality varies throughout the profile. Though reprocessing has improved all the data significantly, (compare Figure 3.22 with Figure 4.1, both figures in folder) the best data occurs towards the centre of the line where several reflection packages occur.

Most of the reflection packages are as identified by Hall et al. (1992), except that they are more focused and distinct in the current profile. Unconformity "U" and package "G" were not identified by Hall et al. (1992). The two non-reflective section below (part of "D") and above reflector "R" (part of "B") were not previously identified (Figure 4.1).

4.2. Description of the seismic line

4.2.1 Reflections

Reflector "R"

As illustrated on Figure 4.2 (in folder) and interpreted on Figures 4.3 - 4.6, the seismic character of the section changes across a strong reflector at 0.2 to 0.6 s

Legend of Figure 4.3.

a	Anguille
c	Codroy
b	Barachois
BSG1	Memorial University drill hole

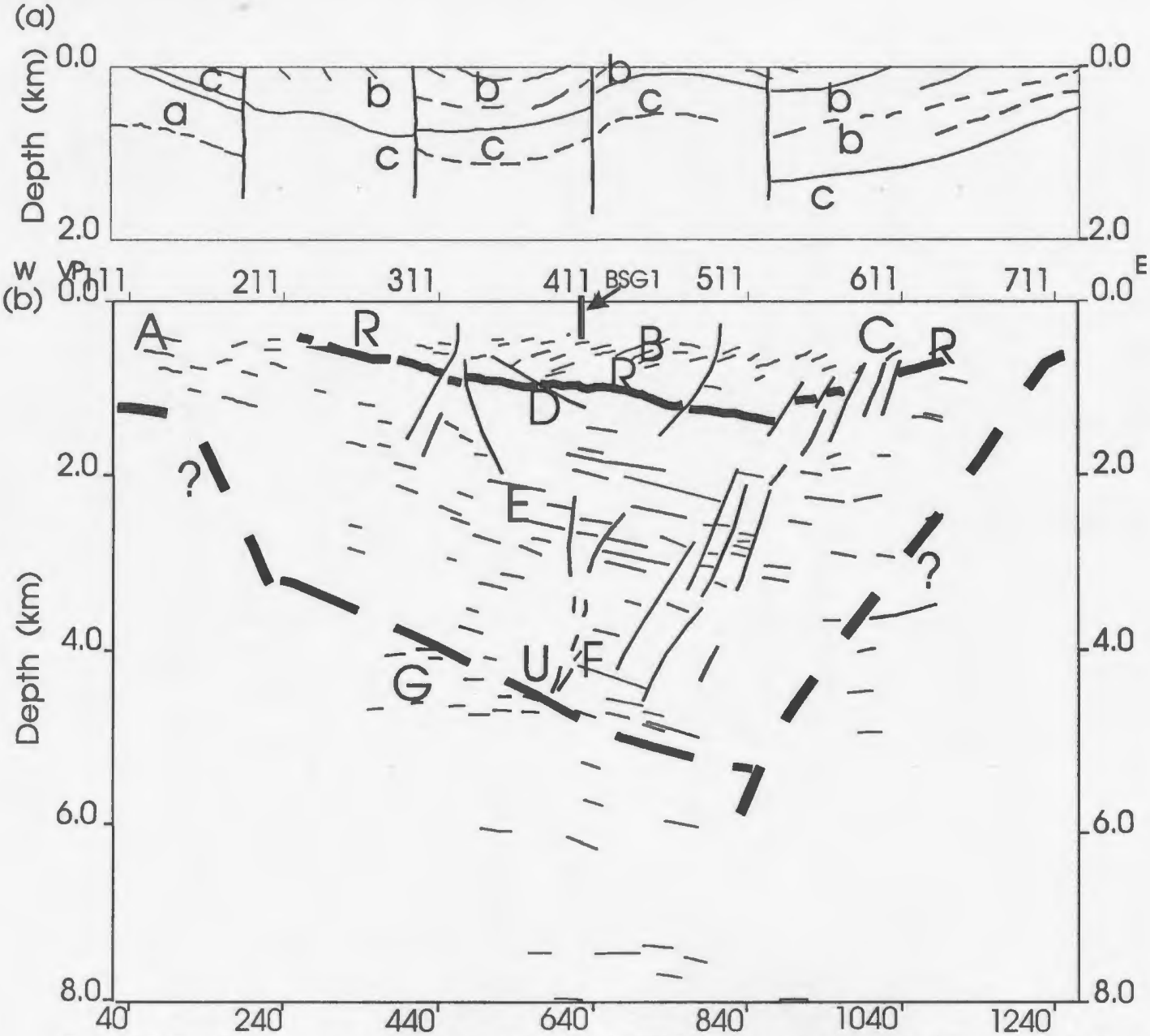

Figure 4.3. The St. George coalfield basin. (a) Knight's (1983) cross section projected onto the seismic profile. (b) Line drawing of the seismic profile taken from the reflectors picked on figure 4.2.

TWT. On the east, this reflector marked "R" can only be traced as small fragments which are separated from each other by faults. Reflector "R" divides the section into two groups of strata, i.e. westward-dipping reflectors (package "B" and "C") above the "R" and eastward pre-dominantly dipping packages "D" to "F" below (Hall et al.,1992).

Package "A"

This package consists of high amplitude discontinuous events at the west end of the seismic line. The dominant frequency of this package is about 30 Hz. The depth extent is about 0.6 s at dips of about 15°. There is a dip reversal at about VP 170, probably indicating the presence of a fault.

The high amplitude events give way downwards to a low amplitude zone with horizontal discontinuous events, similar to those observed in the deeper parts of the sections.

Package "B"

"B" is a relatively high amplitude package with most of the events dipping west at an angle of 20°, though some events are gently east dipping at angles $\leq$ 10°. A few folds which correlate well with the surface geology can be recognised.

This package loses its coherent reflectors above "R" to the west near VP 250 where it appears to be offset by a steep fault. Eastward at TWT larger than 0.3-0.45

seconds the package gives way to a much less reflective package overlying reflector "R" from VP 411 to 570.

Package "C" is probably part of "B".

Package "D"

Beneath reflector "R", this package is about 0.8 km to 1 km thick, if an average velocity of 4 km/s is assumed for the seismic section. It is present from VP 230 to 550 and appears to be fault-bounded at its eastern and western limits. This package which is both low reflective and of low amplitude, dips towards the east. It is cut by minor and major faults and it appears irregularly bedded.

Package "E"

Package "E" is present from VP 160 to 630 and is about 1.4 km thick. This package exhibits strong parallel reflectors that dip to the east but become nearly horizontal towards at their eastern extent. Dip reversals occur at about VP 590.

The package is faulted in a very complex manner towards the east end of the seismic profile (VP 550 to 671).

Package "F"

This package consists of brief series of strong but discontinuous reflectors at a depth of approximately 5 km. The section between "E" and "F" is weakly reflective,

though the events, where focused, dip towards the east. Below "F" there are discontinuous straight reflectors which are bounded at their top by unconformity "U".

Package "G"

This package comprises discontinuous straight reflectors and is separated from "F" by unconformity "U". It has generally low reflectivity except below "F", where events are clear. Package "G" appears to be interrupted occasionally by a few eastward dipping events. These may result from shear zones in the crystalline basement. Alternatively this would also imply that package "G" could represent two rocks of different ages, i.e. Lower Palaeozoic and Precambrian.

Unconformity "U"

Unconformity "U" separates "F" from "G". The seismic character and the eastward dips of "F" compared to those of "G" makes it possible to identify this event. It is clear in the centre of the section between 1.8 to 2.5 s TWT, but is not visible in the eastern and western faulted parts of the section.

4.2.2. Faults

The whole seismic section is cut by several steep normal faults. Many of these are minor without any pattern, though a few of them that are marked in Figure 4.2 adhere to an extensional pattern with minor compressional features present.

At the east end in the vicinity of VP 540 to 611, a complex fault system is interpreted. Again, no clear pattern of extension or compression can be established, and it is likely that a cross-section through a shear zone is being imaged. This is consistent with the regional geology, as the Cabot (Long Range Fault), a regional strike-slip feature, occurs only 5 km to the east of the seismic profile. Near the top of the section, reflector "R" is displaced by movements on faults in this shear zone (see figure 4.2).

At VP 380, 2-way time 0.4 s, reflector "R" appears to have been cut by a low angle reverse fault. To check the validity of this feature, the Fresnel width of this part of the seismic line was analyzed. The Fresnel width (w) is given by (Kleyn, 1984)

$$w = (2\ z\ \lambda)^{\frac{1}{2}} \qquad (4.1)$$

where z is depth and λ is the wavelength. If the dominant period is taken to be 20 ms, and velocity to be 3300 m/s, then w is $\approx$ 300 m. This means that the horizontal resolution at such a depth (0.4 s) is about 300 m. Therefore, the fault which is about 200 m wide may not be resolved exactly, therefore, the thrust fault may not be a true event based on this argument of Fresnel width. Nevertheless, this event could be real because after migration, which enhances lateral resolution, this fault is still evident.

The two faults, marked with question marks, on either side of the seismic section tend to limit either eastward or westward extension of packages "D" to "F". The fault

from 0.5 to 6 m (Figure 4.3) maybe a growth fault controlling sedimentation in a half-graben. This is a very common situation in the Horton subbasins in the Magdalene Basin (Durling and Mariller, 1993). It possible that packages "D" to "F" extend further than mapped here, but deformation along these growth faults prevents the detection of these packages.

4.3. Interpretation of the seismic line

4.3.1 Introduction

There are number of possible geological interpretations of reflector "R", packages "A" to "G" and unconformity "U". The interpretation made here will utilize all the geological and geophysical information available, especially surface geology, local drill hole data, nearby published and unpublished seismic lines, regional seismic character in the Maritimes Basin and the Bay St. George Subbasin, and regional geological setting.

4.3.2 Reflector "R"

There are four possible geological interpretations for reflector "R", as interpreted by Hall et al. (1992):

1) Anguille/Codroy contact;

2) Codroy/Pre-Carboniferous basement contact;

3) a décollement within the basin;

4) marine Codroy/non-marine Codroy-Barachois contact.

It should be noted however, that the third interpretation is not mutually exclusive of any of the other three.

The first interpretation of "R" as Anguille/Codroy is alluring. From the character of "R", it looks similar to a regional reflector that has been identified in offshore and onshore seismic in the Maritimes Basin as the Horton/Windsor contact (Nickerson, pers.comm.), which is chrono-and litho-stratigraphically equivalent to the Anguille/Codroy Group contact (Hall et al., 1992). A second, similar observation arises from these observations. Seismic profiles described and illustrated in St. George's Bay (see Figures 2.8 and 2.9) by Kilfoil (1988), Miller et al. (1990) and Langdon (1991) show a very similar reflector that is interpreted as near base Codroy upon Pre-Carboniferous rocks. This reflector defines a deep half graben beneath the bay.

In either of the above two situations, the strong reflection character near the base of the Codroy is probably related to the presence of evaporites in the Codroy Road Formation (see figure 2.3). In either case, regarding the seismic profile at hand, if "R" is interpreted to represent the near-base-Codroy, then the unconformity "U" would represent the contact between Pre-Codroy rocks (Anguille and/or Lower Palaeozoic) and the Precambrian.

The third interpretation calls for a décollement within the Carboniferous succession. This is favoured by the angular discordance reflectors in overlying

packages "B" on "R" and the contrast in deformation between strata above and below "R" as has been noted by Hall et al. (1992). Knight (1983) indicated that such a décollement could explain anomalous structural relationships that occur around the northern end of the Anguille Anticline, especially the marked contrast between the degree of deformation within the evaporitic and fine grained strata of the Codroy Group (Codroy Road Formation) and within the Anguille Group and the conformably overlying Ship Cove Formation limestones. The décollement is most likely to occur at the base of the evaporitic sediments of the Codroy Road Formation which could be the low amplitude non-reflective package above reflector "R" from VP 411 to VP 581. If this interpretation is correct, then "R" would combine elements of interpretation 1 and 3 or 2 and 3 (Hall et al., 1992).

As a fourth possible interpretation, reflector "R" could be a prominent limestone bed known as the Crabbes limestone (Bell, 1948; Knight 1983). This unit attains a thickness of up to 15 m in coastal sections of St. George's Bay and separates beds of the lower Codroy Group from non-marine strata belonging to the upper Codroy Group and the Barachois Group. It is most probable that the limestone is not the cause of the reflector, because it may be too thin to be responsible for the strong and continuous character of "R". Nonetheless, its position between contrasted lithologies may cause it to be coincident with the reflector.

4.3.3. Packages "A" to "G"

From Knight's (1982) geological mapping, package "A" contains sedimentary strata of the lower Codroy Group and the underlying Fischell's Brook Member of the Anguille Group. These rest unconformably upon Precambrian crystalline rocks that are known to be the core of the Flat Bay Anticline and are imaged by the horizontal low amplitude discontinuous reflectors below 0.4 to 0.6 s TWT. However, the demarcation between the sediments and the Precambrian cannot be determined from the seismic profile. The boundary marked in figures 4.3 to 4.6 at either end of the basin is structural rather than stratigraphic.

The interpretation of packages "B" to "E" is difficult to make on the basis of seismic character alone. Their interpretation depends on the most reasonable interpretation of reflector "R". If "R" is the Codroy/Anguille or the Carboniferous/basement boundary accentuated or modified by basal evaporitic décollement, then "B" must include either Codroy and Barachois strata, or both.

If "R" is indeed the 8Codroy/Anguille contact, packages "D" and probably "E" belong to the Anguille Group, which would be approximately 2.0 to 2.2 km thick.

In this scenario "D" consists of the uniform red sandstone of the Spout Falls Formation plus conglomerates of the Fischell's Brook Member. The low reflective nature of "D" is characteristic of sandstones and conglomerates as has been identified in the Gulf of Mexico (Stuart and Caughey, 1977). The reflective nature of "E" is typical of lacustrine and deltaic rocks of the Snake's Bight and Friars Cove

Formations. "E" has same seismic character as Horton (Anguille) Group sediments in the Magdalen Basin (Durling pers. comm.,1993). Package "E" appears to be continuous in the west and may be the same as package "A".

4.3.4 Unconformity "U"

The interpretation of "U" will depend on the interpretation of reflector "R" and packages "A" to "G". If "R" is Anguille/Codroy contact with "F" as the Lower Palaeozoic, then "U" is the Lower Palaeozoic/Precambrian contact. If lower Palaeozoic is absent, then "U" is the Carboniferous/Precambrian boundary. Alternatively "U" could be the Carboniferous/Lower Palaeozoic contact, if "F" is interpreted to belong to the Anguille Group and part of "G" to be Lower Palaeozoic.

4.4. Geological Models

4.4.1 Introduction

Some combinations of the alternative interpretations are feasible. In Figures 4.4 to 4.6, three of the most probable alternatives are shown. All the models are based solely on the alternative interpretations of reflector "R" and unconformity "U". Each of models A to C implies a different likely range for the Carboniferous underlying "R" (Hall et al., 1992) and different types of basement underlying "U".

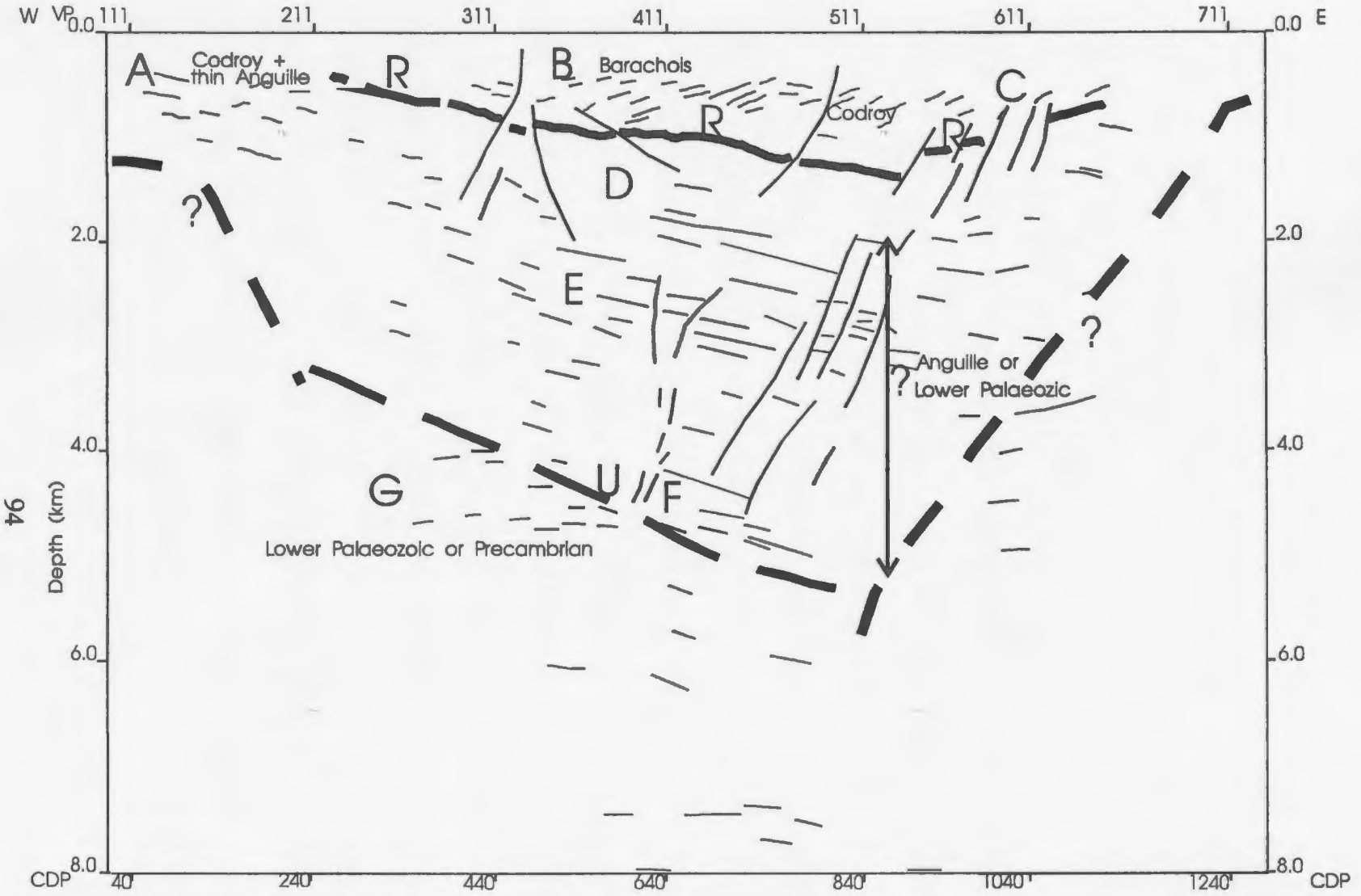

Figure 4.4. Model A - "R" as the Anguille/Codroy contact with or without decollement . The rock units are as indicated in the figure.

4.4.2 Model A - "R" as the Anguille/Codroy contact with or without décollement

Figure 4.4 illustrates model A, which interprets "R" as the Anguille/Codroy contact with or without décollement. This model as discussed by Hall et al. (1992), is a compelling model because "R" can be correlated with Horton/Windsor contact as in offshore and onshore seismic interpretations of the Maritimes Basin (Nickerson, pers. comm., Durling and Mariller, 1990). This would imply that Codroy and Barachois Groups occur above "R", overlying the Anguille Group. The low reflective package overlying "R" could represent Codroy Group especially the Codroy Road Formation. Packages "D" and "E" may include Lower Palaeozoic Carbonates and flysch, but this is unlikely in this model because the erosional truncation of the Lower Palaeozoic is missing. The magnetic field data suggest that the Grenville basement is at depth below the Barachois syncline, because of the rapid loss of amplitude, short wavelength anomalies which characterise the field over exposed basement under the adjacent Flat Bay anticline, and immediately east of the Long Range fault (Fig 2.7). The gravity field across the Barachois syncline shows a low with an amplitude of 10-15 mGal (depending on the choice of regional field). The Barachois/Codroy sequence has a density contrast of 0.22 Mg/m^3 (see Table 2.2) with basement and a thickening of this sequence from 0 to 1 km at the axis of the syncline would thus explain an anomaly of 9.2 mGal. This is barely enough to explain the observed low. It is thus likely that Anguille also underlies the syncline. From model A, 2.3 km of Anguille (to include reflector package E), given a density contrast of 0.09 Mg/m^3 with basement, would

contribute no more than 8.7 mGal to the gravity low. Given that these estimates are directly from the 2-D slab formula (Telford et al., 1990), they overestimate the gravity effect, especially for 'tight' structures. It is concluded that model A provides match to the gravity data. "U" would probably be the contact between the Late Devonian to Carboniferous rocks and the Precambrian basement if the Lower Palaeozoic is missing in this model. Otherwise, "U" could be the Lower Palaeozoic/Precambrian contact if "F" is Lower Palaeozoic. Alternatively "U" could be Carboniferous/Lower Palaeozoic boundary (see Figure 4.4)

Anguille Group would correspond to Package "D" and probably "E" also (i.e Spout Falls, Friars Cove and Snake's Bight Formations). From the seismic profile at hand it is obvious that packages "D" and "E" are conformable to each other. This would mean that "E" is confined to a down-faulted block that lay east of the upthrust Grenvillian basement that now occupies the core of the Flat Bay Anticline (Hall et al., 1992). Anguille Group is likely to be about 2.0 to 2.2 km thick or more if all the way down to "U", contrasting greatly with the approximate 200 m mapped around the Flat Bay Anticline and forming part of package "A" in the seismic profile. If package "F" is included, the total thickness is about 4 km, which is usual for Horton (Anguille Group equivalent) subbasins in the Magdalene Basin (Durling and Marillier, 1993).

From this seismic profile, it can be observed that Anguille Group is not deformed much. The strata are generally flat lying, though interrupted by faults here and there. This can be explained, possibly, by the nature of Precambrian basement which is

crystalline and magnetic compared to the non-crystalline and non-magnetic basement beneath the Anguille Mountains where the Anguille Group is quite deformed.

The Lower Palaeozoic may be either confined to package "F" or absent in this model. Deformation at the east end of the seismic profile (VP 511 to 640) probably indicates salt movements and basal detachment. There is a possibility that a shear zone is being imaged here i.e. from VP 511 to 640, TWT 0.2 s to 0.6 s. Surface geology, nearby drill holes and the apparent conflict of overlying west dipping reflectors with "R" at the west end of the line, suggest that Barachois Group may rest directly upon "R" from VP 250 to VP 390. This would mean that if Codroy Group is present in the west end of the line, it must be very thin (< 200 m). Otherwise, it is evident that the Codroy Group may be present from VP 390 to 590.

4.4.3 Model B - "R" as the Codroy - Barachois upon Pre-Late Devonian-Carboniferous basement with or without décollement

Figure 4.5 shows model B, where "R" is interpreted as the Codroy-Barachois upon Pre-Carboniferous basement plus or minus décollement. This model, proposed by Hall et al. (1992) incorporates the interpretation of packages "B" and "C" as in model A. However, "R" would mark the Codroy-Barachois/Pre-Carboniferous contact. The Pre Carboniferous basement rocks would likely include Lower Palaeozoic orogenic flysch ("D") and carbonates ("E") of the Anticosti Platform which overlay the Precambrian crystalline basement. In this model, unconformity "U" would separate Lower

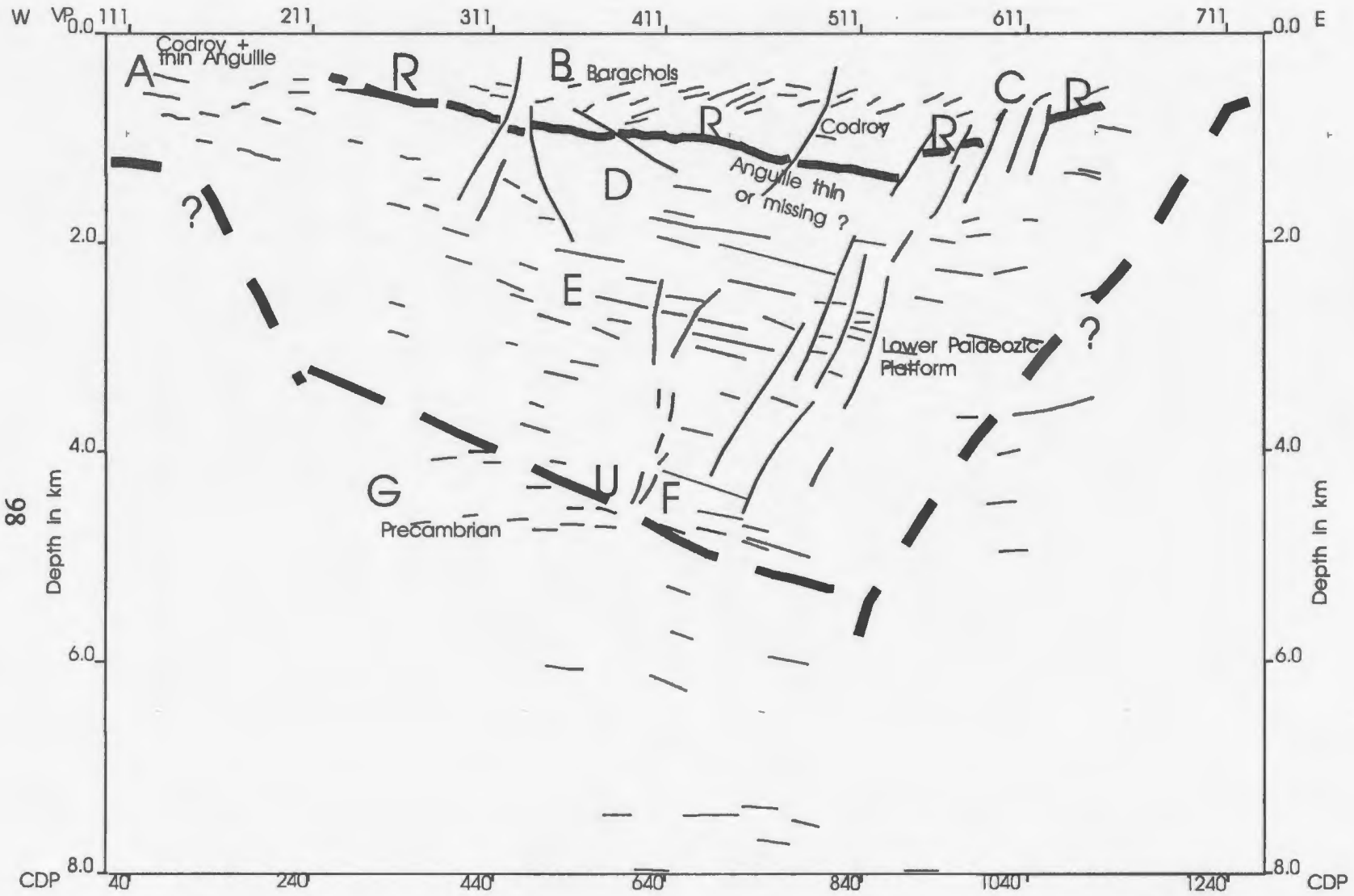

Figure 4.5. Model B - "R" as the Codroy-Barachois upon Pre-late Devonian/ Carboniferous basement with or without Decollement.

Palaeozoic from Precambrian basement. The highly reflective nature of "E" suggests sediments above crystalline basement rather than intra-crystalline basement reflectivity, though some southeast dips in Grenville basement are observed in Lithoprobe data in deep seismic data in the area (Quinlan et al., 1992). From the magnetic field data (Fig. 2.7) it is evident, as discussed previously, that the Grenville basement is at great depth. From the discussion of the gravity effect of model A, it would be recalled that the gravity effect of Barachois/Codroy, separated from basement at reflector "R" is less than 9.2 mGal. This is less than the observed low, suggesting that basement (Lower Palaeozoic or Grenville) does not immediately underlie reflector "R". Structural relationships of "B" and "C" reflectors to "R" require some basal detachment. In both models A and B, it is possible that the Crabbes Brook Fault may represent the outcrop expression of the detachment zone because "R" approaches the surface close to the mapped location of the Crabbes Fault. Outcrop in this section of the seismic line is poor and it is impossible to verify this idea without some more research especially deep drilling.

Model B has less integrity because erosional truncation at the top of the Lower Palaeozoic ("D" and "E") below Carboniferous strata cannot be seen in the seismic profile.

4.4.4 Model C - A non-marine downlap within a half graben

Model C, which is non-marine downlap within a half graben (Figure 4.6), is based

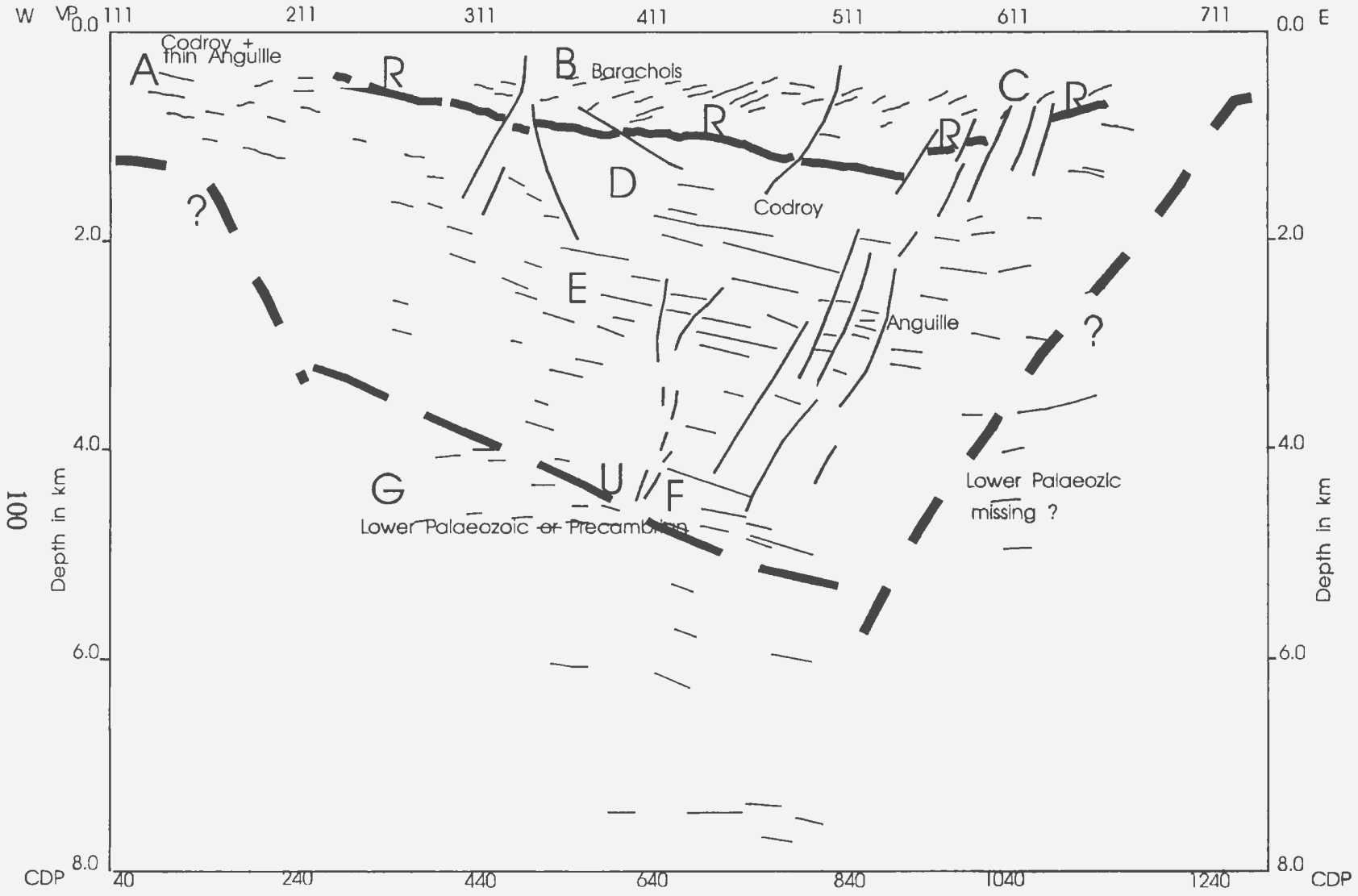

Figure 4.6. Model C - Non-marine downlap within a half graben.

on Reflector "R" as marking Crabbes limestone, the top of Viséan marine sedimentation in the basin (Hall et al., 1992). In this model package "D" would be marine Codroy Group comprising evaporites, thin limestone and fine grained grey and red beds of the Codroy Road Formation and Jeffrey's Village Members. The implication here would be that the Codroy Group (package "D") would overly the Anguille Group (package "E"). It is unlikely that "E" is lower Palaeozoic strata conserved in a down-faulted outlier beneath the basin because erosional truncation at the top of "E" is missing. "E" rests unconformably on either Lower Palaeozoic or Precambrian crystalline basement "G", though the possibility that Lower Palaeozoic is present at "F" cannot be ruled out. The low reflective package between "E" and "F" appears to be conformable with "F". But, this is not very clear from the seismic profile, therefore "F" may be or may be not Lower Palaeozoic.

In this model Codroy Group would be approximately 1.2 km thick overlying 1.0 km of Anguille. The Anguille is a full graben as in model A, bounded by faults on either side. However, the faults that define this graben cannot be placed exactly on the seismic profile because of the many minor faults that cut the whole section.

Packages "B" and "C" are interpreted as non-marine sediments that infilled a half-graben nestled east of the Long Range Fault and south of the Steel Mountain anorthosite. One of the predominant features of these packages ("B and "C") is the west dipping reflectors that intercept "R" at some points and may imply stratigraphic downlap. The downlap dipped at angles generally less than 20° for the reflectors.

This dip is a permissible repose for an offlaping sedimentary wedge deposited on a large alluvial fan (Hall et al., 1992).

Timing of the half-graben formation is not certain, but could have occurred during deposition of Windsor subzone C and even younger, since the Crabbes Limestone is likely not younger than early subzone C (Mamet, 1968; Knight 1983). The half-graben evolved from late Viséan through Westphalian as indicated by the age of the local coals (Hacquebard, 1972; Knight, 1983; Solomon, 1986). The east trending events with post-Codroy movements identified from seismic and potential fields data in offshore Bay St. George (Kilfoil, 1988) may suggest a linked subsidence history of onshore and offshore of the subbasin. The fault system, though complex, suggests that the basin may have been opened by strike slip movements but, later deformed by compressional forces.

The Barachois Group, though dominated by sandstones, contains some intervals dominated by shale and coal measures. Therefore, this could be imaged by the folded reflectors (Barachois syncline) in the middle of the seismic profile (VP 501 to 511). The east dipping packages would then consist of thick sandstone dominated sequences separated by fine grained (shale/mudstone/sandstone) intervals, a few tens to a hundred metres thick (the strongly imaged, westward dipping reflectors), reflecting pulses of basin subsidence coupled with relative uplift of source areas (Heward, 1978; Blair and Bilodeau, 1988). As the half graben grew wider and the source terrane retreated, the basin formed a complex floodplain of rivers and swampy to forested

overbank areas (coal bearing Barachois) (Hall et al., 1992).

Chapter 5: Conclusions

Reprocessing of this seismic profile has yielded significant results. In previous processing DMO was not at all applied to the data, therefore it can be concluded that DMO is a powerful tool in improving data quality. In the current project, more features have been unveiled especially unconformity "U", clear distinction of the reflection packages ("A" to "G") and clear identification of faults (see figures 3.20 and 4.1). It is now easier to interpret the seismic profile. There is a clue now that the basin may be limited downwards by "U". The clear distinction of the packages ("A" to "G") have made it easier to place boundaries between the different possible rock units.

There is no new data, either seismic or potential fields or drill hole data, that has been acquired in this area since this seismic line was interpreted by Hall et al. (1992). The unveiling of unconformity "U" has made it possible to constrain the basin downwards. "U" could be either Lower Palaeozoic/Precambrian boundary or Carboniferous/Lower Palaeozoic boundary or even Carboniferous/Precambrian boundary. Reflector "R" is most likely to be a décollement being imaged within the Carboniferous rocks. Therefore, models A and B are more likely than C. Model B requires a thick Lower Palaeozoic sequence in order that Grenville basement be deep enough to satisfy the magnetic field character. Since there is no surface evidence of any Lower Palaeozoic in this area, model B is regarded as somewhat less likely than model A. Moreover, the gravity anomaly map favours model A.

The structure of the basin from the current study is that of half graben as modelled

by Kilfoil (1988), Miller et al. (1990) and Hall et al. (1992). But, the depth and width extent of the basin is still uncertain. From the models, it appears that the basin could be as shallow as 2 km or as deep as 5 km. This contrasts with the 2-4 km models of Kilfoil (1988).

More research, especially deep drill holes and seismic reflection data, is needed to verify the above findings.

References

Bell, W.A. 1948. Early Carboniferous Strata of St. George's Bay area. Geological Survey of Canada, Memoir 314, 112 p.

Belt, E.S. 1969. Newfoundland Carboniferous Stratigraphy and its relation to the Maritimes Ireland. In Kay M. (Ed), Symposium on Stratigraphy and Structure Bearing on Continental Drift in the Northern American Ocean, Gander Meeting, 1967, AAPG, Memoir 12, p 734 - 753.

Biondi, B. and Ronen, J. 1987. Dip Moveout in Shot Profiles, Geophysics, 52, p 1473-1482.

Blair, T.C. and Bilodeau, W.L. 1988. Development of the tectonic cyclotherms in rift, pull-apart and foreland basins: Sedimentary response to episodic tectonism. Geology, 16, p 517-520.

Dobrin, M.B., and Savit, C. H. 1988. Introduction to Geophysical Prospecting. New York, McGraw-Hill, 897p.

Durling, P.W. and Marillier, F.J.Y. 1990. Structural trends and basement rock subdivisions in the western Gulf of St. Lawrence, northern Appalachians. Atlantic Geology 26, p 79-95.

_____ 1993. Structural elements of the Magdalen Basin, Gulf of St. Lawrence, from seismic reflection data; in Research, Part D; Geological Survey of Canada, Paper 93-1D, p 147-154.

Hacquebard, P.A. 1972. The Carboniferous of Eastern Canada. In Comptes Rendus,

7e Congrèss International de Stratigraphie et de Géologie du Carbonifère, Krefeld, Bd, 1, p 69-90.

Hall, J., Langdon, G., Roberts, B., Hawkins, D., Fagan, A., Knight, I and Kilfoil, G. 1992. Reflection seismic imaging of the Carboniferous St.George coalfield, Western Newfoundland: a reappraisal of Palaeozoic stratigrahic thickness. Bulletin of Canadian Petroleum Geology, 40, p 321-334.

Heward, P.A. 1978. Aluvial fan sequence and megasequence models: with examples from Westphalian D- Stephanian B coalfields, northern Spain: In A.D. Mial (ed). Fluvial sedimentology. Canadian Society of Petroleum Geologists, Memoir 5, p 669-702.

Kilfoil, G.J. 1988. An integrated gravity, magnetic and seismic interpretation of the Carboniferous Bay St. George subbasin, western Newfoundland. Unpublished M.Sc. thesis, Memorial University of Newfoundland, 168 p.

Kilfoil, G.J. and Bruce, P.A. 1991. Gridded Aeromagnetic data. 200 m grid cell (Ver.1.0), Newfoundland by 1:250000 NTS, map area, Newfoundland Dept. of Mines and Energy, Open File, Newfoundland (2063).

Kleyn, A.H. 1984. Seismic reflection interpretation. London, Elsevier Applied Science Publishers, 269 p.

Knight, I. 1982. Geology map of the Carboniferous Bay St. George subbasin, western Newfoundland, Map 82-1, Mineral Development Division, Newfoundland and Labrador Department of Mines and Energy.

_____1983. Geology of the Carboniferous Bay St. George Subbasin, western Newfoundland, Memoir 1, Mineral Development Division, Newfoundland and Labrador Department of Mines and Energy, 358 p.

Langdon, G. 1991. Current research into the western Newfoundland Carboniferous - Onshore and offshore. CERR, unpublished report.

Langdon, G.S. and Hall, J. Carboniferous tectonics, Basin development and styles of deformation in the Cabot Strait. In prep.

Larner, K.L., Gibson, B.R., Chambers, R. and Wiggins, R.A. 1979. Simultaneous estimation of the residual static and cross-dip corrections. Geophysics, 44, p 1175.

Mamet, B.L. 1968. Sur une Microfaune du Viséan Supérieur de terre Neuve. Naturaliste Canadien, 95, p 1357-1372.

Miller, H., Kilfoil, G.J., and Peavy, S.T. 1990. An integrated geophysical interpretation Carboniferous Bay St. George Subbasin, western Newfoundland. Bulletin of Canadian Petroleum Geology, 38, p 320-331.

Murthy, G.S. and Rao, K.V. 1976. Palaeomagnetism of Steel Mountain and Indian Head anorthosites from western Newfoundland. Canadian Journal of Earth Sciences, 13 p 75-83.

Neidell, N. and Taner, M.T. 1971. Semblance and other coherency measures for multichannel Data. Geophysics, 36, p 482-497.

Peavy, S.T. 1985. A gravity and magnetic interpretation of the Bay St. George

Carboniferous Subbasin in western Newfoundland. Unpublished M.Sc. thesis, Memorial University of Newfoundland, 207 p.

Quinlan, G.M., Hall, J., Williams, H., Wright, J., Colman-Sadd, S.P., O'Brien, S.J., Stockmal, G.S. and Marillier, F. 1992. Lithoprobe onshore reflection transects across the Newfoundland Appalachians. Canadian Journal of Earth Sciences, 29, p 1865-1877.

Rietsch, E. 1980. Estimation of the signal-to-noise ratio of seismic data with an application to stacking. Geophysical prospecting, 28, p 531-550.

Riley, G.C. 1962. Stephenville map-area, Newfoundland. Geophysical Survey of Canada, Memoir 232, 72 p.

Robinson, E.A. 1983. Seismic Velocity Analysis and the Convolutional Model. Boston, International Human Resources Development Corporation, 290 p.

Schillereff, S. and Williams, H. 1979. Geology of the Stephenville Map area, Newfoundland. In: Current Research, Part A. Geological Survey of Canada, Paper 79-1A, p 327-332.

Solomon, S. 1986. Sedimentary and Fossil-fuel potential of the Upper Carboniferous Barachois Group, western Newfoundland. Unpublished M.Sc. thesis, Memorial University of Newfoundland, 256 p.

Spector, A. 1969. Report on Interpretation of aeromagnetic data, St. George's Bay, Newfoundland. British Newfoundland Exploration Limited. Unpublished report, open file PB (157), Newfoundland and Labrador Department of Mines

and Energy.

STARPAK Processing Manual, 1989.

Stuart, C.J. and Caughey, C.A. 1977. Seismic facies and sedimentology of terrigenous Pleistocene deposits in Northwest and Central Gulf of Mexico. In: C.E. Payton (Ed). The seismic Stratigraphy - applications to hydrocarbon exploration, AAPG, Memoir 26, p 249-275.

Telford, W.M., Geldart, L.P. and Sheriff, R.E. 1990. Applied Geophysics. New York, Cambridge University Press, pp 770.

Vernall, P. 1954. Gravity Survey of the Bay St. George area, Southwest Newfoundland. Geological survey of Newfoundland, Unpublished report, Open file 12B (63).

Wiggins, R. A., Larner, K.L. and Wisecup, R.D. 1976. residual static analysis as a general linear inverse problem. Geophysics, 41, p 922.

Williams, H. 1978. Tectonic Lithofacies map of the Appalachian Orogen. Memorial University of Newfoundland, Map 1.

_____ 1985. Geology, Stephenville Map area, Newfoundland. Geological Survey Of Canada, Map 1579A (1:1,000,000).

Wilson, J.T. 1962. Cabot fault, an Appalachian equivalent of San Adreas and Great Glen Faults and some implications for continental displacement. Nature, 195, p. 135-138.

Yilmaz, O. 1987. Seismic Data Processing. Investigations in Geophysics volume 2,

Society of Exploration Geophysicists.

Appendix A

This appendix contains the values used to calculate field statics corrections and elevation values.

Abbreviations are as follows; ti is the intercept time (ms); vb is the velocity of the bedrock (km/s); zw is the thickness of the weathered layer (m); Es is the elevation (m) and Td is the static correction (ms).

Appendix A

Table A.1. FIELD STATICS SPECIFICATIONS.

station	ti	vb	zw	Es	Td
101	5	3.6	6.013	124	5.886
103	10	3.6	12.03	124.5	4.411
105	13	3.6	15.63	124.9	3.498
107	15	3.6	18.04	125.3	2.852
109	15	3.6	18.04	125.8	2.713
111	15	3.6	18.04	126.2	2.602
113	15	3.6	18.04	126.7	2.463
115	15	3.6	18.04	127.1	2.352
117	15	3.6	18.04	127.5	2.241
119	16	3.6	19.24	128	1.835
121	18	3.6	21.65	128.2	1.245
123	20	3.6	24.05	127.5	0.905
125	25	3.6	30.07	126.8	−0.24
127	27	3.6	32.47	125.7	−0.47
129	29	3.6	34.88	124.5	−0.67
131	28	3.6	33.67	123.3	−0.07
133	25	3.6	30.07	122.1	1.068
135	23	3.6	27.66	120.9	1.936
137	22	3.6	26.46	119.7	2.537
139	21	3.625	25.18	118.5	3.046
141	20	3.625	23.98	117.3	3.646
143	19	3.625	22.78	116.9	4.025
145	18	3.625	21.58	116.6	4.376
147	18	3.625	21.58	116.3	4.459
149	18	3.625	21.58	115.9	4.57
151	19	3.65	22.71	115.6	4.291
153	20	3.65	23.91	115.2	4.13
155	22	3.65	26.3	114.9	3.672
157	24	3.65	28.69	114.6	3.214
159	26	3.65	31.08	114.2	2.783
161	29	3.7	34.47	113.9	1.838
163	32	3.7	38.04	112.6	1.37
165	35	3.725	41.49	109.5	1.266
167	38	3.75	44.92	107.4	0.878

Appendix A

Table A.1. FIELD STATICS SPECIFICATIONS.

169	41	3.8	48.22	109.8	−0.84
171	44	3.85	51.49	112.1	−2.53
173	46	3.9	53.58	114.3	−3.9
175	47	4	54.27	115.3	−4.89
177	47	4.05	54.05	116.4	−5.38
179	45	4.125	51.45	117.4	−5.35
181	41	4.2	46.63	118.5	−4.71
183	38	4.3	42.93	118.6	−4.18
185	35	4.35	39.41	118.7	−3.45
187	31	4.45	34.7	118.8	−2.54
189	28	4.525	31.21	118.9	−1.84
191	25	4.6	27.76	119	−1.11
193	22	4.675	24.34	119.1	−0.35
195	19	4.75	20.95	119.2	0.421
197	17	4.8	18.7	119.3	0.941
199	16	4.85	17.56	119.4	1.149
201	14	4.9	15.34	119.5	1.686
203	14	4.9	15.34	120.4	1.503
205	14	4.925	15.32	121.2	1.298
207	14	4.925	15.32	122	1.136
209	15	4.9	16.43	122.8	0.689
211	17	4.85	18.66	123.7	−0.06
213	19	4.775	20.92	124.5	−0.74
215	22	4.65	24.37	125.3	−1.63
217	24	4.5	26.79	126.2	−2.15
219	26	4.3	29.37	127	−2.51
221	28	4.15	31.96	127.8	−2.93
223	29	4	33.49	129	−3.12
225	30	3.8	35.28	130.3	−3.17
227	30	3.675	35.76	131.5	−3.12
229	30	3.45	36.82	132.7	−2.72
231	29	3.25	36.79	133.2	−1.91
233	27	3.1	35.34	133.4	−0.91
235	25	3	33.54	133.7	−0.16
237	22	2.9	30.38	134	0.803

Appendix A

Table A.1. FIELD STATICS SPECIFICATIONS.

239	20	2.825	28.32	134.3	1.422
241	17	2.8	24.29	134.6	2.03
243	14	2.8	20	134.2	2.785
245	13	2.8	18.58	133.9	3.096
247	12	2.8	17.15	133.6	3.408
249	12	2.8	17.15	133.2	3.551
251	12	2.8	17.15	132.9	3.658
253	15	2.8	21.43	132.6	3.152
255	17	2.8	24.29	132.2	2.887
257	19	2.8	27.15	131.9	2.586
259	19	2.8	27.15	131.6	2.693
261	19	2.8	27.15	131.5	2.729
263	17	2.8	24.29	131.3	3.208
265	15	2.8	21.43	131.1	3.688
267	10	2.8	14.29	130.9	4.78
269	8	2.8	11.43	131	5.153
271	8	2.8	11.43	131	5.153
273	8	2.8	11.43	131	5.153
275	8	2.8	11.43	131.1	5.117
277	8	2.8	11.43	131.2	5.081
279	8	2.8	11.43	131.4	5.01
281	7	2.8	10	131.6	5.143
283	7	2.8	10	131.8	5.071
285	7	2.8	10	132.4	4.857
287	7	2.8	10	132.9	4.678
289	9	2.8	12.86	133.5	4.056
291	12	2.8	17.15	134	3.265
293	15	2.8	21.43	134.6	2.438
295	15	2.8	21.43	134.5	2.474
297	15	2.8	21.43	133.8	2.724
299	16	2.8	22.86	133.1	2.77
301	16	2.8	22.86	132.4	3.02
303	16	2.8	22.86	133.3	2.698
305	16	2.8	22.86	134.4	2.305
307	16	2.8	22.86	135.5	1.913

Appendix A

Table A.1. FIELD STATICS SPECIFICATIONS.

309	16	2.8	22.86	136.7	1.484
311	18	2.85	25.27	137.8	0.513
313	23	2.85	32.28	138.9	−0.92
315	26	2.85	36.5	140.1	−1.97
317	27	2.85	37.9	141.2	−2.56
319	28	2.85	39.3	142.4	−3.19
321	28	2.9	38.67	143.8	−3.86
323	28	2.9	38.67	144.6	−4.14
325	28	2.9	38.67	145.4	−4.41
327	28	2.95	38.09	146.3	−4.88
329	28	3	37.57	147.1	−5.29
331	28	3.05	37.09	147.8	−5.66
333	27	3.1	35.34	148.3	−5.72
335	25	3.125	32.54	148.8	−5.47
337	22	3.15	28.48	149.3	−4.98
339	18	3.15	23.3	149.8	−4.19
341	17	3.175	21.89	150.3	−4.14
343	16	3.2	20.5	150.6	−4.03
345	14	3.2	17.93	150.8	−3.61
347	13	3.2	16.65	150.9	−3.4
349	12	3.2	15.37	150.4	−3.01
351	10	3.2	12.81	150	−2.4
353	9	3.2	11.53	149.5	−2.01
355	7	3.2	8.967	149.1	−1.4
357	5	3.2	6.405	148.6	−0.76
359	3	3.2	3.843	148.2	−0.16
361	2	3.225	2.549	147.9	0.167
363	2	3.225	2.549	148.1	0.105
365	1	3.225	1.275	148.3	0.285
367	0	3.25	0	148.4	0.492
369	0	3.25	0	151	−0.31
371	0	3.25	0	153	−0.92
373	0	3.3	0	154.3	−1.3
375	0	3.3	0	155.6	−1.7
377	0	3.3	0	156.8	−2.06

Appendix A

Table A.1. FIELD STATICS SPECIFICATIONS.

379	0	3.3	0	156.8	−2.06
381	0	3.3	0	158.1	−2.45
383	0	3.3	0	159.4	−2.85
385	0	3.33	0	160.4	−3.12
387	0	3.33	0	161.5	−3.45
389	1	3.33	1.251	162.5	−4
391	3	3.33	3.752	163.6	−4.83
393	4	3.33	5.003	164.6	−5.38
395	5	3.33	6.254	165.7	−5.96
397	5	3.33	6.254	166.7	−6.26
399	5	3.33	6.254	167.6	−6.53
401	5	3.33	6.254	168.4	−6.77
403	5	3.33	6.254	169.2	−7.01
405	5	3.33	6.254	170.3	−7.34
407	5	3.33	6.254	171.3	−7.65
409	4	3.33	5.003	172.3	−7.7
411	3	3.33	3.752	173.3	−7.75
413	2	3.33	2.501	174.4	−7.83
415	4	3.33	5.003	175.4	−8.63
417	7	3.33	8.755	176.4	−9.68
419	6	3.33	7.504	177.4	−9.73
421	6	3.33	7.504	177.9	−9.88
423	5	3.33	6.254	178.3	−9.75
425	4	3.33	5.003	178.4	−9.53
427	4	3.33	5.003	178.6	−9.59
429	4	3.33	5.003	178.7	−9.62
431	4	3.33	5.003	178.6	−9.59
433	4	3.33	5.003	178.2	−9.47
435	4	3.33	5.003	177.9	−9.38
437	4	3.33	5.003	177.5	−9.26
439	4	3.33	5.003	177.2	−9.17
441	4	3.33	5.003	176.8	−9.05
443	5	3.33	6.254	176.5	−9.21
445	6	3.33	7.504	176.4	−9.43
447	7	3.33	8.755	176.4	−9.68

Appendix A

Table A.1. FIELD STATICS SPECIFICATIONS.

449	8	3.33	10.01	176.3	−9 9
451	9	3.33	11.26	176.3	−10.1
453	9	3.33	11.26	176.2	−10.1
455	10	3.33	12.51	176.1	−10.3
457	10	3.33	12.51	176.1	−10.3
459	10	3.33	12.51	175.8	−10.2
461	10	3.33	12.51	175.6	−10.2
463	10	3.33	12.51	175.3	−10.1
465	12	3.33	15.01	176.5	−11
467	14	3.33	17.51	177.7	−11.8
469	14	3.33	17.51	178.9	−12.2
471	14	3.33	17.51	180.1	−12.5
473	14	3.33	17.51	181.4	−12.9
475	14	3.33	17.51	182.6	−13.3
477	14	3.33	17.51	183.8	−13.6
479	13	3.33	16.26	185	−13.8
481	12	3.33	15.01	186.2	−13.9
483	11	3.33	13.76	187.4	−14
485	10	3.33	12.51	188.2	−14
487	9	3.33	11.26	188.4	−13.8
489	8	3.33	10.01	188.4	−13.5
491	7	3.33	8.755	188.4	−13.3
493	6	3.33	7.504	188.3	−13
495	5	3.33	6.254	188.3	−12.8
497	6	3.33	7.504	188.3	−13
499	7	3.33	8.755	188.2	−13.2
501	7	3.33	8.755	186.8	−12.8
503	7	3.33	8.755	185.4	−12.4
505	7	3.33	8.755	184.4	−12.1
507	7	3.33	8.755	183.4	−11.8
509	7	3.33	8.755	182.4	−11.5
511	6	3.33	7.504	181.5	−11
513	5	3.33	6.254	180.5	−10.4
515	4	3.33	5.003	179.5	−9.86
517	4	3.33	5.003	178.5	−9.56

Appendix A

Table A.1. FIELD STATICS SPECIFICATIONS.

519	2	3.33	2.501	177.5	−8.76
521	0	3.33	0	176.5	−7.96
523	0	3.33	0	175.5	−7.66
525	0	3.33	0	174.8	−7.45
527	0	3.33	0	174.2	−7.27
529	0	3.33	0	175.5	−7.66
531	0	3.33	0	177.5	−8.26
533	0	3.33	0	178.7	−8.62
535	0	3.33	0	179.7	−8.92
537	0	3.33	0	180.8	−9.25
539	0	3.33	0	181.9	−9.58
541	1	3.33	1.251	183	−10.2
543	2	3.33	2.501	184.1	−10.7
545	4	3.33	5.003	185.4	−11.6
547	5	3.33	6.254	186.6	−12.2
549	7	3.33	8.755	186.3	−12.6
551	10	3.33	12.51	185.9	−13.3
553	12	3.33	15.01	185.5	−13.7
555	11	3.33	13.76	183.6	−12.8
557	10	3.33	12.51	181.7	−12
559	10	3.33	12.51	179.8	−11.4
561	10	3.33	12.51	177.9	−10.9
563	12	3.33	15.01	176	−10.8
565	14	3.33	17.51	175	−11
567	17	3.33	21.26	175.9	−12
569	18	3.33	22.51	172.9	−11.4
571	14	3.33	17.51	171.9	−10.1
573	10	3.33	12.51	171.7	−9.01
575	12	3.33	15.01	173.9	−10.2
577	13	3.33	16.26	176.1	−11.1
579	13	3.33	16.26	178.4	−11.8
581	12	3.33	15.01	180.6	−12.2
583	11	3.33	13.76	182.8	−12.6
585	10	3.33	12.51	184.3	−12.8
587	8	3.33	10.01	185.5	−12.7

Appendix A

Table A.1. FIELD STATICS SPECIFICATIONS.

589	6	3.33	7.504	186	−12.3
591	7	3.33	8.755	186.5	−12.7
593	8	3.33	10.01	187	−13.1
595	6	3.33	7.504	187.6	−12.8
597	5	3.33	6.254	188.1	−12.7
599	3	3.33	3.752	188.6	−12.3
601	2	3.33	2.501	189.3	−12.3
603	2	3.33	2.501	190.1	−12.5
605	5	3.33	6.254	191.3	−13.7
607	3	3.33	3.752	192.5	−13.5
609	2	3.33	2.501	193.7	−13.6
611	3	3.33	3.752	195	−14.3
613	4	3.33	5.003	196.2	−14.9
615	5	3.33	6.254	197.5	−15.5
617	6	3.33	7.504	198.7	−16.1
619	6	3.33	7.504	199.5	−16.4
621	7	3.33	8.755	199.9	−16.7
623	7	3.33	8.755	200.4	−16.9
625	8	3.33	10.01	201.6	−17.5
627	8	3.33	10.01	202.9	−17.9
629	7	3.33	8.755	204.2	−18
631	7	3.33	8.755	205.4	−18.4
633	10	3.33	12.51	206.7	−19.5
635	12	3.33	15.01	206.8	−20.1
637	10	3.33	12.51	206.8	−19.6
639	7	3.33	8.755	206.8	−18.8
641	0	3.33	0	206.8	−17.1
643	0	3.33	0	206.9	−17.1
645	0	3.33	0	206.4	−16.9
647	0	3.33	0	206	−16.8
649	0	3.33	0	205.6	−16.7
651	0	3.33	0	205.8	−16.8
653	0	3.33	0	206.4	−16.9
655	0	3.33	0	207	−17.1
657	0	3.33	0	207.6	−17.3

Appendix A

Table A.1. FIELD STATICS SPECIFICATIONS.

659	0	3.33	0	208.2	−17.5
661	0	3.33	0	208.8	−17.7
663	0	3.33	0	209.4	−17.8
665	0	3.33	0	210.1	−18
667	0	3.33	0	210.7	−18.2
669	0	3.33	0	211.3	−18.4
671	1	3.33	1.251	211.7	−18.8
673	3	3.33	3.752	212.1	−19.4
675	5	3.33	6.254	212.5	−20
677	7	3.33	8.755	212.9	−20.6
679	10	3.33	12.51	213.3	−21.5
681	15	3.33	18.76	213.6	−22.8
683	18	3.33	22.51	213.5	−23.6
685	20	3.33	25.01	214.3	−24.3
687	22	3.33	27.52	215.1	−25
689	25	3.33	31.27	216	−26.1
691	31	3.33	38.77	216.4	−27.7
693	40	3.33	50.03	216.9	−30.1
695	70	3.33	87.55	217.2	−37.7
697	74	3.33	92.55	217.4	−38.7
699	75	3.33	93.8	217.6	−39
701	76	3.33	95.05	217.7	−39.3
703	76	3.33	95.05	217.9	−39.4
705	75	3.33	93.8	218.5	−39.3
707	73	3.33	91.3	219.2	−39
709	72	3.33	90.05	219.9	−39
711	70	3.33	87.55	220.5	−38.7
713	68	3.33	85.05	221.2	−38.4
715	67	3.33	83.8	221.9	−38.3
717	67	3.33	83.8	221.8	−38.3
719	67	3.33	83.8	221.5	−38.2
721	67	3.33	83.8	221.1	−38.1
723	67	3.33	83.8	220	−37.8
725	67	3.33	83.8	216.9	−36.8
727	67	3.33	83.8	213.8	−35.9

Appendix A

Table A.1. FIELD STATICS SPECIFICATIONS.

729	67	3.33	83.8	210.7	−35
731	67	3.33	83.8	207.5	−34
733	67	3.33	83.8	207	−33.9
735	67	3.33	83.8	200.3	−31.8

Appendix B

DMO Theory

The impulse response in time-space coordinates of the DMO operator derived by Biondi and Ronen (1987) is an ellipse:

$$\left(\frac{t}{t_i}\right)^2 + \left(\frac{x - x_i}{x_i}\right)^2 = 1 \qquad \text{(B.1)}$$

where t_i is the location of the impulse and x represents full offset. The above equation is only part of the operator, no amplitude information is included in it. Amplitude information is ignored at this point due to its uncertainty. It would be expensive to perform DMO using equation B.1. Therefore, a change of variables has to be made that transforms equation B.1.

Let $x = \exp(p)$, $x_0 = \exp(p_0)$

$t = \exp(s)$, $t_0 = \exp(s_0)$, then:

$$(\exp(s - s_0))^2 + (\exp(p - p_0) - 1)^2 = 1 \qquad \text{(B.2)}$$

Equation B.2 is more pleasing than equation B.1 because the form of the curve does not change with (s_0, p_0), therefore convolution applies and a fast algorithm could be written.

Appendix B

But, the change of variables involves a logarithmic stretch which will usually increase the size of the shot record. The amount of increase is dependent on the frequency and wavenumber content of the data, and also on the start time and near offset. The transformation makes time zero and offset zero to map to infinity in the p and s domains. There must be a non-zero start time and a non-zero offset. DMO in shot records is a compromise. The offset direction is log transformed so vectoring could be used, and the time axis is left as it is, to avoid additional data to process. The reason x axis is chosen to be transformed is that normalised wavenumbers for a moved-out shot tend to be lower as compared to the normalised frequencies, therefore this direction would be less sensitive to the transformation.

After log transforming x axis, equation B.1 becomes:

$$(\frac{t}{t_i})^2 + (\exp(p - p_0) - 1)^2 = 1 \qquad (B.3)$$

If p is made the subject of the formula in equation B.3, the following expression is obtained:

$$p = p_i + \log(1 \pm \sqrt{1 - (\frac{t}{t_i})^2}) \qquad (B.4)$$

Appendix B

A plot of equation B.4 is shown in figure B.1. Figure B.2 shows the plot of the same equation with different p_0's and t_0's. Note that the form of the curve does not change with p_0, rather it changes with t_0.

Equation B.3 can now be used to produce an algorithm that will perform DMO. Consider the following integral;

$$g(t,p) = \int_t^{\infty} Af\left(s, p - \log\left[1 - \sqrt{1 - \left(\frac{t}{s}\right)^2}\right]\right) ds$$

$$+ \int_t^{\infty} Bf\left(s, p - \log\left[1 + \sqrt{1 - \left(\frac{t}{s}\right)^2}\right]\right) ds \qquad (B.5)$$

where f(t,p) is the stretched NMO-corrected shot record, g(t,p) is the stretched zero offset section and A and B are arbitrary functions to be determined. It is hoped that this integral will give the proper t-p relationship by substituting a delta function at some location for the function f, i.e let $f(s,p) = \Delta(s-t_0)*\Delta(p-p_0)$, and solve the integral:

$$g(t,p) = \int_t^{\infty} A\Delta(s - t_0) * \Delta\left(p - p_0 - \ln\left[1 - \sqrt{1 - (t/s)^2}\right]\right) ds$$

Appendix B

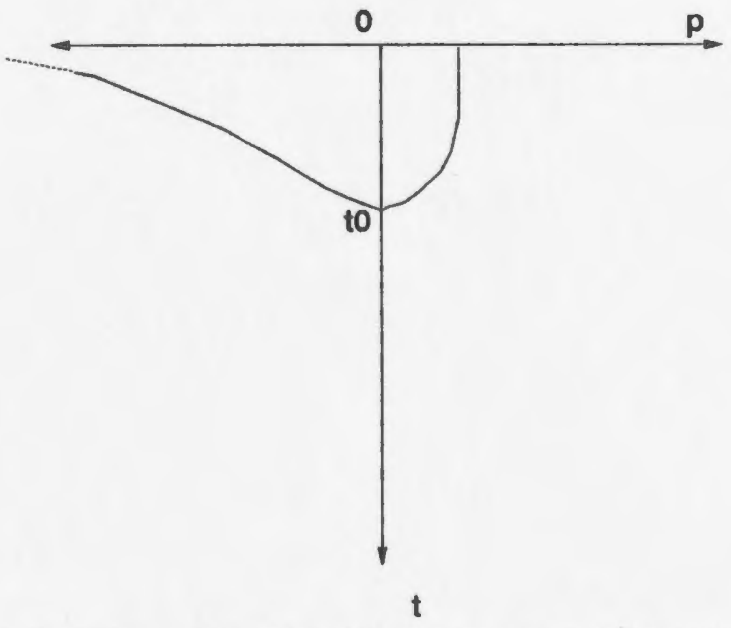

Figure B.1. Plot of equation B.4. P0 was set to zero for this plot (Biondi and Ronen, 1987).

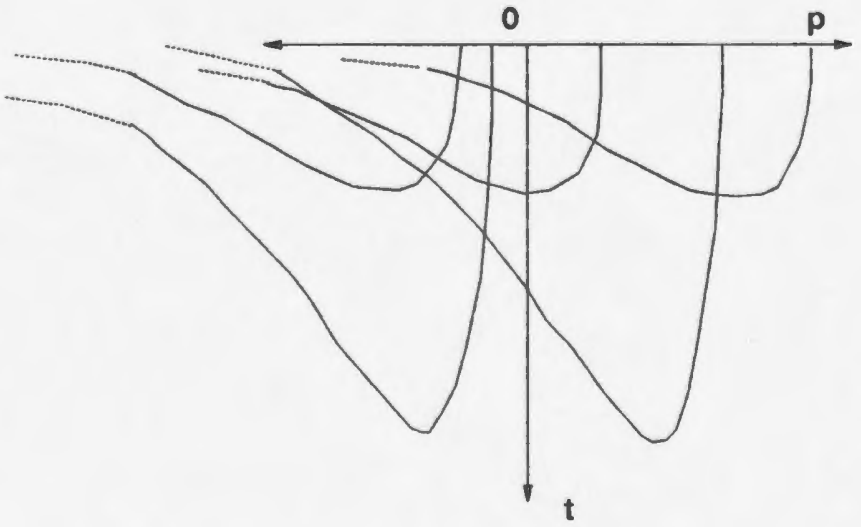

Figure B.2. Plot of equation B.4 for different values for P0's and t0 's (Biondi and Ronen, 1987).

Appendix B

$$+ \int_{t}^{\infty} B\Delta(s-t_0) * \Delta(p - p_0 - \ln\left[1 + \sqrt{1 - (t/s)^2}\right]) ds \quad (B.6)$$

By the definition of the delta function, the above integral will only have non-zero values when s is equal to t_0, and

$$p - p_0 - \log\left(1 - \sqrt{1 - (t/s)^2}\right) = 0 \quad (B.7)$$

and

$$p - p_0 - \log\left(1 + \sqrt{1 - (t/s)^2}\right) = 0 \quad (B.8)$$

Substituting t_0 for s in the above equations, we arrive at equation B.4, the desired time response. Applying Fourier transform in p on the above equation the following expression is obtained:

$$g(t,k) = \int_{t}^{\infty} Af(s,k)\, e^{jk\ln\left(1 - \sqrt{1 - (t/s)^2}\right)} ds$$

$$+ \int_{t}^{\infty} Bf\ (s,k)\, e^{jkln(1\ +\ \sqrt{1\ -\ (t/s)^2})}\ ds \qquad \text{(B.9)}$$

There are no restrictions on the values of A and B because the amplitudes of DMO are uncertain. However, a convenient choice of A and B would be the derivatives of

$$\log\ (1\ -\ \sqrt{1\ -\ (t/s)^2} \qquad \text{(B.10)}$$

and

$$-\ \log(1\ -\ \sqrt{1\ +\ (t/s)^2} \qquad \text{(B.11)}$$

with respect to s.

The final result after all the analytical computations is:

$$g\ (m\Delta t,k)\ =\ \sum_{n\ =\ m}^{\infty} f(n\Delta t,k)\ \ [e^{jkln[1\ -\ \sqrt{1\ -\ (\frac{m}{n}\ +\ 1)^2}]}$$

$$-\ e^{jkln[1\ -\ \sqrt{1\ -\ (\frac{m}{n})^2}]}\ -\ e^{jkln[1\ +\ \sqrt{1\ -\ (\frac{m}{n\ +\ 1})^2}]}$$

$$+\ e^{jkln[1\ +\ \sqrt{1-\frac{m^2}{n}}]} \qquad \text{(B.12)}$$

where t = m * dt and s = n * dt. The above expression is the operator used to DMO in shot records.

Figure 4.2. Main r
of the seismic prof
reflection packages;
0.2 to 0.6 s TWT; t
unconformity "U" i

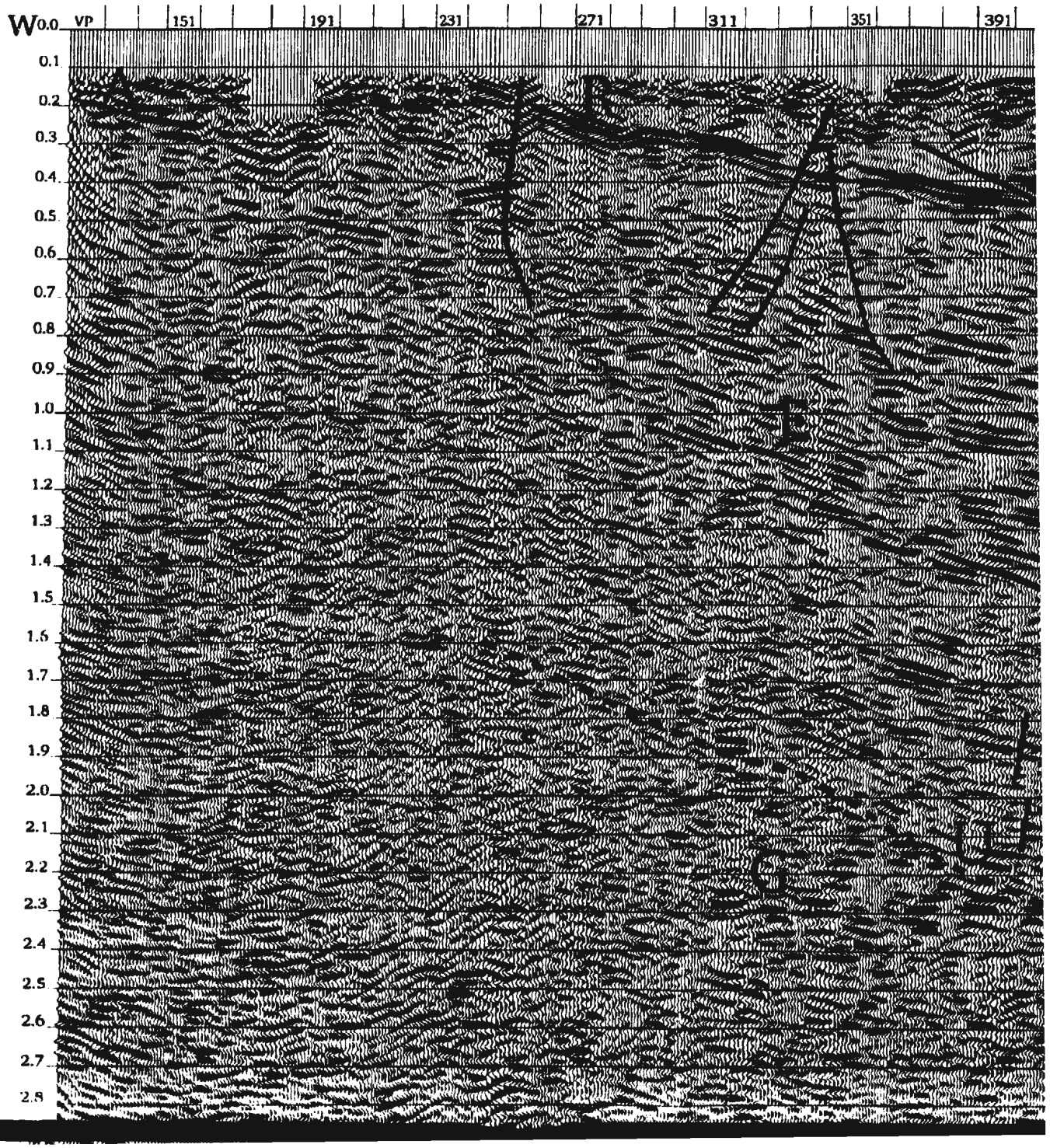

2. Main reflection packages, faults and unconformity smic profile. Packages "A" to "G" mark the main packages; "R" is a major reflector which extends from s TWT; the faults are shown as vertical thin lines and ity "U" is shown by a dashed line.

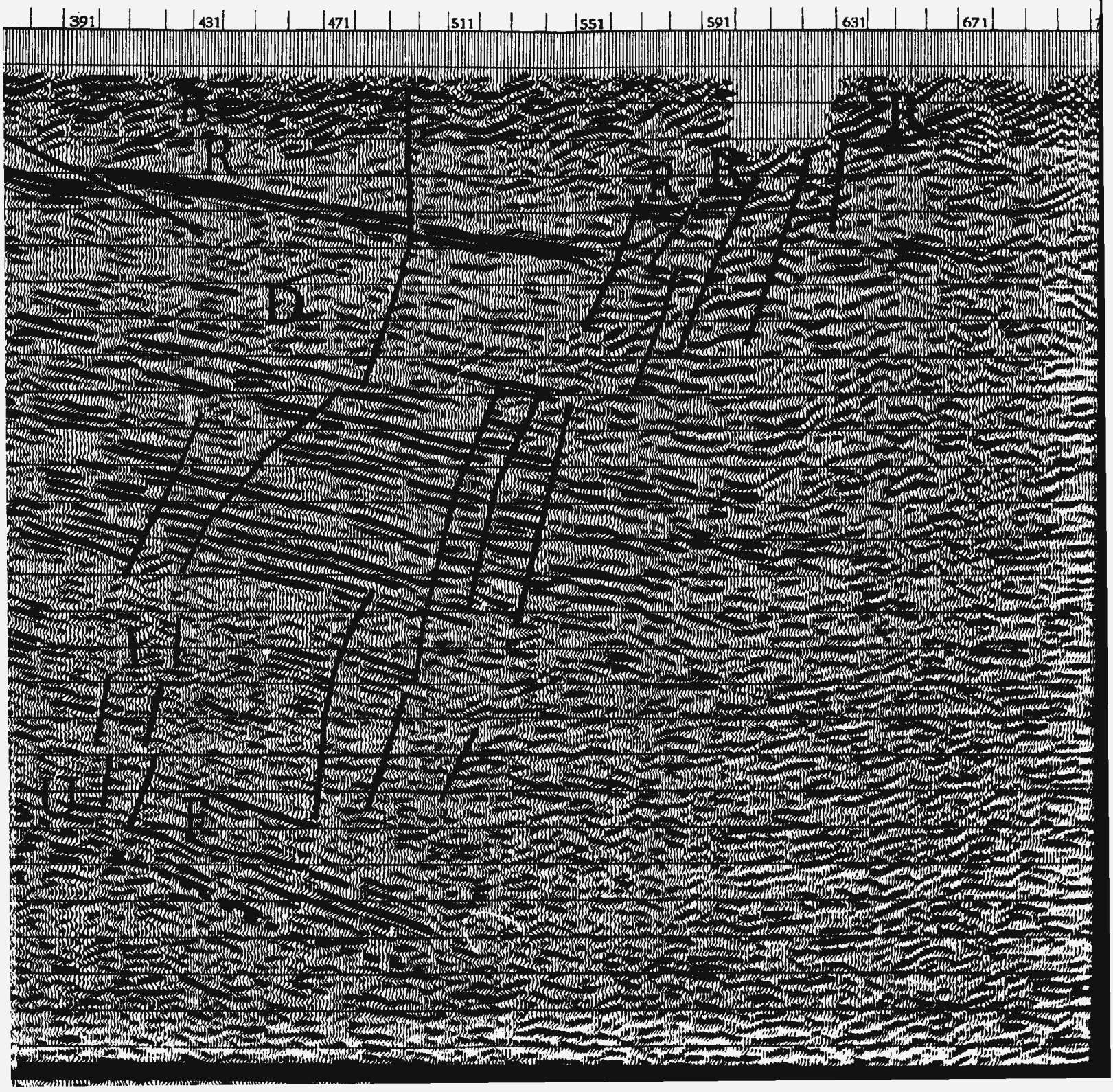

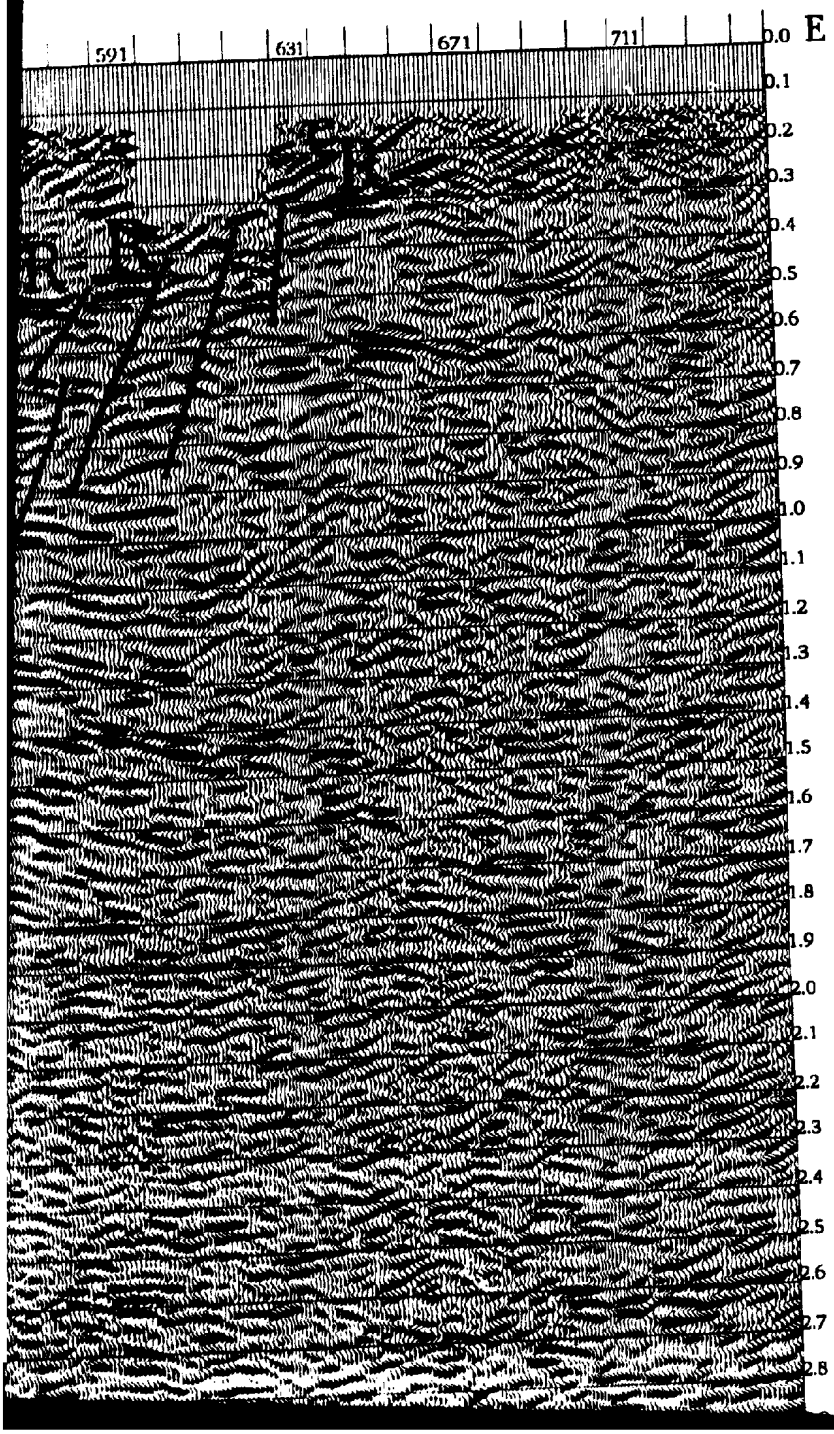
591
631
671
711
E
0.0
0.1
0.2
0.3
0.4
0.5
0.6
0.7
0.8
0.9
1.0
1.1
1.2
1.3
1.4
1.5
1.6
1.7
1.8
1.9
2.0
2.1
2.2
2.3
2.4
2.5
2.6
2.7
2.8

1

Figure 4.1. The seismic profile as processed previously. N
the difference in focus of events as compared to figure 3.21
this section unconformity "U" cannot be identified.
demarcation between one package to the other is not clear.

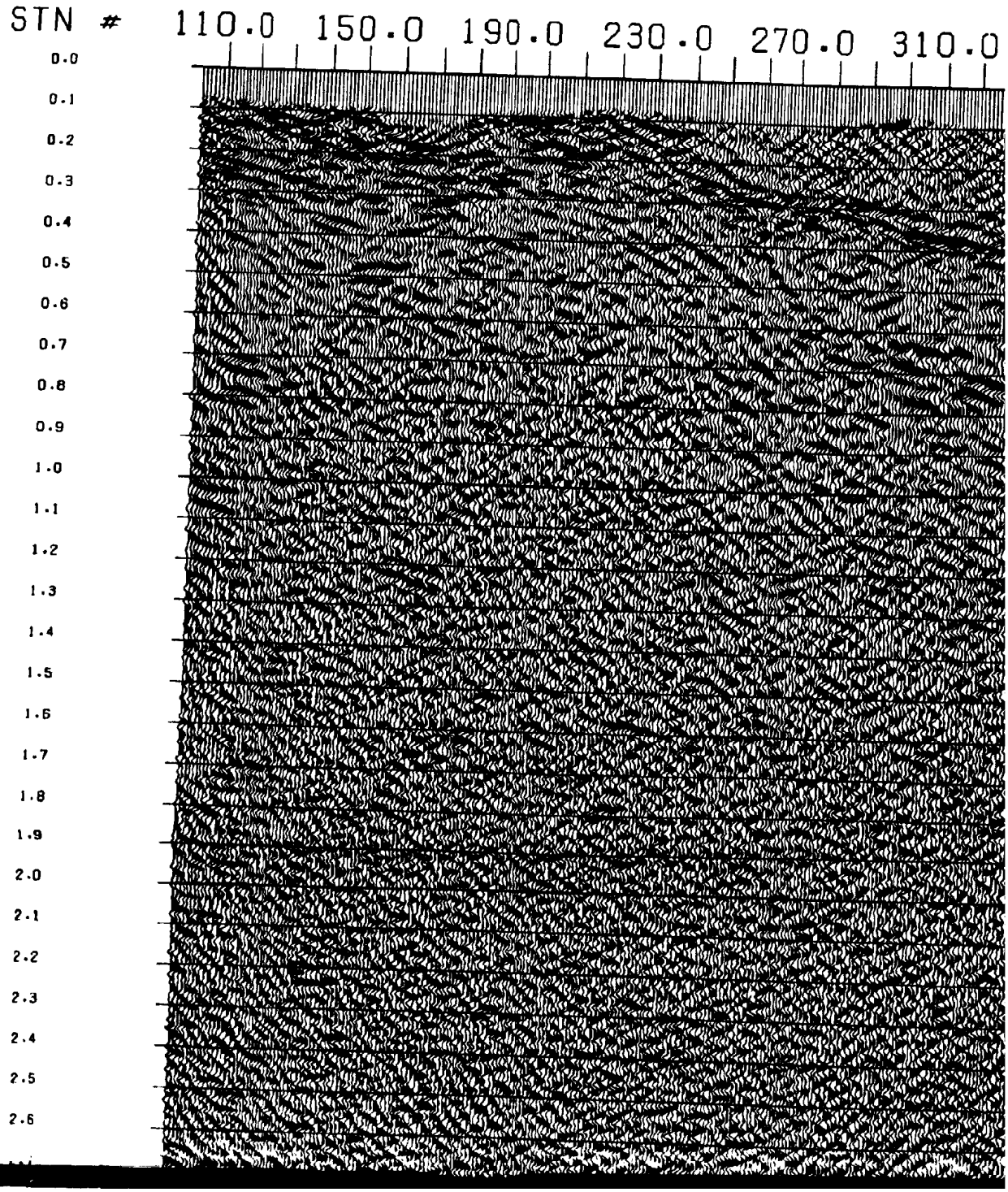

previously. Note
to figure 3.21. In
identified. The
r is not clear.

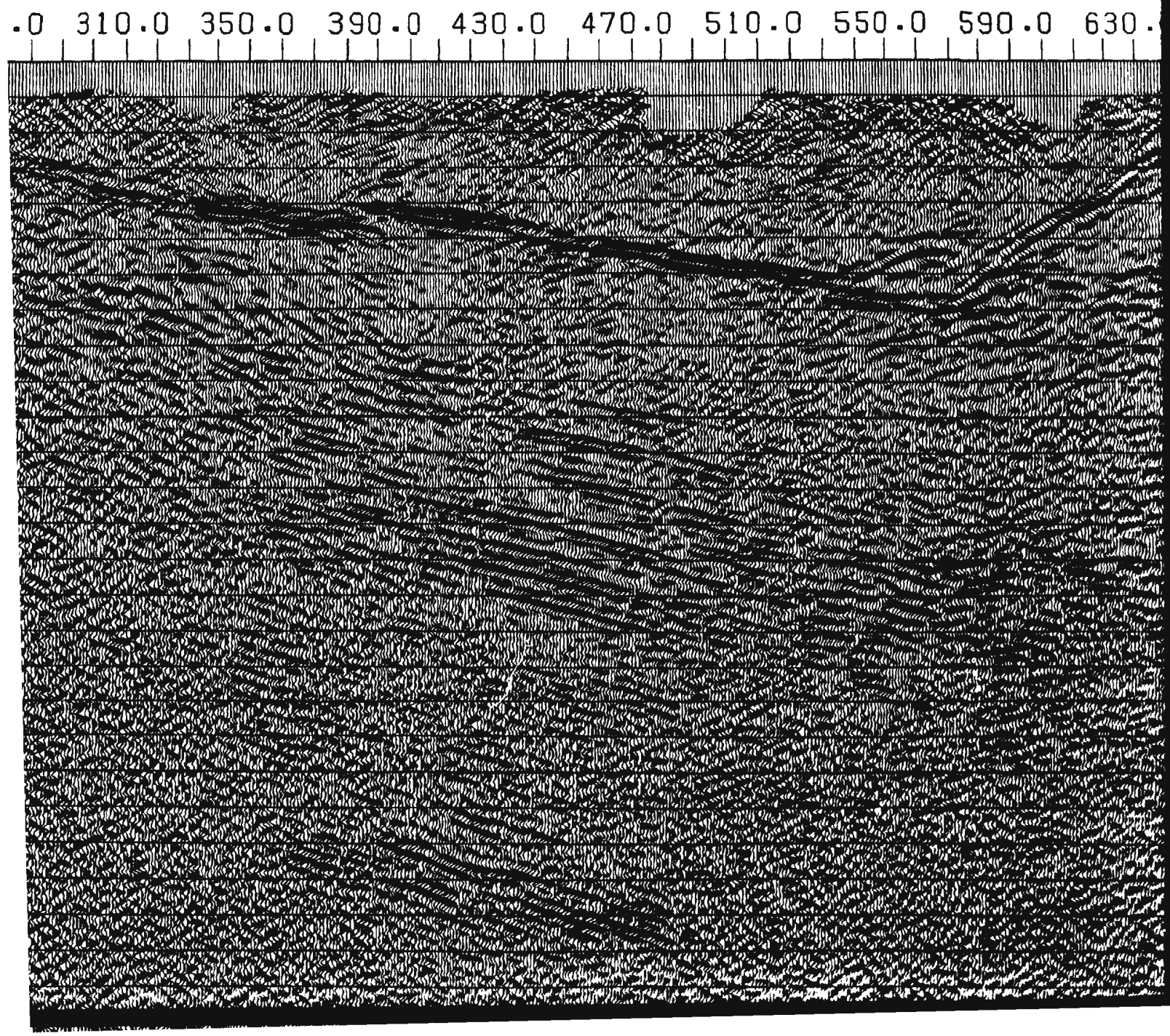

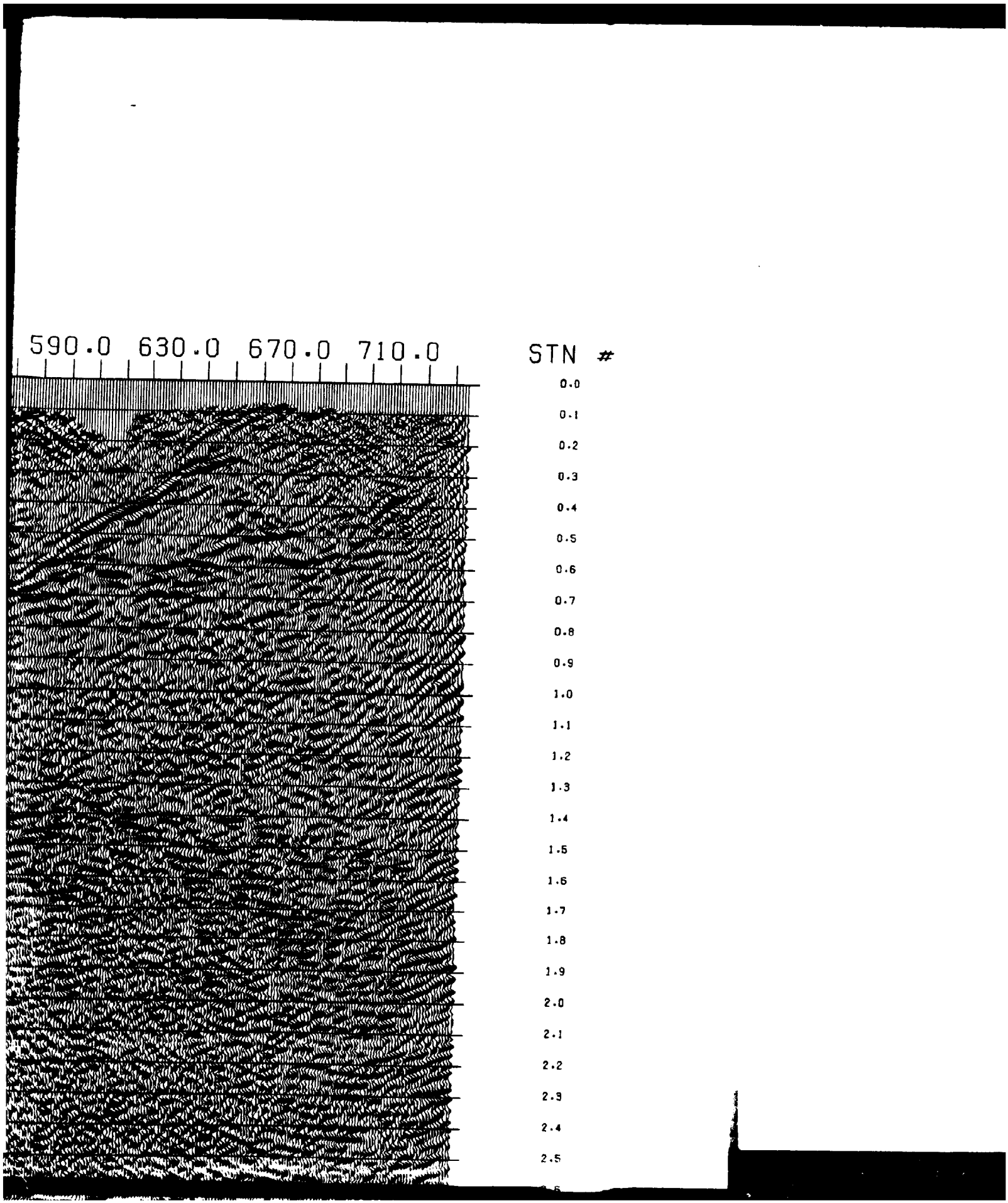
590.0
630.0
670.0
710.0
STN #
0.0
0.1
0.2
0.3
0.4
0.5
0.6
0.7
0.8
0.9
1.0
1.1
1.2
1.3
1.4
1.5
1.6
1.7
1.8
1.9
2.0
2.1
2.2
2.3
2.4
2.5

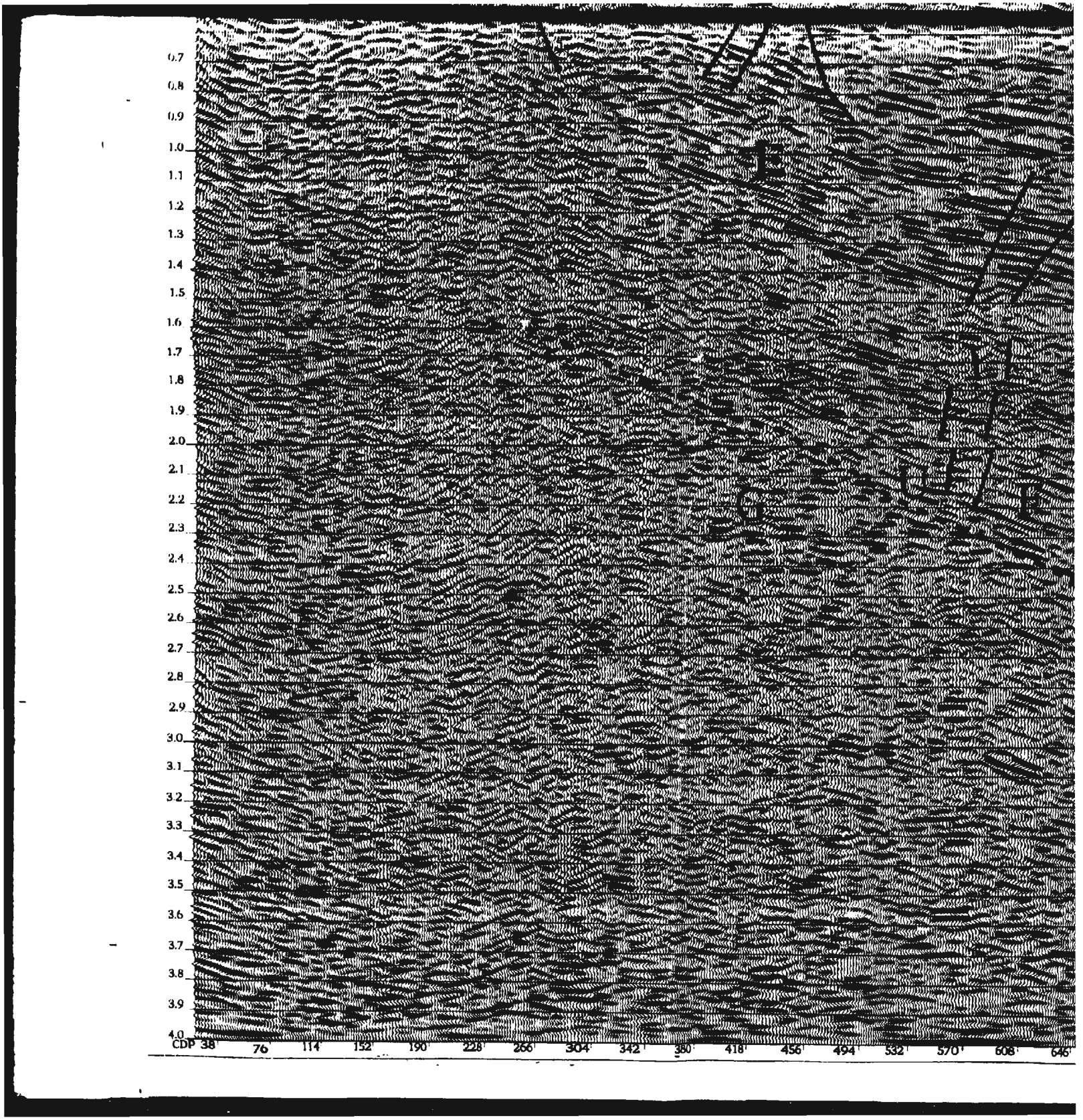
0.7
0.8
0.9
1.0
1.1
1.2
1.3
1.4
1.5
1.6
1.7
1.8
1.9
2.0
2.1
2.2
2.3
2.4
2.5
2.6
2.7
2.8
2.9
3.0
3.1
3.2
3.3
3.4
3.5
3.6
3.7
3.8
3.9
4.0
CDP 38
76
114
152
190
228
266
304
342
380
418
456
494
532
570
608
646

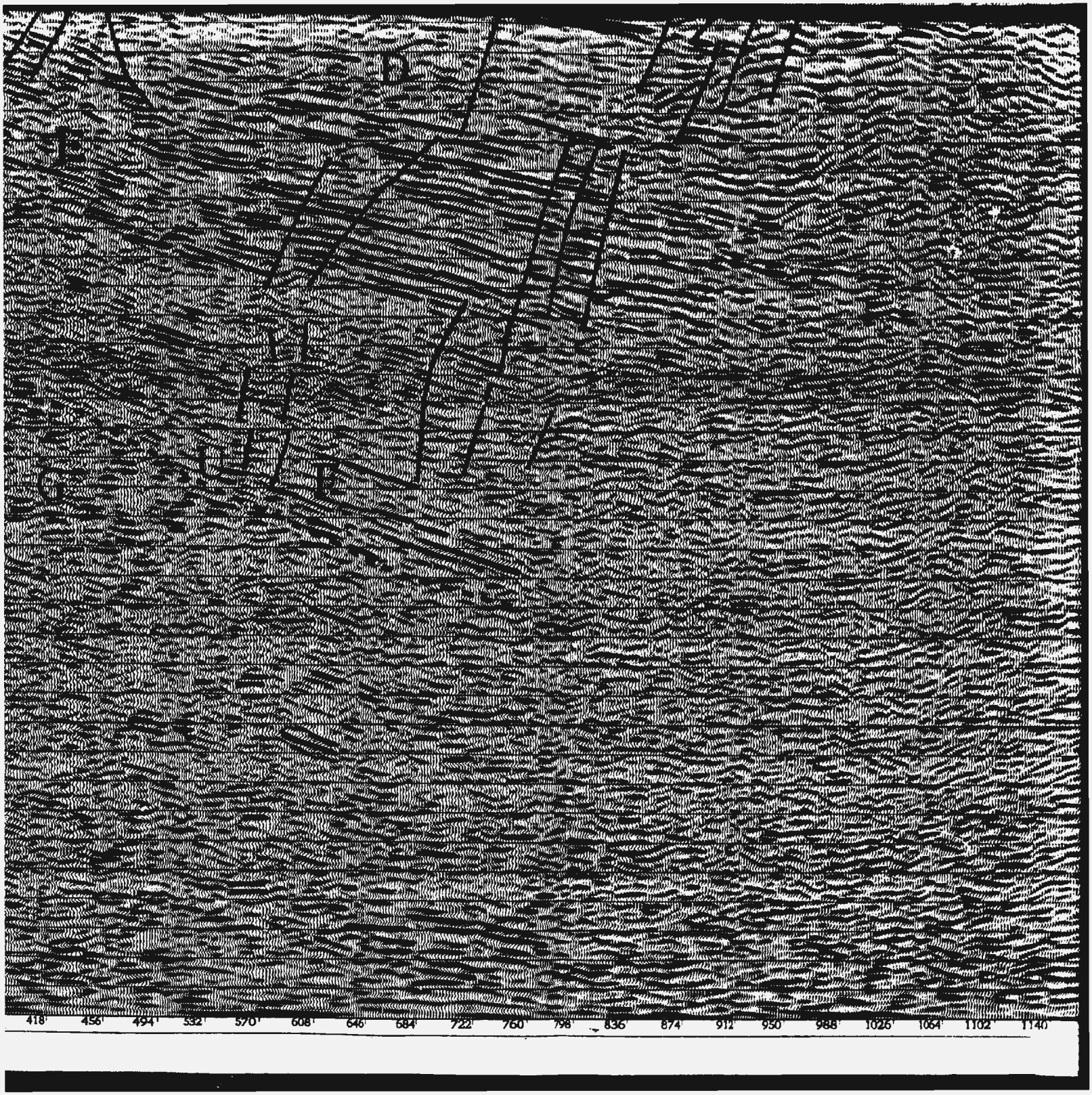
418'
456'
494'
532'
570'
608'
646'
684'
722'
760'
798'
836'
874'
912'
950'
988'
1026'
1064'
1102'
1140'

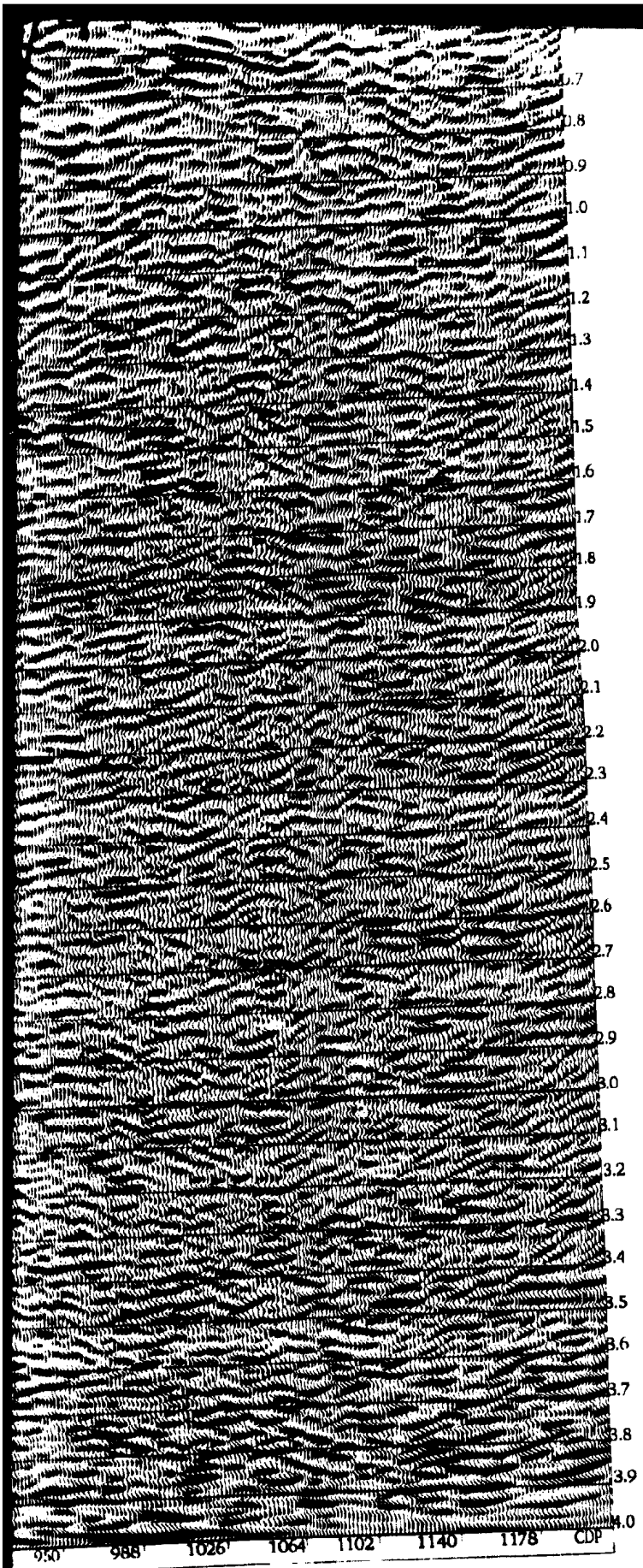
0.7
0.8
0.9
1.0
1.1
1.2
1.3
1.4
1.5
1.6
1.7
1.8
1.9
2.0
2.1
2.2
2.3
2.4
2.5
2.6
2.7
2.8
2.9
3.0
3.1
3.2
3.3
3.4
3.5
3.6
3.7
3.8
3.9
4.0
950
988
1026
1064
1102
1140
1178
CDP

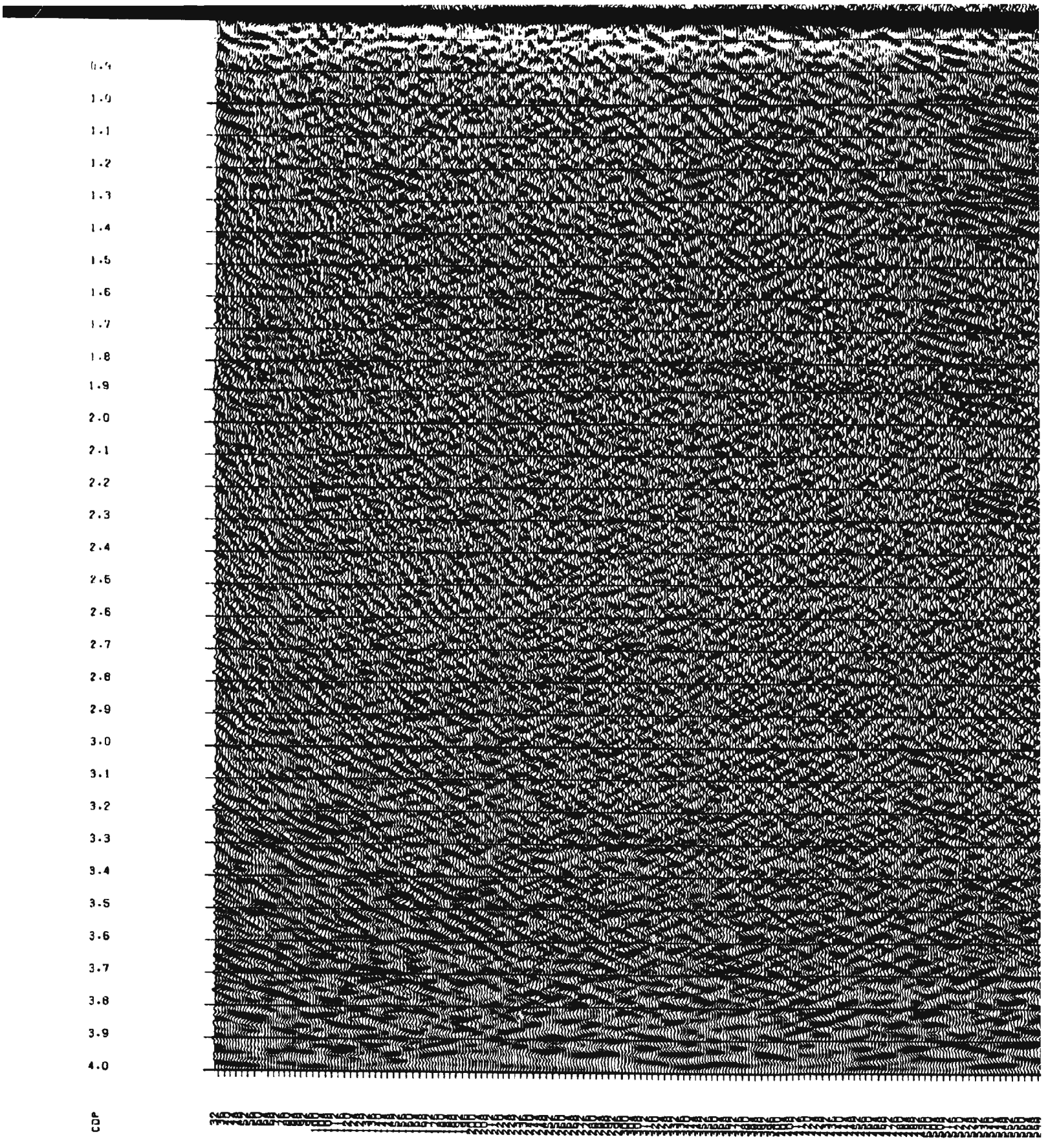
1.0
1.1
1.2
1.3
1.4
1.5
1.6
1.7
1.8
1.9
2.0
2.1
2.2
2.3
2.4
2.5
2.6
2.7
2.8
2.9
3.0
3.1
3.2
3.3
3.4
3.5
3.6
3.7
3.8
3.9
4.0
CDP

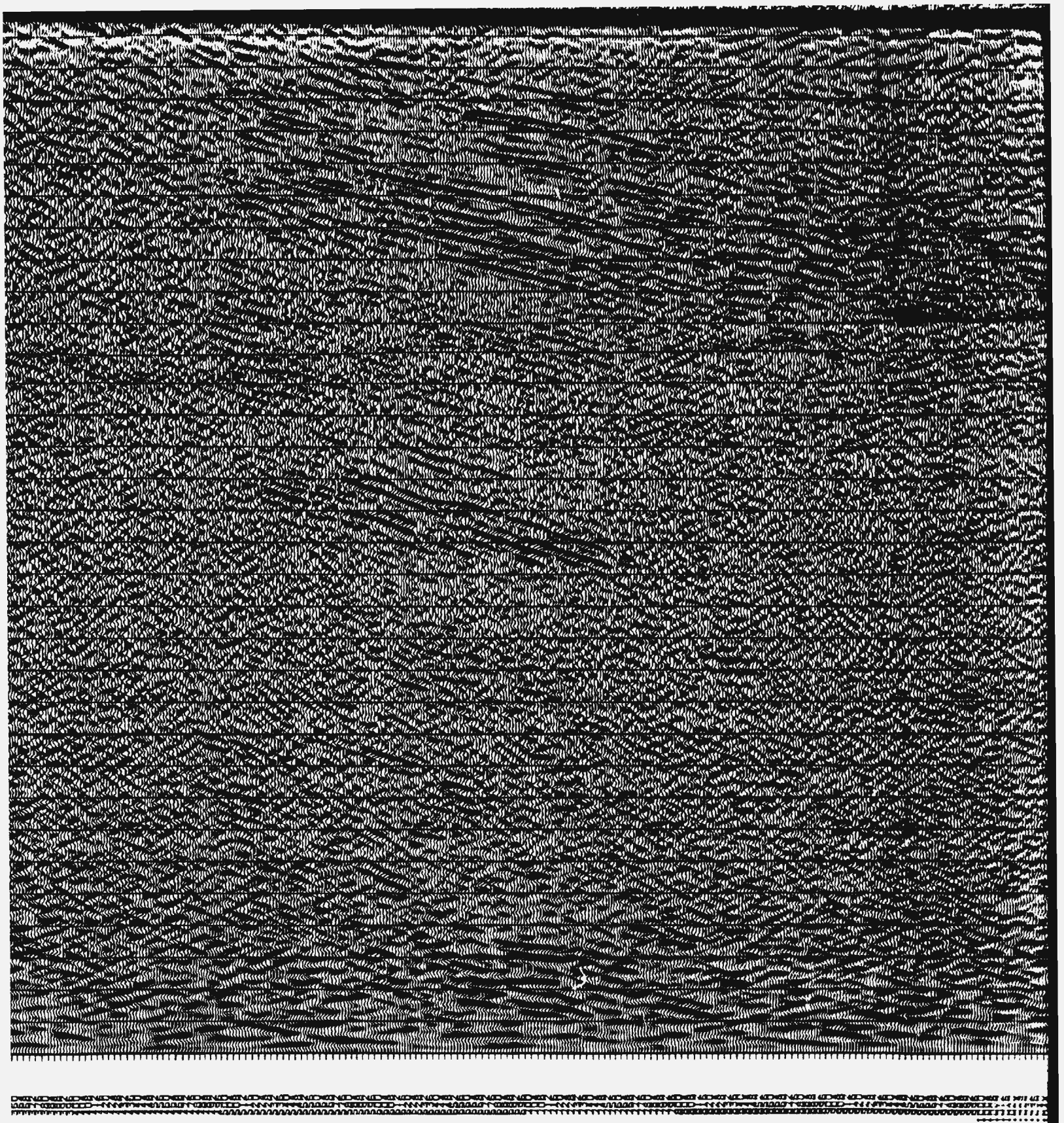

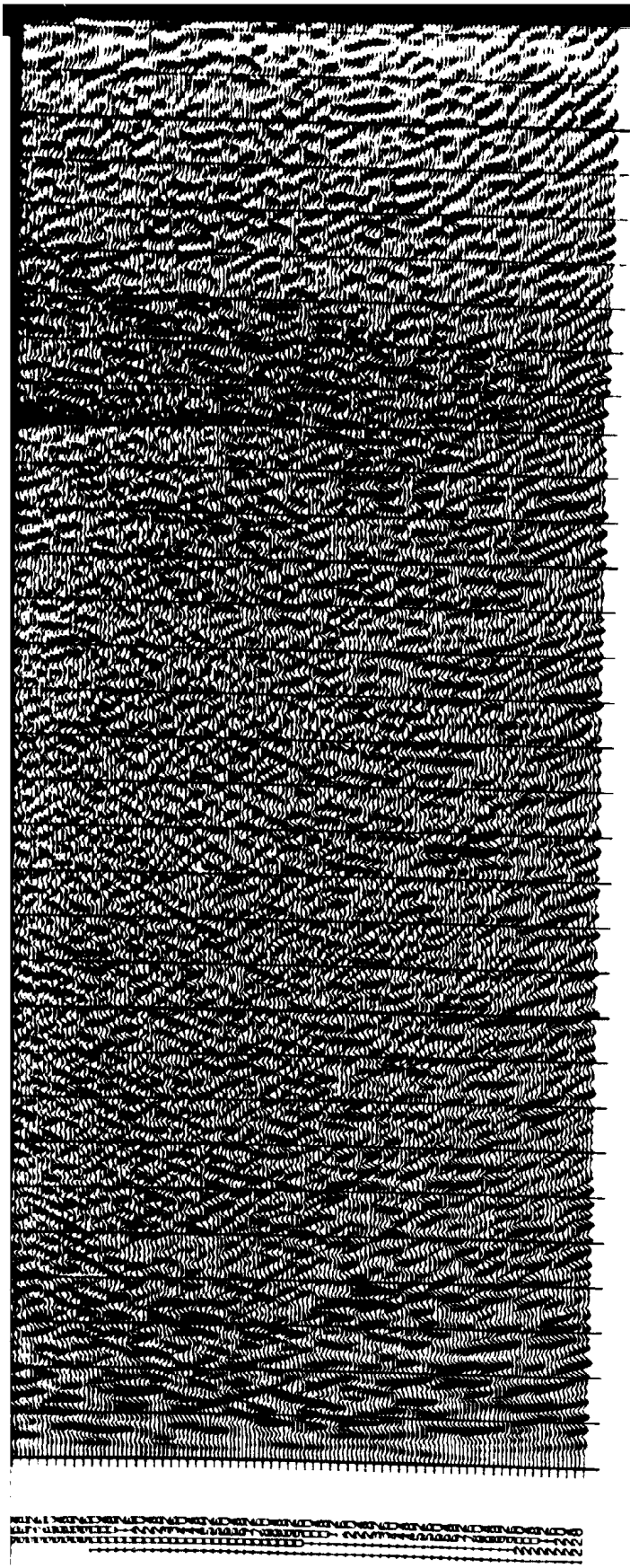

0.9
1.0
1.1
1.2
1.3
1.4
1.5
1.6
1.7
1.8
1.9
2.0
2.1
2.2
2.3
2.4
2.5
2.6
2.7
2.8
2.9
3.0
3.1
3.2
3.3
3.4
3.5
3.6
3.7
3.8
3.9
4.0

CDP

Figure 3.16.
stack proces

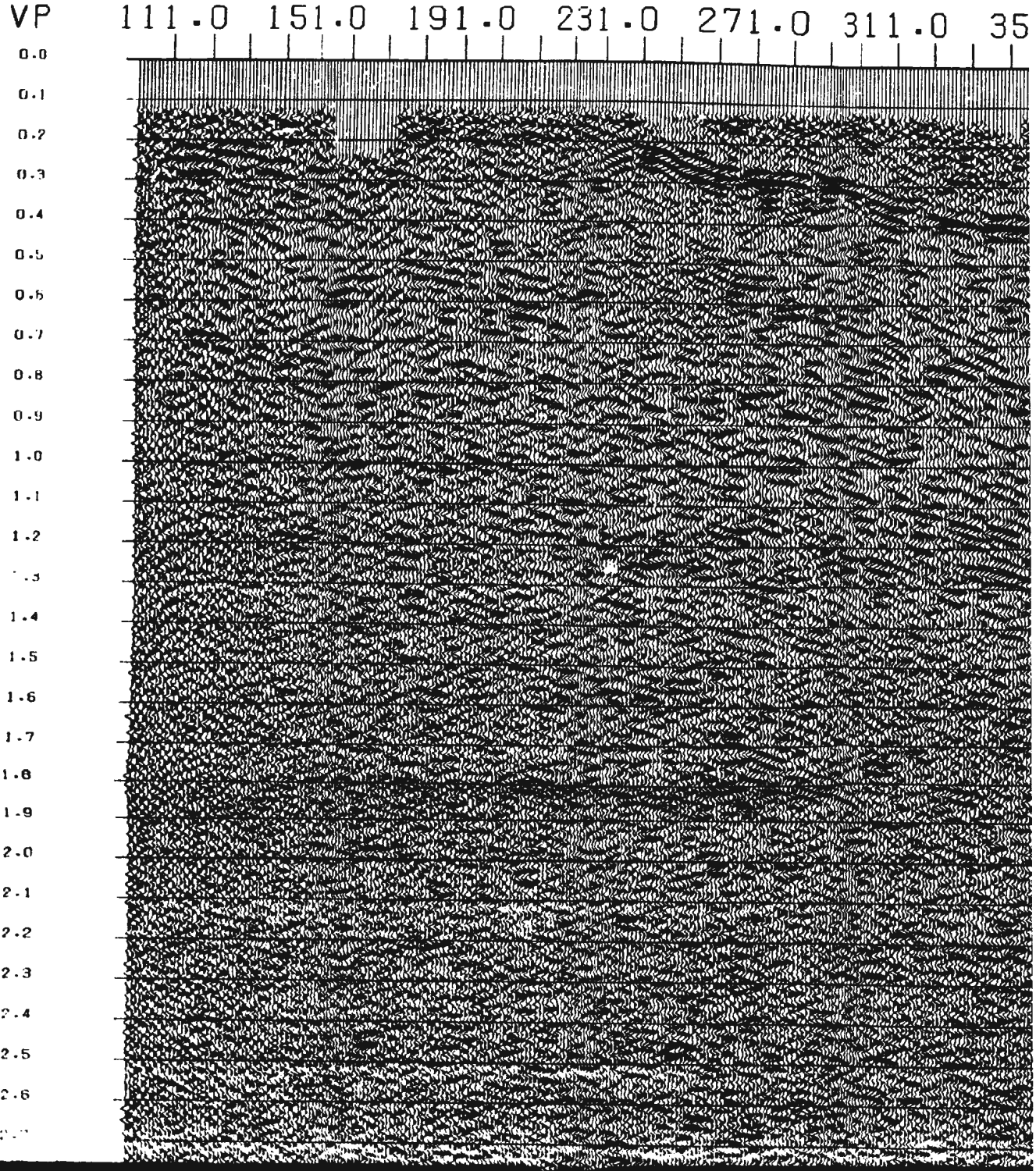

Figure 3.16. Stacked section after DMO correction, with no post stack processing.

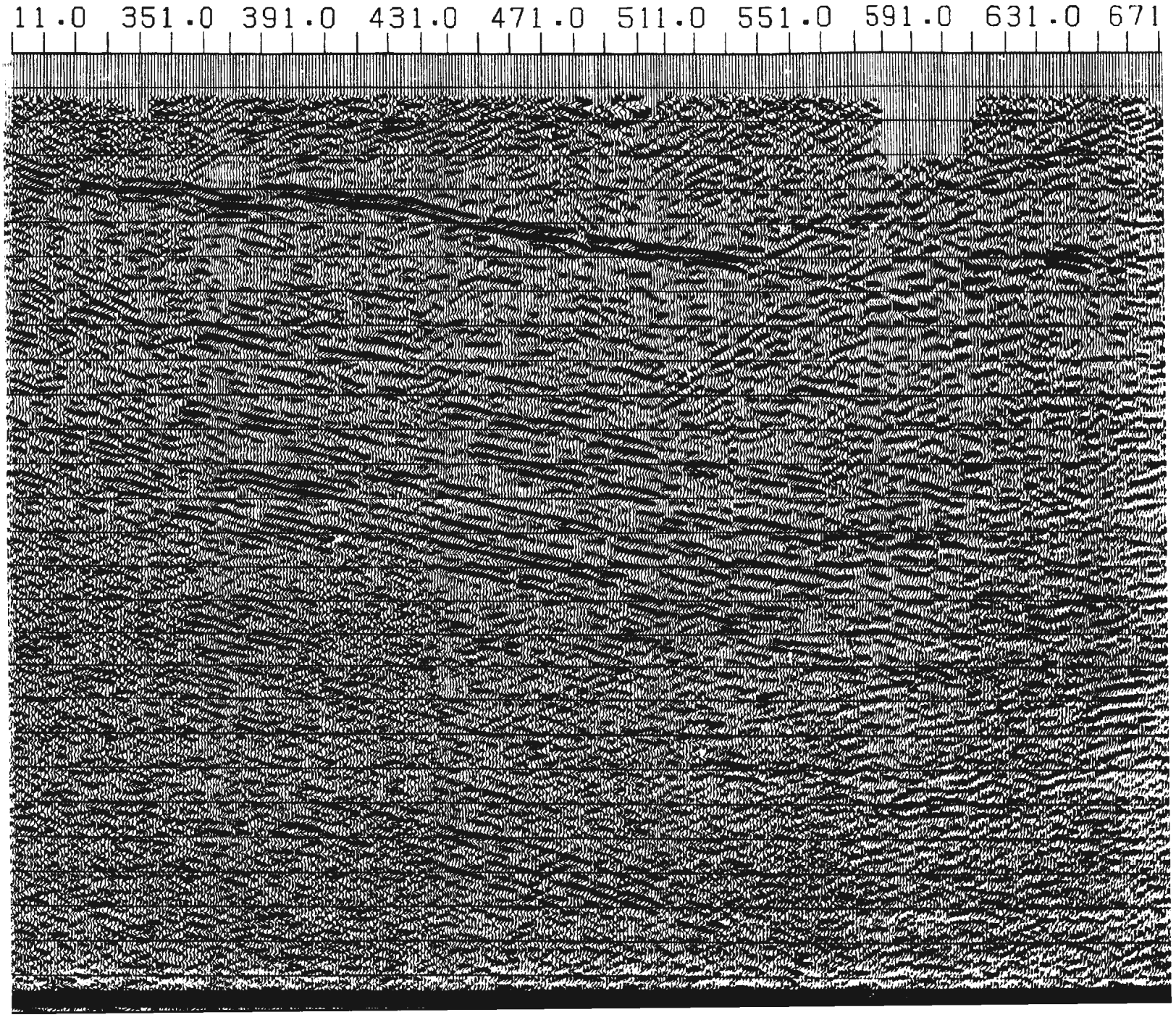

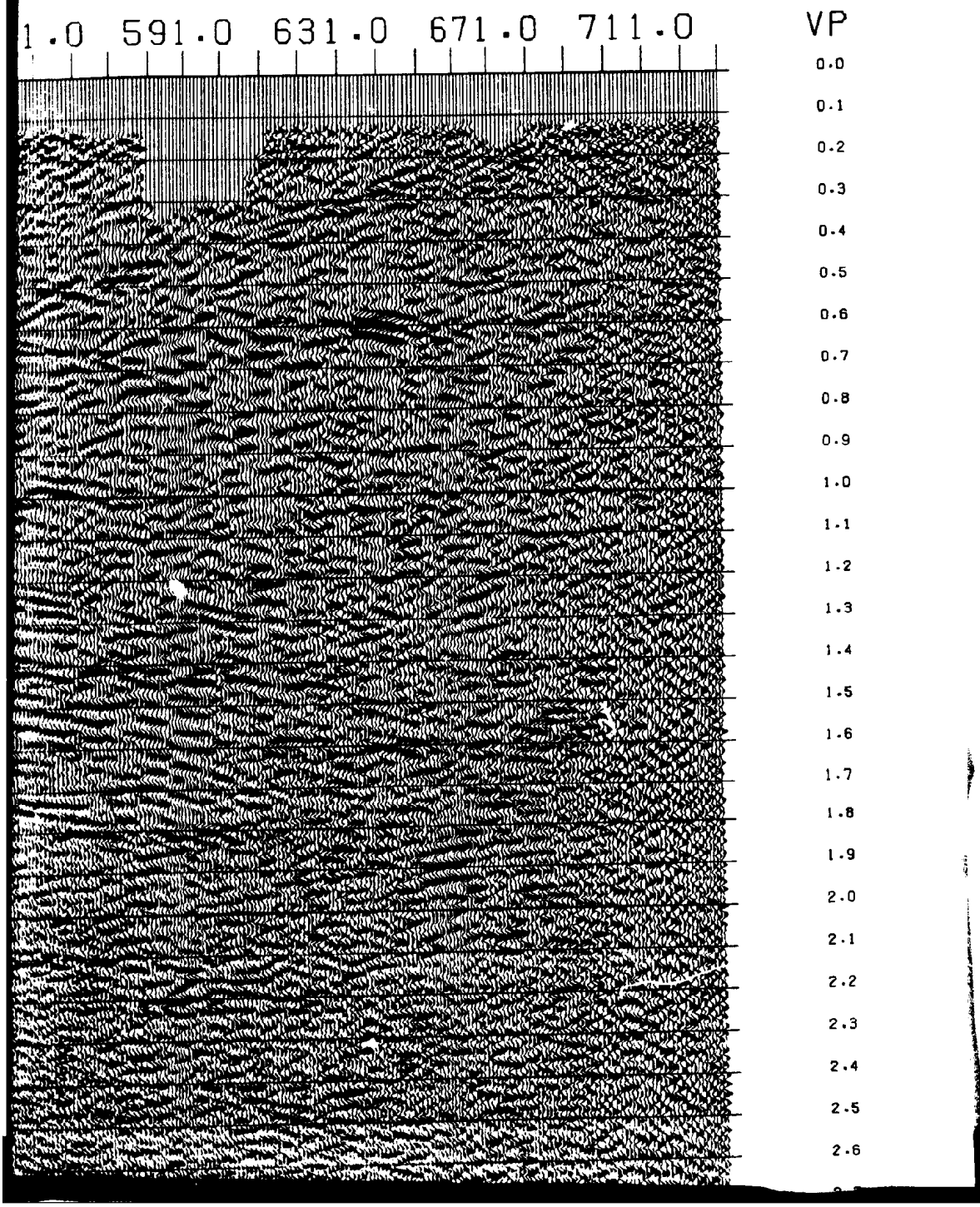

VP

0.0
0.1
0.2
0.3
0.4
0.5
0.6
0.7
0.8
0.9
1.0
1.1
1.2
1.3
1.4
1.5
1.6
1.7
1.8
1.9
2.0
2.1
2.2
2.3
2.4
2.5
2.6

Figure 3.12. Velo

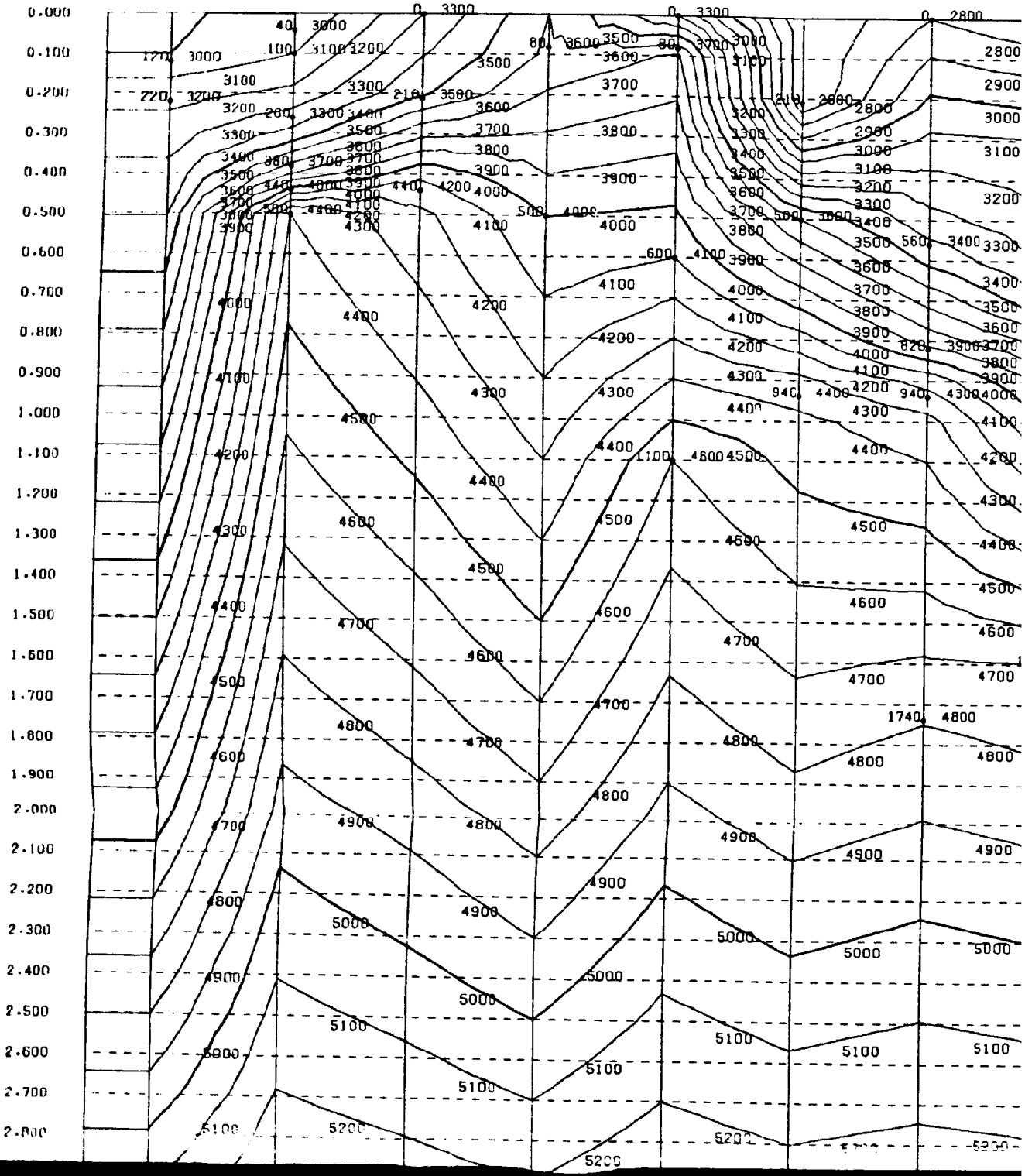

elocity field contours after DMO correction.

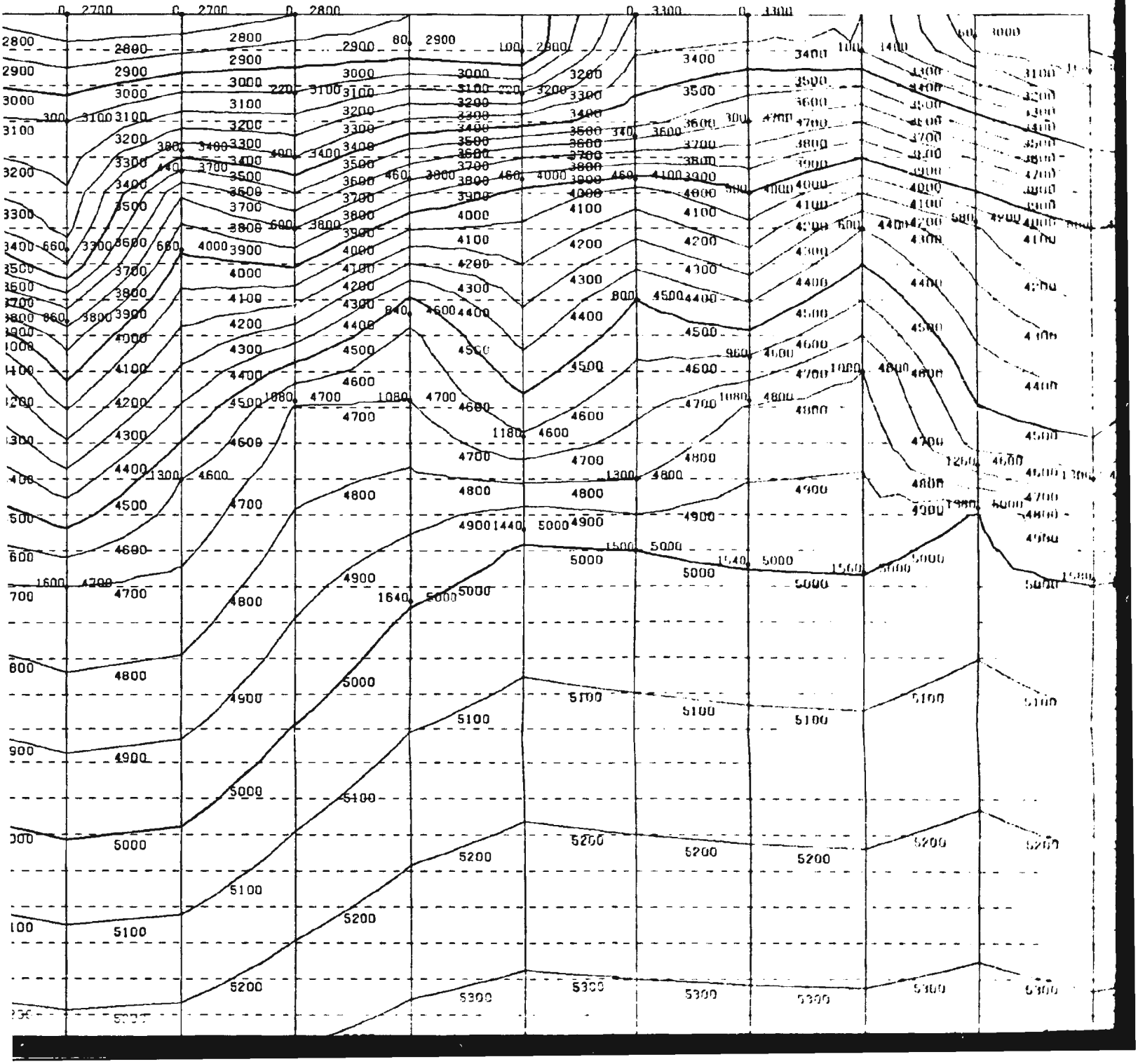

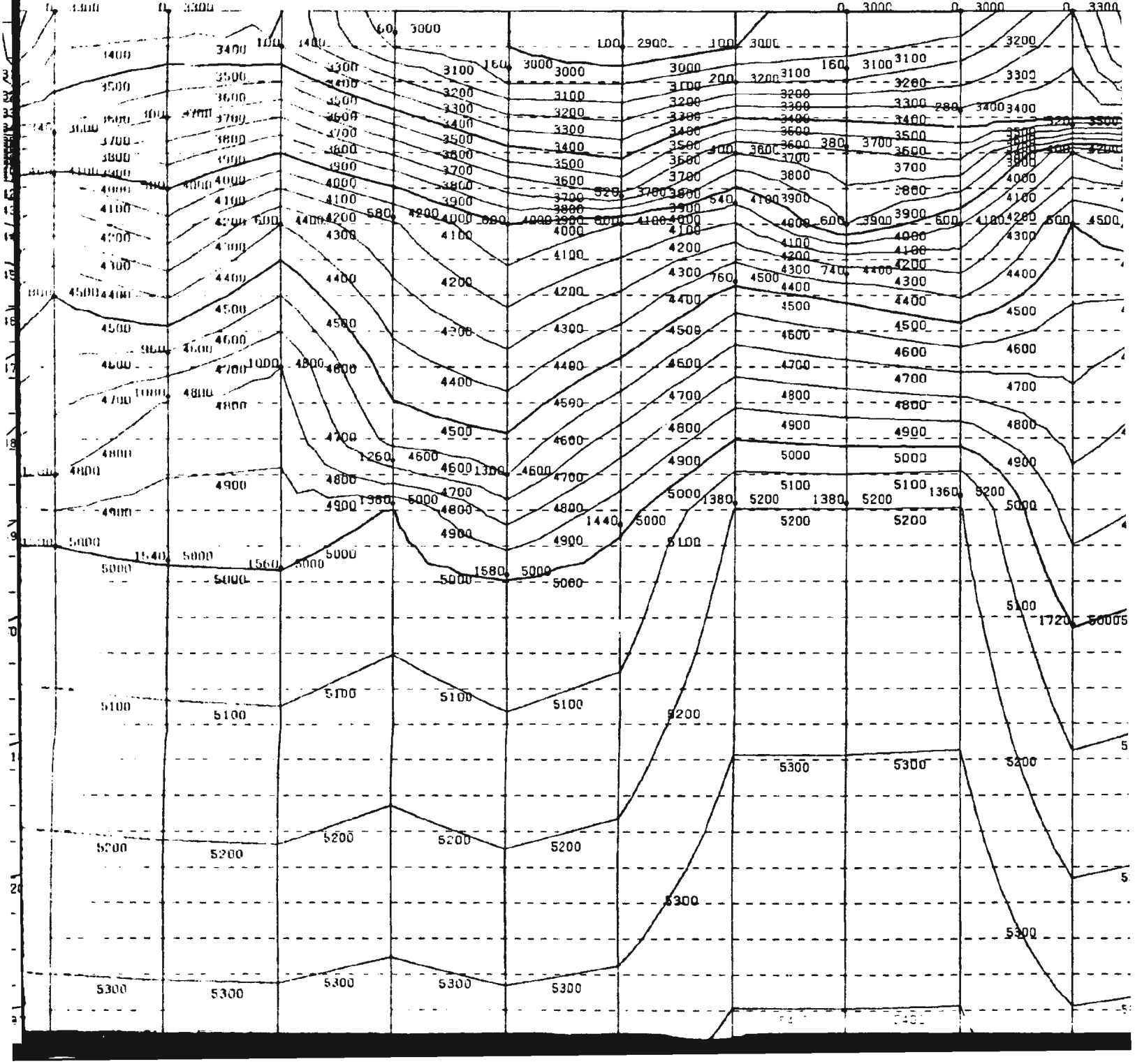

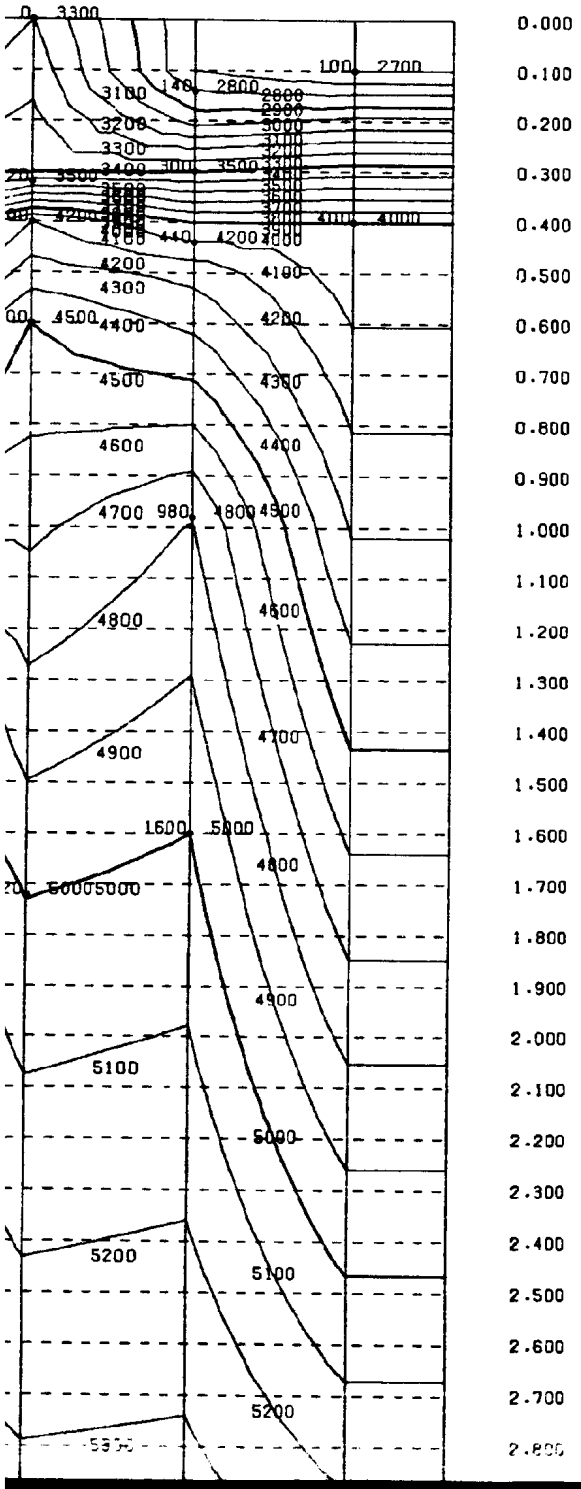
0.000
0.100
0.200
0.300
0.400
0.500
0.600
0.700
0.800
0.900
1.000
1.100
1.200
1.300
1.400
1.500
1.600
1.700
1.800
1.900
2.000
2.100
2.200
2.300
2.400
2.500
2.600
2.700
2.800

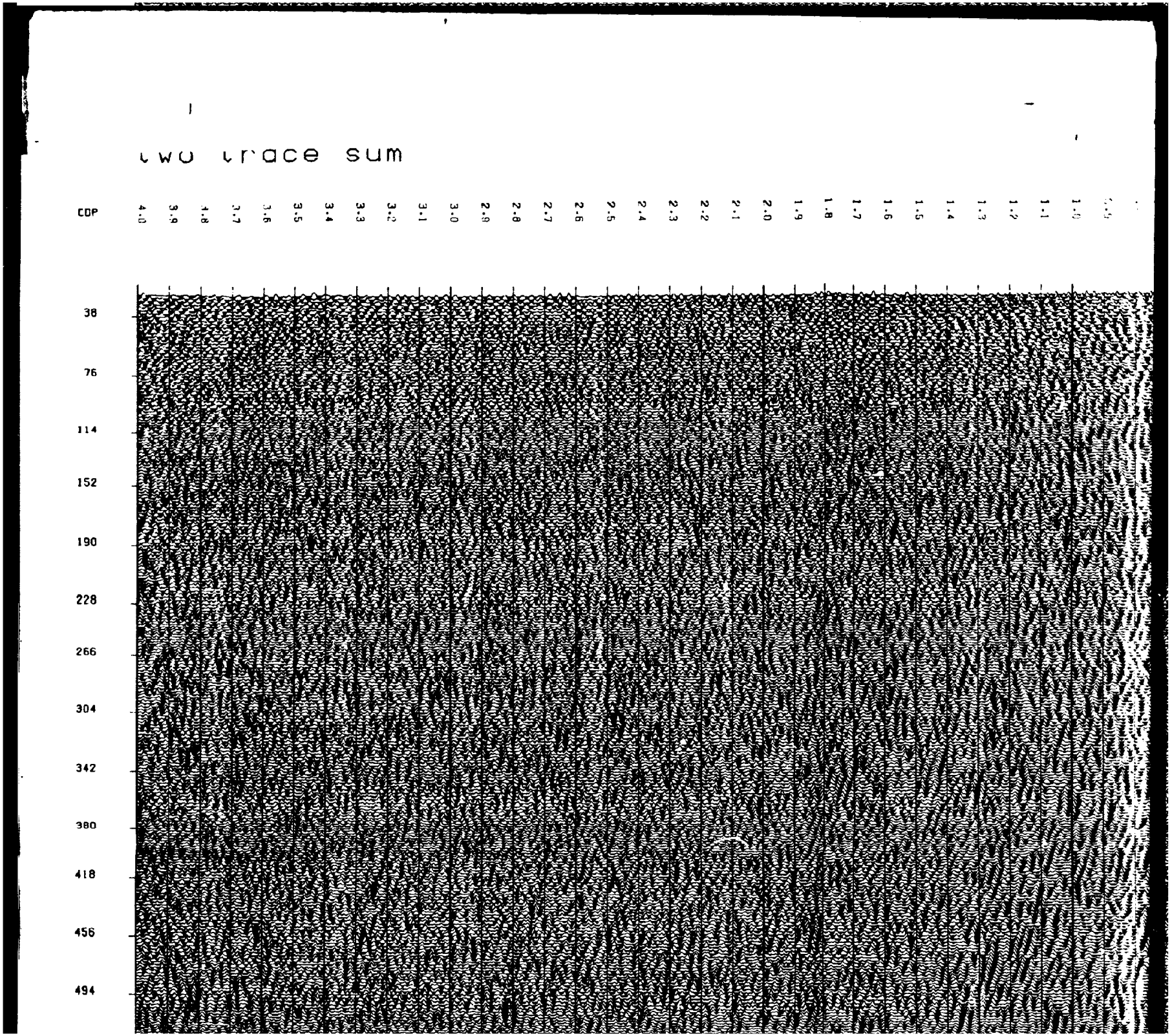
two trace sum
CDP
4.0
3.9
3.8
3.7
3.6
3.5
3.4
3.3
3.2
3.1
3.0
2.9
2.8
2.7
2.6
2.5
2.4
2.3
2.2
2.1
2.0
1.9
1.8
1.7
1.6
1.5
1.4
1.3
1.2
1.1
1.0
38
76
114
152
190
228
266
304
342
380
418
456
494

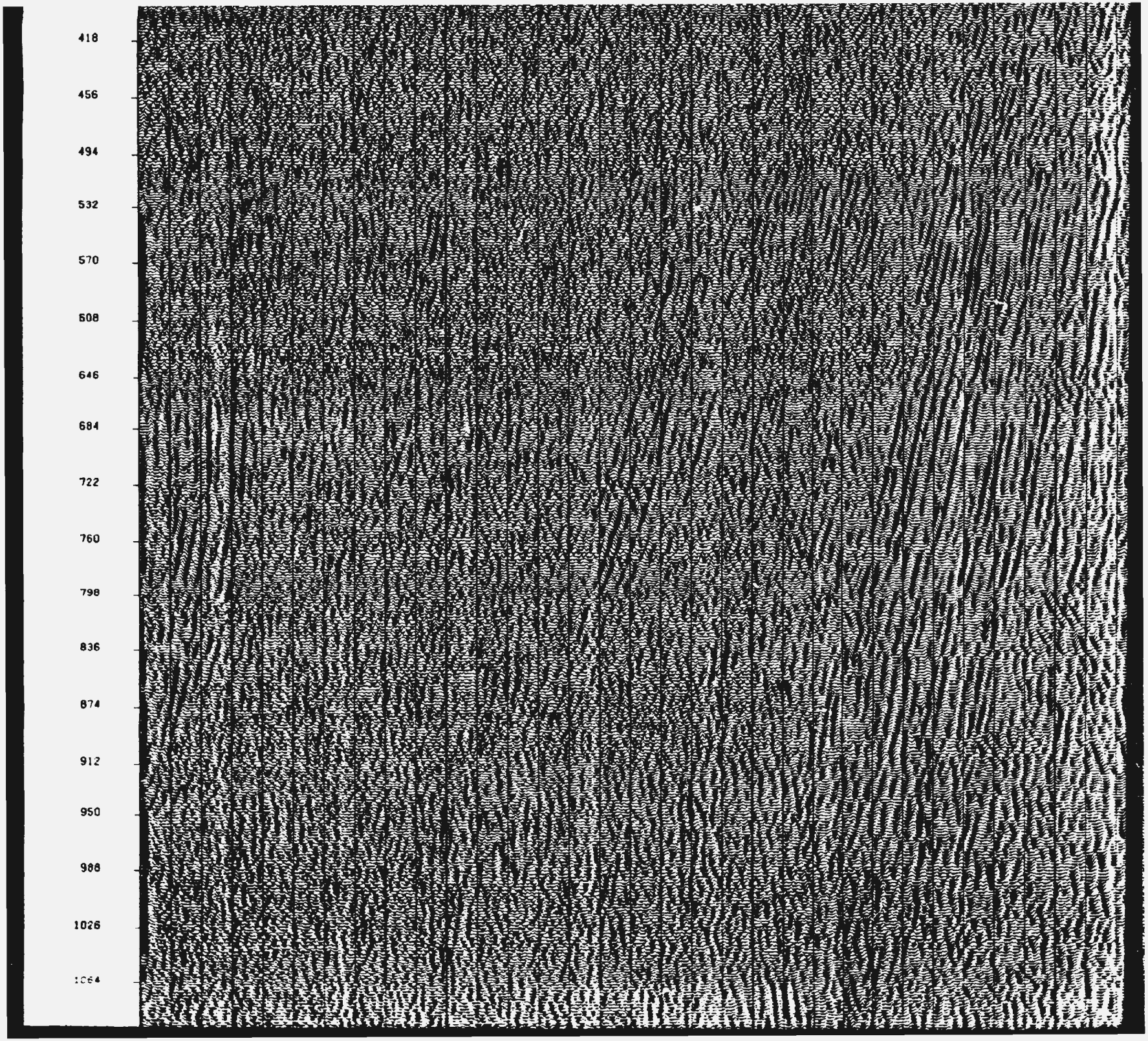
418
456
494
532
570
608
646
684
722
760
798
836
874
912
950
988
1026
1064

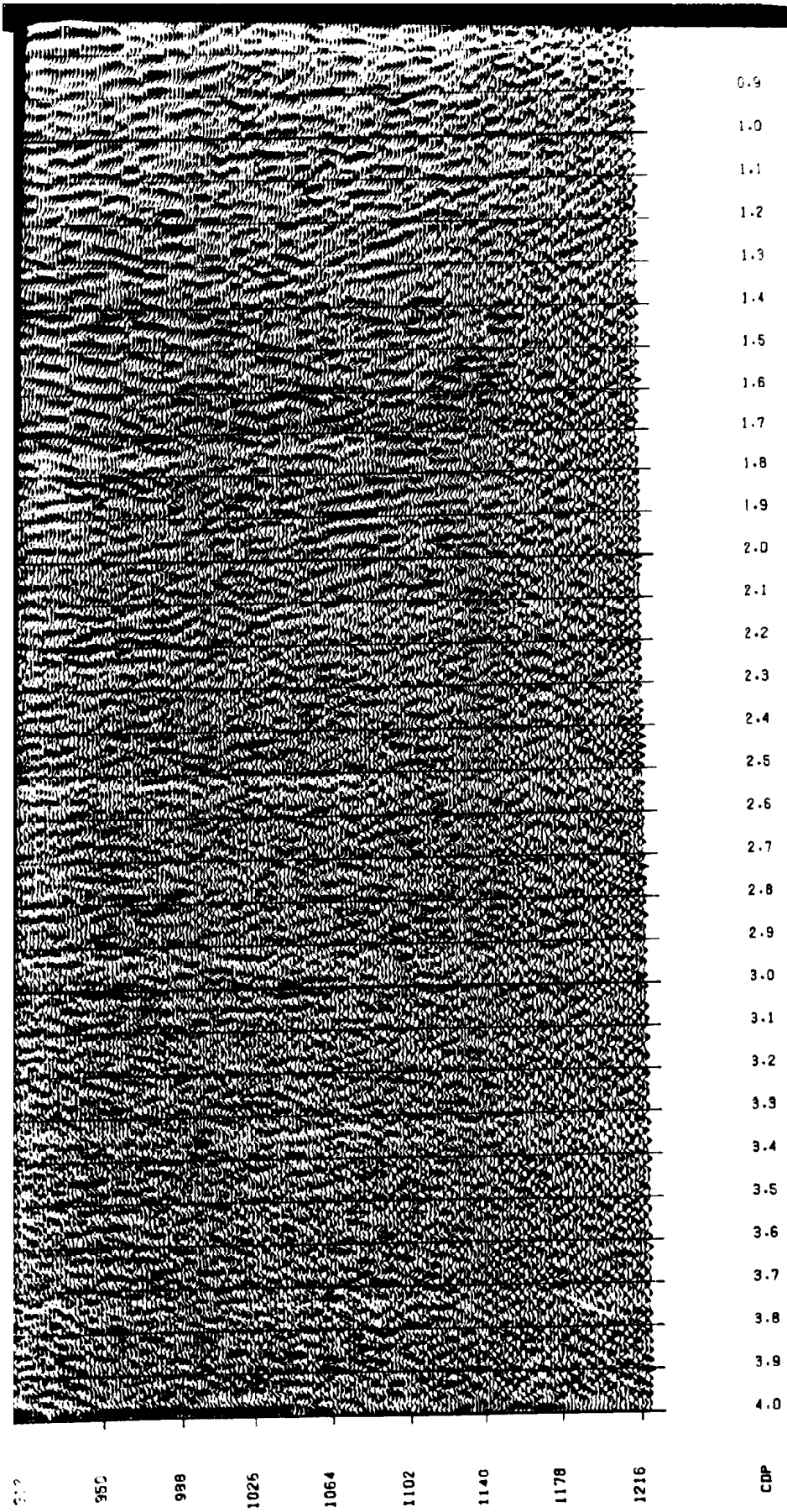
0.9
1.0
1.1
1.2
1.3
1.4
1.5
1.6
1.7
1.8
1.9
2.0
2.1
2.2
2.3
2.4
2.5
2.6
2.7
2.8
2.9
3.0
3.1
3.2
3.3
3.4
3.5
3.6
3.7
3.8
3.9
4.0
950
988
1026
1064
1102
1140
1178
1216
CDP

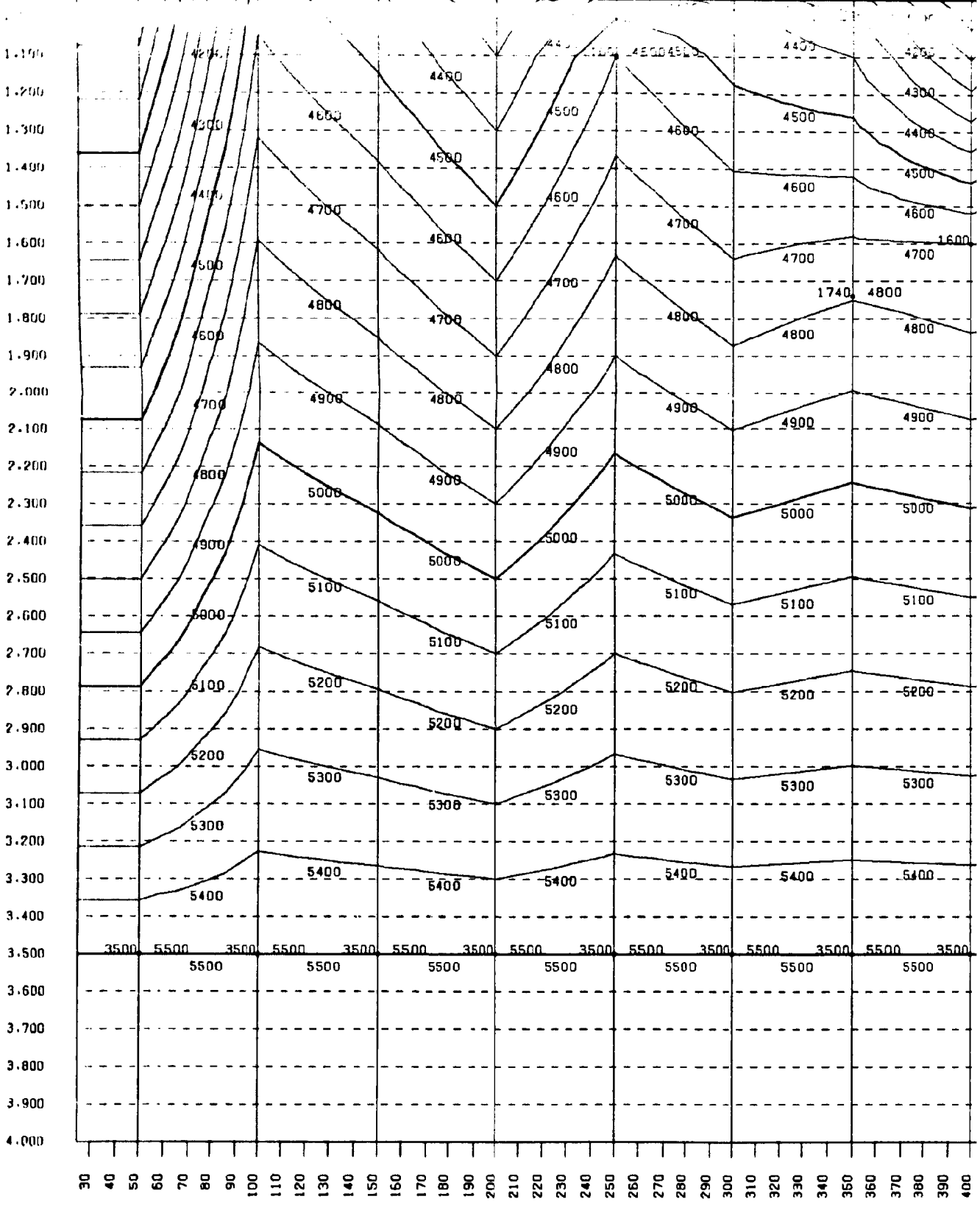
1.100
1.200
1.300
1.400
1.500
1.600
1.700
1.800
1.900
2.000
2.100
2.200
2.300
2.400
2.500
2.600
2.700
2.800
2.900
3.000
3.100
3.200
3.300
3.400
3.500
3.600
3.700
3.800
3.900
4.000
30 40 50 60 70 80 90 100 110 120 130 140 150 160 170 180 190 200 210 220 230 240 250 260 270 280 290 300 310 320 330 340 350 360 370 380 390 400
3500 5500
5500

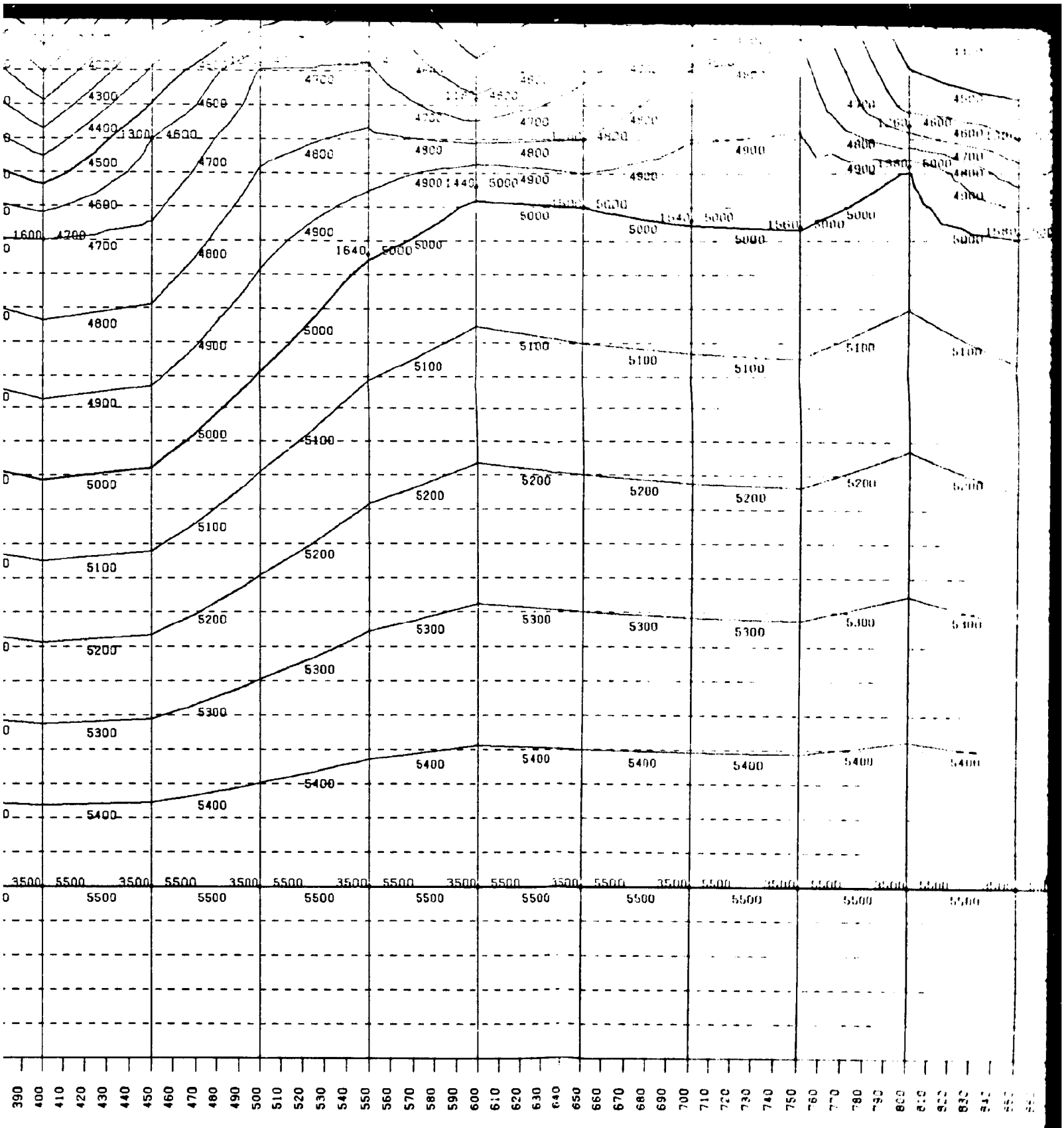

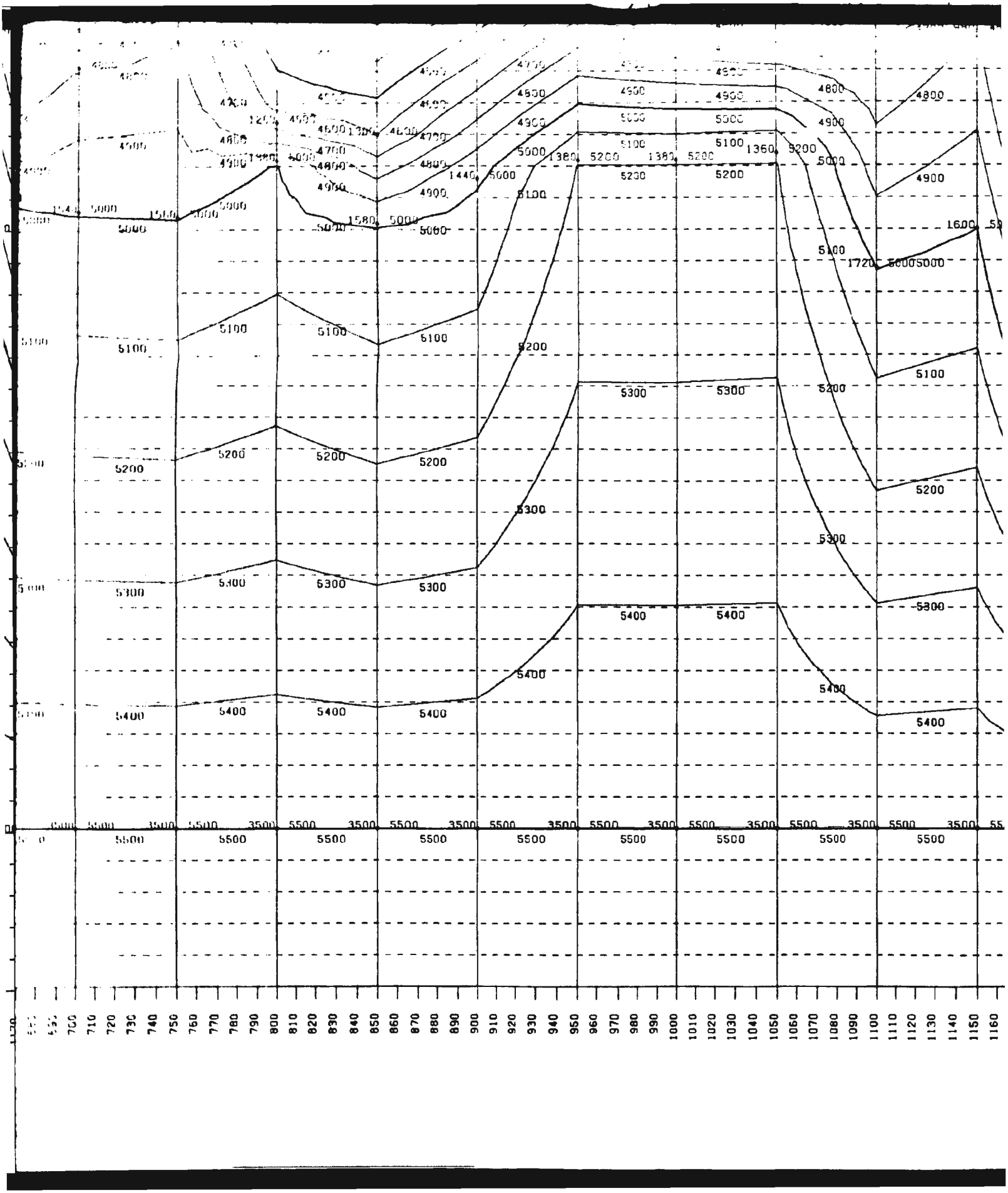

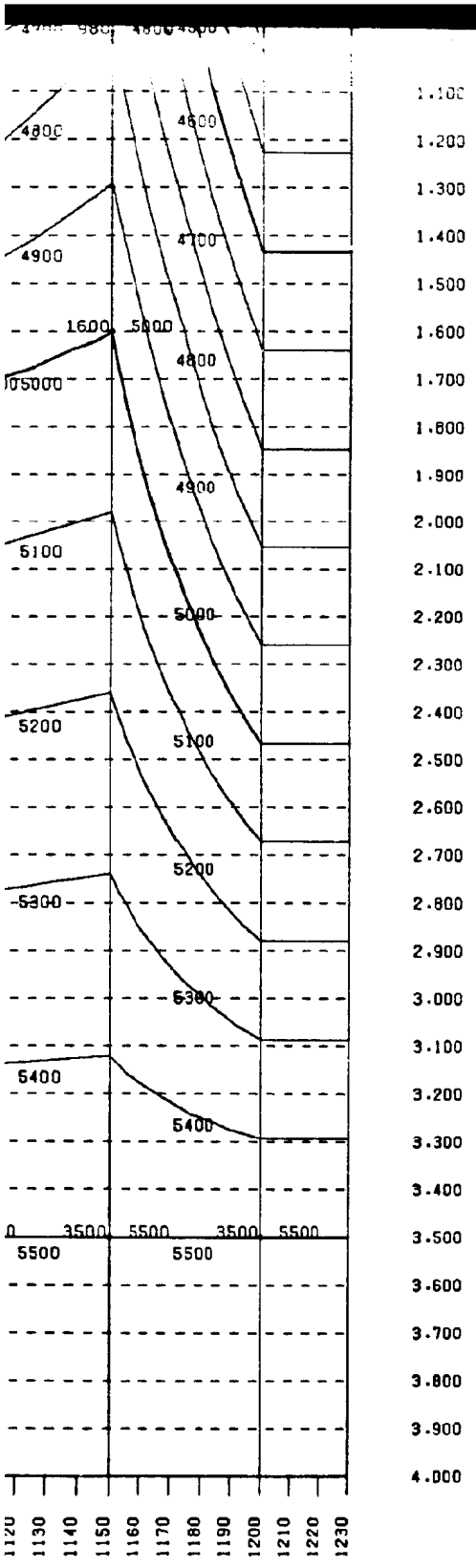
4800
4600
4900
4700
1600
5000
4800
05000
4900
5100
5000
5200
5100
5200
5300
5300
5400
5400
0
3500
5500
3500
5500
5500
5500
1120
1130
1140
1150
1160
1170
1180
1190
1200
1210
1220
1230
1.100
1.200
1.300
1.400
1.500
1.600
1.700
1.800
1.900
2.000
2.100
2.200
2.300
2.400
2.500
2.600
2.700
2.800
2.900
3.000
3.100
3.200
3.300
3.400
3.500
3.600
3.700
3.800
3.900
4.000

Figure 3.11. Velocity field

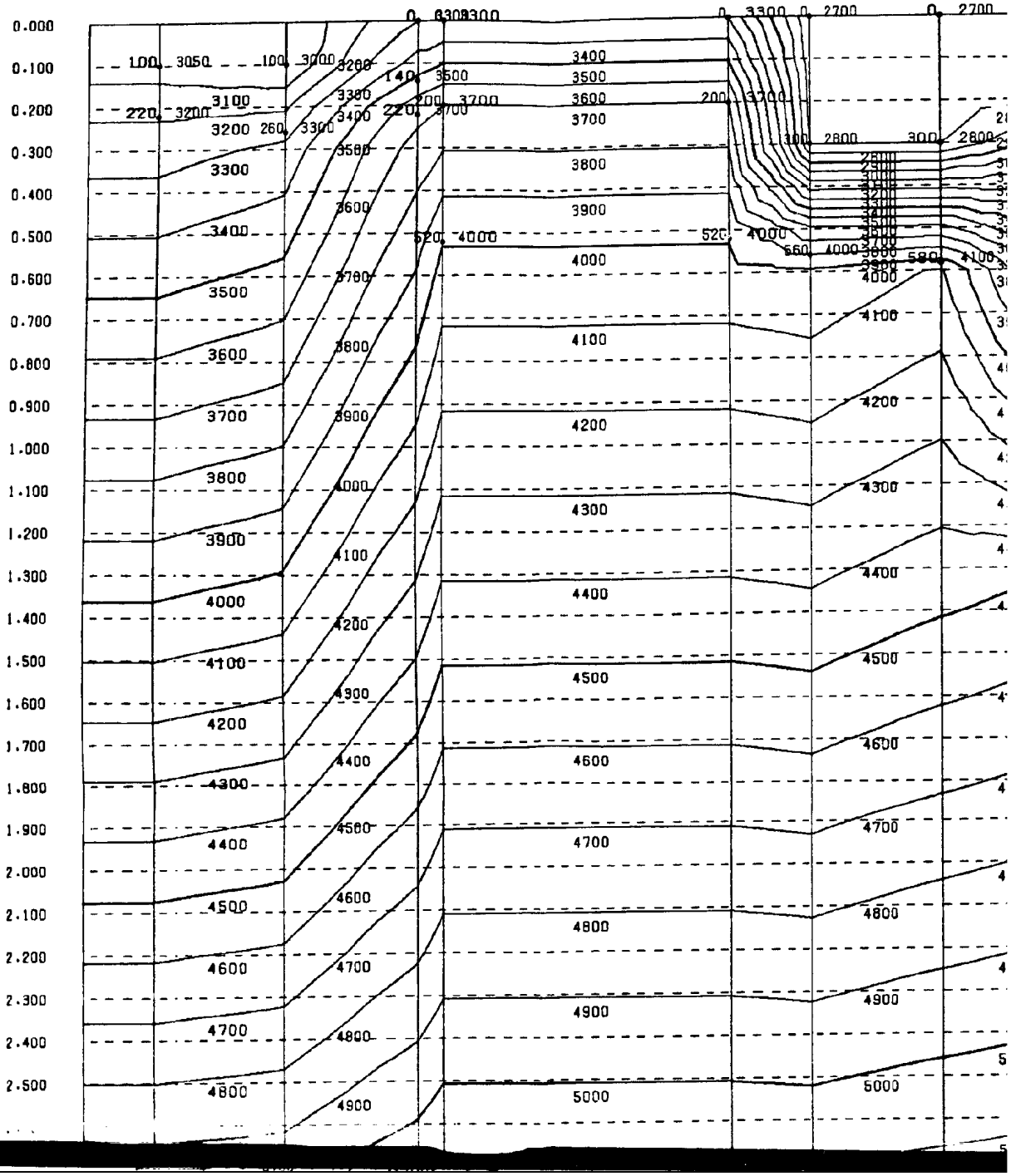

city field contours before DMO correction.

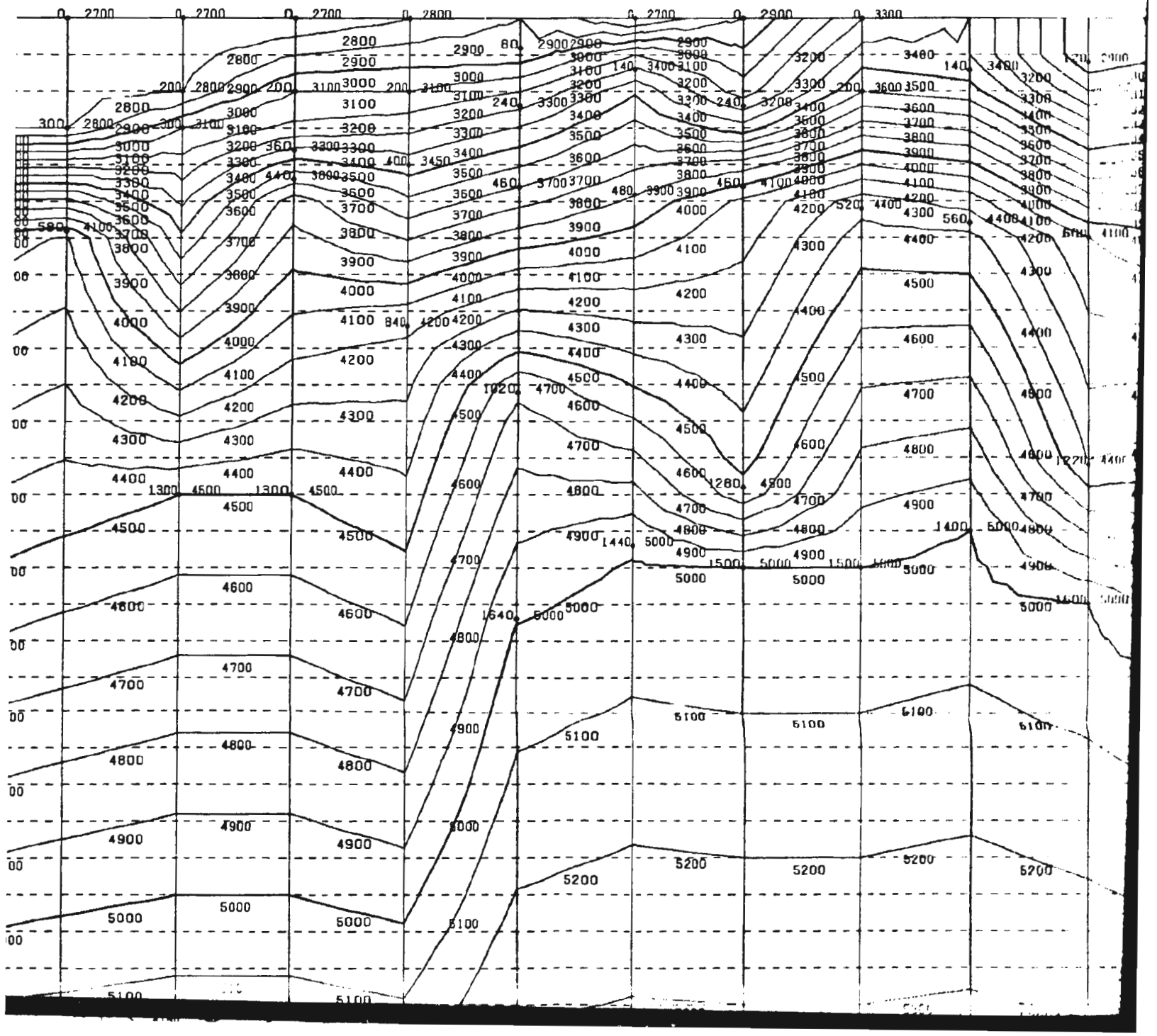

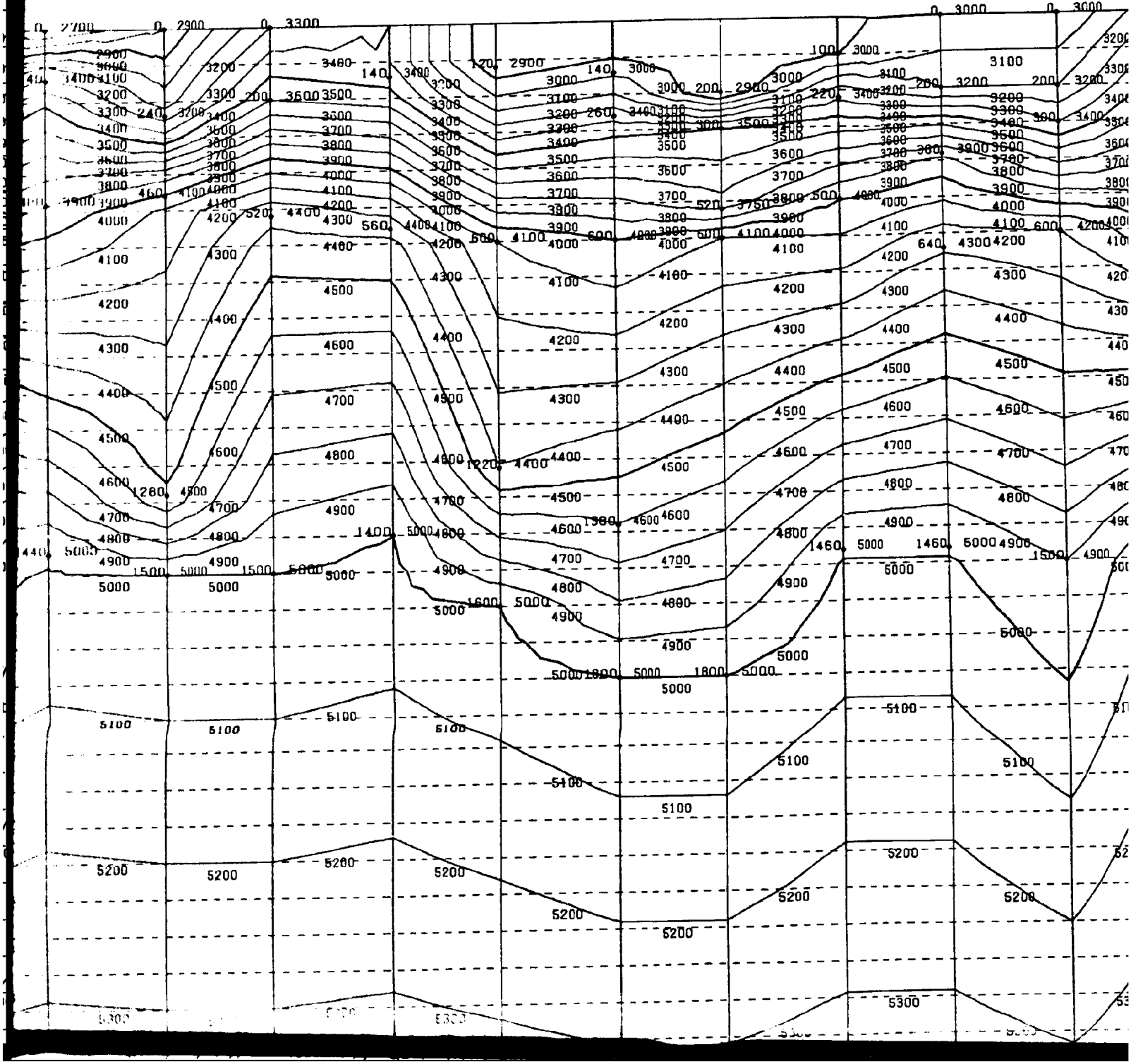

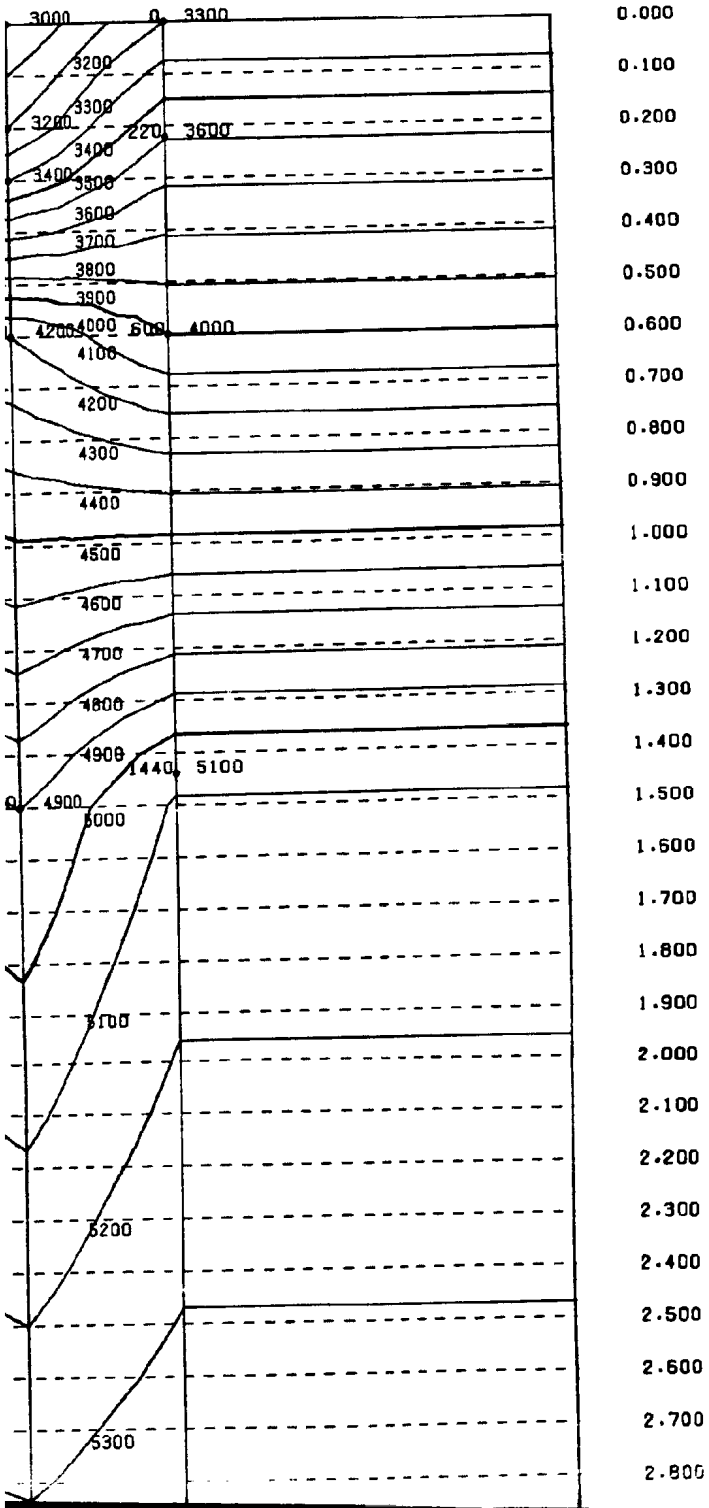
3000
0
3300
3200
3300
3200
220
3600
3400
3400
3500
3600
3700
3800
3900
4200
4000
600
4000
4100
4200
4300
4400
4500
4600
4700
4800
4900
1440
5100
4900
5000
5100
5200
5300
0.000
0.100
0.200
0.300
0.400
0.500
0.600
0.700
0.800
0.900
1.000
1.100
1.200
1.300
1.400
1.500
1.600
1.700
1.800
1.900
2.000
2.100
2.200
2.300
2.400
2.500
2.600
2.700
2.800

ost-nmo
gc

Figure 3.22. Final display of the processed profile. This is a 1:1 section if an average velocity of 4 km/s is assumed for the whole section.

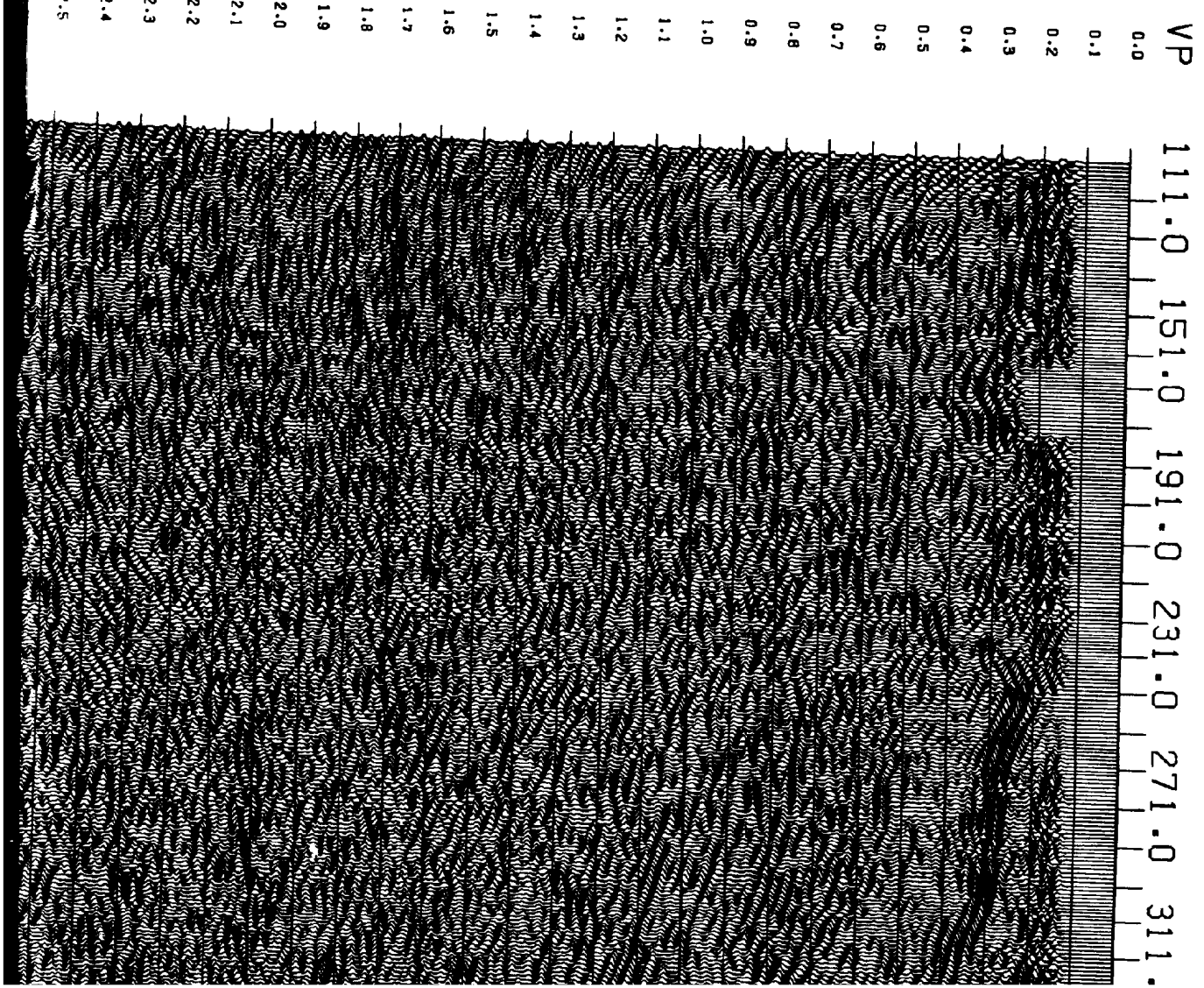

311.0
351.0
391.0
431.0
471.0
511.0
551.0
591.0

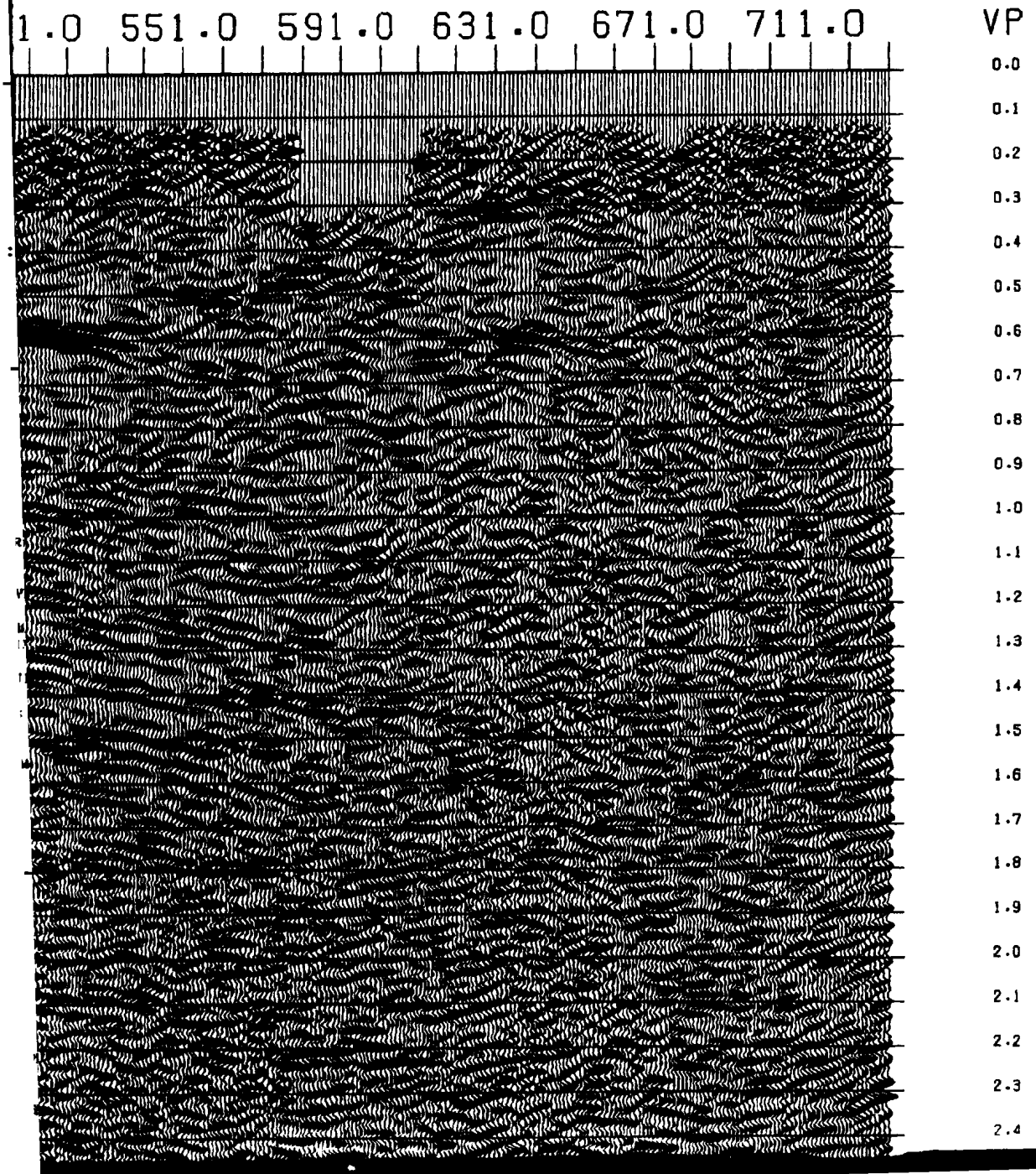

CENTRE FOR

MEMORIAL UN

LINE:

S.P.

AREA:

TITLE

ACQUISITION

SHOT BY:

ENERGY SOURCE:
TYPE:
SWEEP PARAMETE
SWEEP LENGTH:
SOURCE ARRAY:
SHOTPOINT INTER

RECEIVING ARRANGE
FOLD OF RECORD
GROUP INTERVAL:
NUMBER OF GROU
STATION GAP AT
GEOPHONES/GROUP

INSTRUMENTATION:
RECORDING SYSTE
PRE-AMP GAIN:
FILTERS:
RECORD FORMAT:
RECORD LENGTH:
SAMPLE RATE:

PROCESSING

PROCESSED BY:

1. APPLICATION OF

2. APPLICATION OF

3. DMO CORRECTION

FOR EARTH RESOURCES RESEARCH

UNIVERSITY OF NEWFOUNDLAND

LINE: ROBINSONS RIVER
(PASTURE ROAD)

L.P. 1 – 318

REA: BAY ST. GEORGE – WESTERN NFLD

ITLE: FINAL STACK

W

ION

CAPILANO GEOPHYSICAL LTD.

CE:

VIBROSEIS

AMETERS: 20 HZ – 90 HZ, 500 MS TAPER

GTH: 8 SECONDS

RAY: 4 OVER 30 M, MOVE UP 8 M

INTERVAL: 40 M

RANGEMENT:

ECORDING: 104 MAXIMUM

ERVAL: 20.0 METRES

GROUPS: 240

P AT SP: 26

GROUP: 12

ION:

SYSTEM: DFS V

AIN: 48 DB

HIGH CUT 128.0 HZ AT 72 DB

MAT: SEG Y, 240 CHANNEL

GTH: 4 SECONDS

E: 2 MS

NG

: CENTRE FOR EARTH RESOURCES RESEARC

MEMORIAL UNIVERSITY OF NEWFOUNDLAND

OF BINNING AND GEOMETRY:
SURVEY DATA SUPPLIED BY CONTRACTOR

OF FIELD STATICS: ELEVATION AND
REFRACTION STATICS
FROM FIRST BREAKS

CTION:

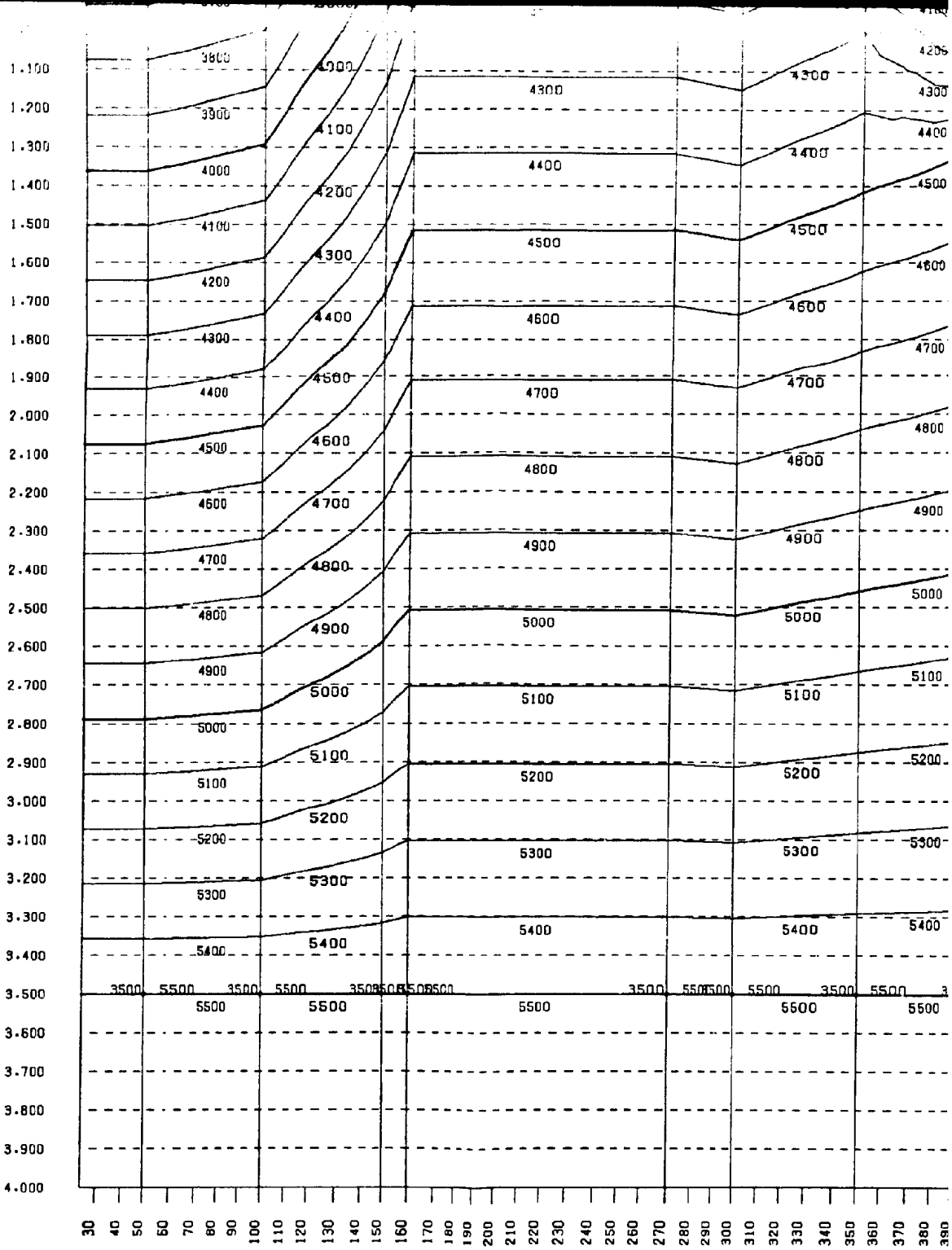
1.100
1.200
1.300
1.400
1.500
1.600
1.700
1.800
1.900
2.000
2.100
2.200
2.300
2.400
2.500
2.600
2.700
2.800
2.900
3.000
3.100
3.200
3.300
3.400
3.500
3.600
3.700
3.800
3.900
4.000
30
40
50
60
70
80
90
100
110
120
130
140
150
160
170
180
190
200
210
220
230
240
250
260
270
280
290
300
310
320
330
340
350
360
370
380
390
3500
5500
4300
4400
4500
4600
4700
4800
4900
5000
5100
5200
5300
5400

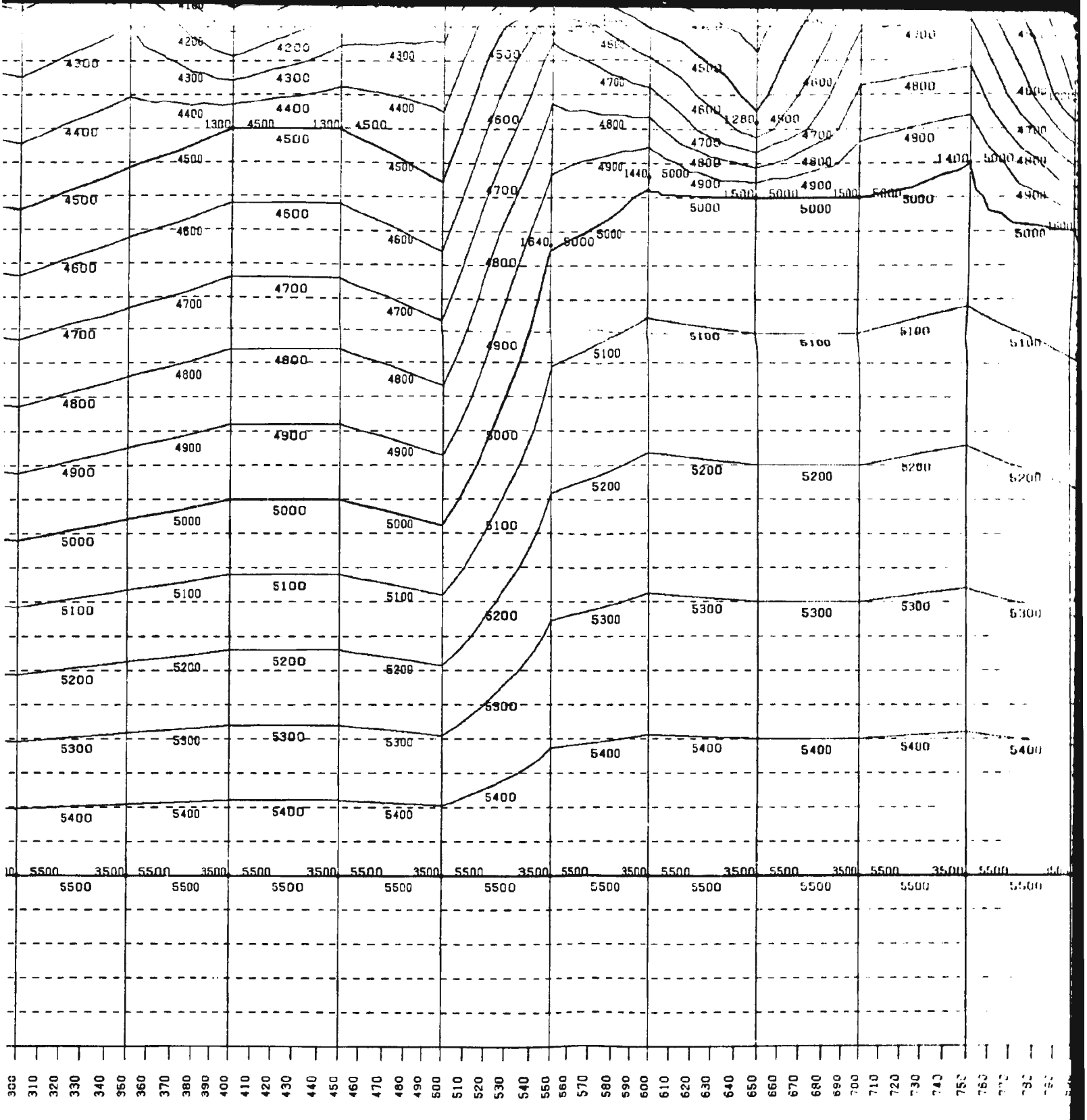

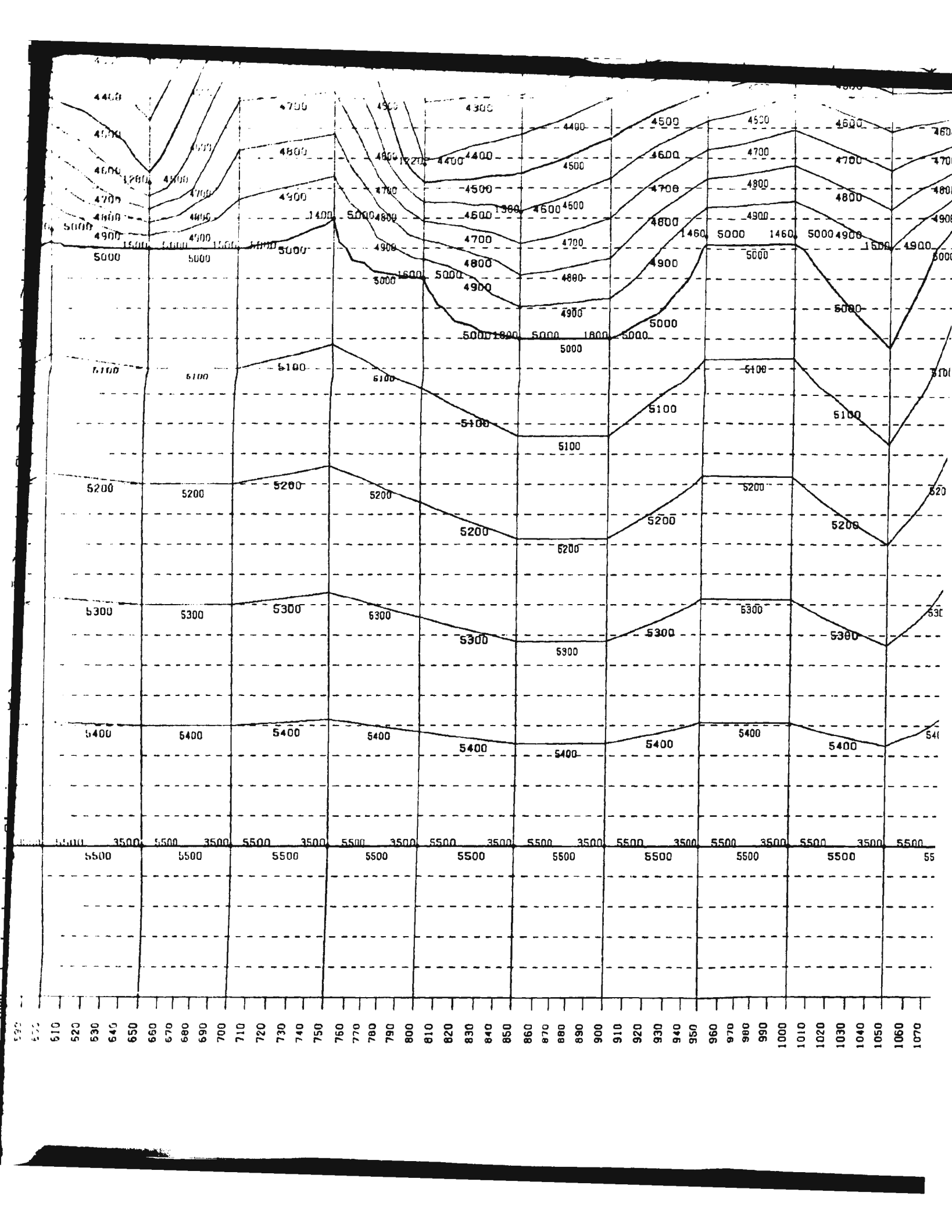

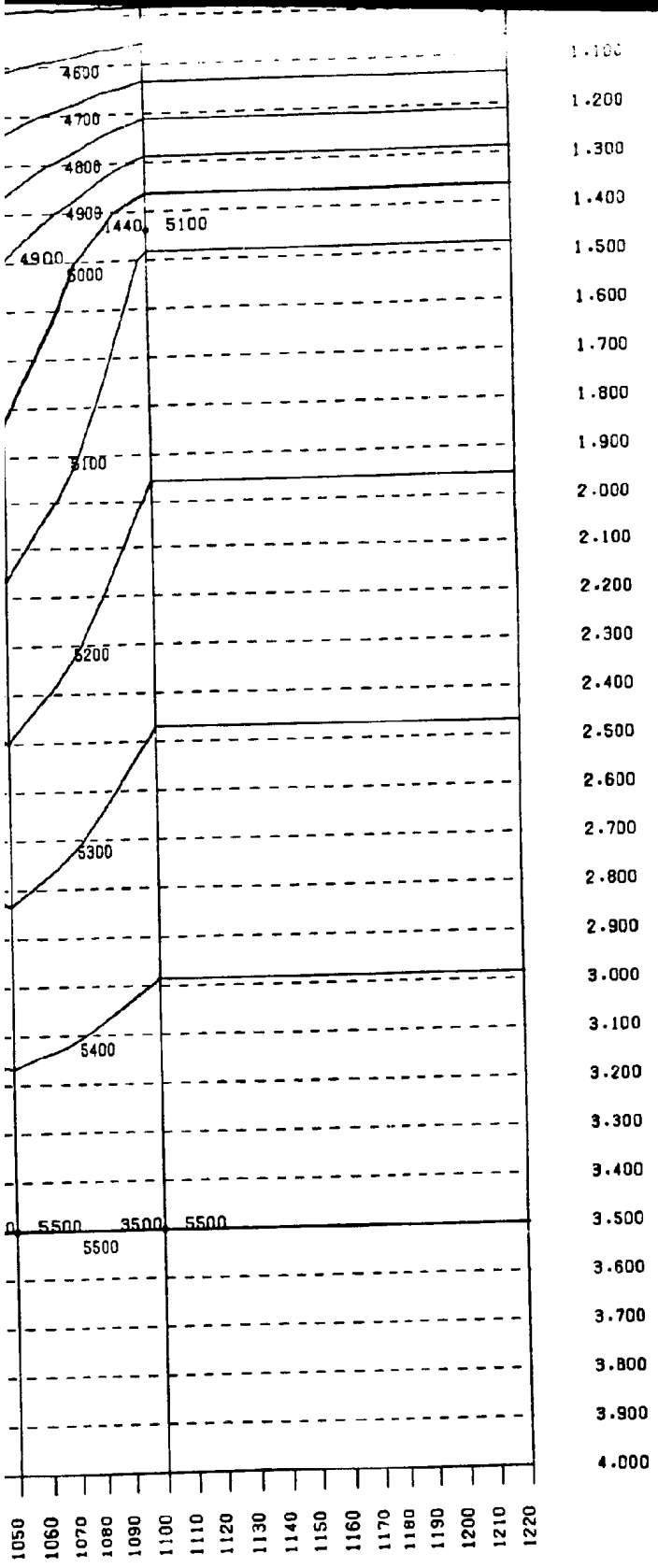
4600
4700
4800
4900
1440
5100
4900
5000
5100
5200
5300
5400
5500
3500
5500
5500
1050
1060
1070
1080
1090
1100
1110
1120
1130
1140
1150
1160
1170
1180
1190
1200
1210
1220
1.100
1.200
1.300
1.400
1.500
1.600
1.700
1.800
1.900
2.000
2.100
2.200
2.300
2.400
2.500
2.600
2.700
2.800
2.900
3.000
3.100
3.200
3.300
3.400
3.500
3.600
3.700
3.800
3.900
4.000

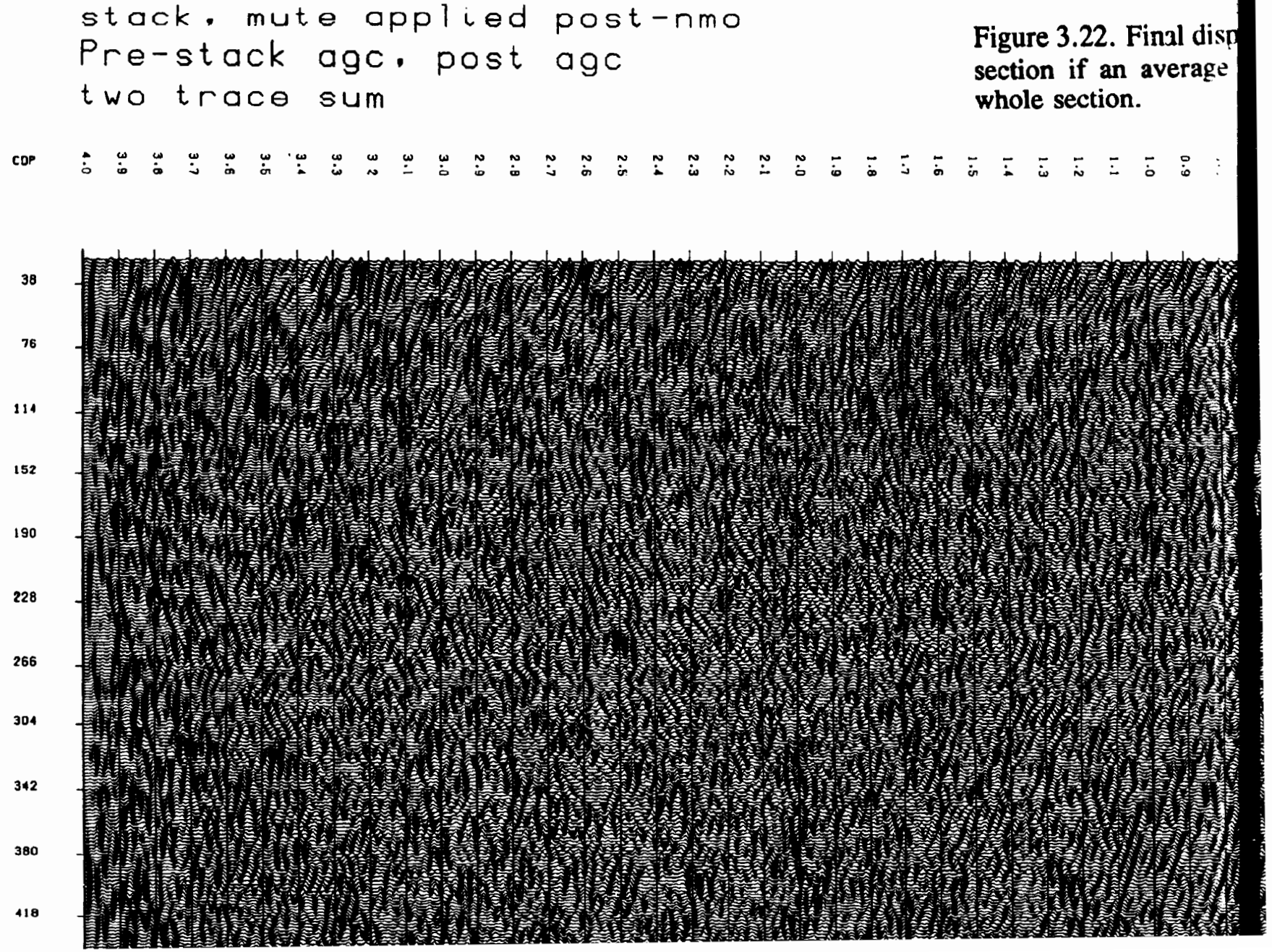

Figure 3.22. Final disp
section if an average
whole section.

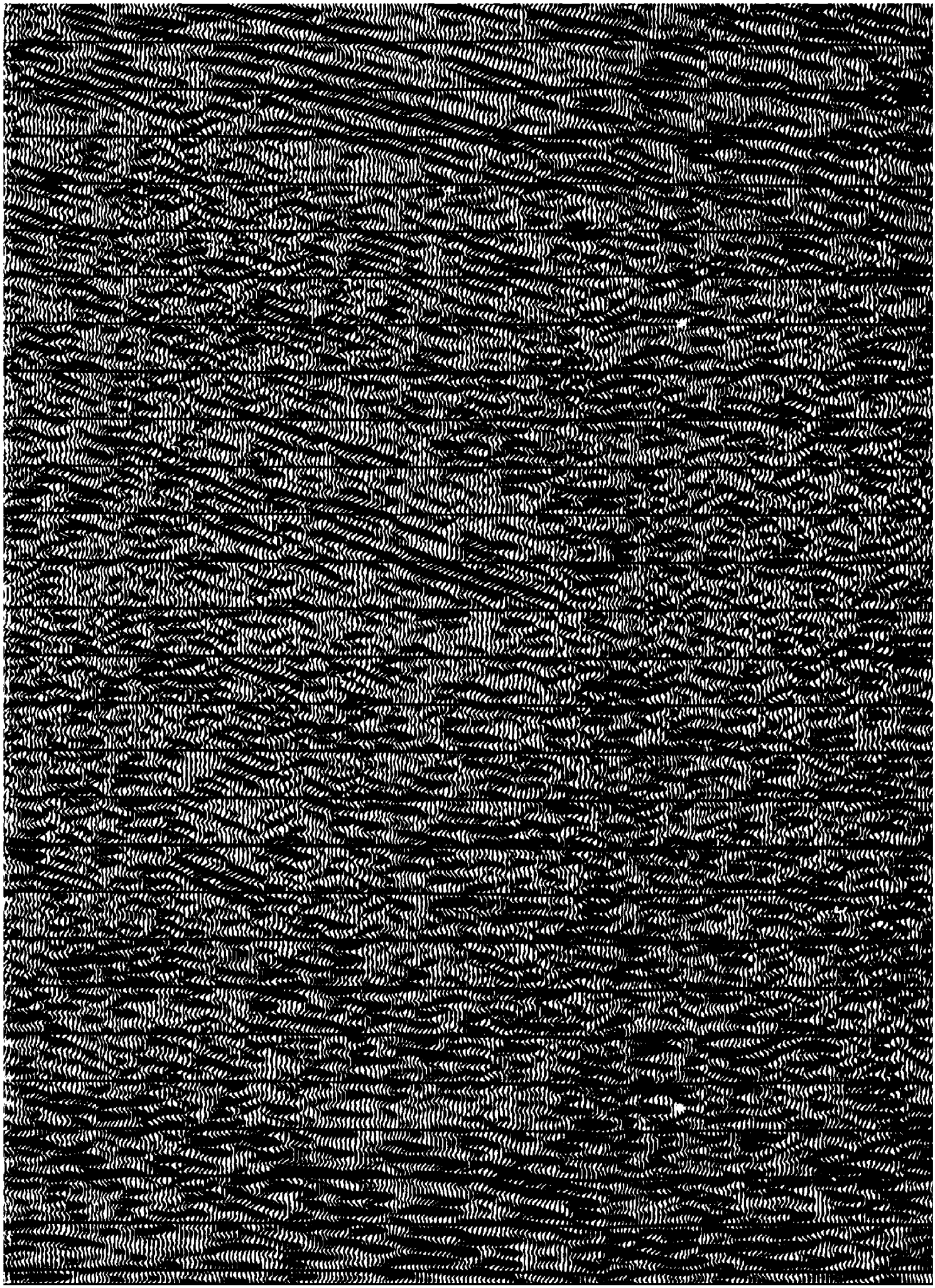

0.9
1.0
1.1
1.2
1.3
1.4
1.5
1.6
1.7
1.8
1.9
2.0
2.1
2.2
2.3
2.4
2.5
2.6
2.7
2.8
2.9
3.0
3.1
3.2
3.3
3.4
3.5
3.6
3.7
3.8
3.9
4.0
798
836
874
912
950
988
1026
1064
1102
1140
1178
1216
CDP

BY:	CAPLANG GEOPHYSICAL LTD.
GY SOURCE:	
PE:	VIBROSEIS
EEP PARAMETERS:	20 HZ - 90 HZ, 500 MS TAPER
EEP LENGTH:	8 SECONDS
URCE ARRAY:	4 OVER 30 M, MOVE UP 8 M
OTPOINT INTERVAL:	40 M
VING ARRANGEMENT:	
LD OF RECORDING:	104 MAXIMUM
OUP INTERVAL:	20.0 METRES
MBER OF GROUPS:	240
ATION GAP AT SP:	26
OPHONES/GROUP:	12
UMENTATION:	
CORDING SYSTEM:	DFS V
E-AMP GAIN:	48 DB
TERS:	HIGH CUT 128.0 HZ AT 72 DB
CORD FORMAT:	SEG Y, 240 CHANNEL
CORD LENGTH:	4 SECONDS
MPLE RATE:	2 MS

OCESSING

ESSED BY:	CENTRE FOR EARTH RESOURCES RESEARC MEMORIAL UNIVERSITY OF NEWFOUNDLAND
PPLICATION OF BINNING AND GEOMETRY:	SURVEY DATA SUPPLIED BY CONTRACTOR
PPLICATION OF FIELD STATICS:	ELEVATION AND REFRACTION STATICS FROM FIRST BREAKS
MO CORRECTION:	
DP GATHER:	MAXIMUM FOLD 104
OTCH FILTER:	REJECTION OF 60 HZ APPLIED IN TIME DOMAIN
MO CORRECTION:	VELOCITY DERIVATION FROM MERVEL VELOCITY ANALYSES, CVNMO AND CONSTANT VELOCITY STACKS (CVS)
ONT MUTE:	PICKED AND APPLIED ON NMO CORRECTED GATHERS
E-STACK AGC:	1000 MS WINDOW
DP STACK:	
TYPE	STANDARD MEAN AMPLITUDE CDP
COVERAGE	6000% - 10400%
ESIDUAL STATICS APPLICATION:	FROM PICKED HORIZON ON DMO CORRECTED STACK
45 DEGREE FINITE DIFFERENCE MIGRATION:	BASED ON VELOCITY ANALYSIS AFTER DMO
ANDPASS FILTER:	0.0 S: 20 HZ TO 90 HZ AT 32 DB/OCT 3.0 S: 20 HZ TO 60 HZ AT 32 DB/OCT
COHERENCY FILTER:	
AUTOMATIC GAIN CONTROL:	AGC BALANCING WINDOW - 500 MS

PLAY

TE:	30/11/1992
STEM	VERSATEC ELECTROSTATIC PLOTTER #7236
AS	0 %
RTICAL SCALE	6 CM/SEC
RIZONTAL SCALE	14 TRACE/CM, 1:13500
LARITY	NORMAL
TUM PLANE	160 METRES

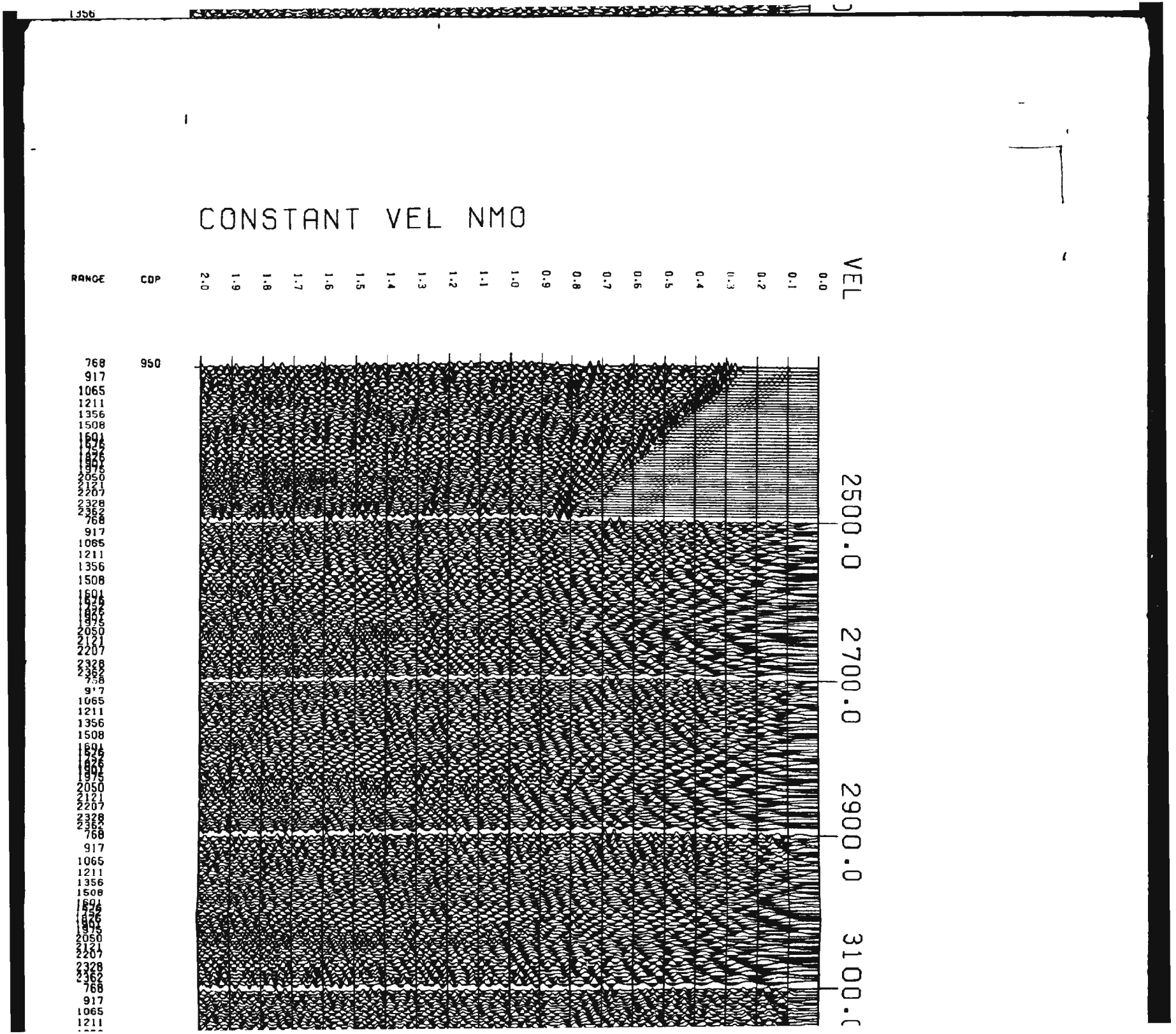
CONSTANT VEL NMO
RANGE
COP
VEL
2.0
1.9
1.8
1.7
1.6
1.5
1.4
1.3
1.2
1.1
1.0
0.9
0.8
0.7
0.6
0.5
0.4
0.3
0.2
0.1
0.0
950
2500.0
2700.0
2900.0
3100.0

(b)

Fig 3.10. (

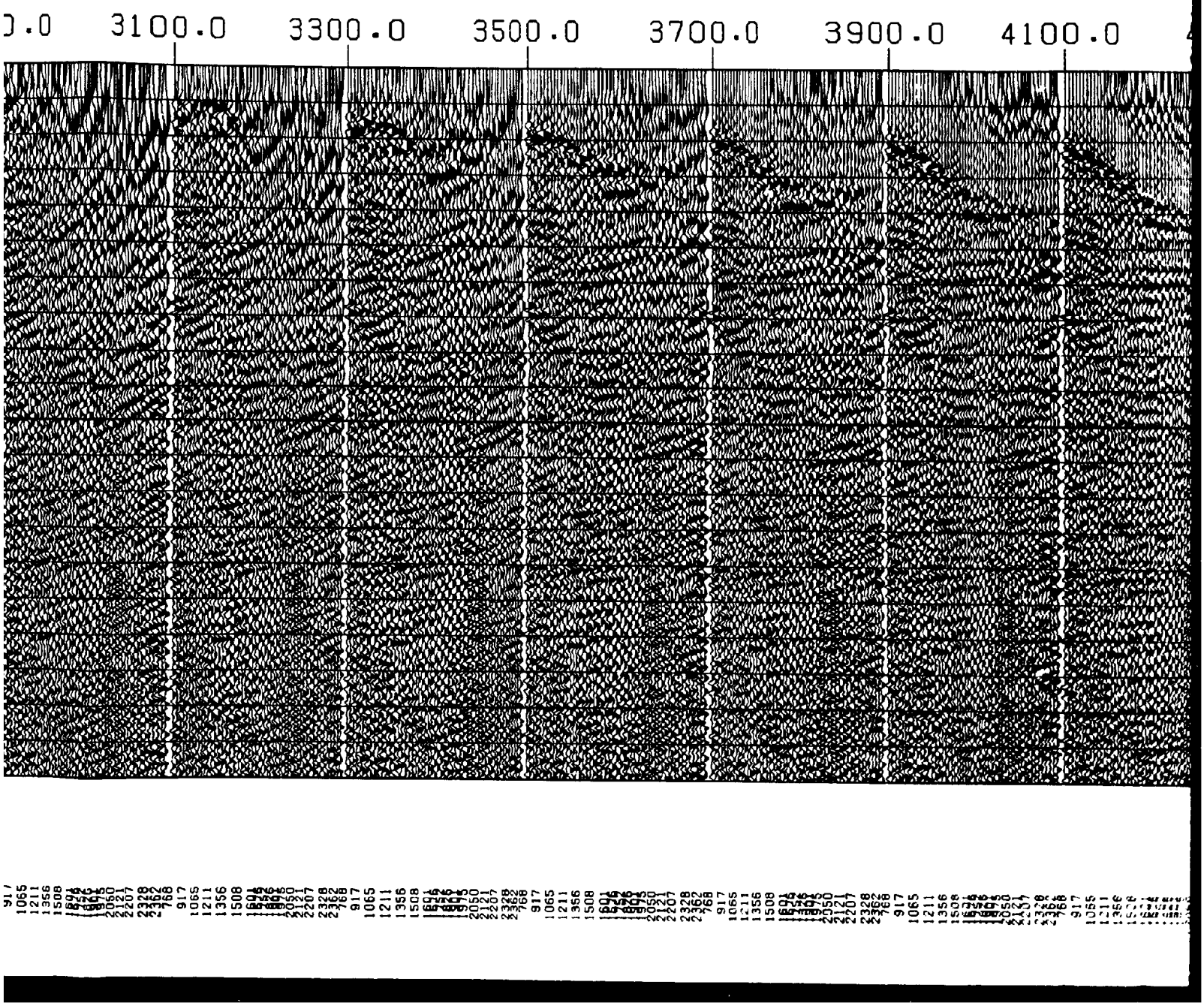

Fig 3.10. (cont.)

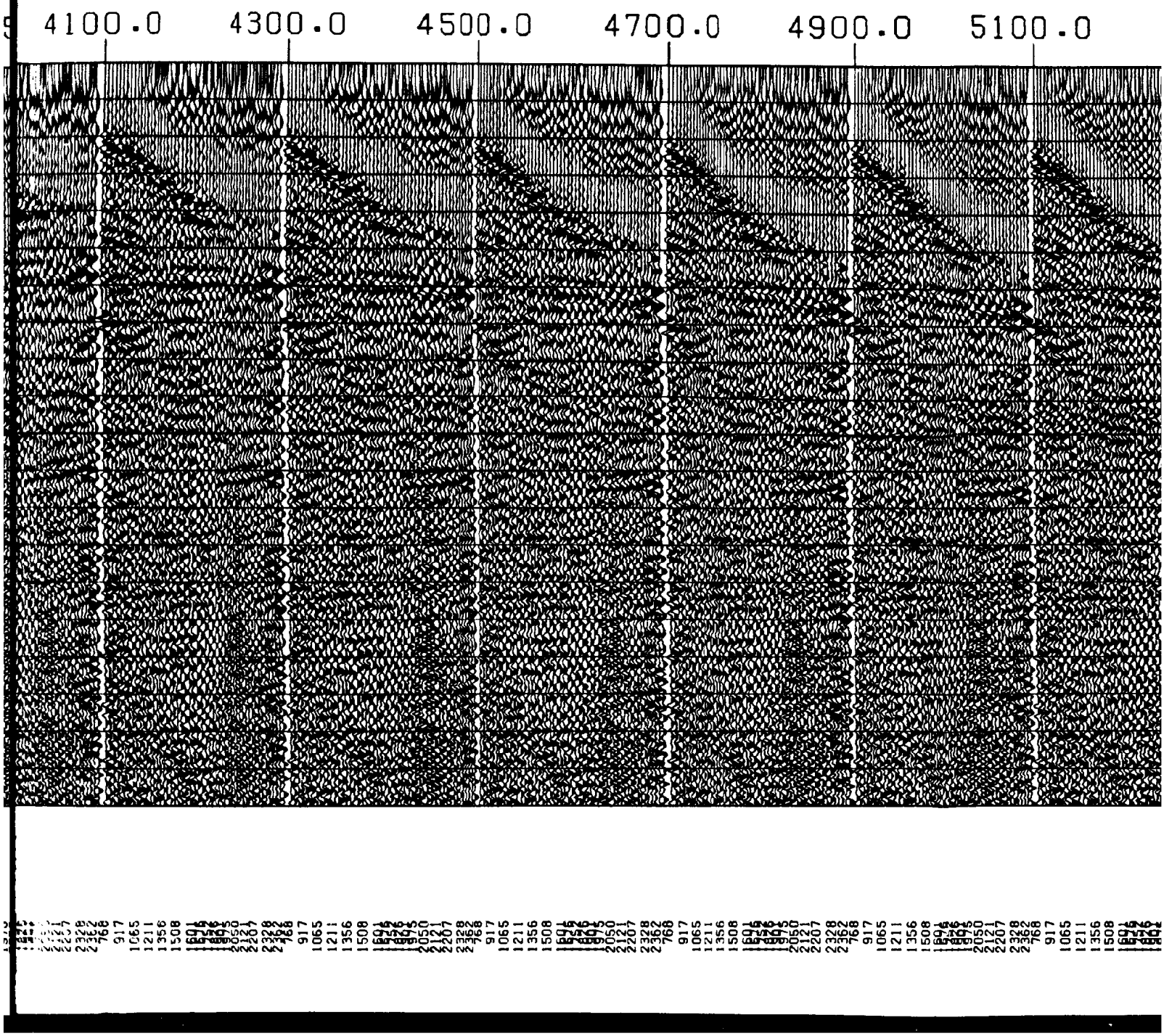

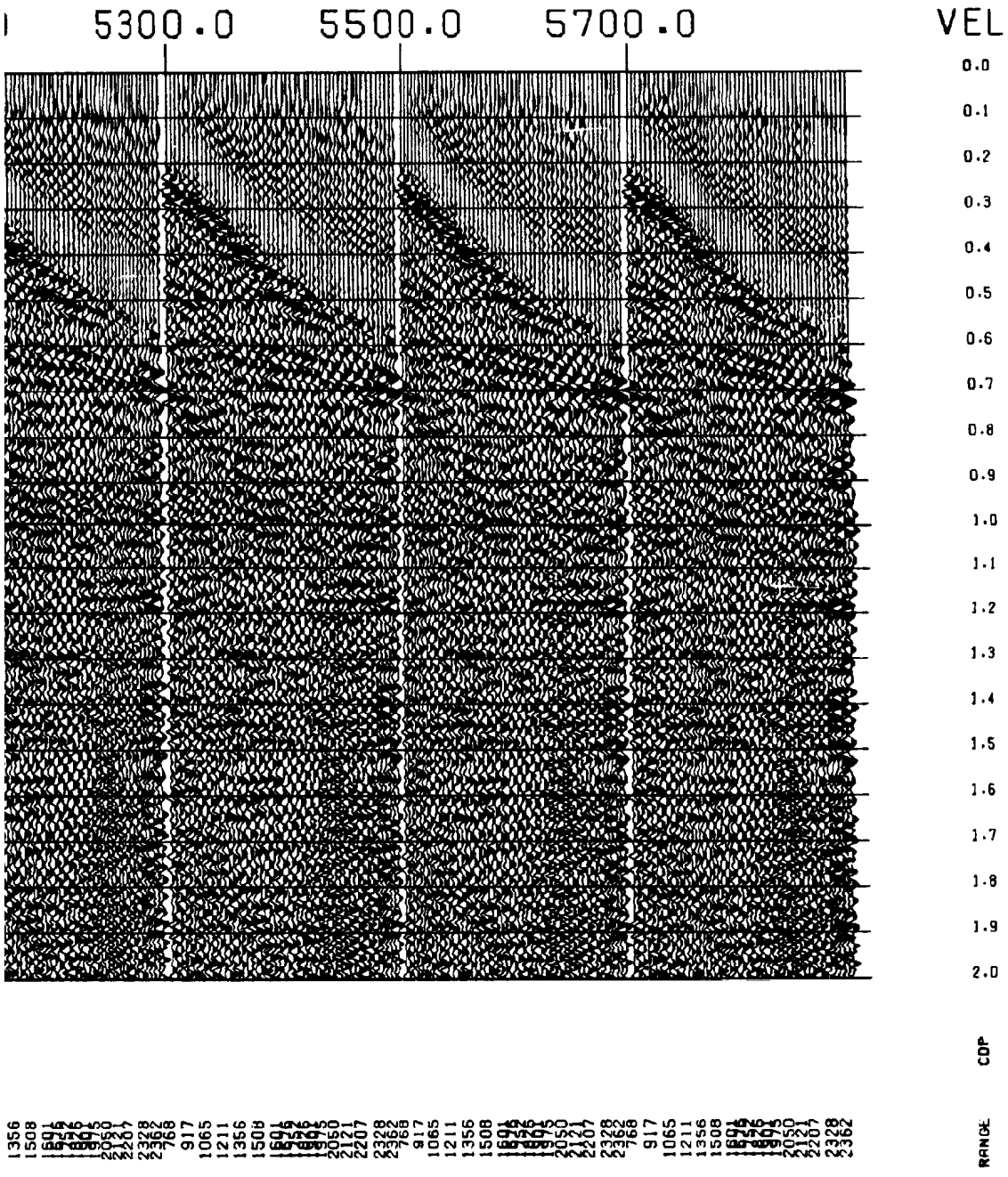
5300.0
5500.0
5700.0
VEL
0.0
0.1
0.2
0.3
0.4
0.5
0.6
0.7
0.8
0.9
1.0
1.1
1.2
1.3
1.4
1.5
1.6
1.7
1.8
1.9
2.0
CDP
RANGE

(a)

Figure 3.10. Constant velocity normal moveout (CVN
CMP 950 after DMO correction. (a) Before DMO co
(b) After DMO correction.

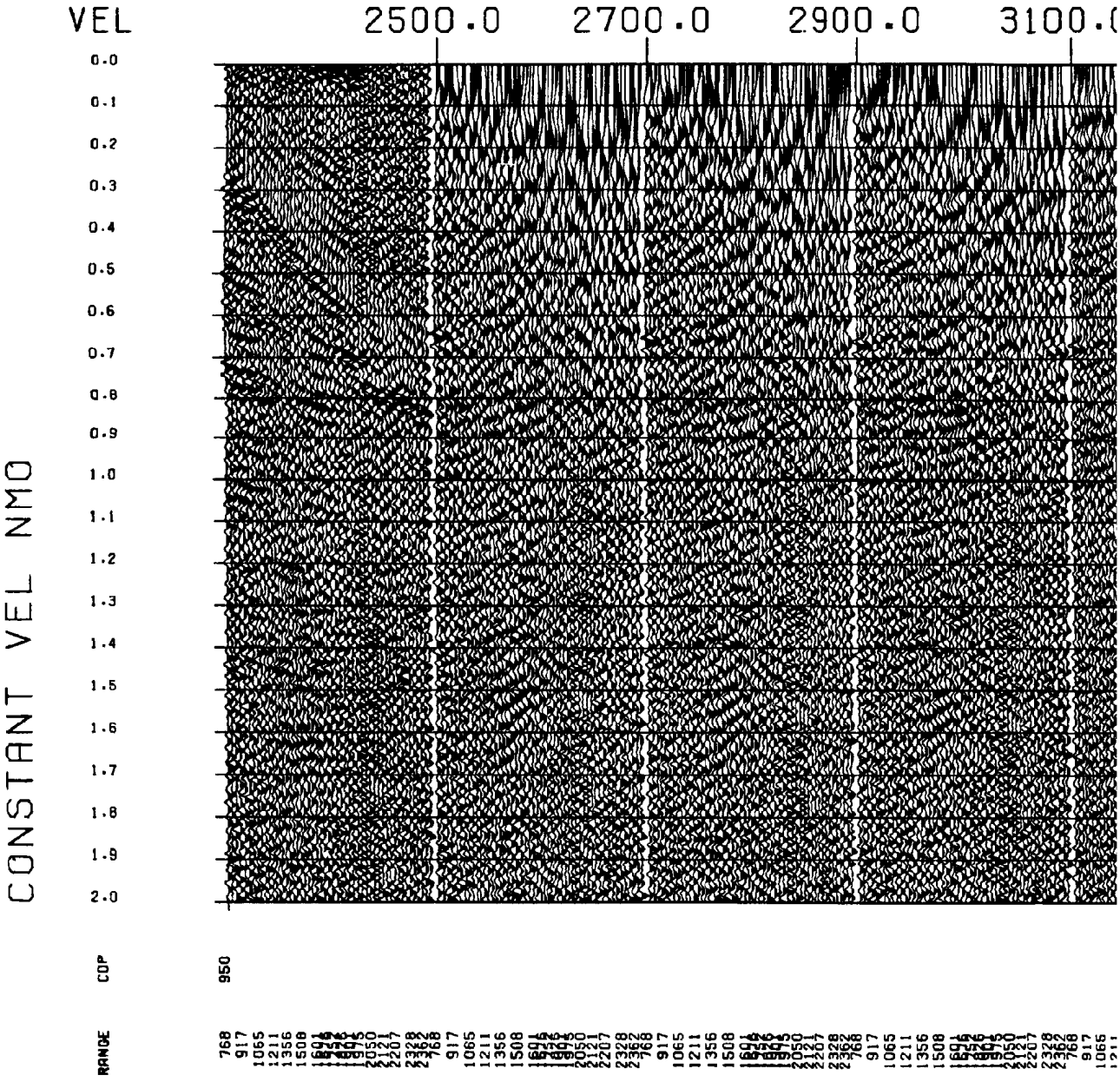

VNMO) of
correction.

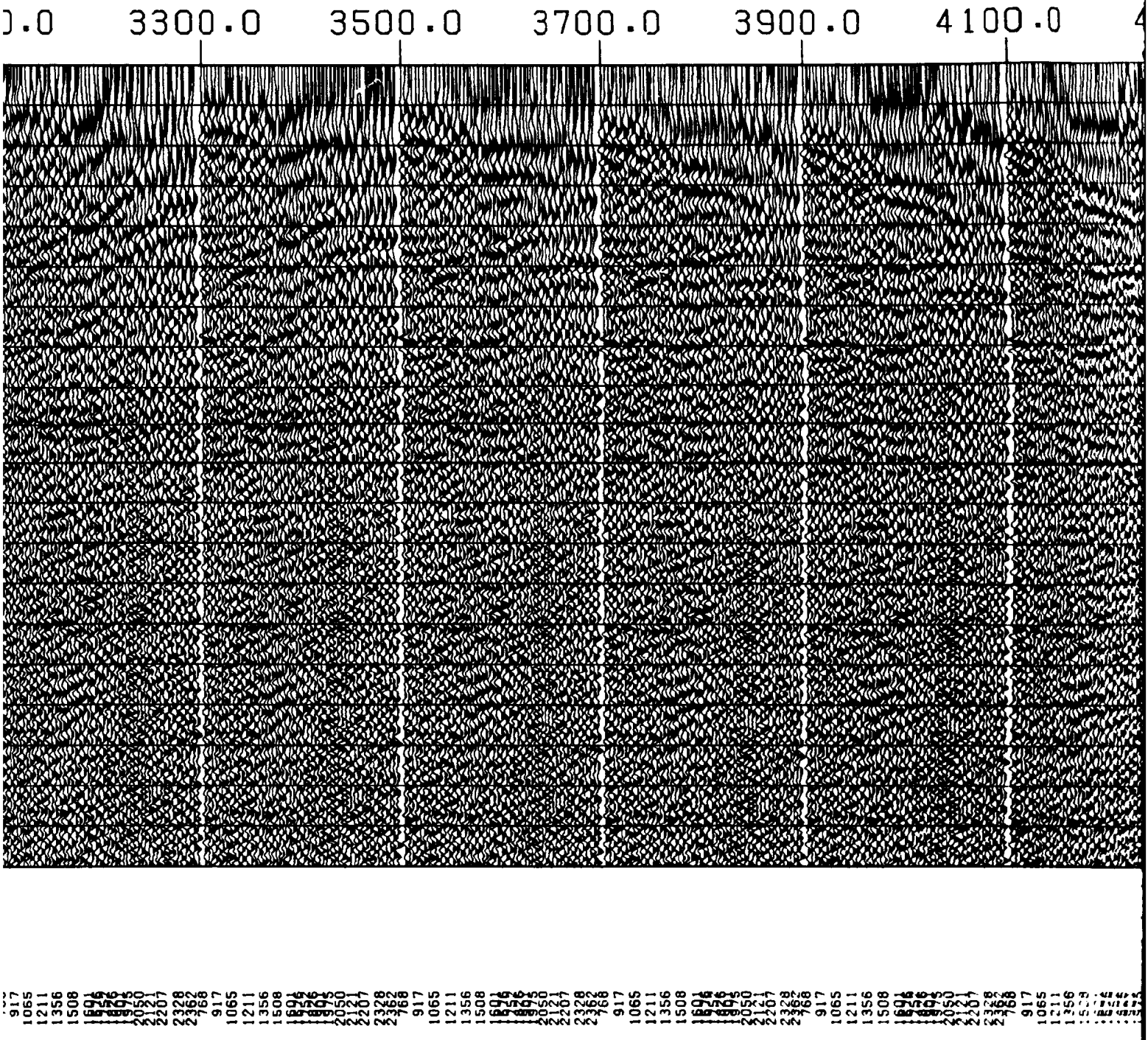

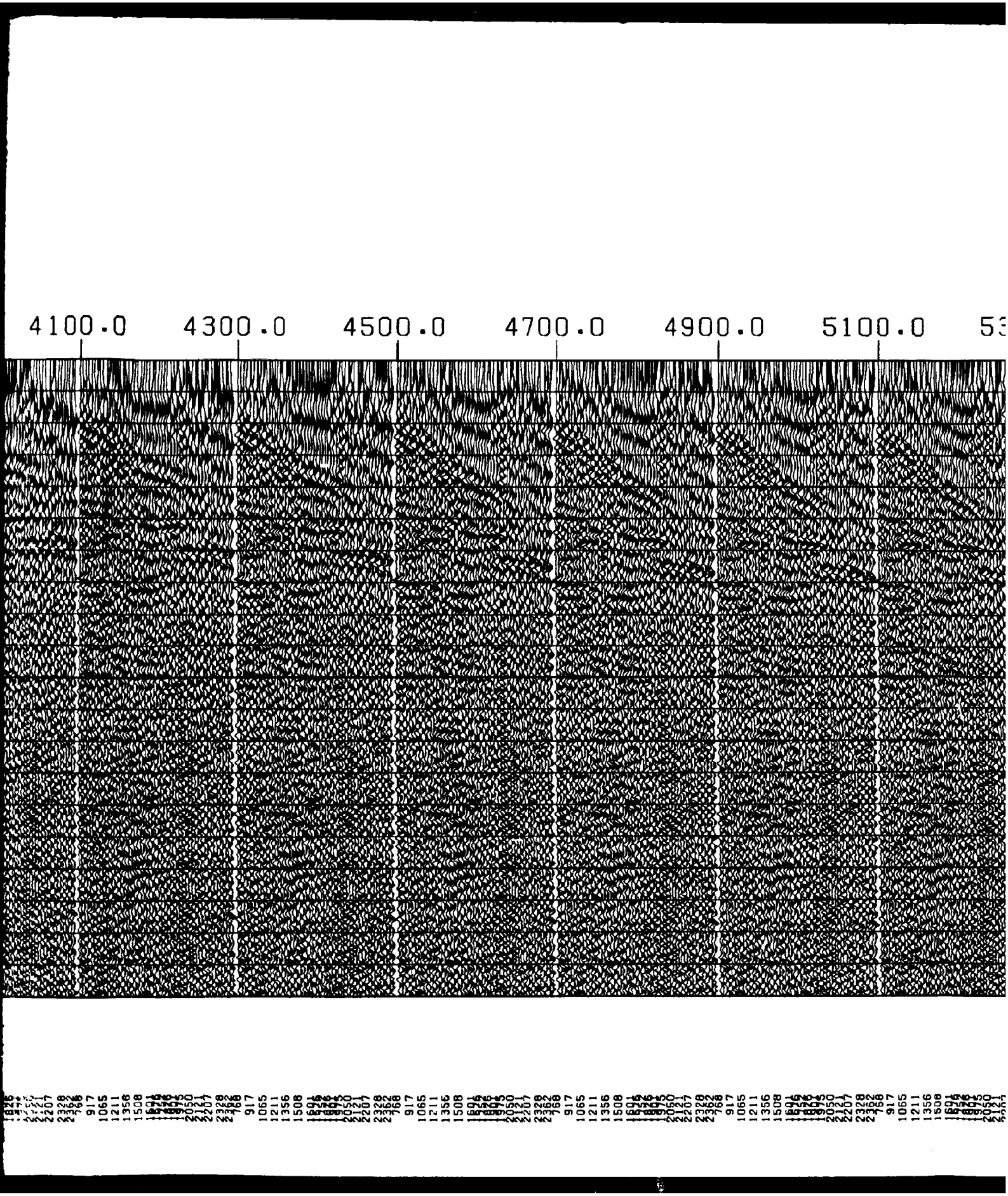
4100.0
4300.0
4500.0
4700.0
4900.0
5100.0
53

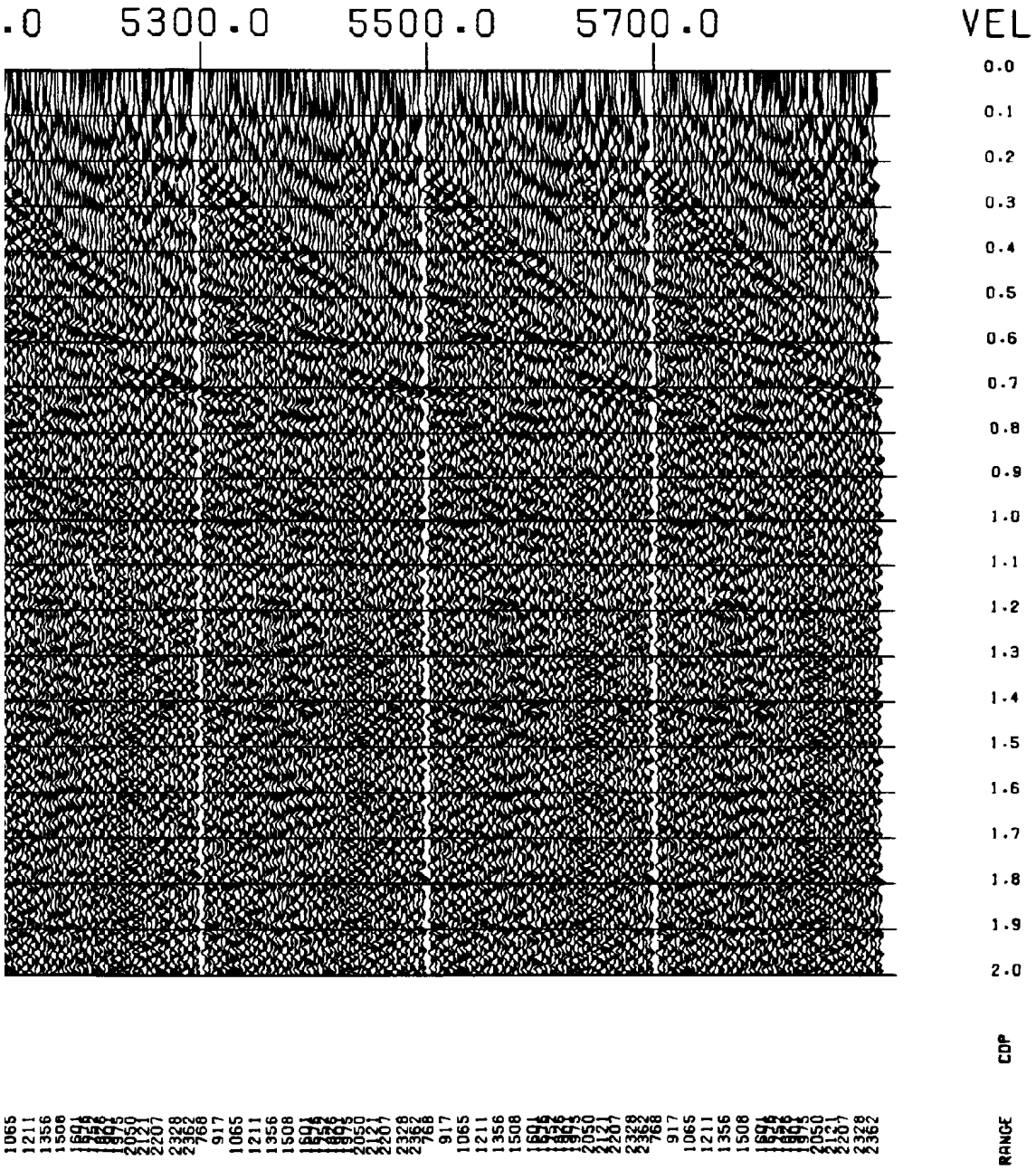
.0
5300.0
5500.0
5700.0
VEL
0.0
0.1
0.2
0.3
0.4
0.5
0.6
0.7
0.8
0.9
1.0
1.1
1.2
1.3
1.4
1.5
1.6
1.7
1.8
1.9
2.0
CDP
RANGE

Figure 3.8. Constant velocity normal moveo
CMP 630 before DMO correction.

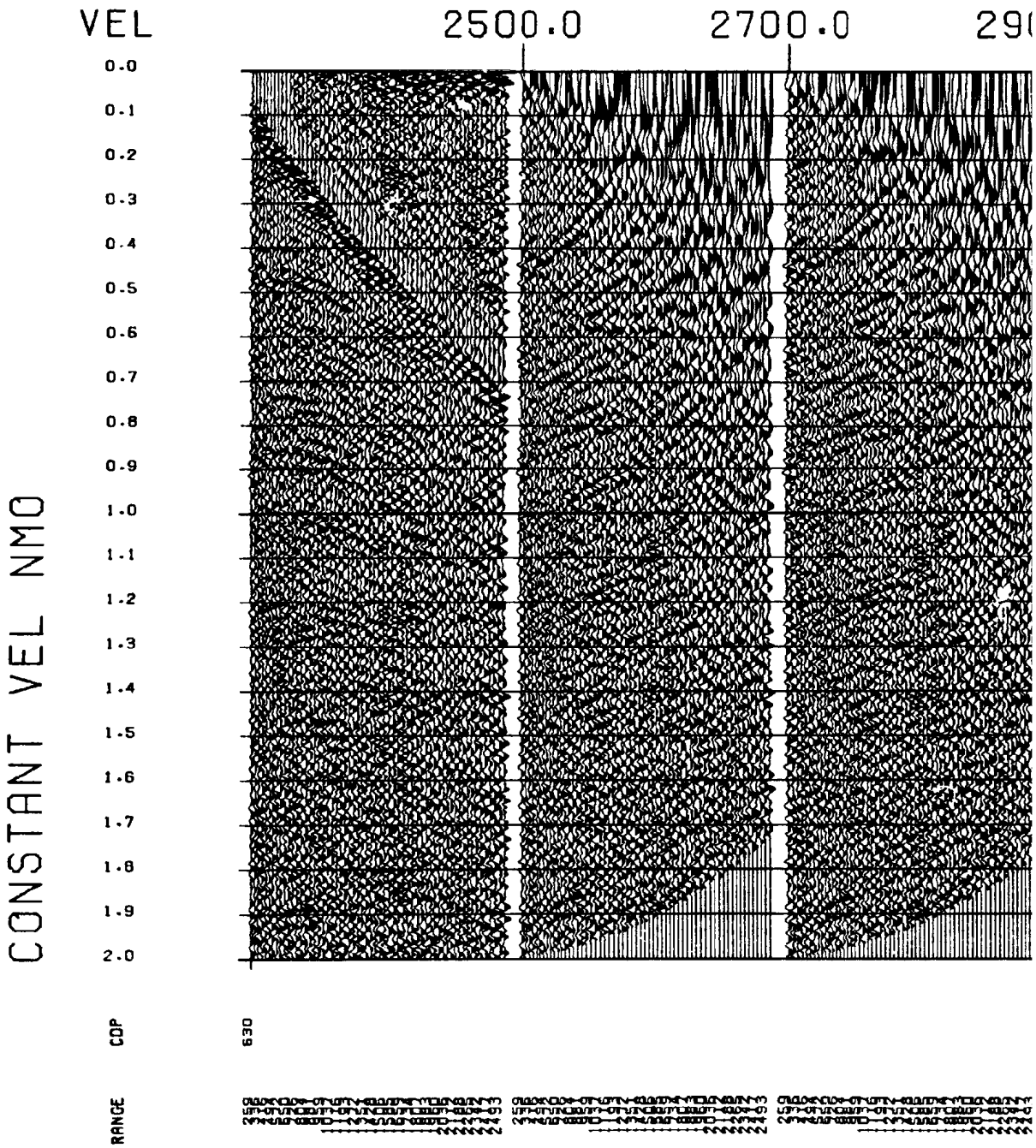

ɔut (CVNMO) of

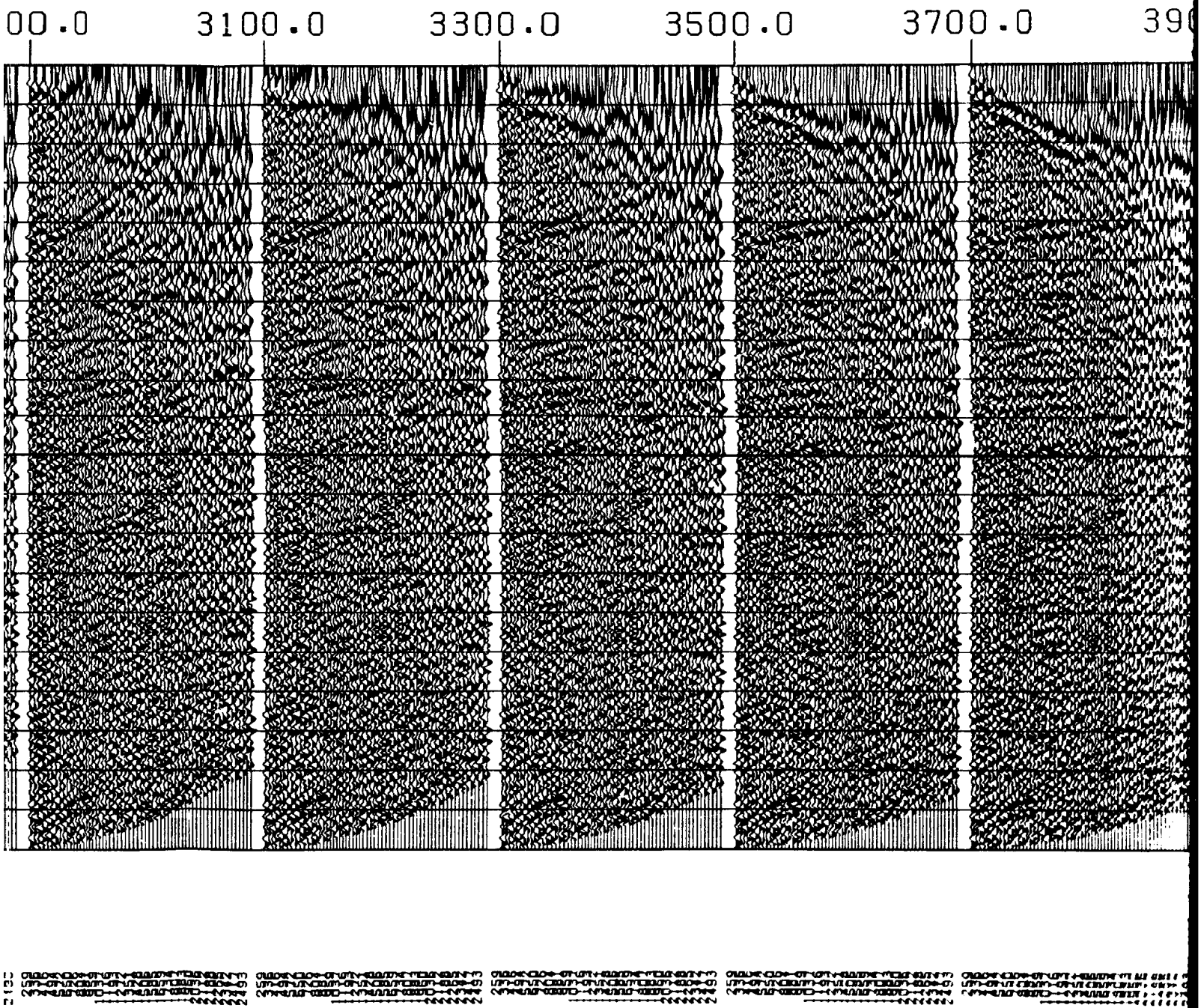

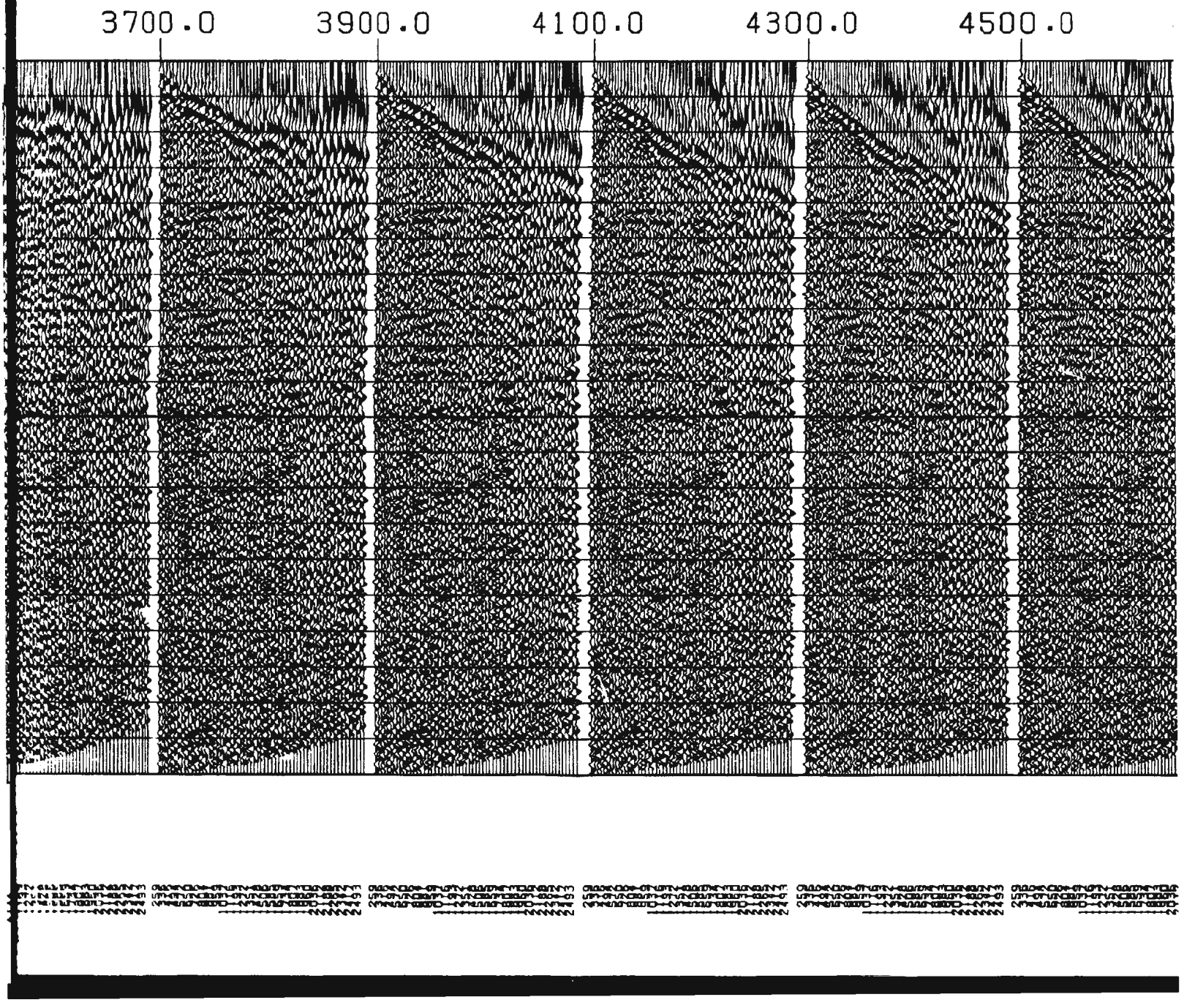
3700.0
3900.0
4100.0
4300.0
4500.0

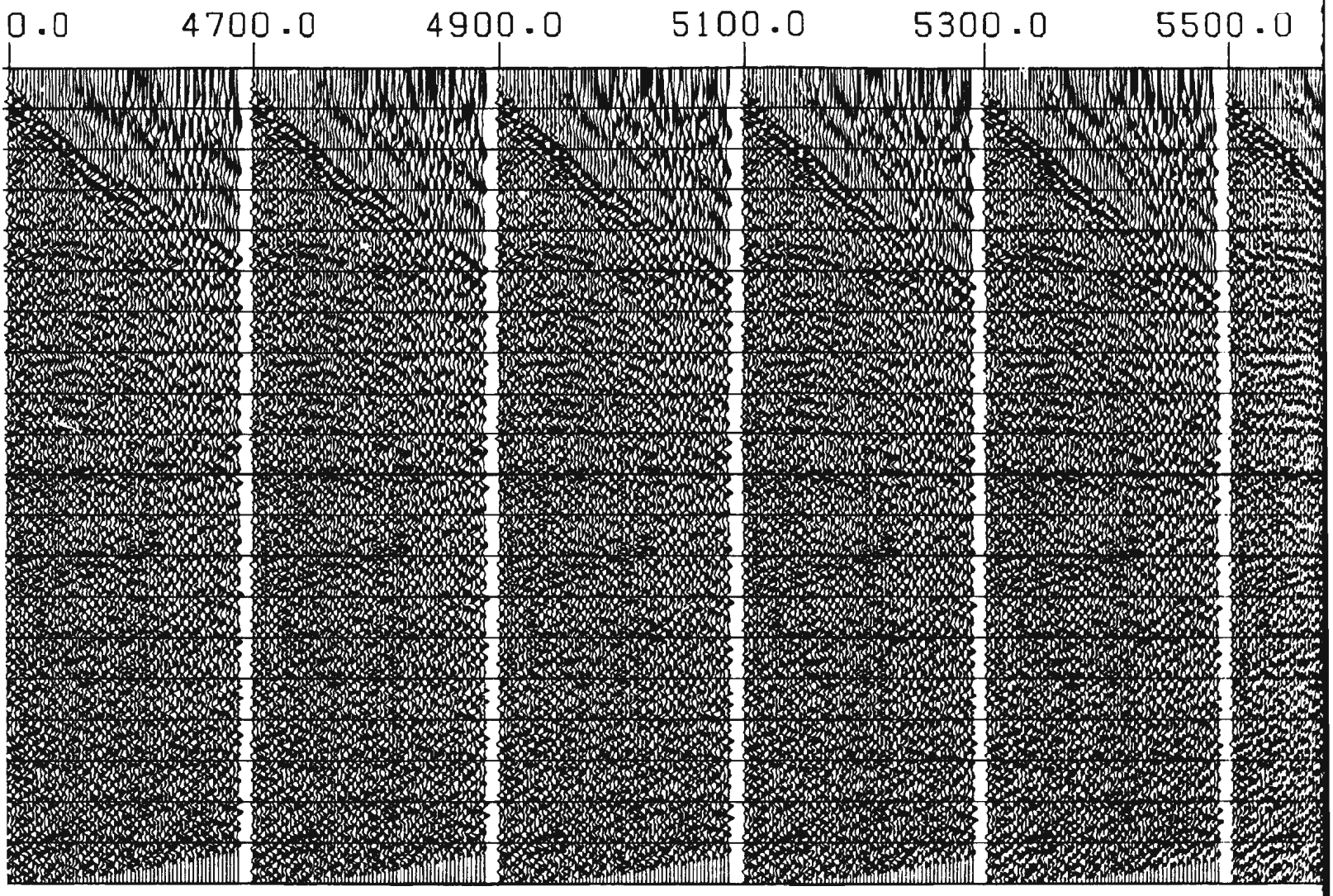
0.0
4700.0
4900.0
5100.0
5300.0
5500.0

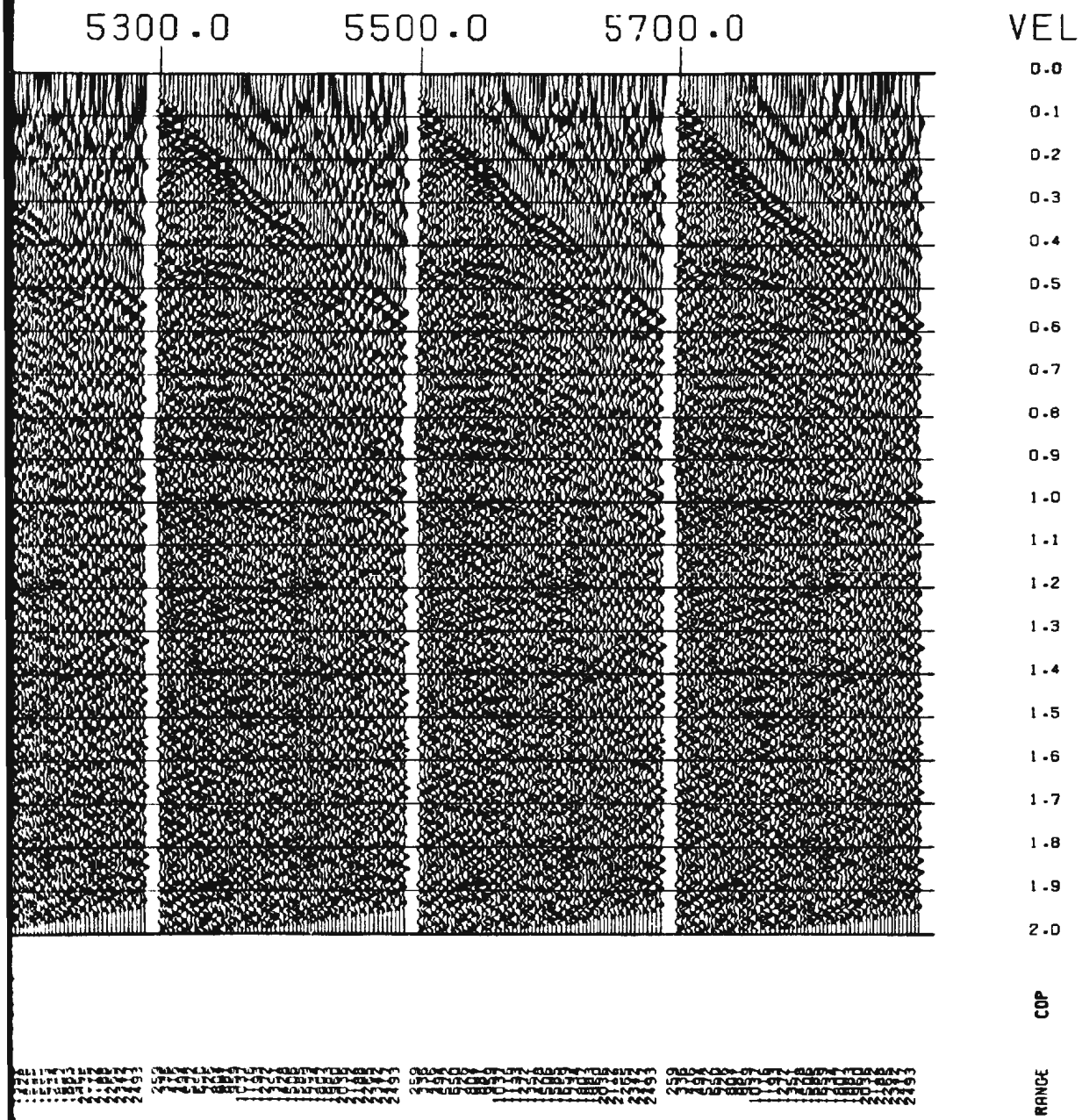
5300.0
5500.0
5700.0
VEL
0.0
0.1
0.2
0.3
0.4
0.5
0.6
0.7
0.8
0.9
1.0
1.1
1.2
1.3
1.4
1.5
1.6
1.7
1.8
1.9
2.0
CDP
RANGE

Figure 3.7 (t). Constant velocity stack of 5500 m/s.

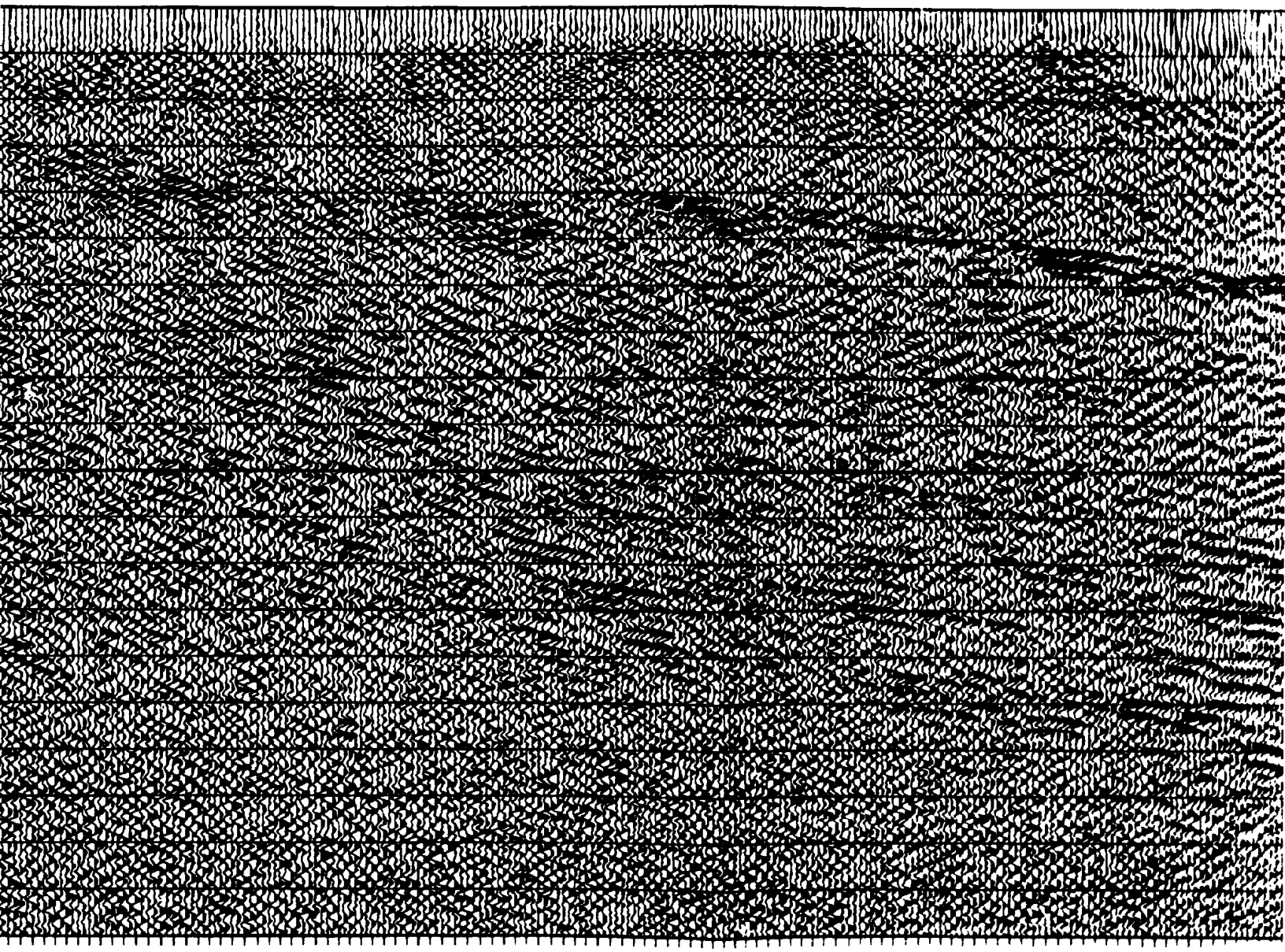

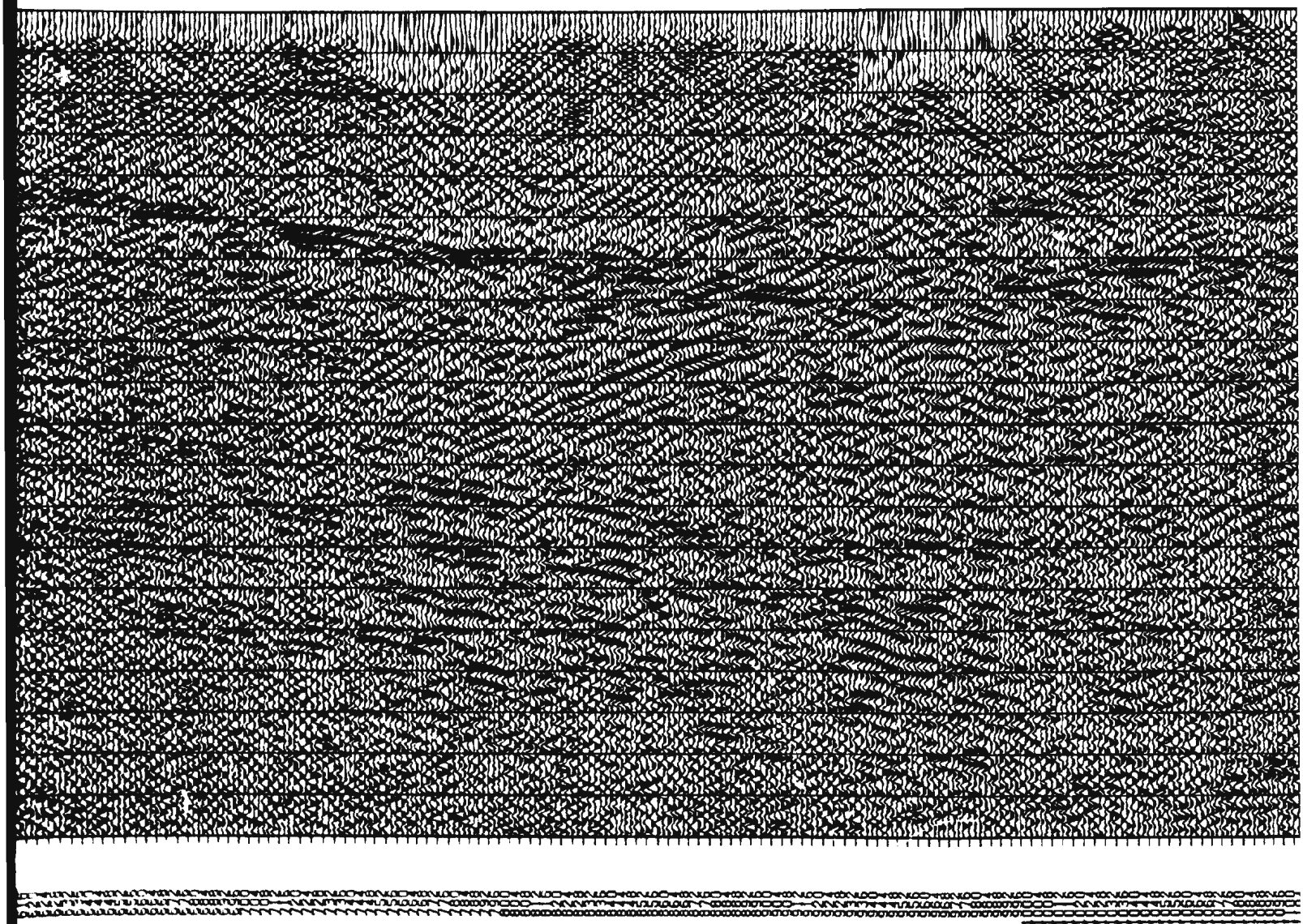

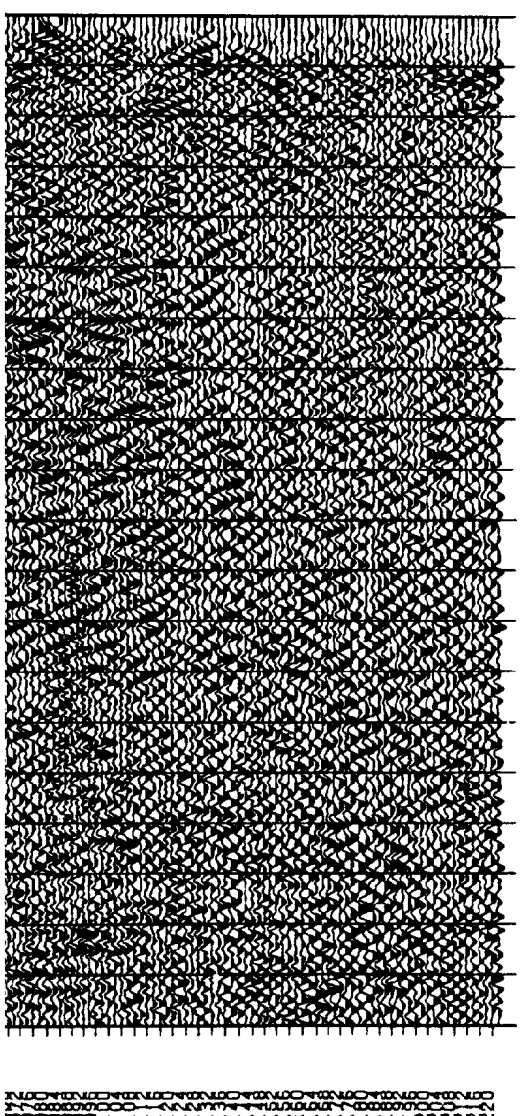
0.0
0.1
0.2
0.3
0.4
0.5
0.6
0.7
0.8
0.9
1.0
1.1
1.2
1.3
1.4
1.5
1.6
1.7
1.8
1.9
2.0
CDP

Figure 3.7 (s). Constant velocity

velocity stack of 5300 m/s.

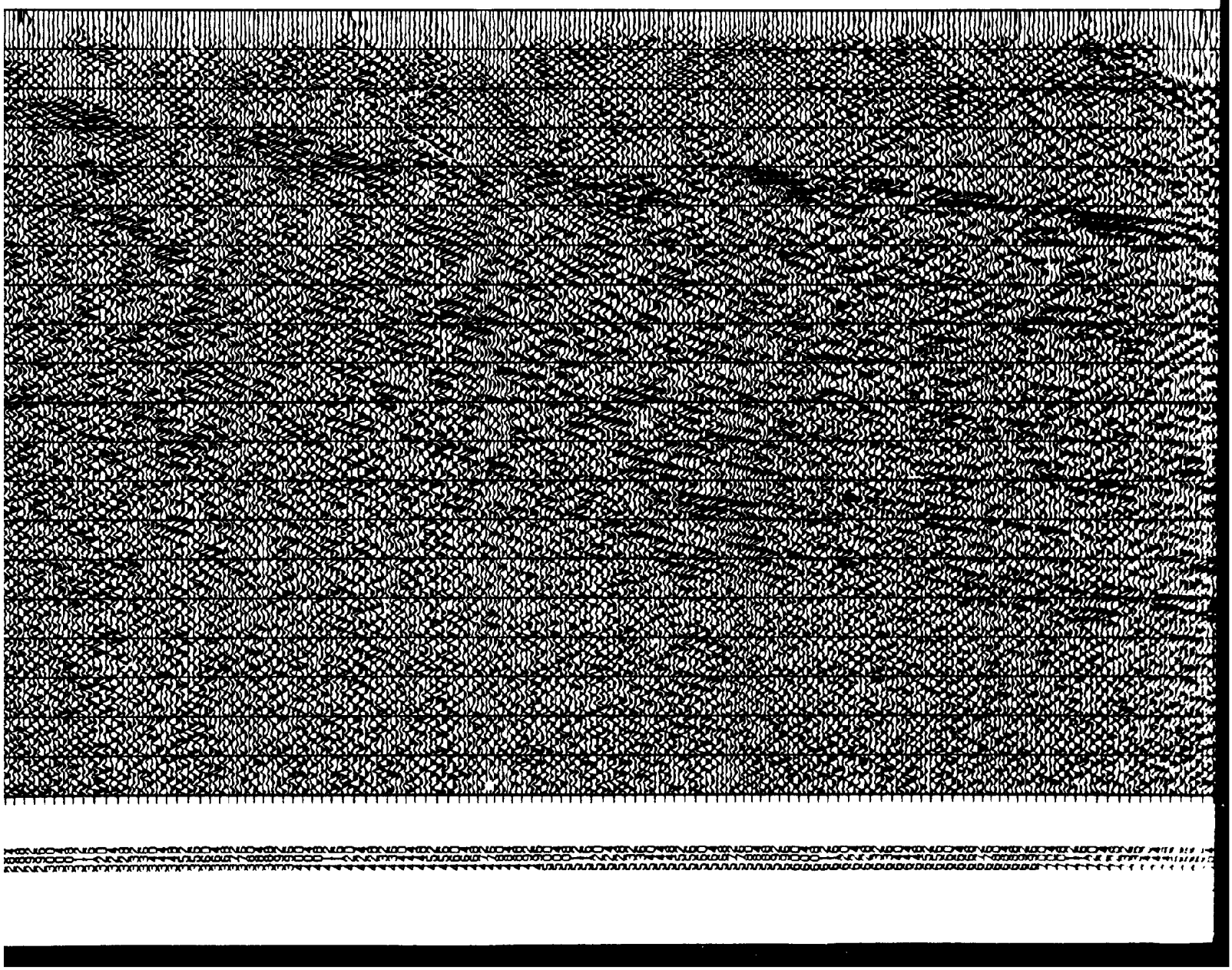

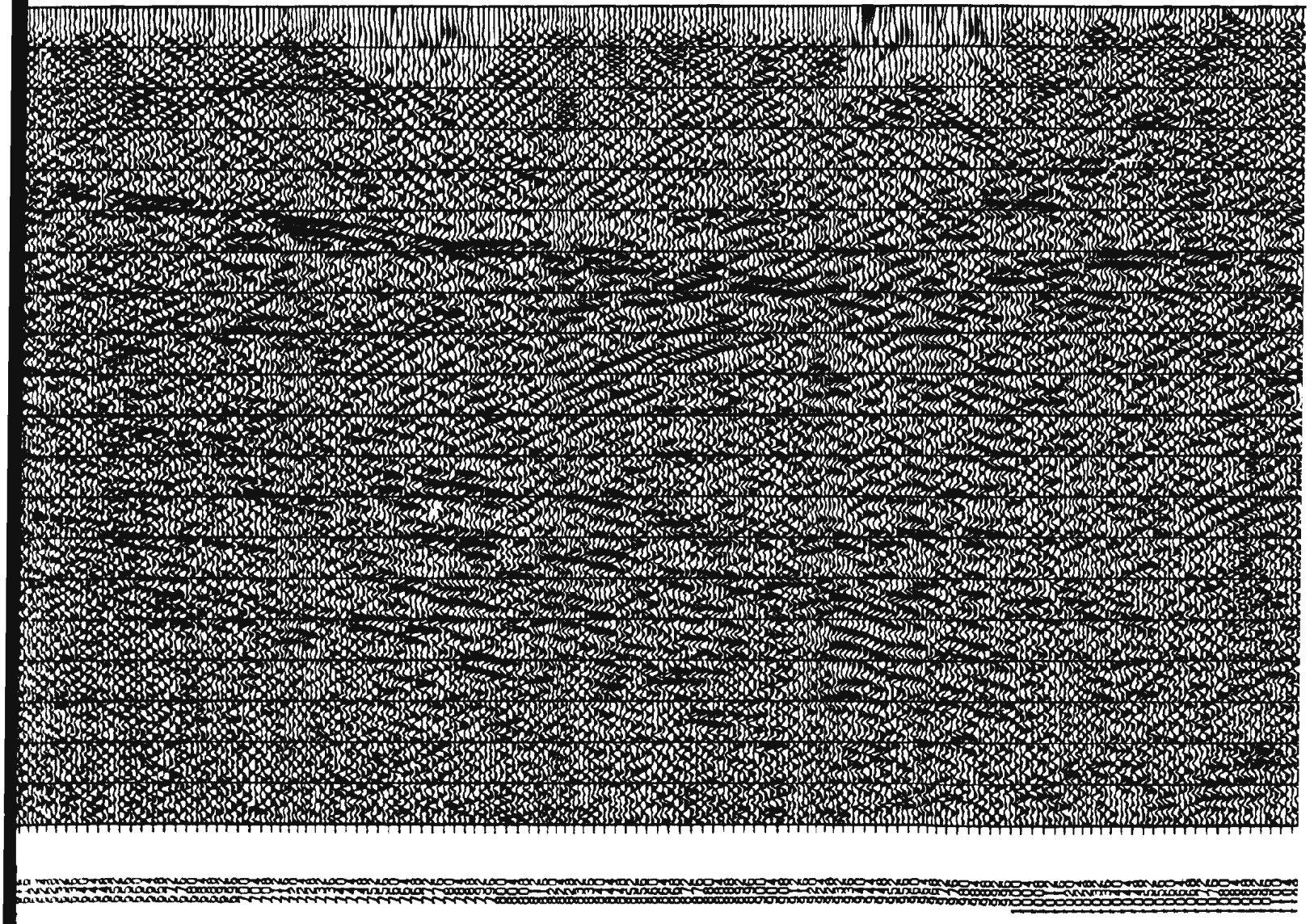

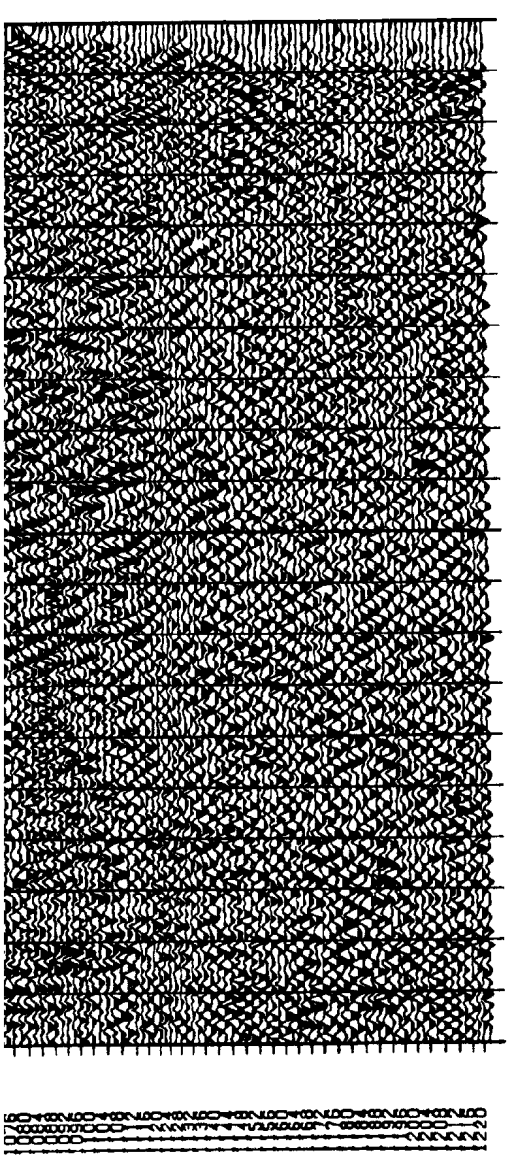
0.0
0.1
0.2
0.3
0.4
0.5
0.6
0.7
0.8
0.9
1.0
1.1
1.2
1.3
1.4
1.5
1.6
1.7
1.8
1.9
2.0
CDP

Figure 3.7 (r). Constant velocity stack of 510(

stack of 5100 m/s.

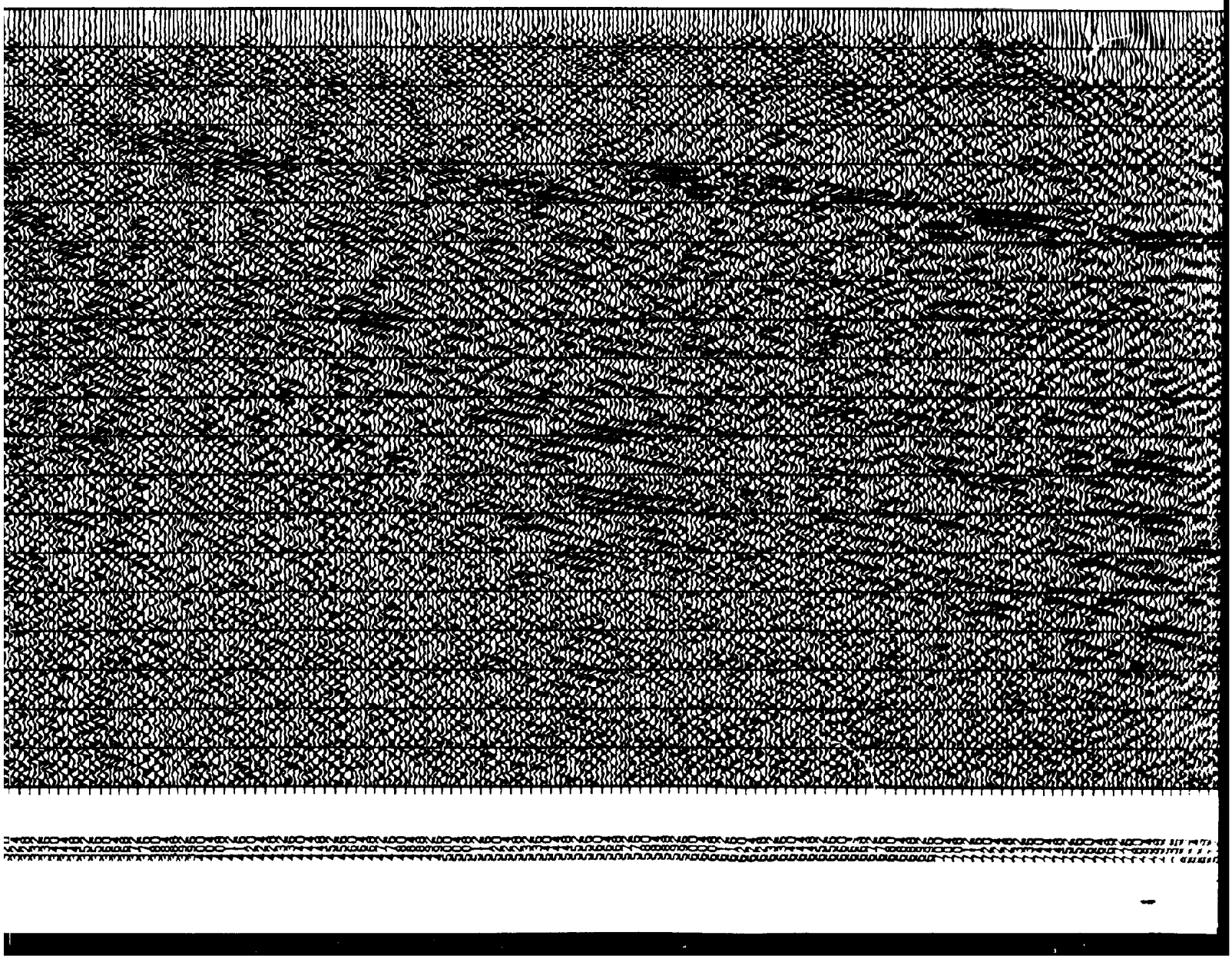

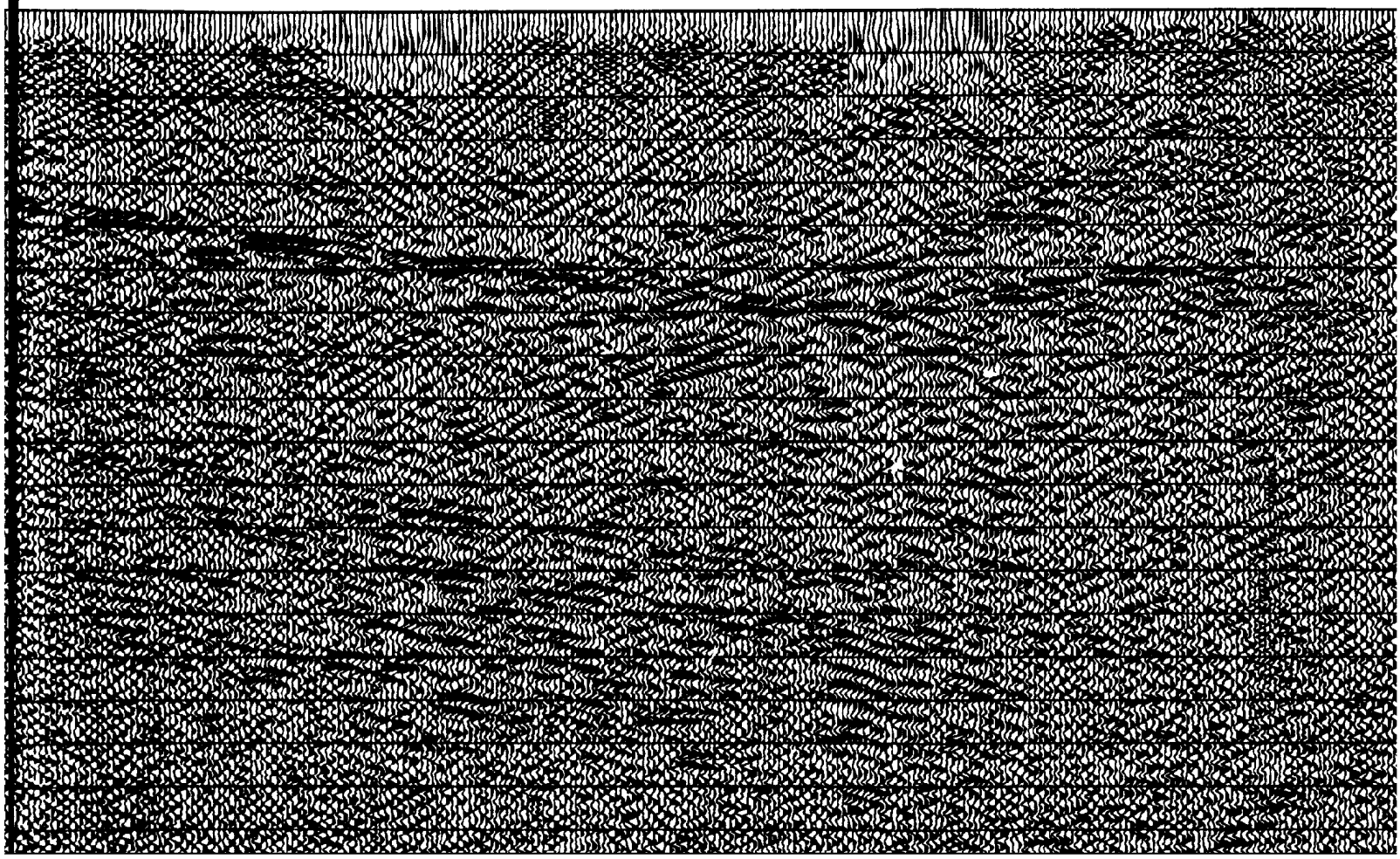

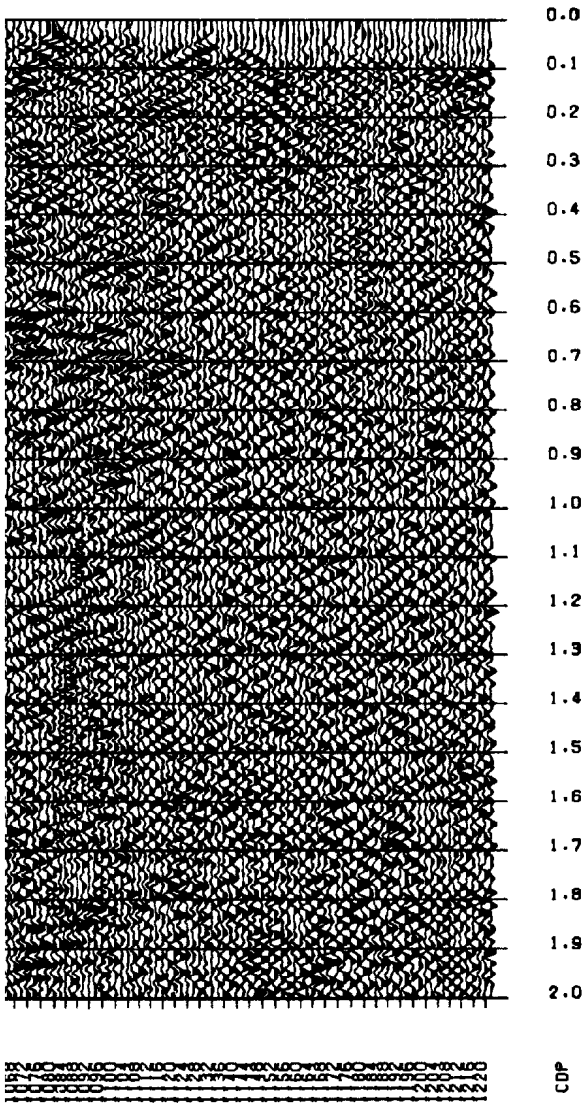
0.0
0.1
0.2
0.3
0.4
0.5
0.6
0.7
0.8
0.9
1.0
1.1
1.2
1.3
1.4
1.5
1.6
1.7
1.8
1.9
2.0

CDP

Figure 3.7 (q). Constant velocity st
events at depth start stacking at sam

velocity stack of 4900 m/s. Note that
ing at same velocity.

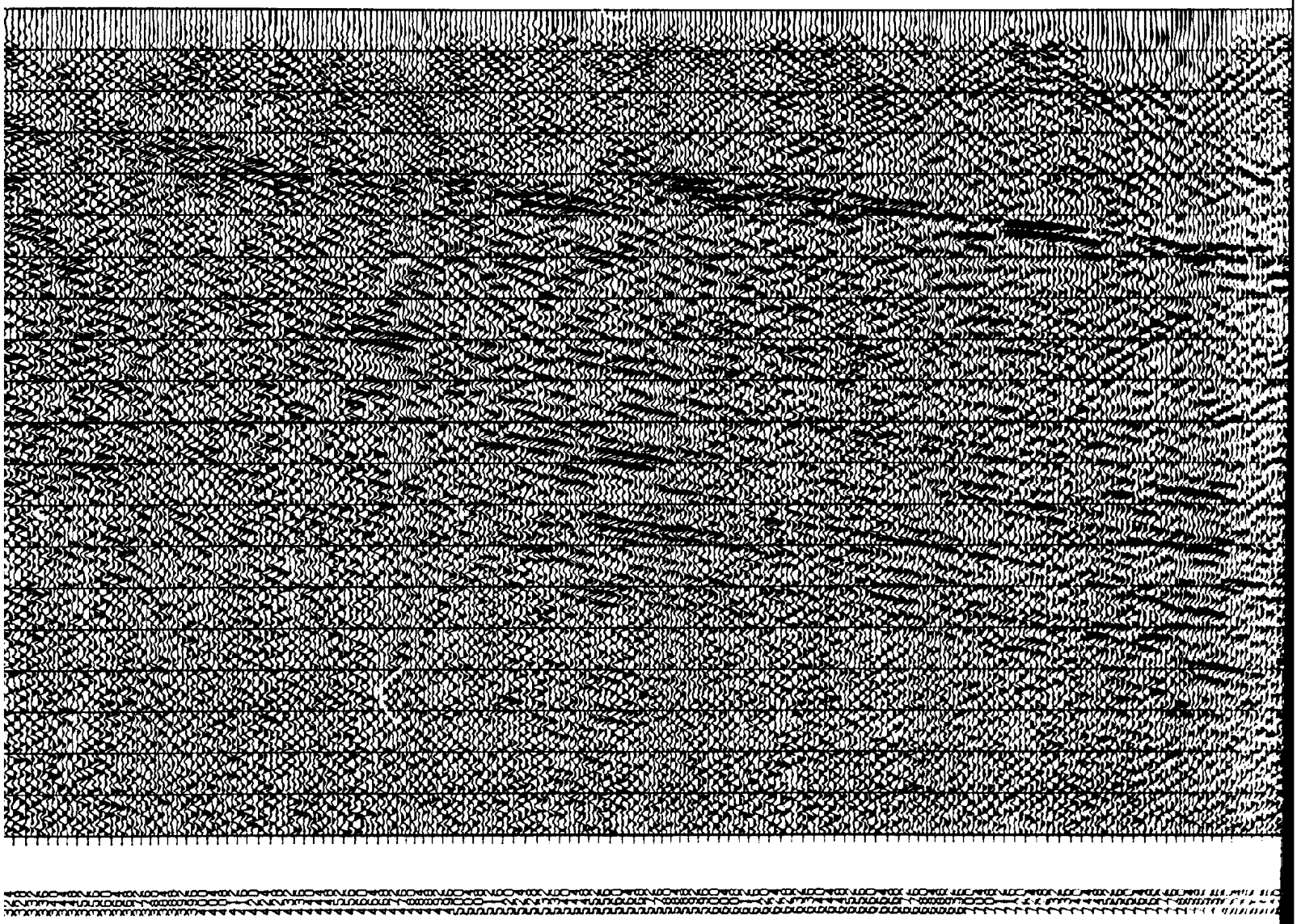

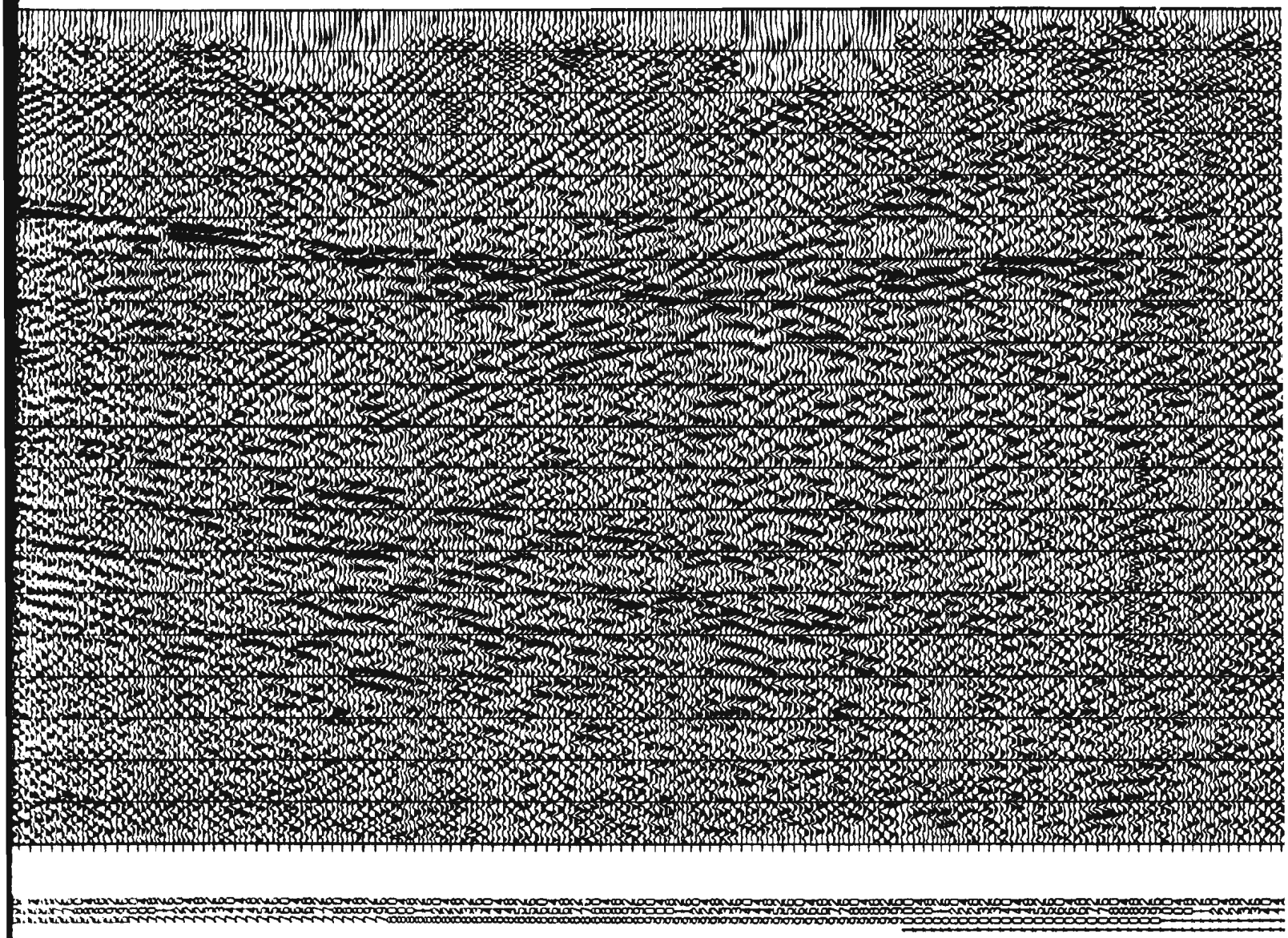

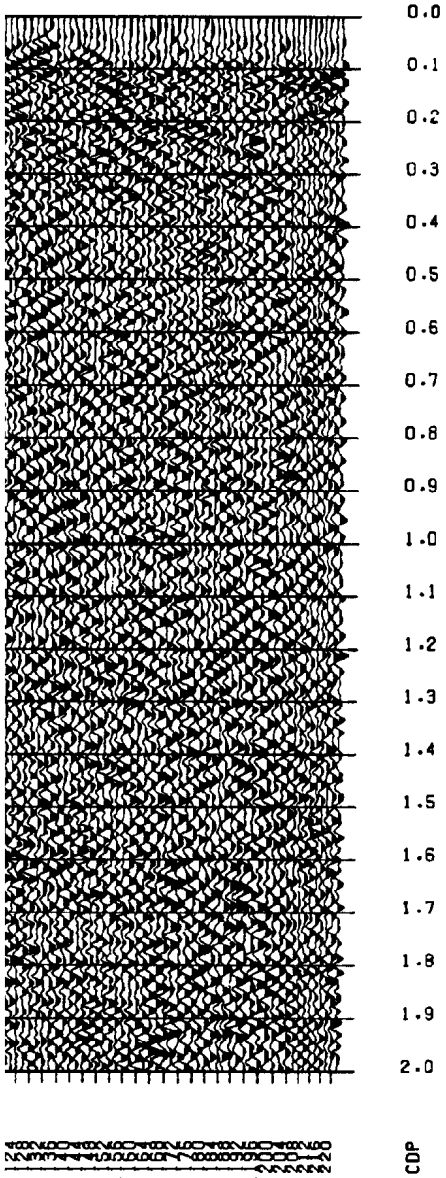
0.0
0.1
0.2
0.3
0.4
0.5
0.6
0.7
0.8
0.9
1.0
1.1
1.2
1.3
1.4
1.5
1.6
1.7
1.8
1.9
2.0
CDP

Figure 3.7 (p). Constant velocity stac
indicate velocity picks.

' stack of 4700 m/s, blue marks

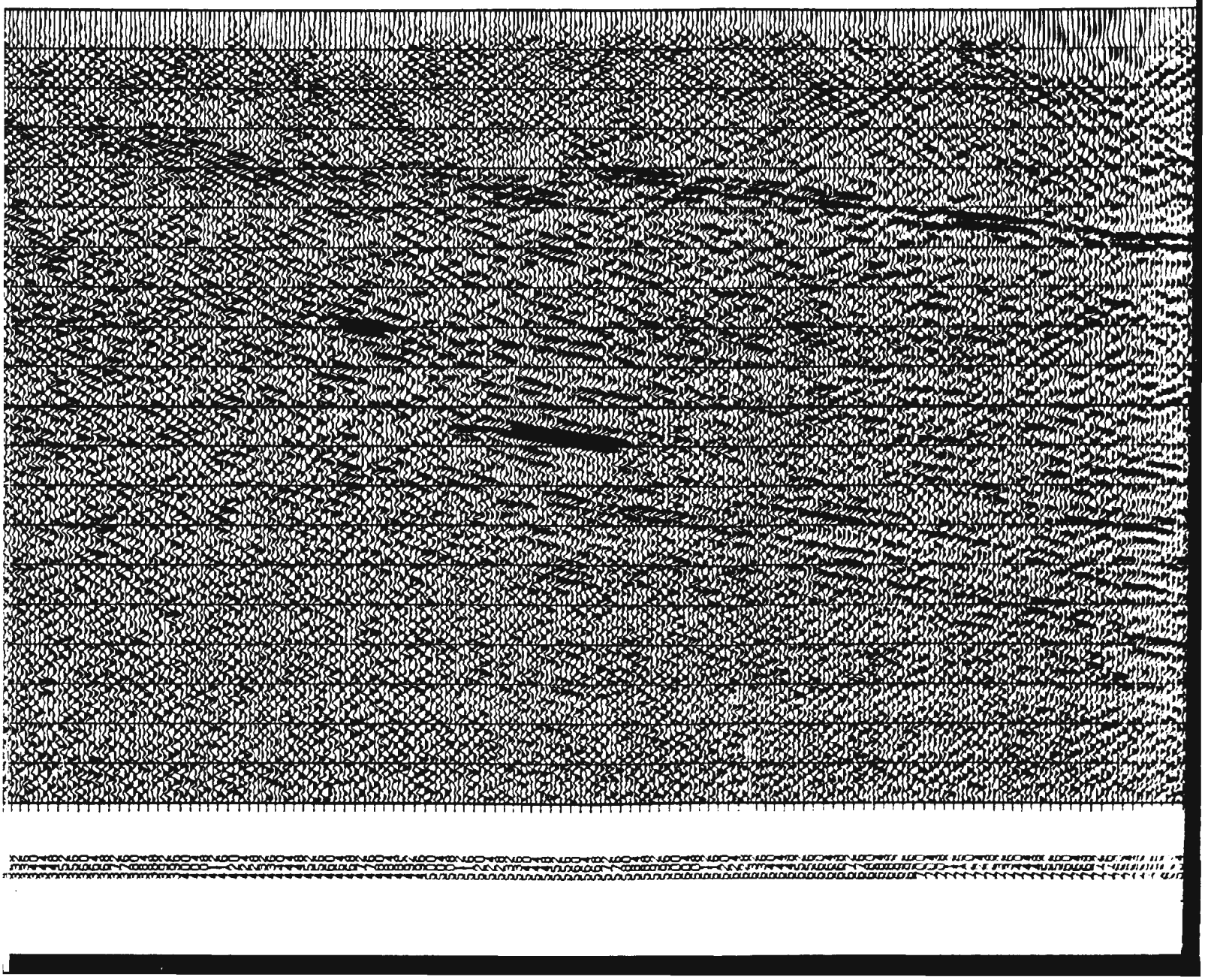

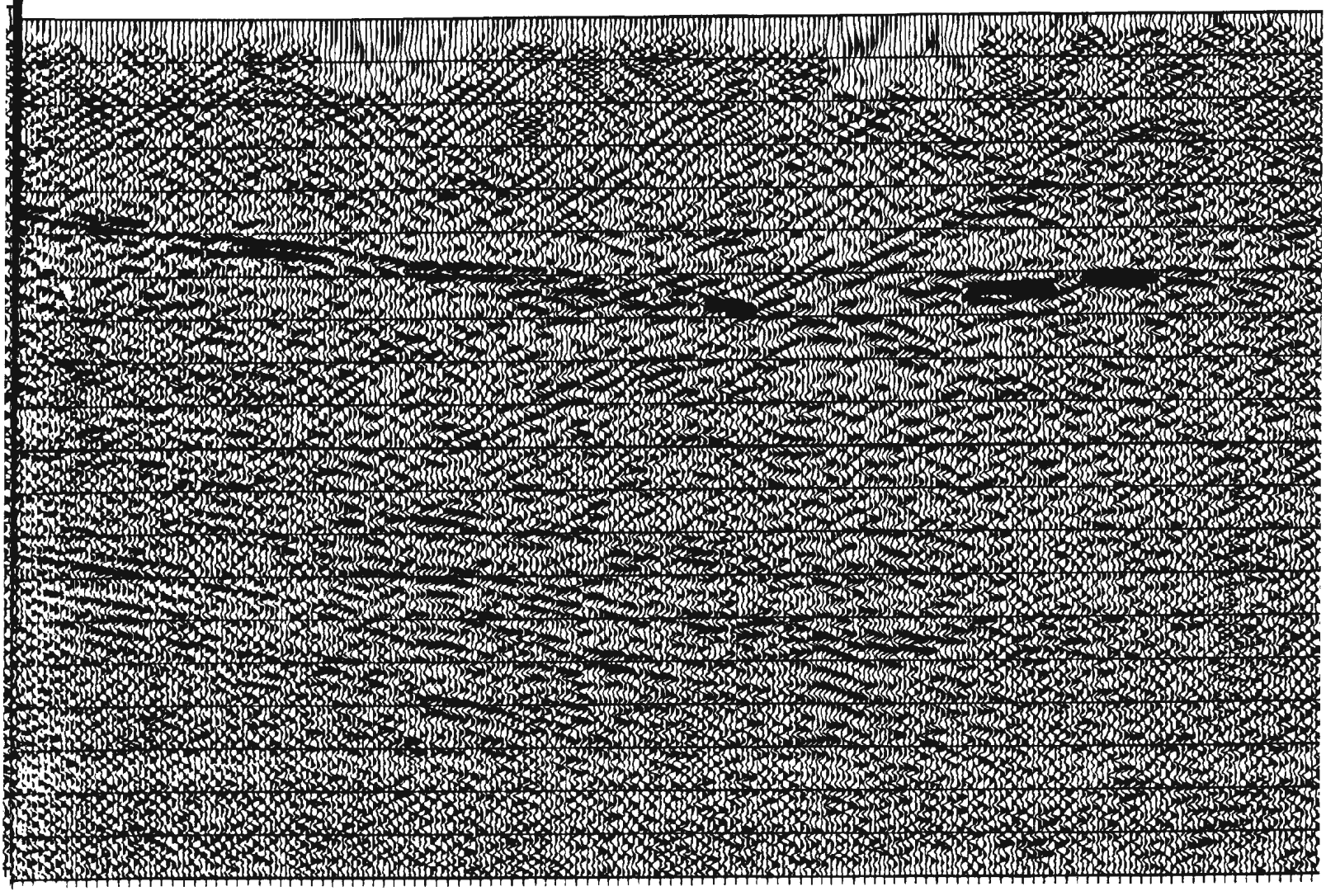

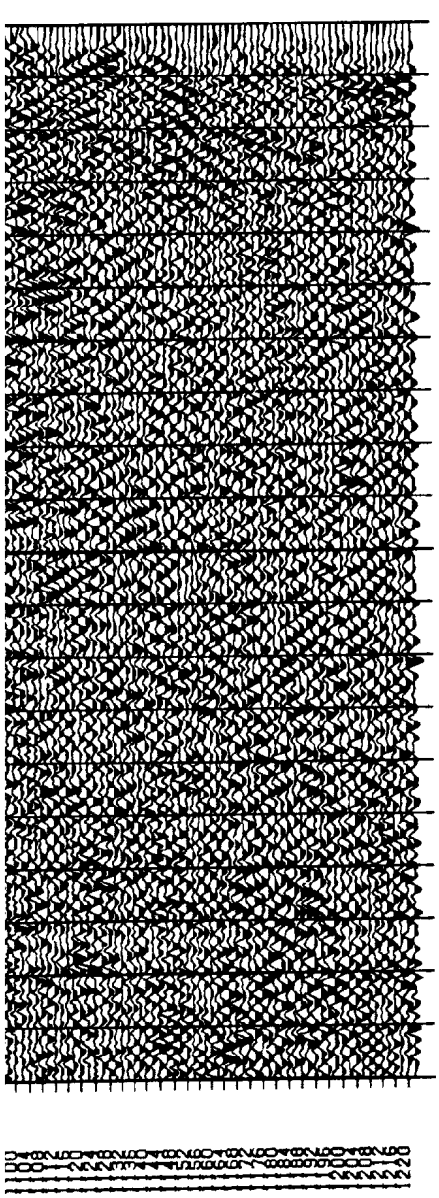
0.0
0.1
0.2
0.3
0.4
0.5
0.6
0.7
0.8
0.9
1.0
1.1
1.2
1.3
1.4
1.5
1.6
1.7
1.8
1.9
2.0
CDP

Figure 3.7 (o). Constant
marks indicate velocity p

(o). Constant velocity stack of 4500 m/s, blue cate velocity picks.

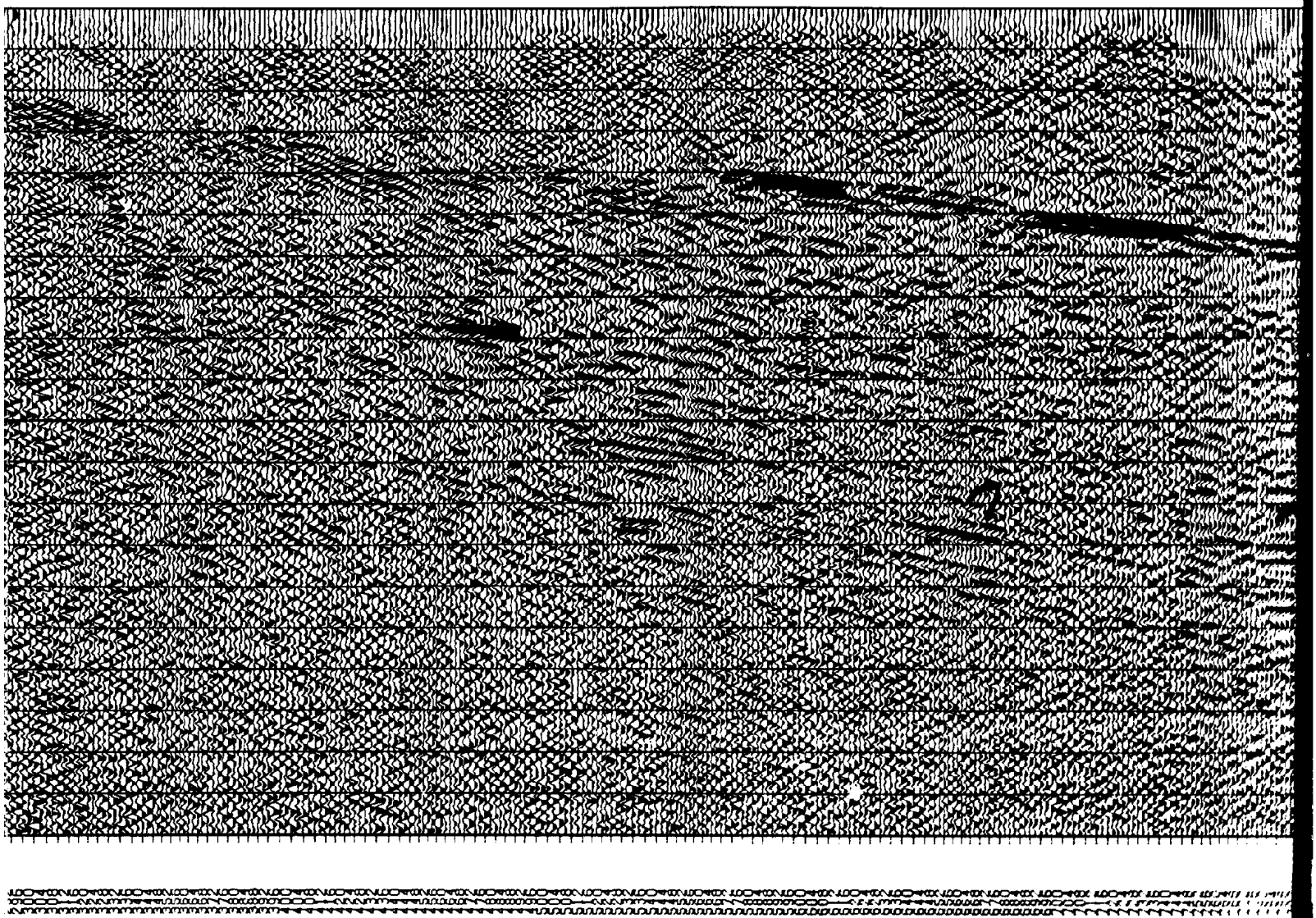

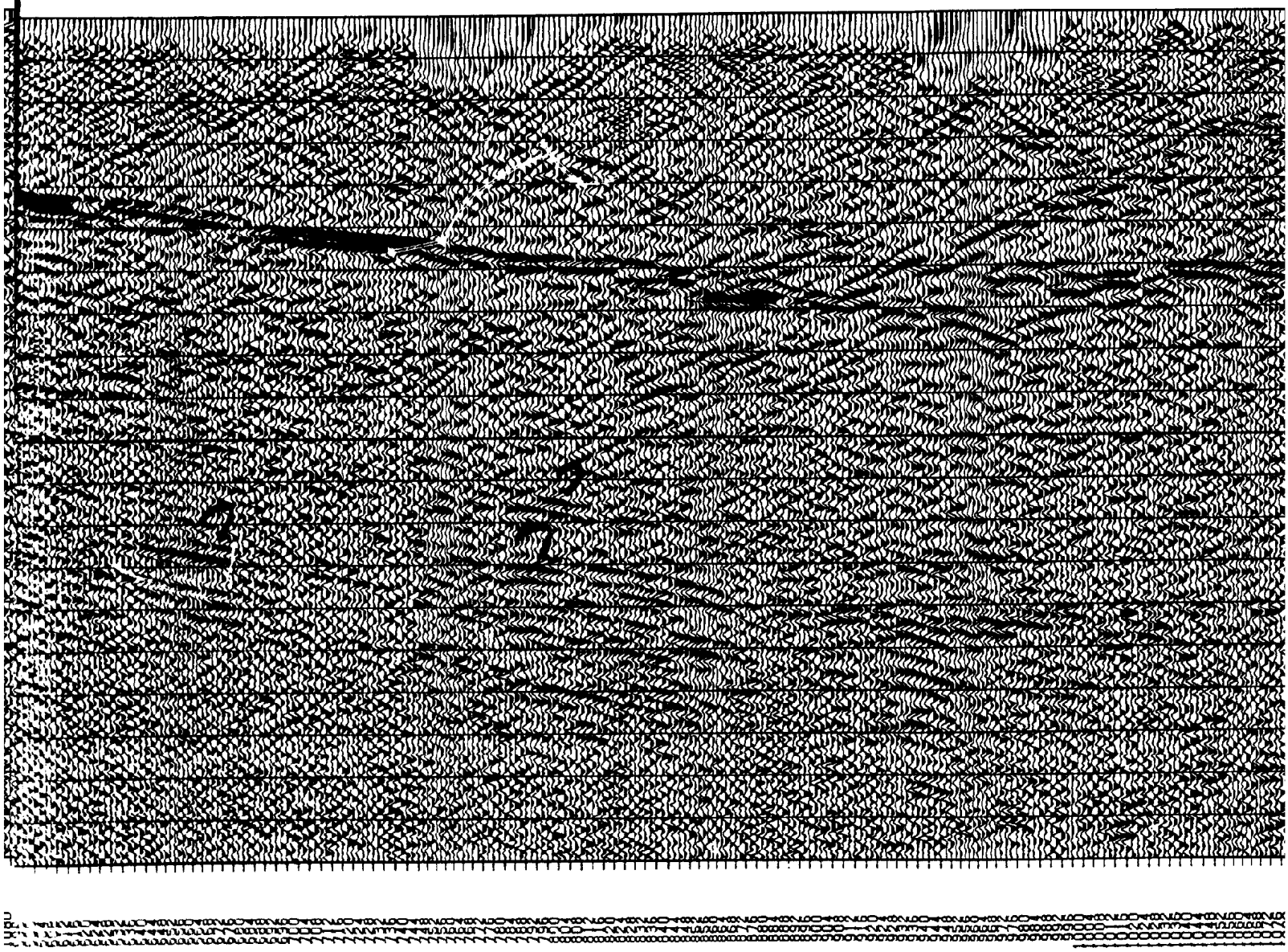

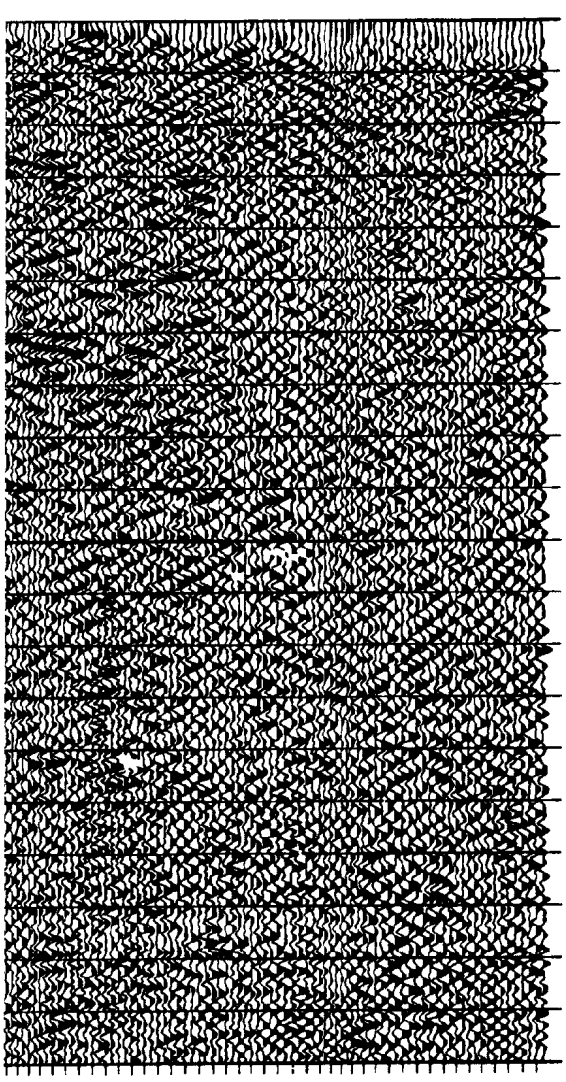

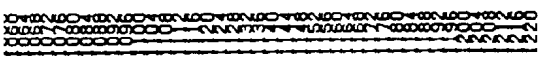

CDP

Figure 3.7 (n). Constant vel
marks indicate velocity pic
multiples at CMPs 800 to 9

velocity stack of 4300 m/s, blue
picks. Notice the likelihood of
) 900, TWT 1.3 s.

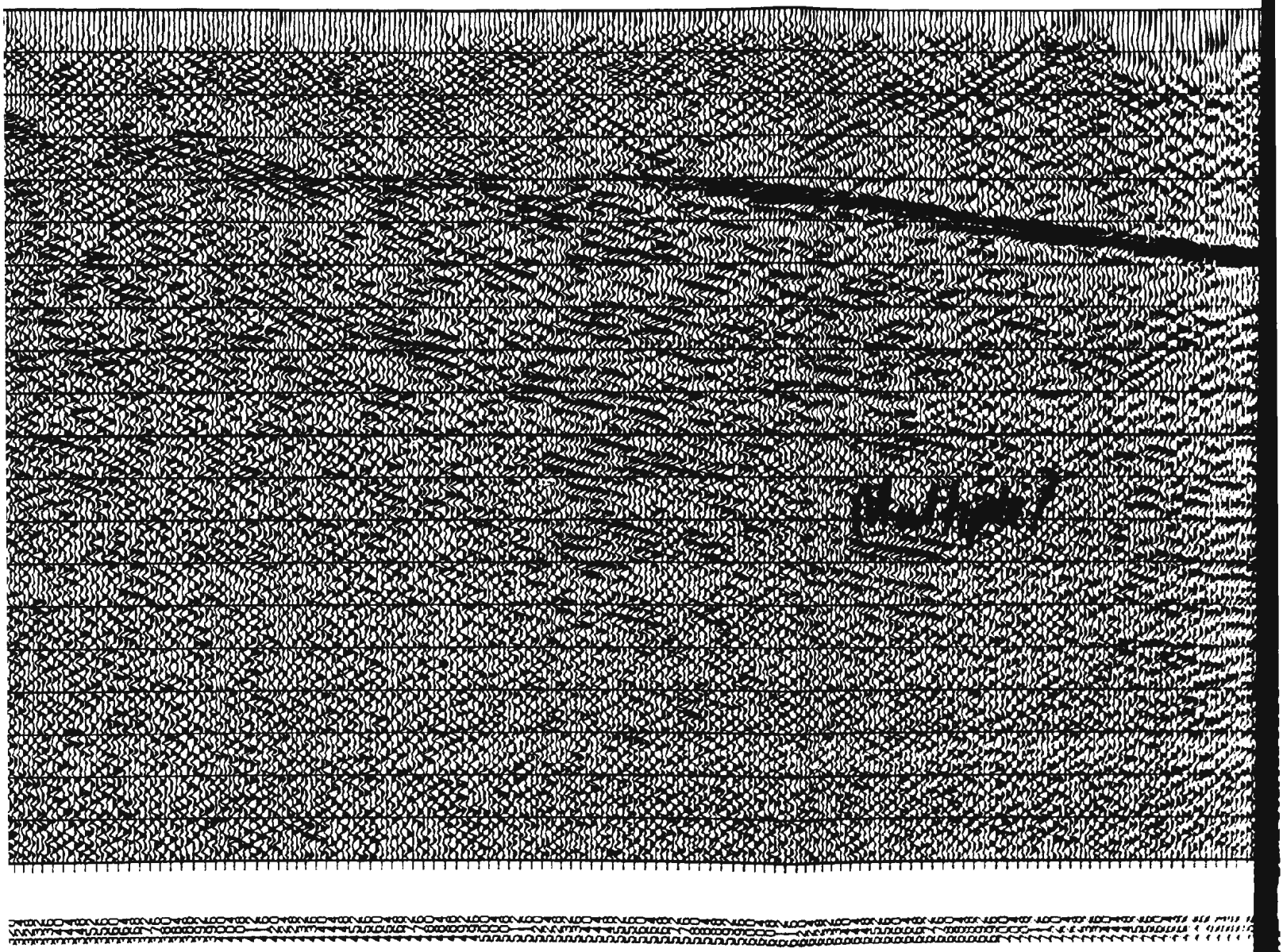

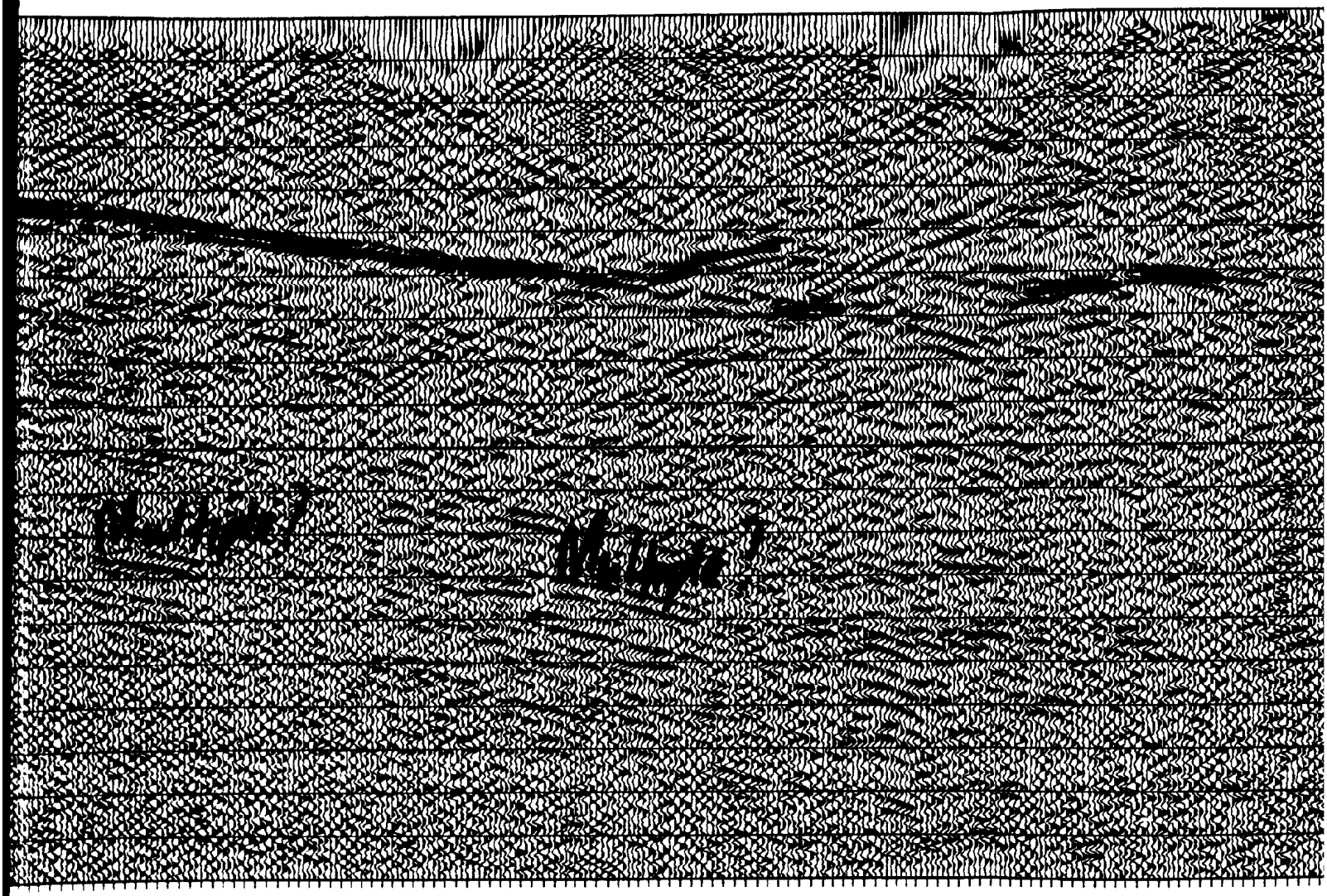

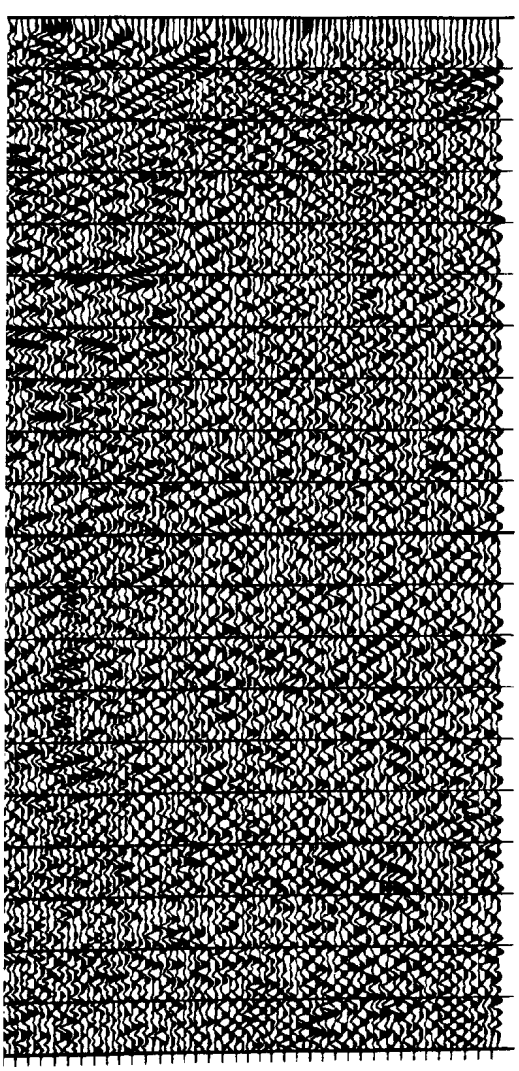
0.0
0.1
0.2
0.3
0.4
0.5
0.6
0.7
0.8
0.9
1.0
1.1
1.2
1.3
1.4
1.5
1.6
1.7
1.8
1.9
2.0
CDP

Figure 3.7 (m). Constant velocity stack of 41C
marks indicate velocity picks.

y stack of 4100 m/s, blue

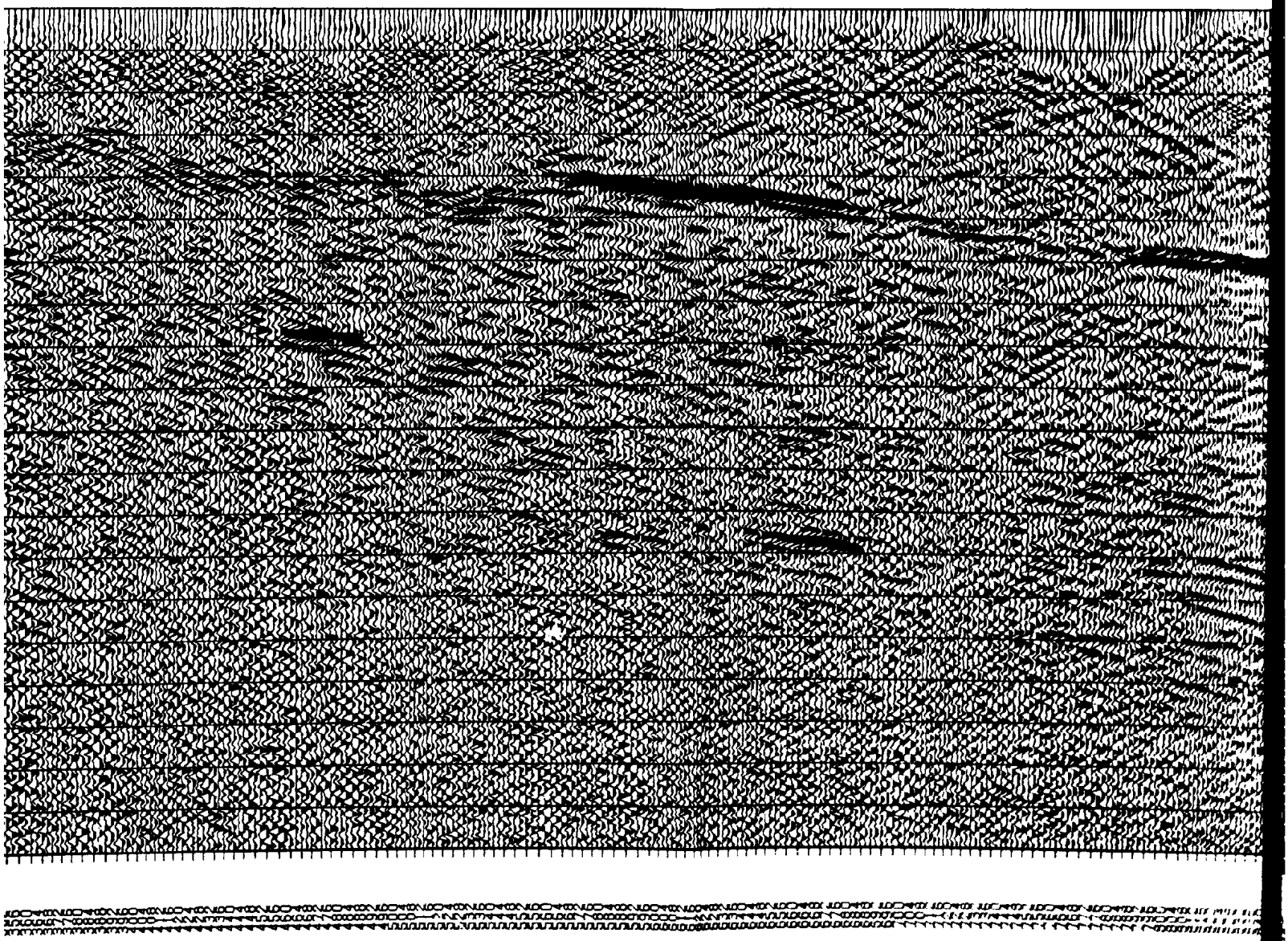

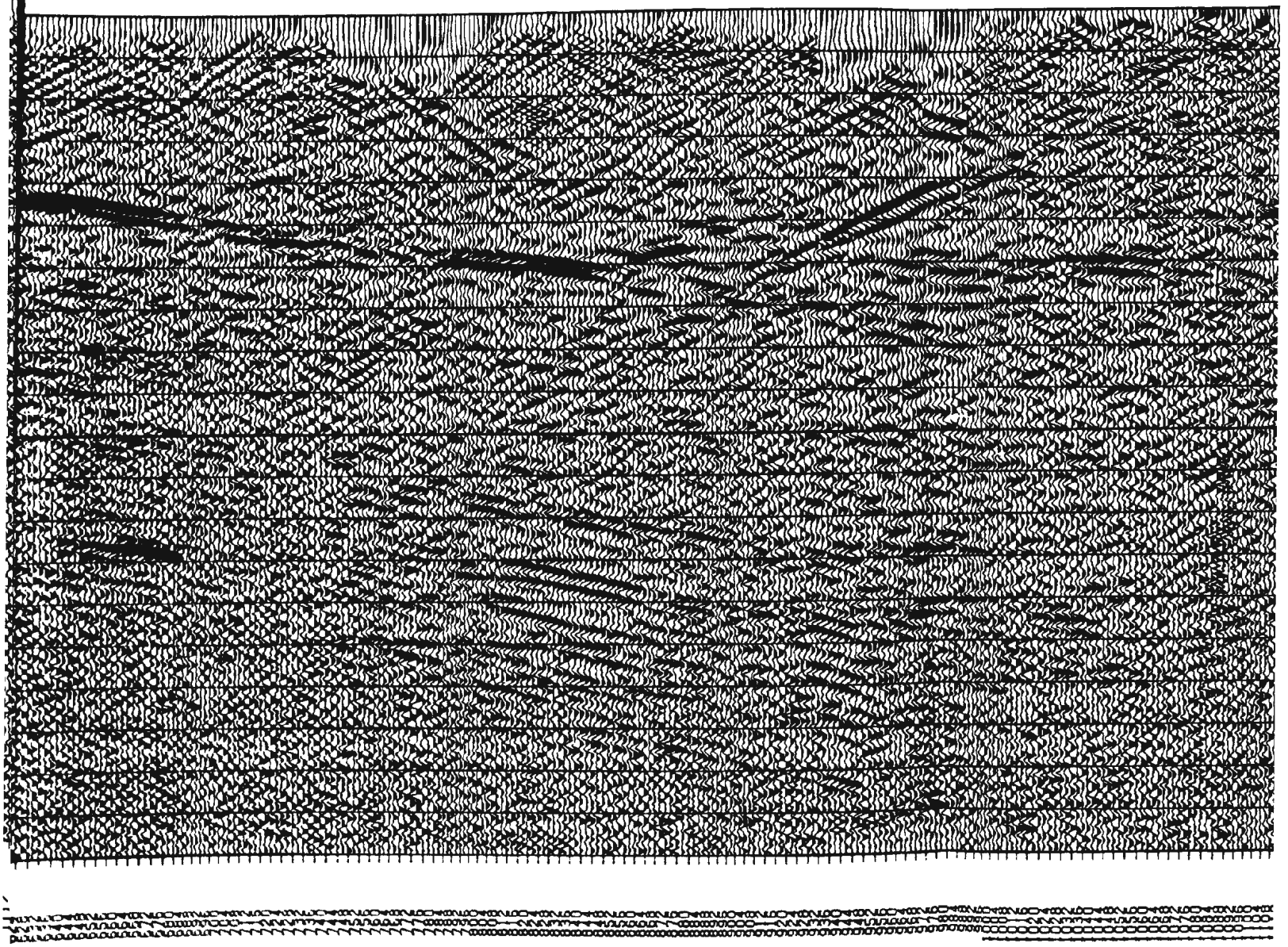

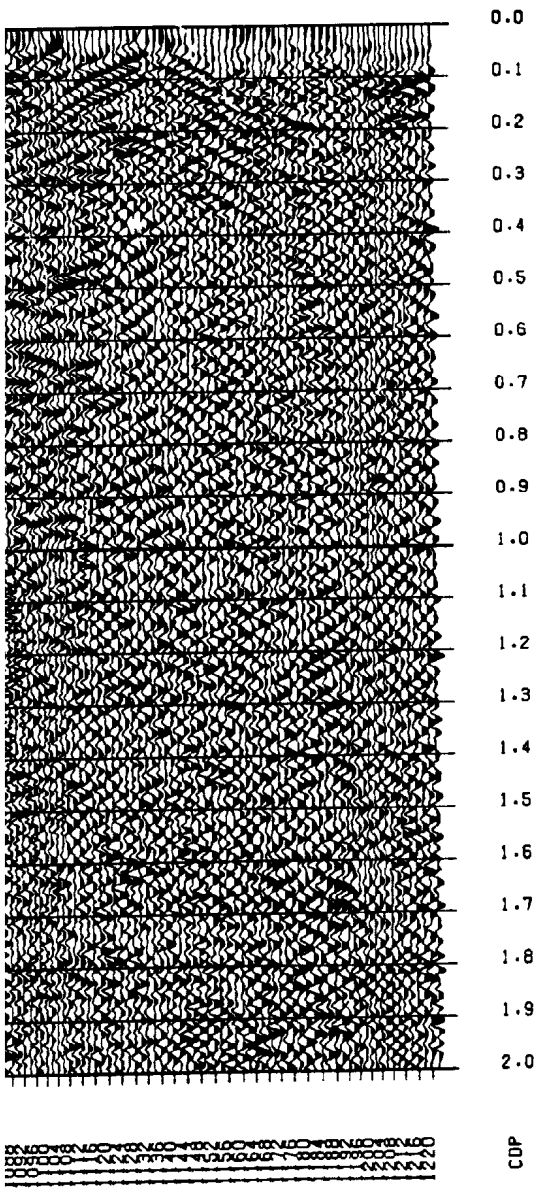
0.0
0.1
0.2
0.3
0.4
0.5
0.6
0.7
0.8
0.9
1.0
1.1
1.2
1.3
1.4
1.5
1.6
1.7
1.8
1.9
2.0
CDP

Figure 3.7 (l). Constant v
marks indicate velocity p

ınstant velocity stack of 3900 m/s, blue
locity picks.

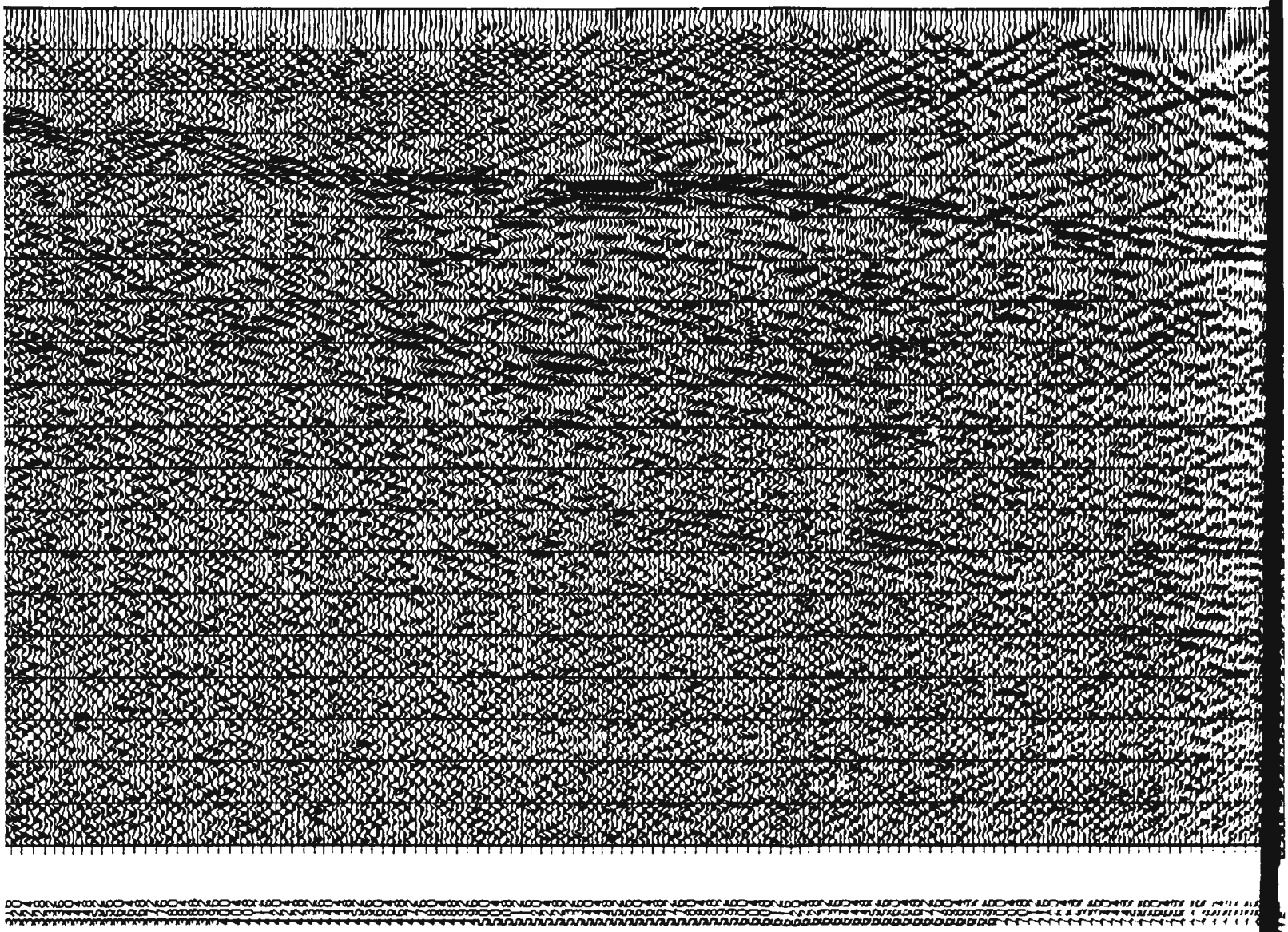

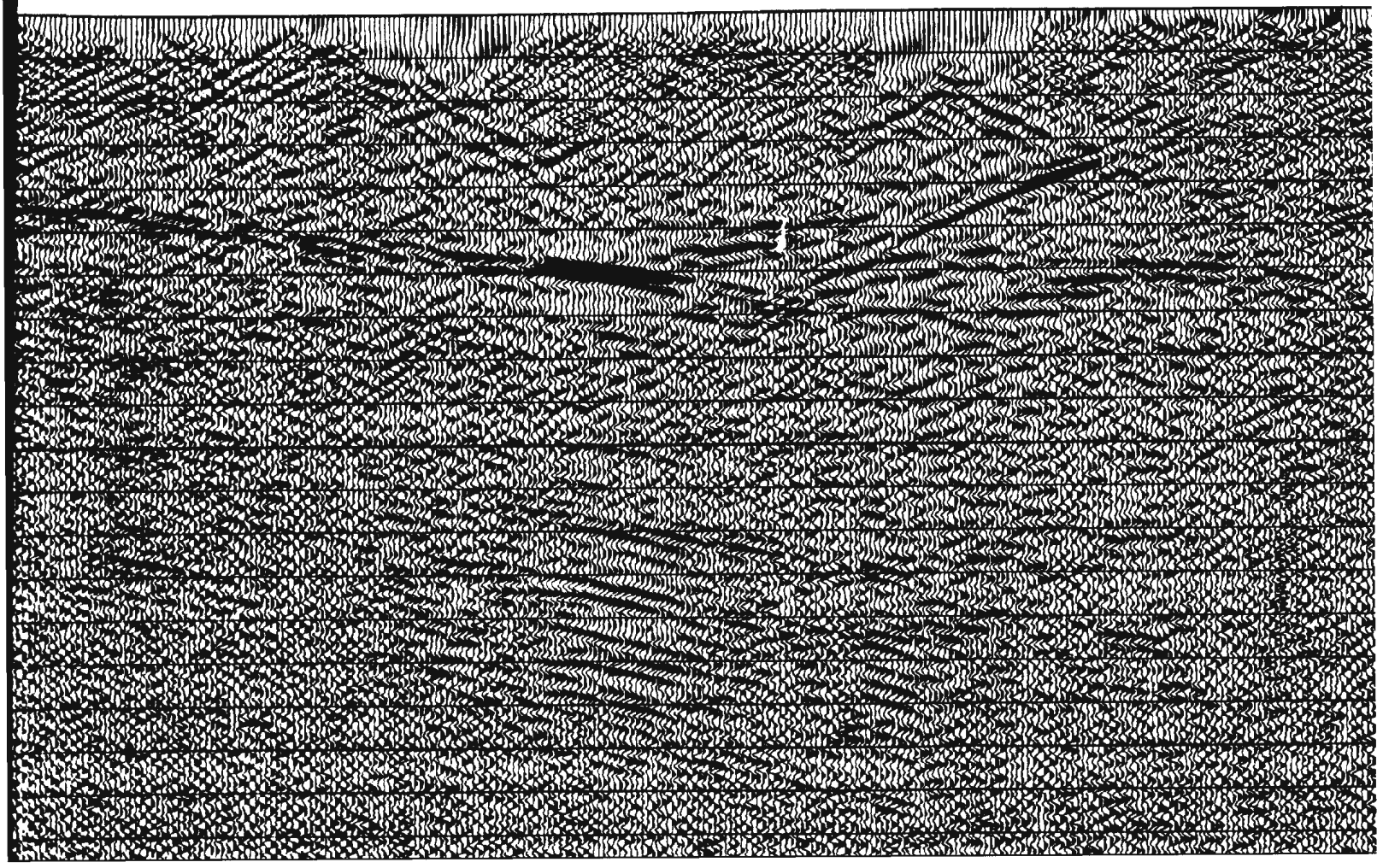

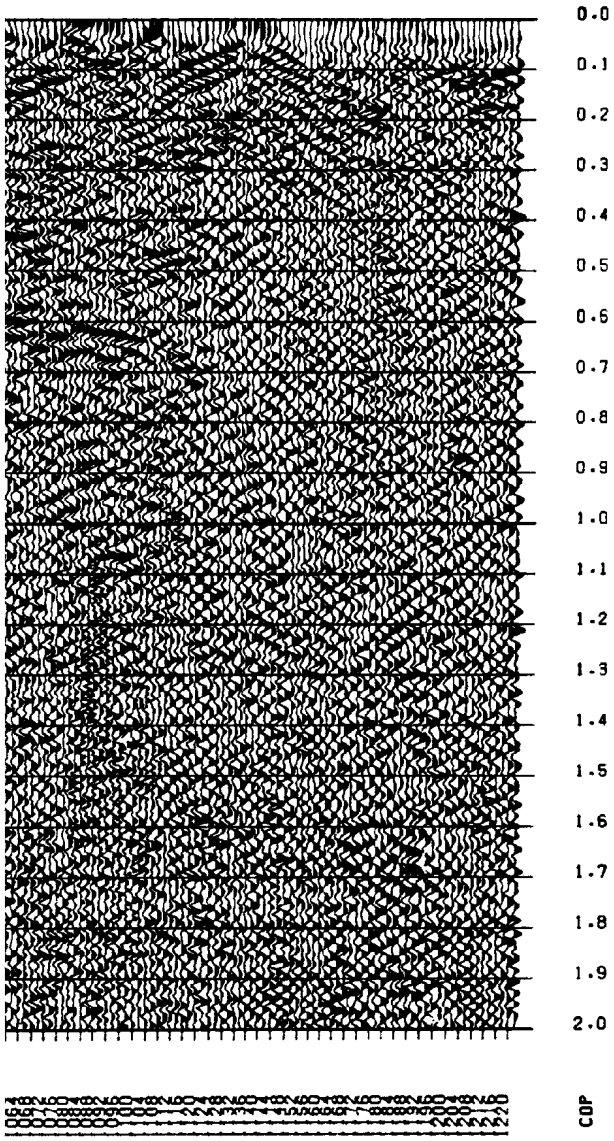
0.0
0.1
0.2
0.3
0.4
0.5
0.6
0.7
0.8
0.9
1.0
1.1
1.2
1.3
1.4
1.5
1.6
1.7
1.8
1.9
2.0
CDP

Figure 3.7 (k). Constant ve
marks indicate velocity pic

:onstant velocity stack of 3700 m/s, blue
elocity picks.

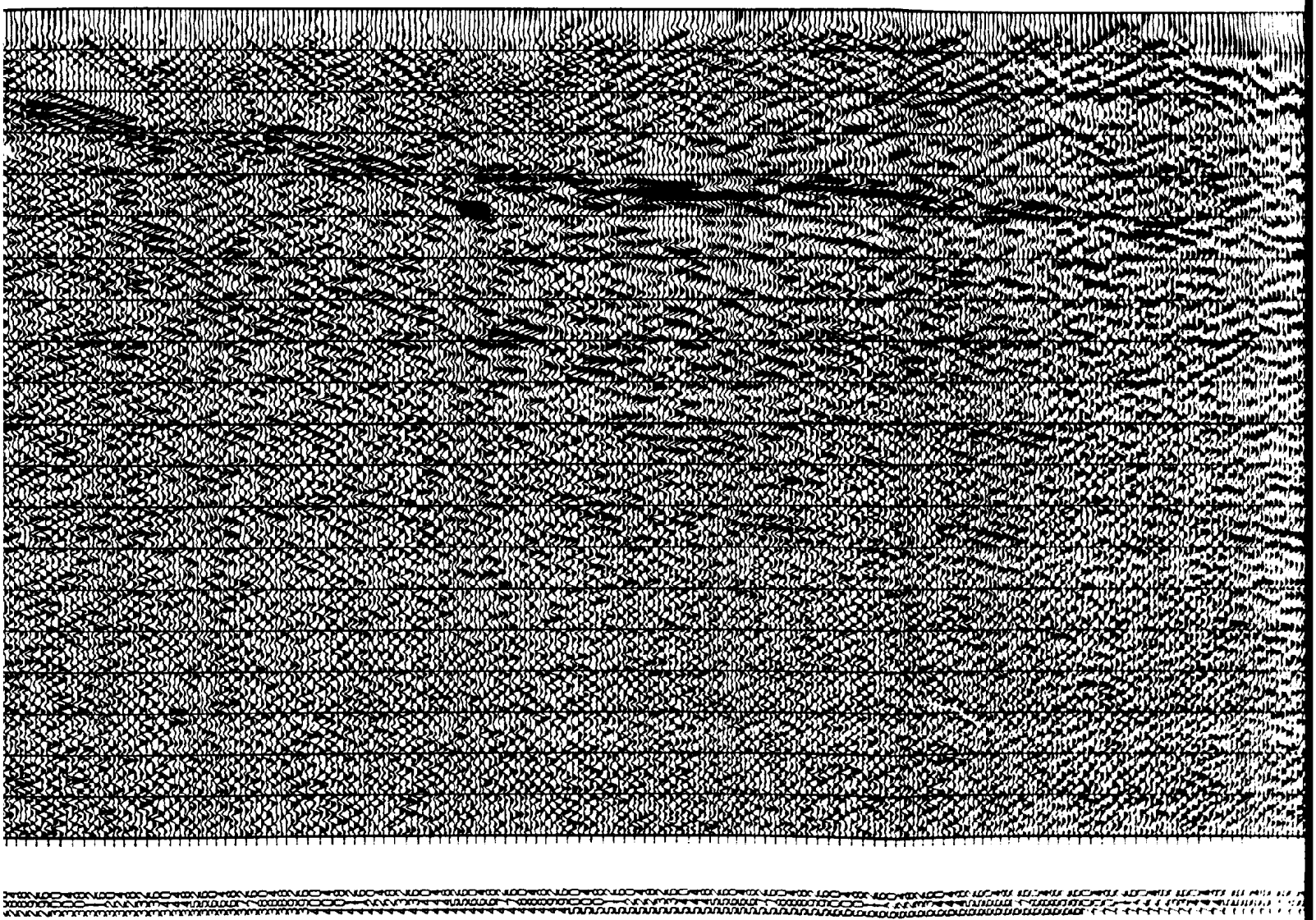

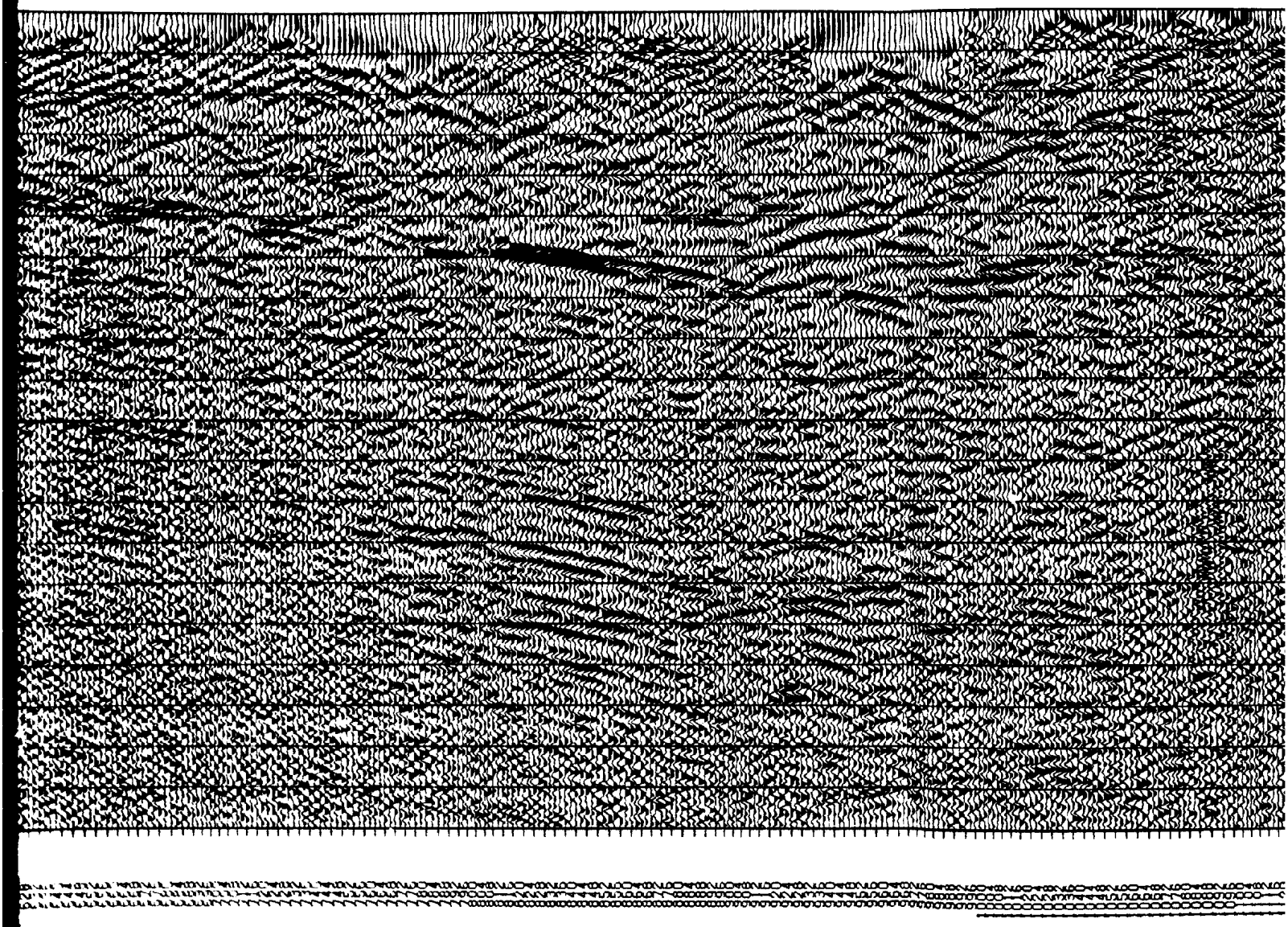

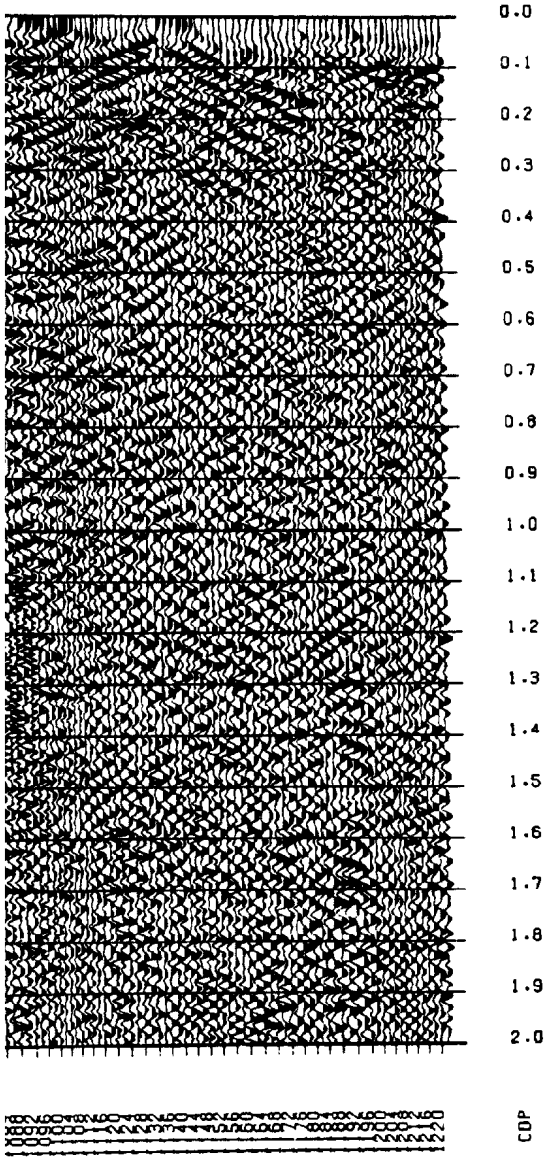
0.0
0.1
0.2
0.3
0.4
0.5
0.6
0.7
0.8
0.9
1.0
1.1
1.2
1.3
1.4
1.5
1.6
1.7
1.8
1.9
2.0
CDP

Figure 3.7 (j). Constant velocit
marks indicate velocity picks.

velocity stack of 3500 m/s, blue
picks.

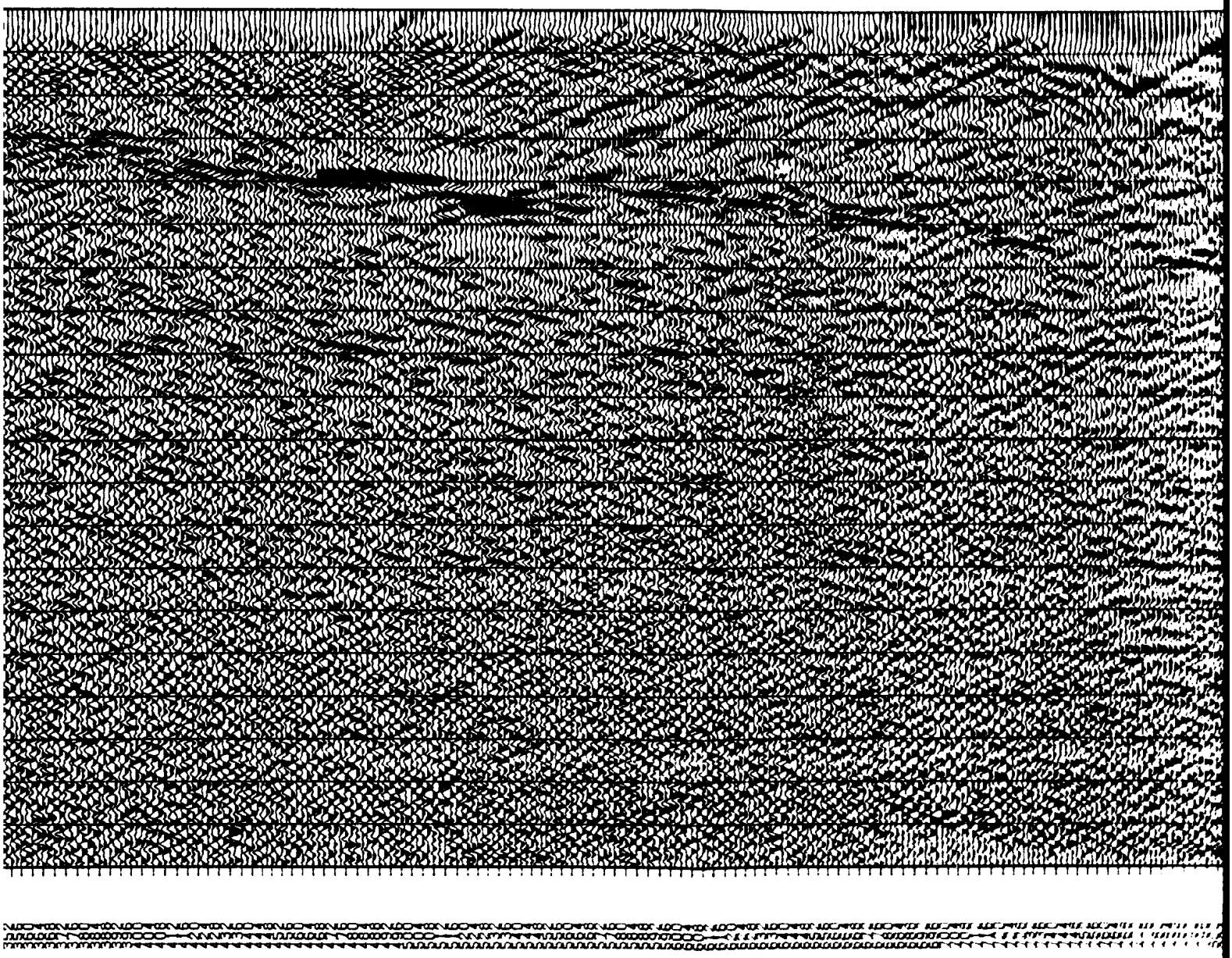

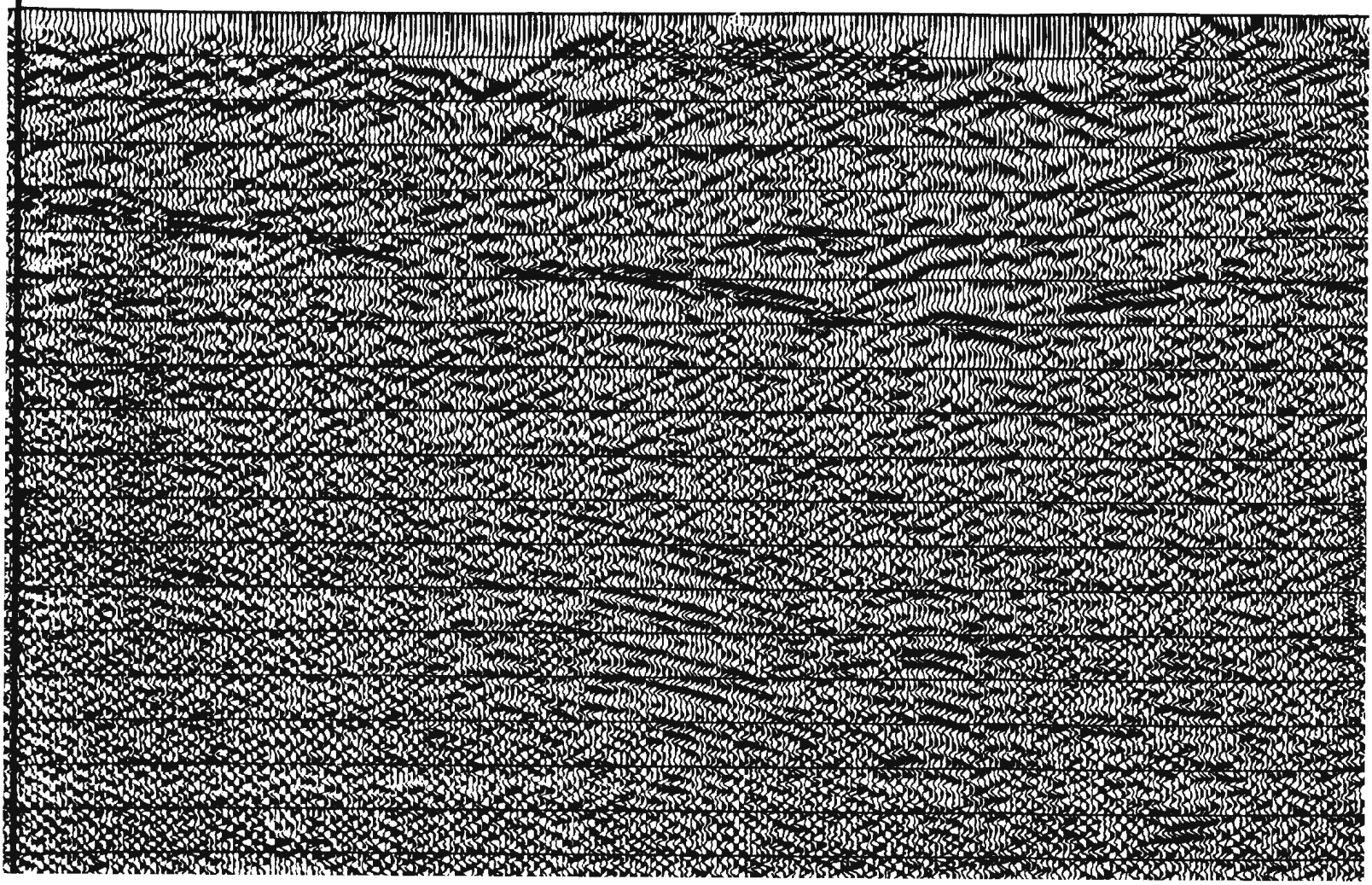

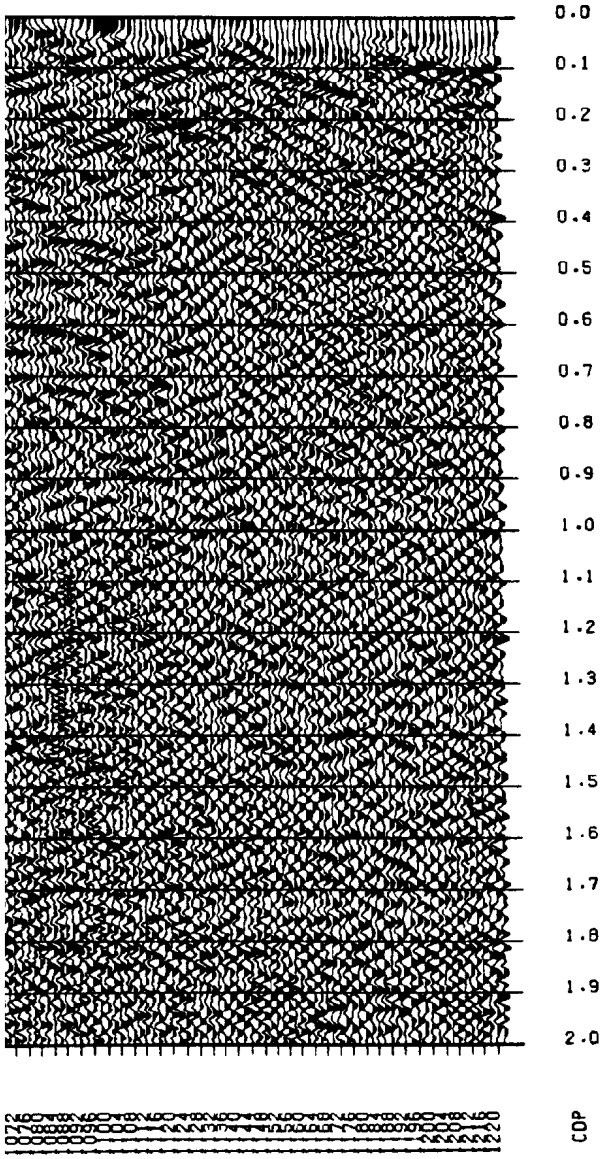
0.0
0.1
0.2
0.3
0.4
0.5
0.6
0.7
0.8
0.9
1.0
1.1
1.2
1.3
1.4
1.5
1.6
1.7
1.8
1.9
2.0

CDP

Figure 3.7 (i). Constant vel
marks indicate velocity pick

(i). Constant velocity stack of 3300 m/s, blue
ate velocity picks.

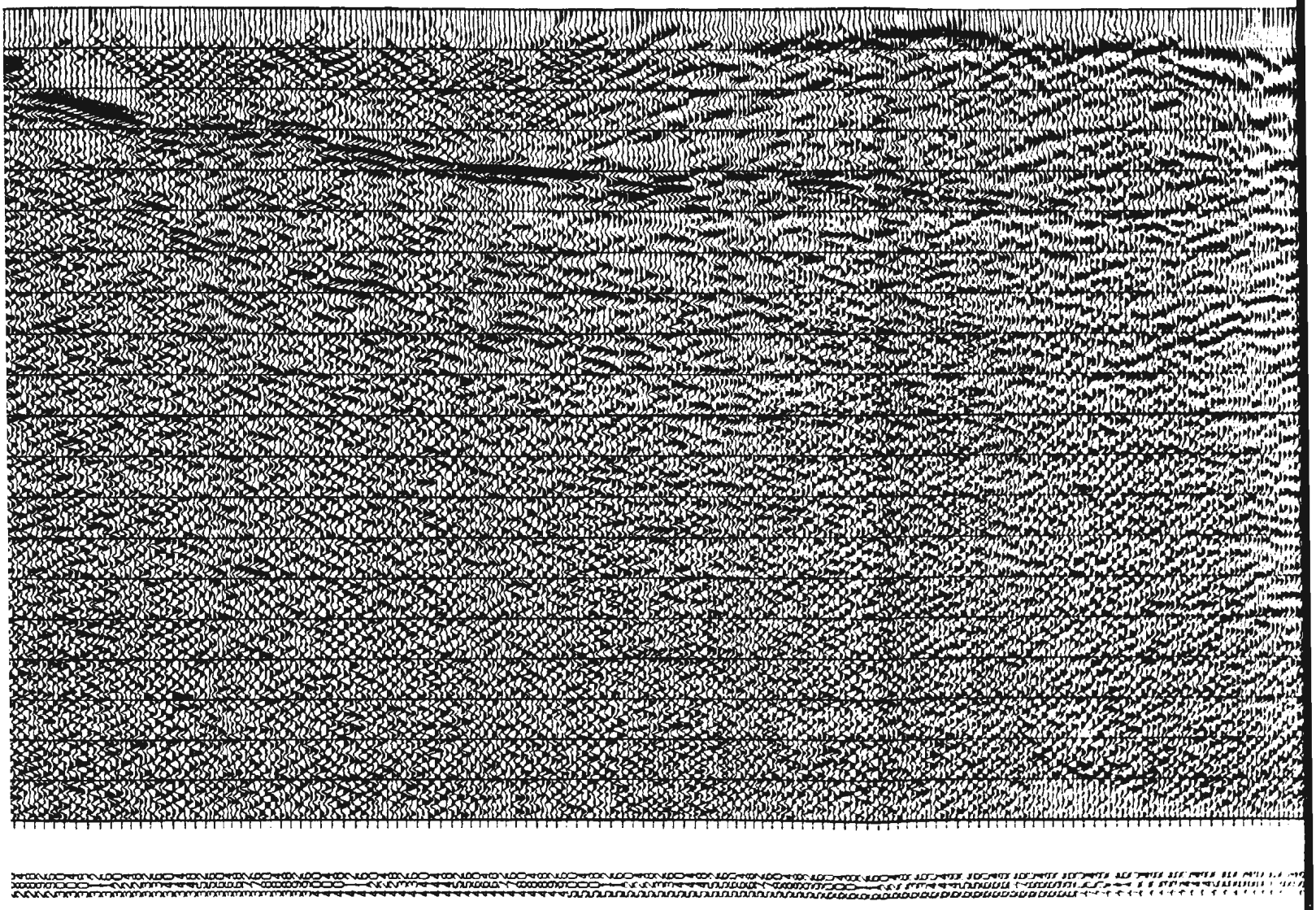

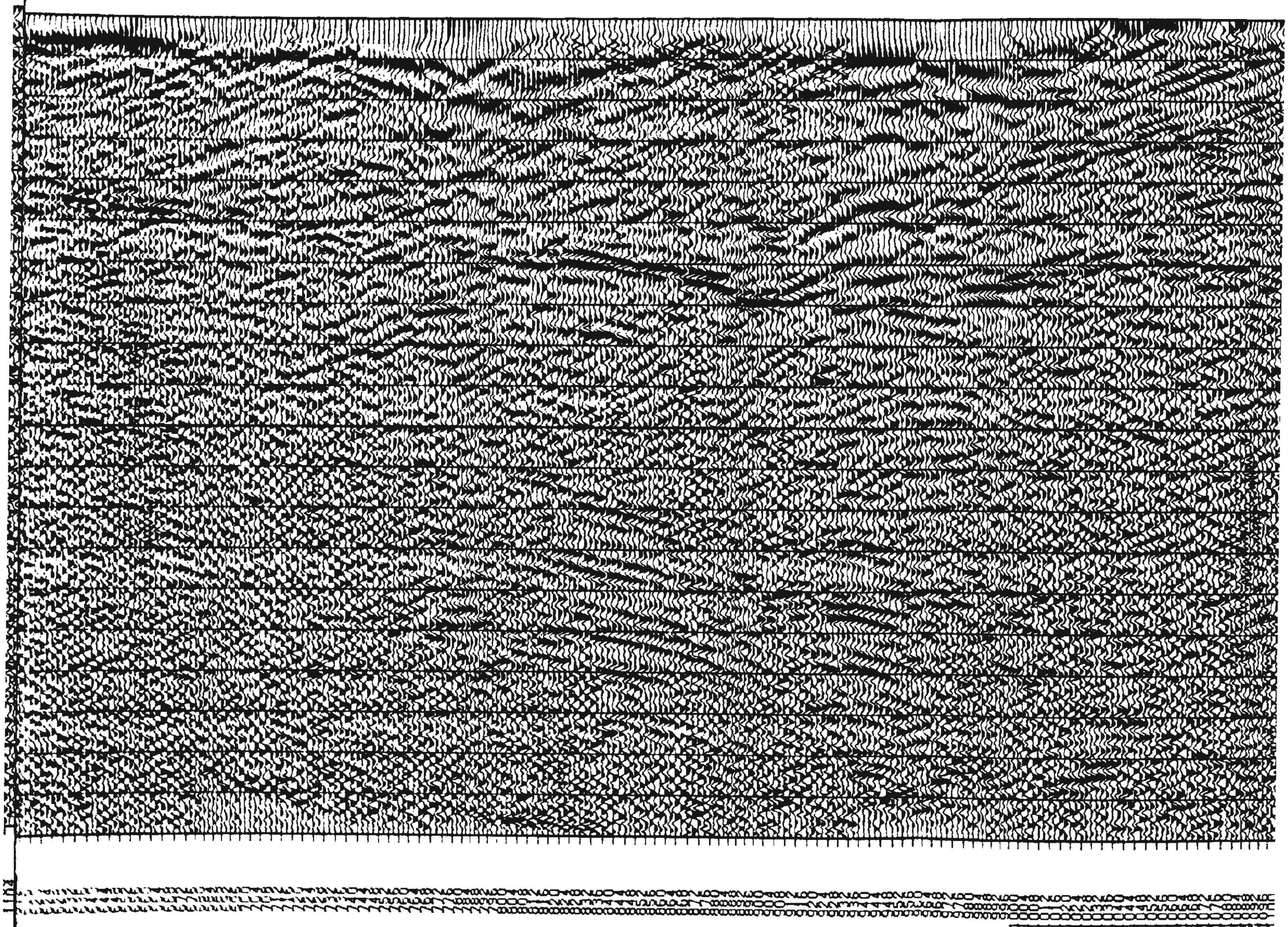

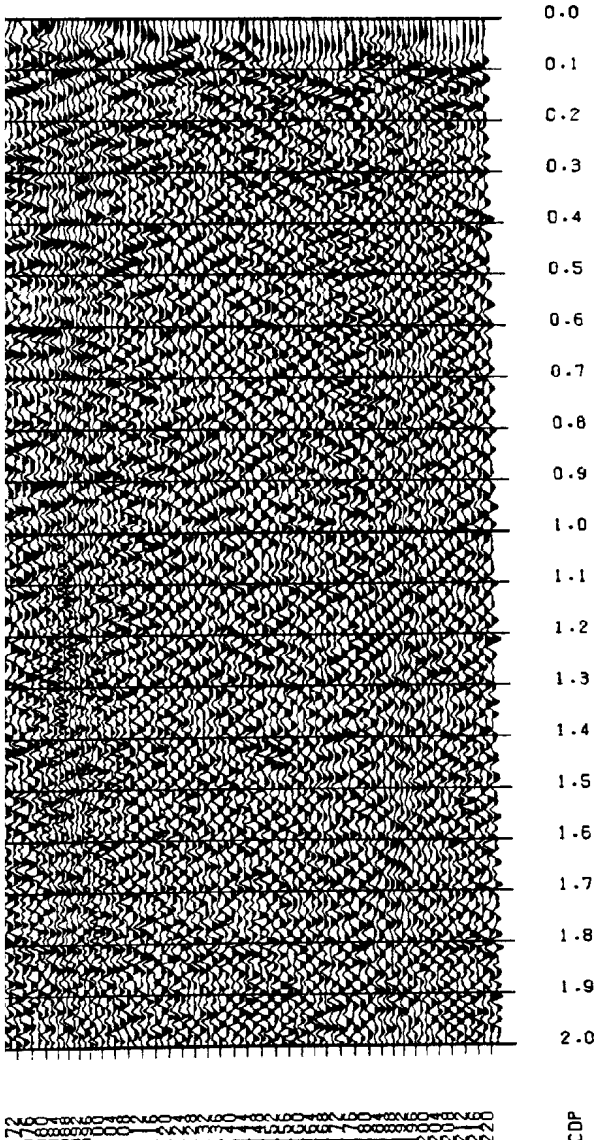
0.0
0.1
0.2
0.3
0.4
0.5
0.6
0.7
0.8
0.9
1.0
1.1
1.2
1.3
1.4
1.5
1.6
1.7
1.8
1.9
2.0
CDP

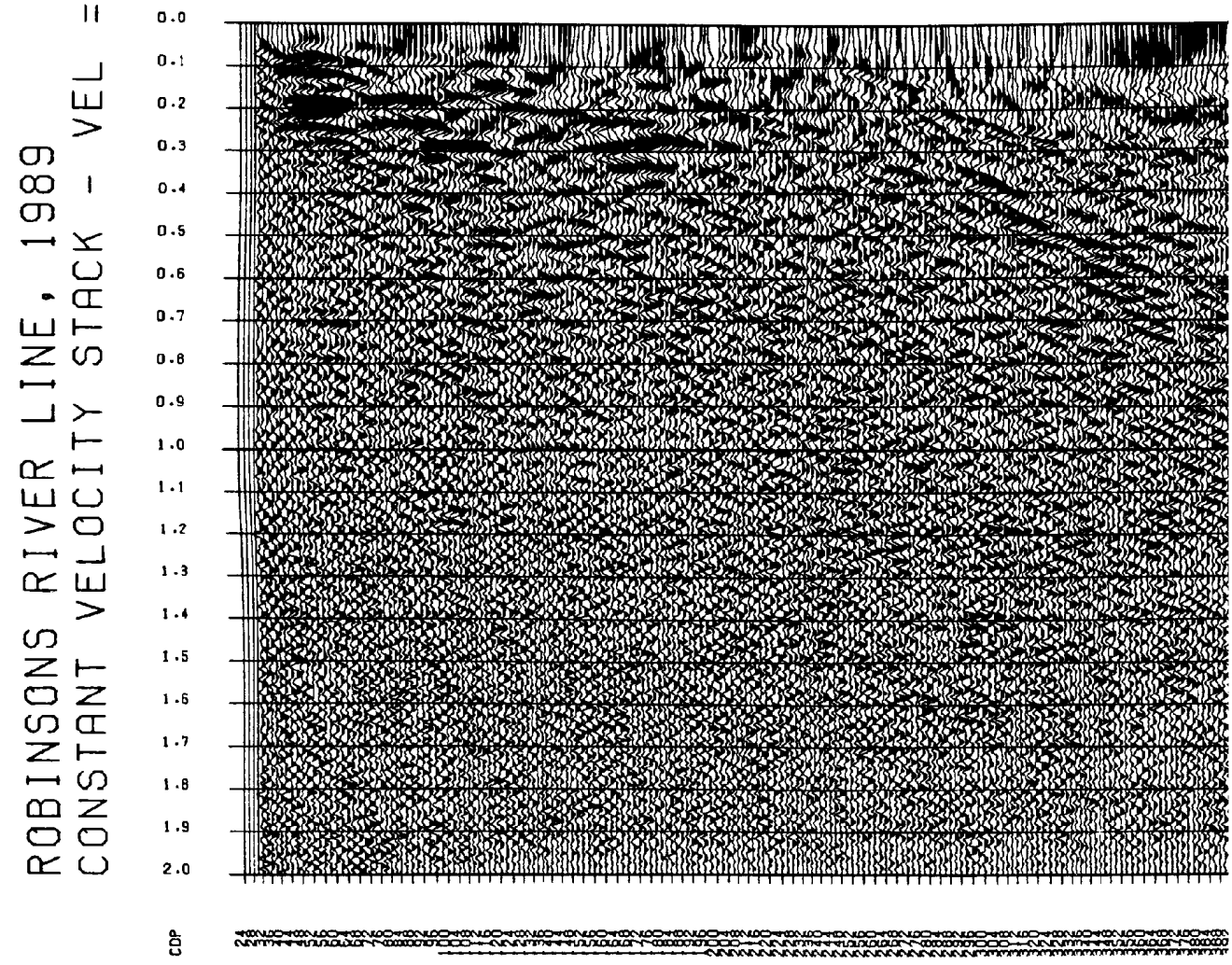

Figure 3.7 (h). Constant velocity stack of 3200 m/ marks indicate velocity picks.

:ack of 3200 m/s, blue

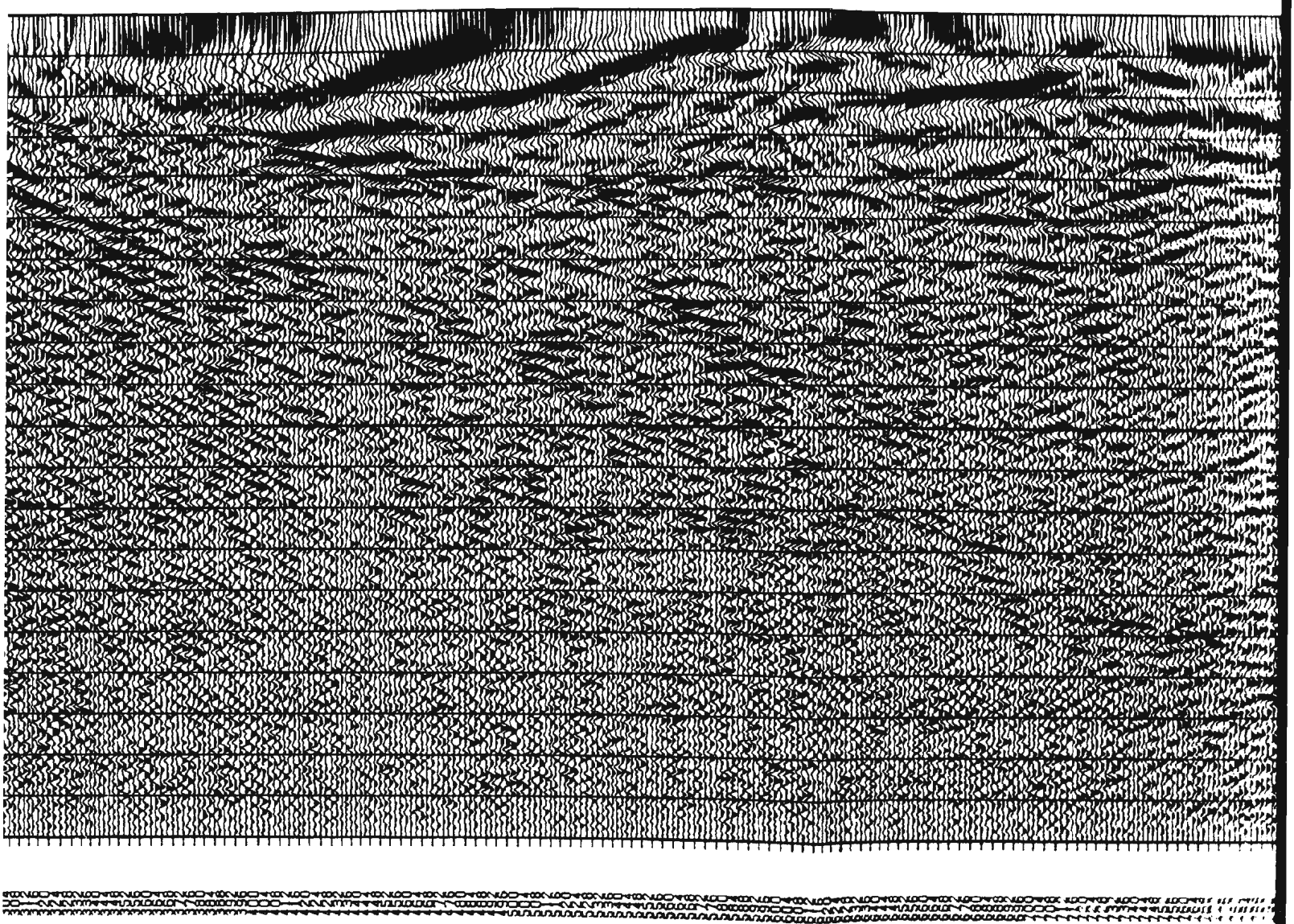

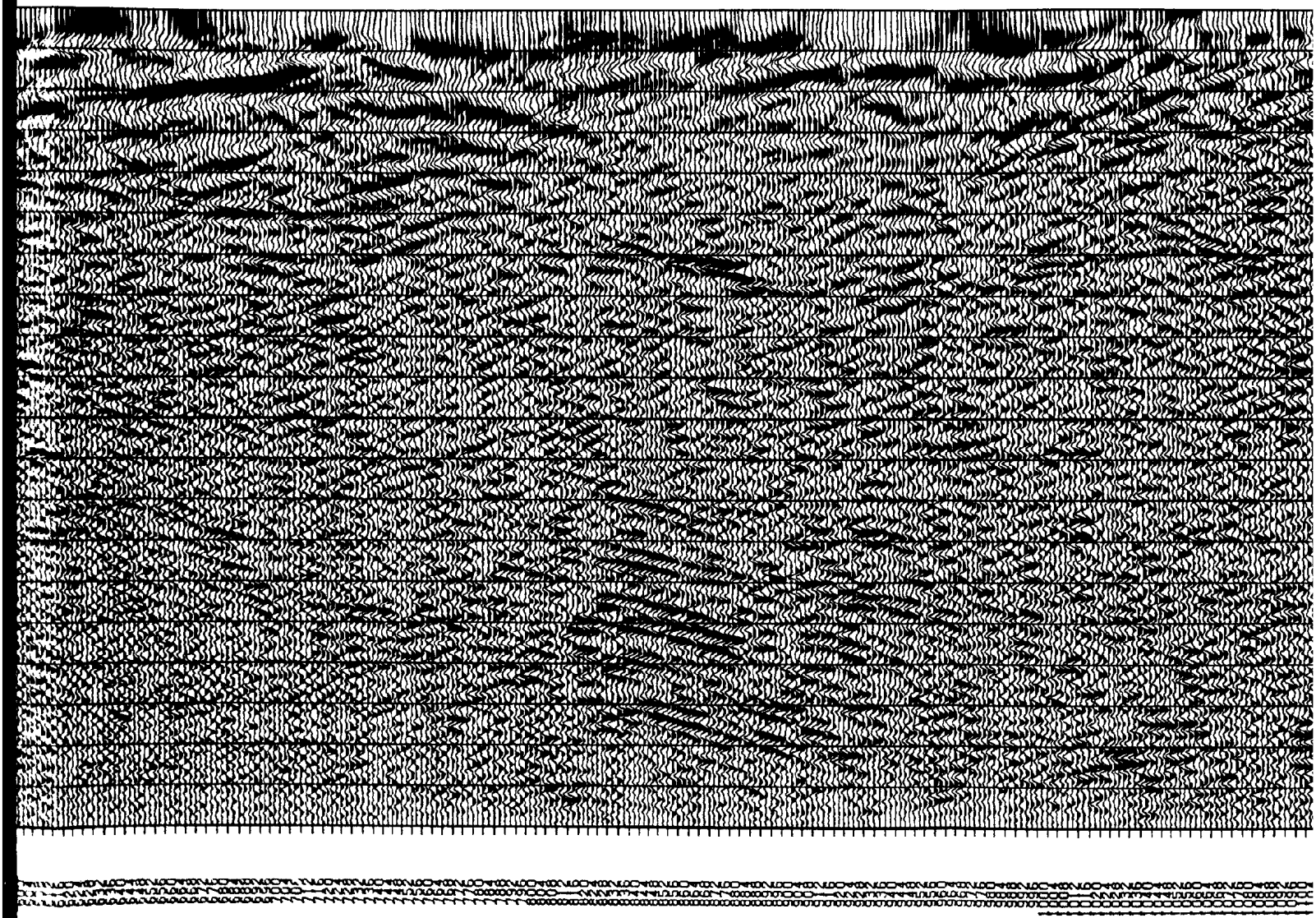

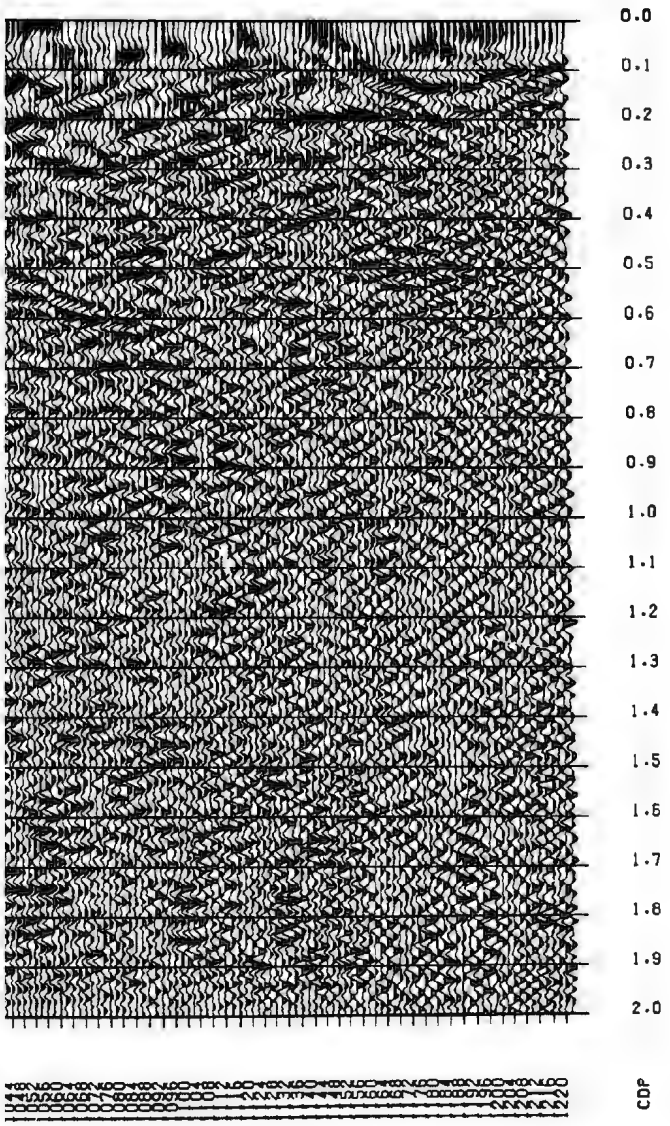
0.0
0.1
0.2
0.3
0.4
0.5
0.6
0.7
0.8
0.9
1.0
1.1
1.2
1.3
1.4
1.5
1.6
1.7
1.8
1.9
2.0
CDP

Figure 3.7 (g). Constant velocity stack. Velocity marks indicate velocity picks.

stack of 3100 m/s, blue

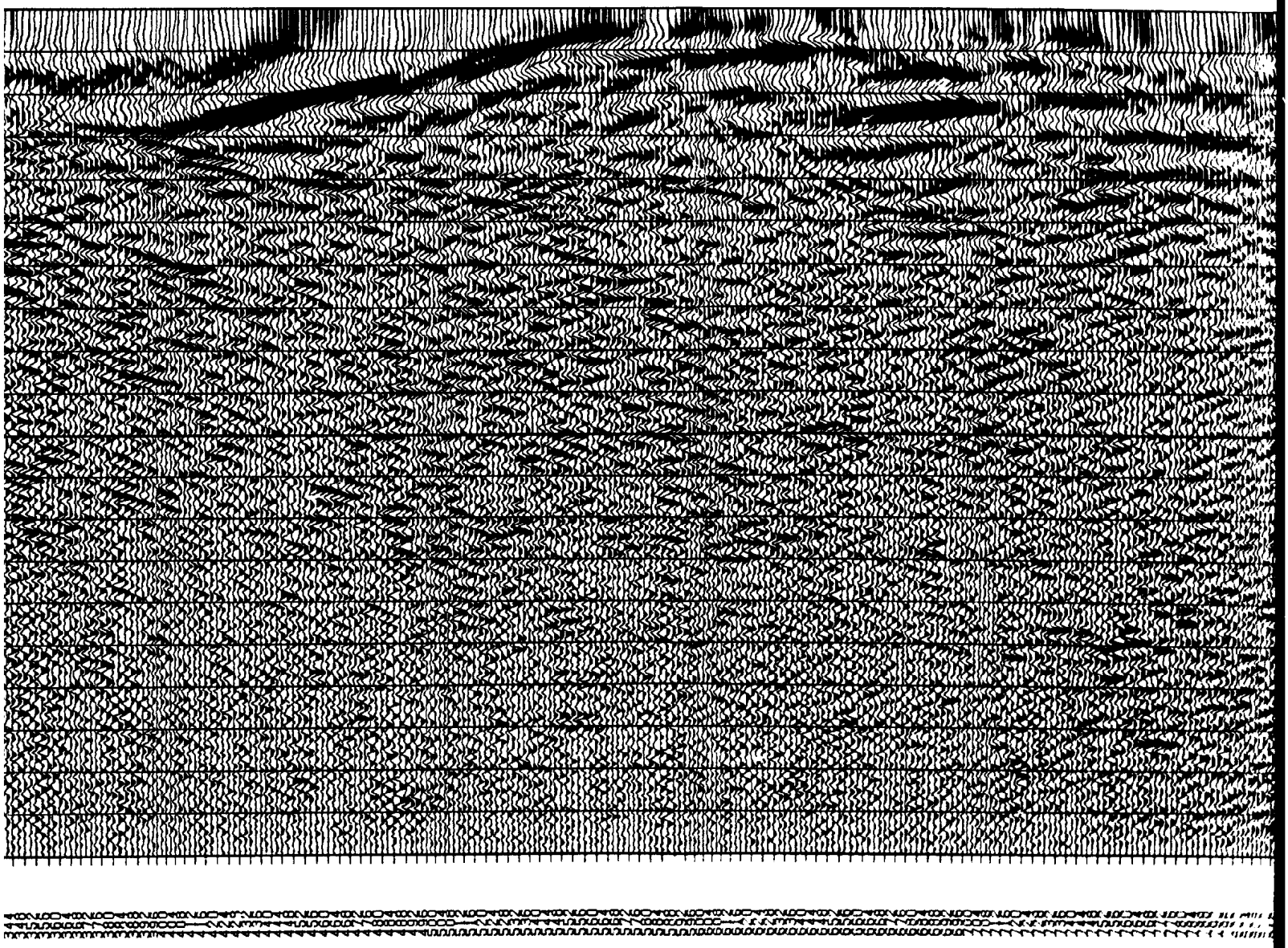

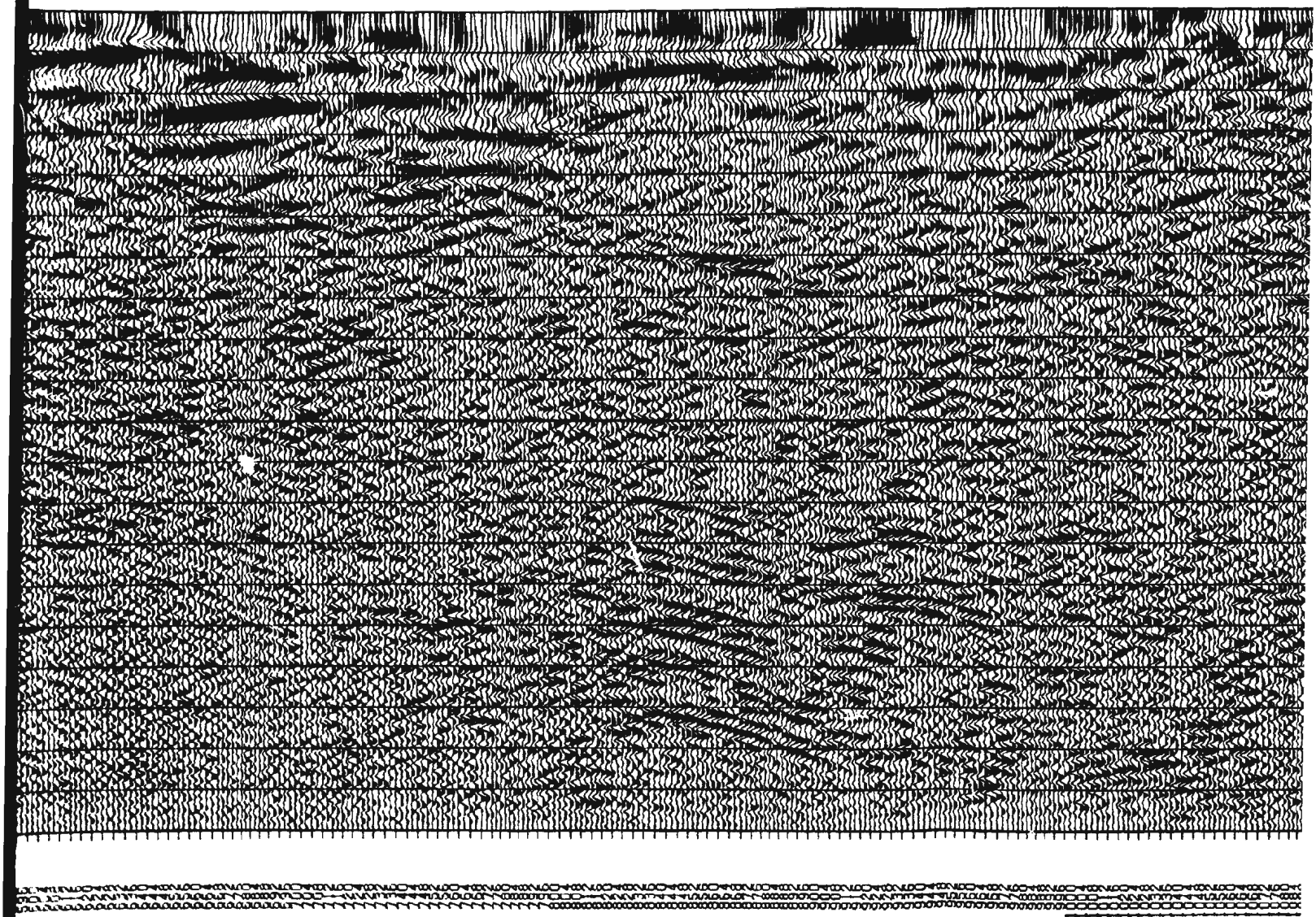

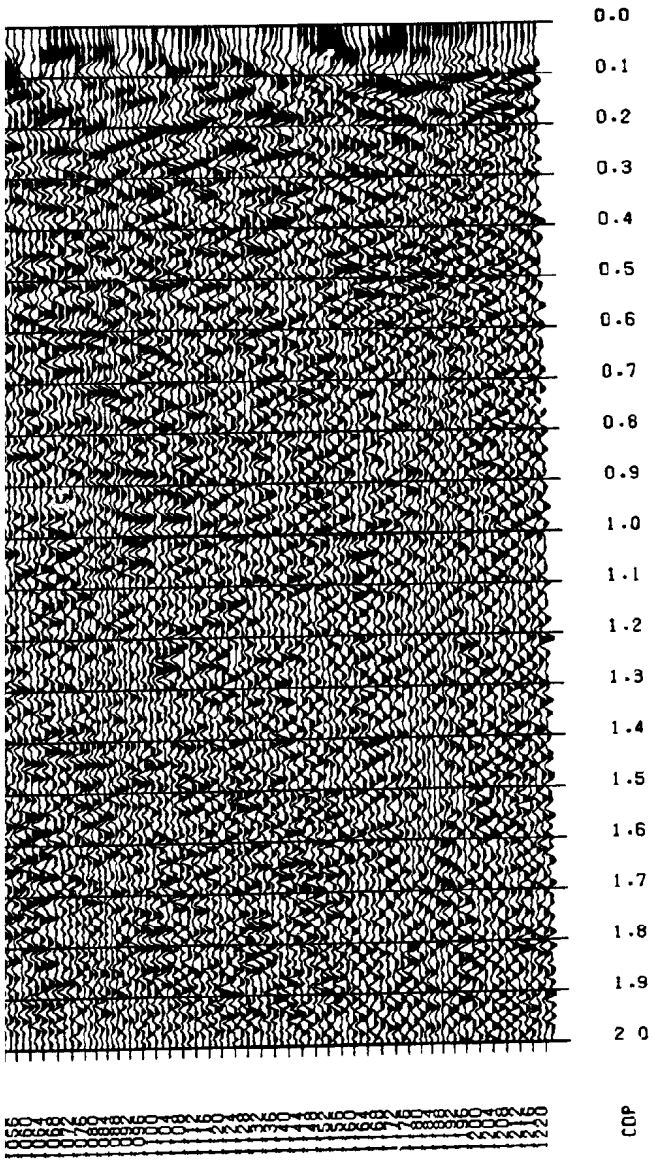
0.0
0.1
0.2
0.3
0.4
0.5
0.6
0.7
0.8
0.9
1.0
1.1
1.2
1.3
1.4
1.5
1.6
1.7
1.8
1.9
2 0
CDP

Figure 3.7 (f). Constant velocity s
marks indicate velocity picks.

y stack of 3000 m/s, blue

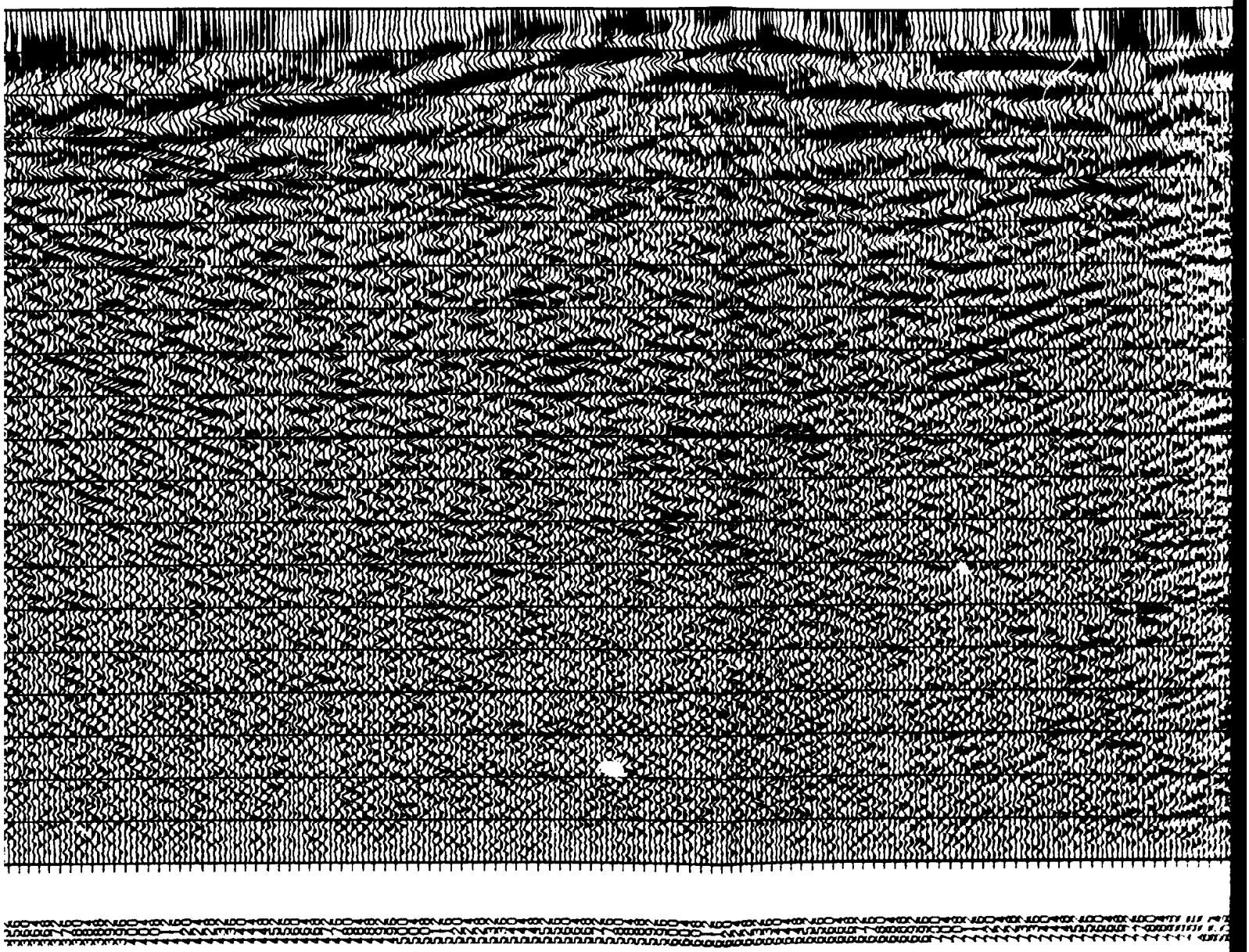

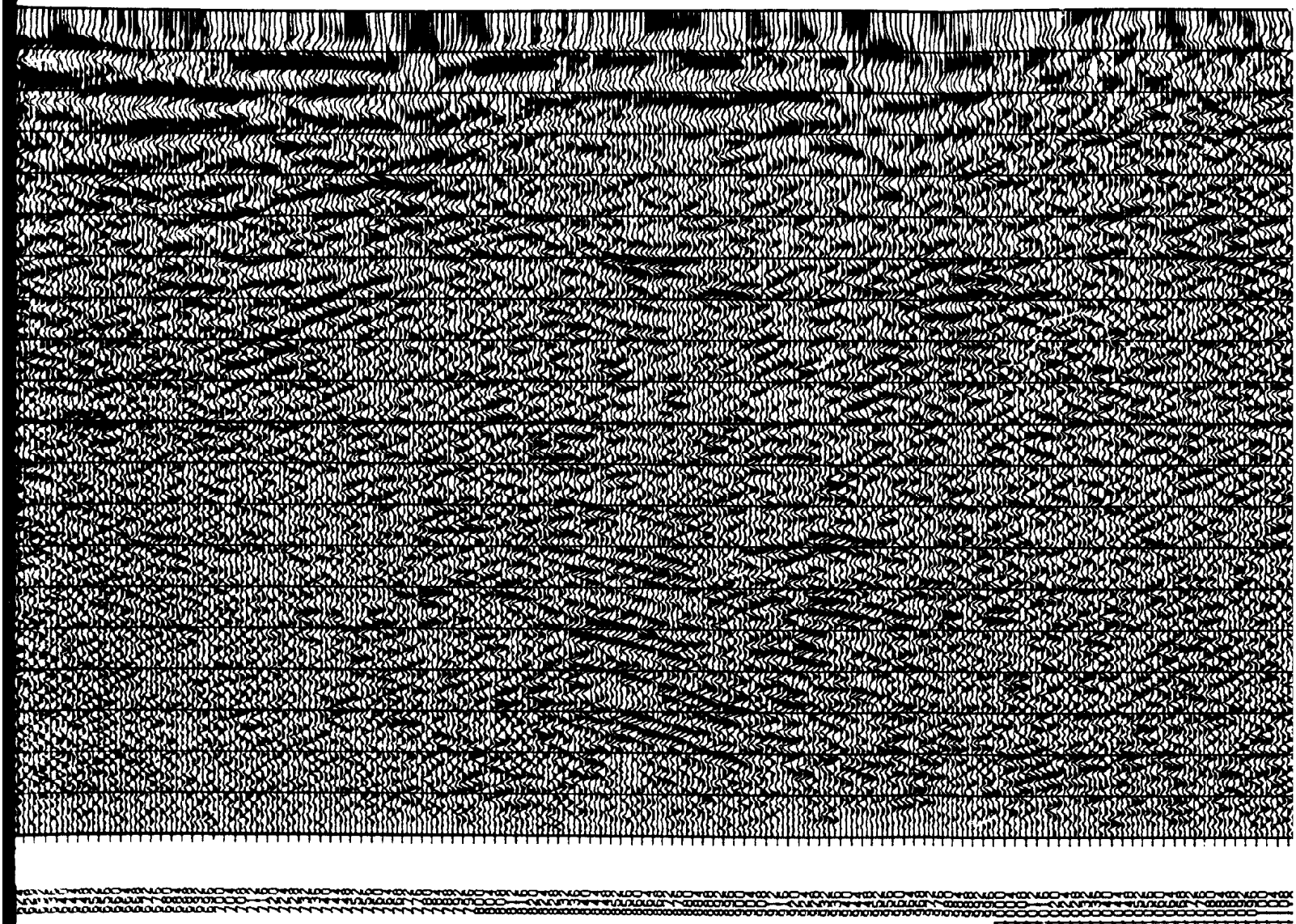

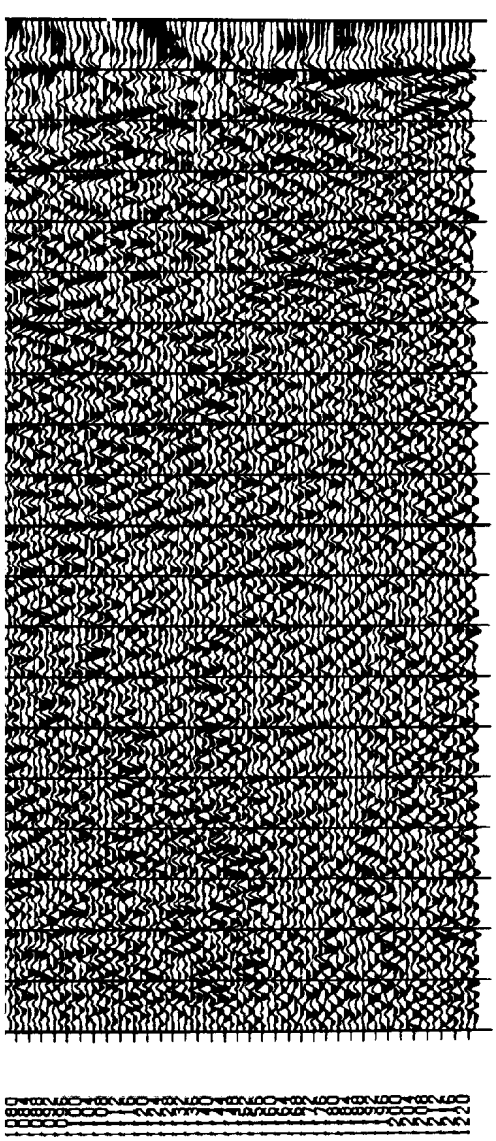
0.0
0.1
0.2
0.3
0.4
0.5
0.6
0.7
0.8
0.9
1.0
1.1
1.2
1.3
1.4
1.5
1.6
1.7
1.8
1.9
2.0
CDP

Figure 3.7 (e). Constant velocity stac
marks indicate velocity picks.

ocity stack of 2900 m/s, blue
s.

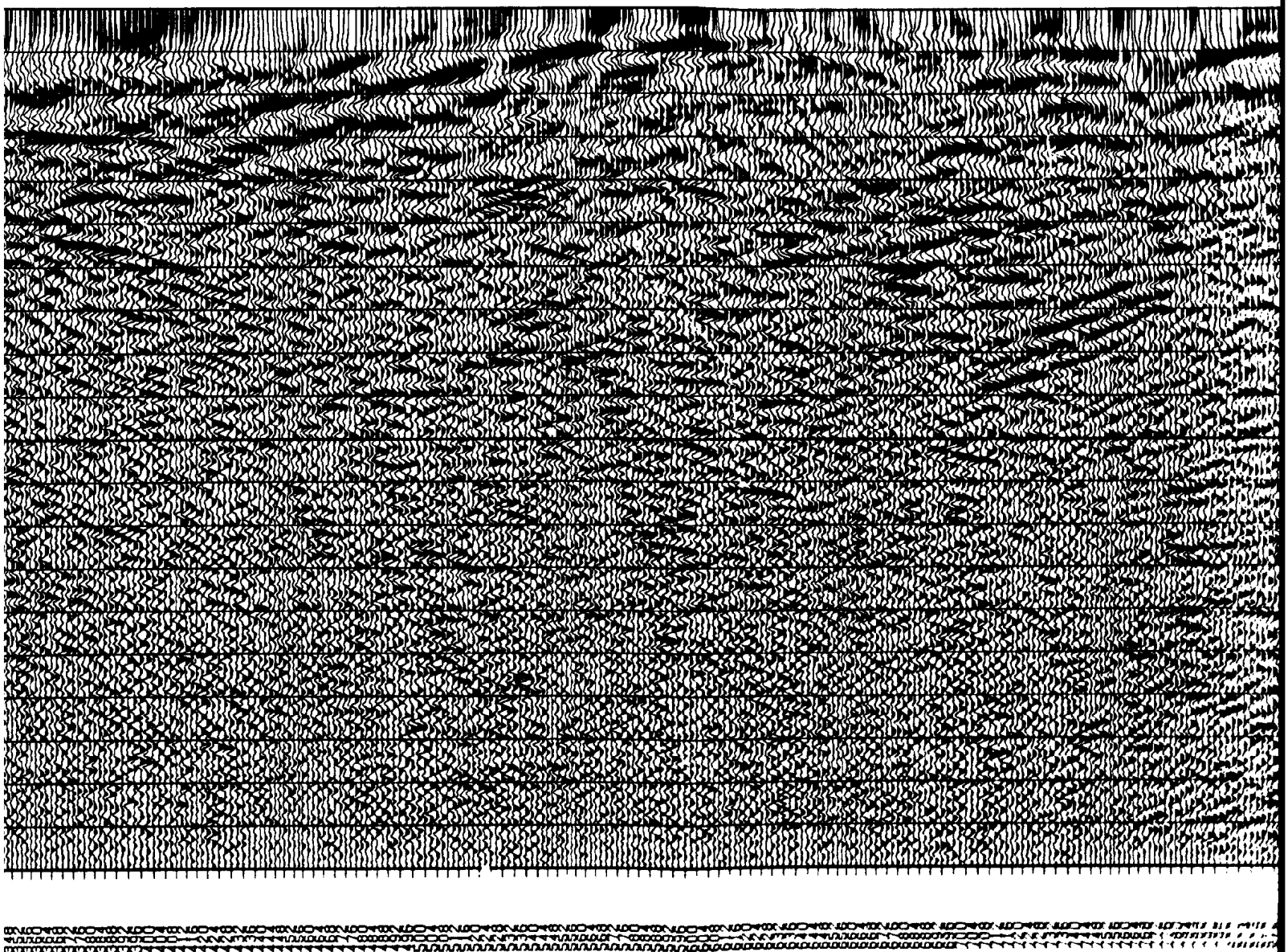

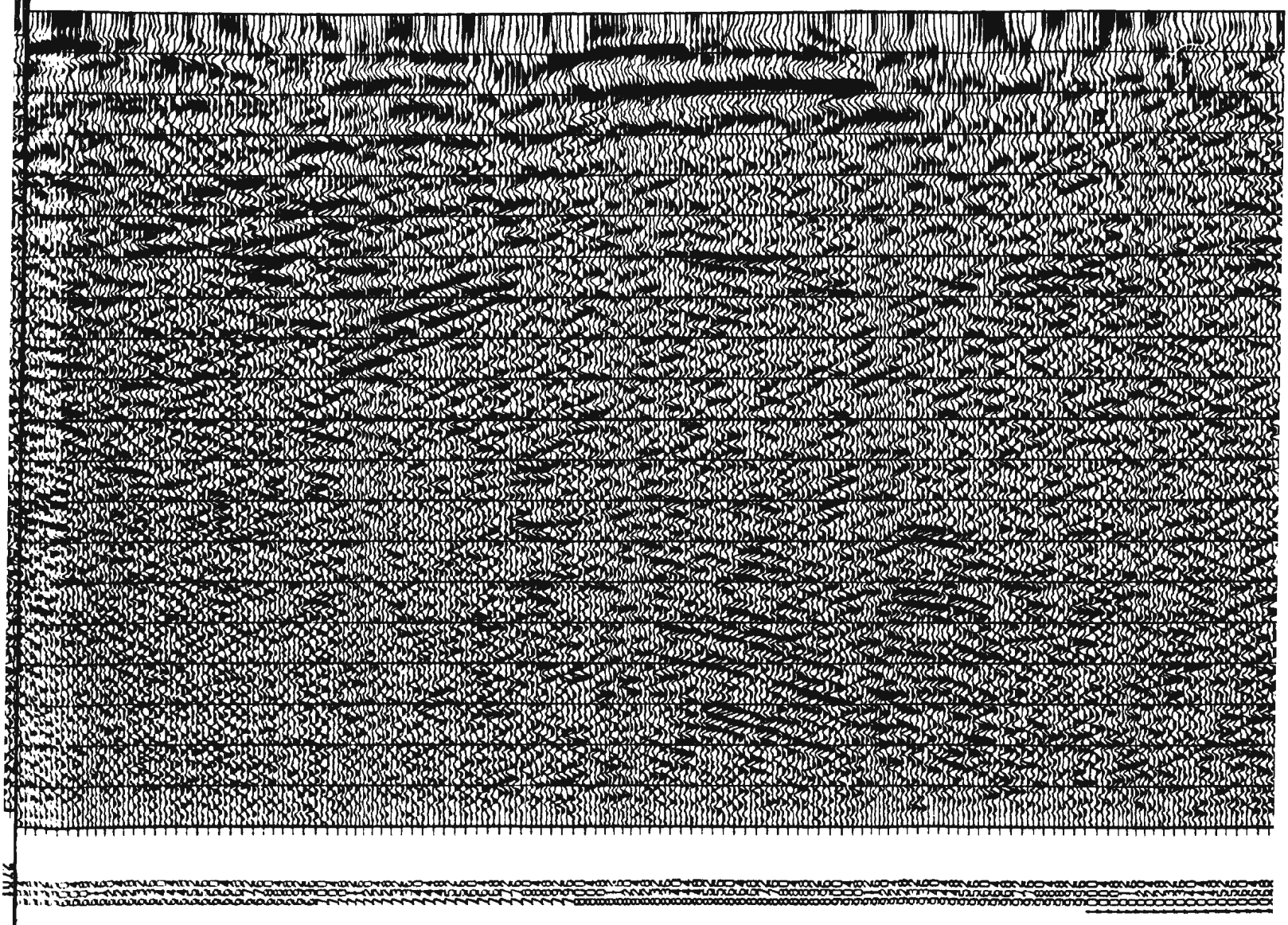

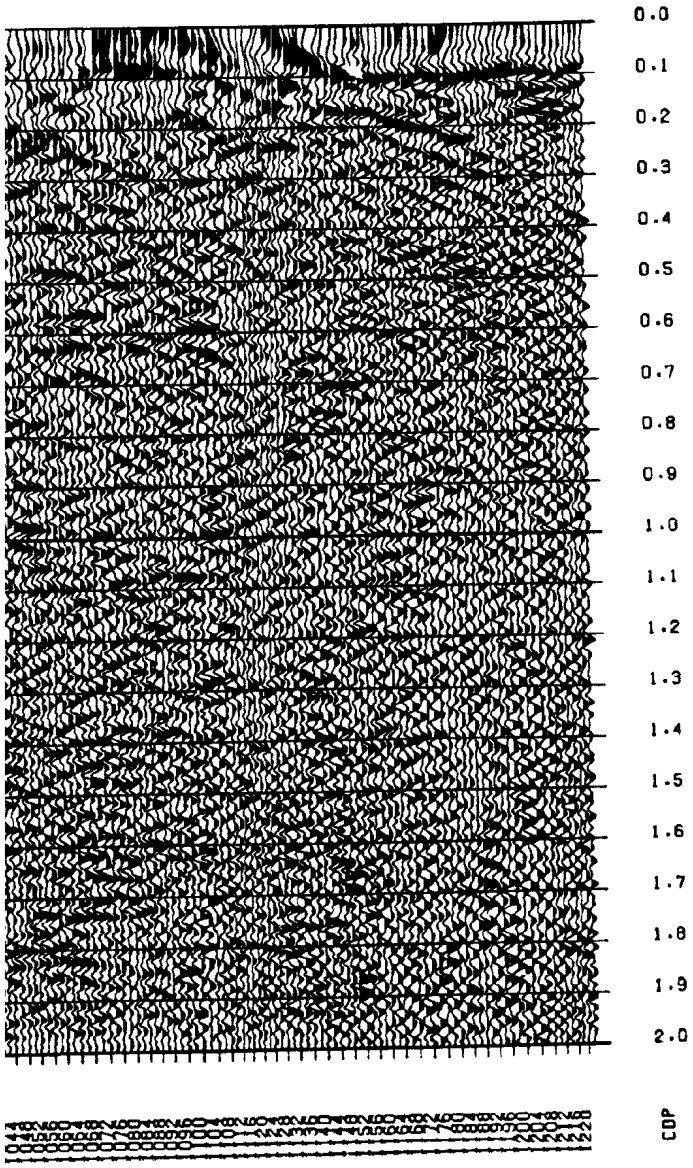
0.0
0.1
0.2
0.3
0.4
0.5
0.6
0.7
0.8
0.9
1.0
1.1
1.2
1.3
1.4
1.5
1.6
1.7
1.8
1.9
2.0
CDP

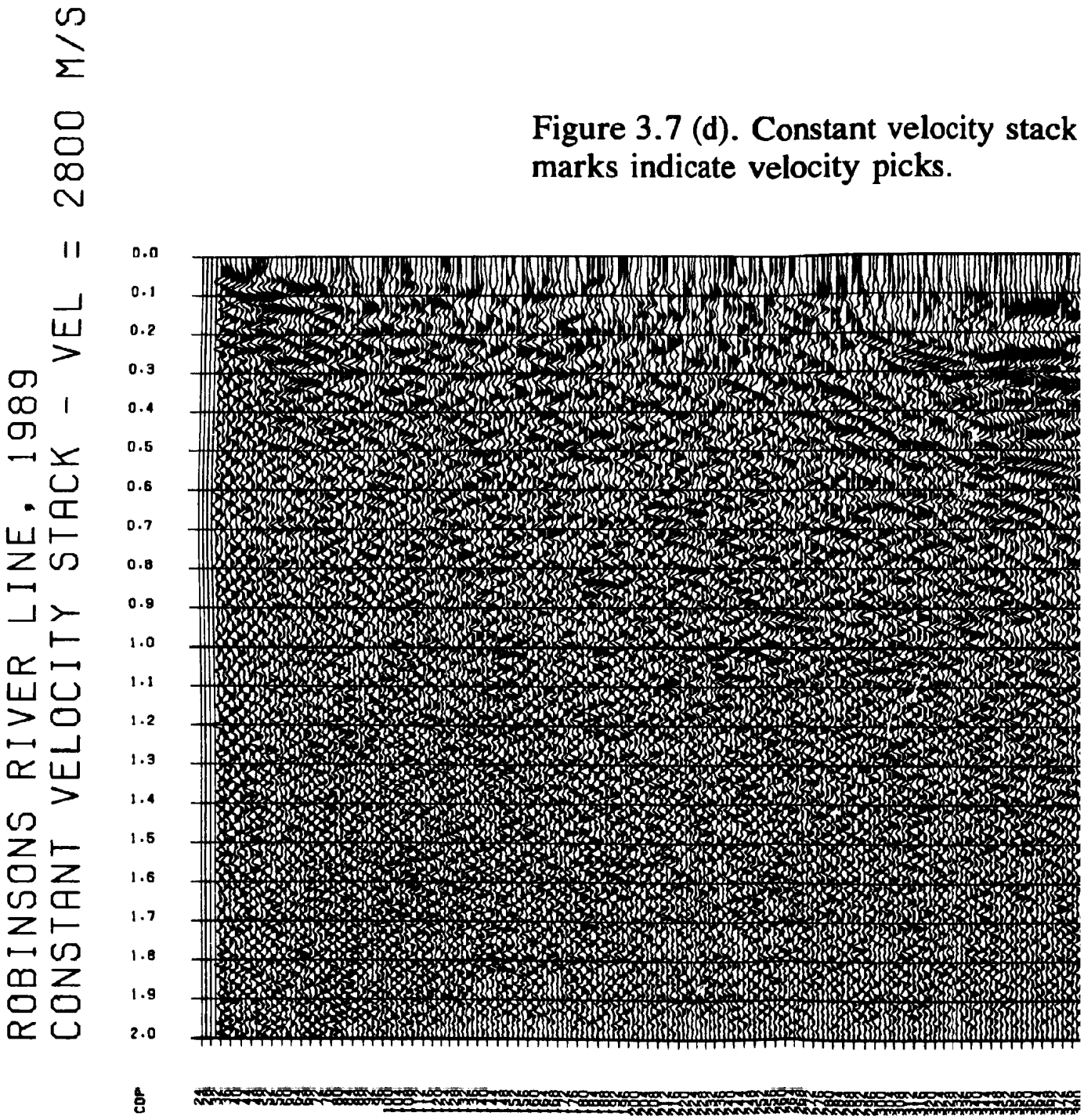

Figure 3.7 (d). Constant velocity stack marks indicate velocity picks.

ck of 2800 m/s, blue

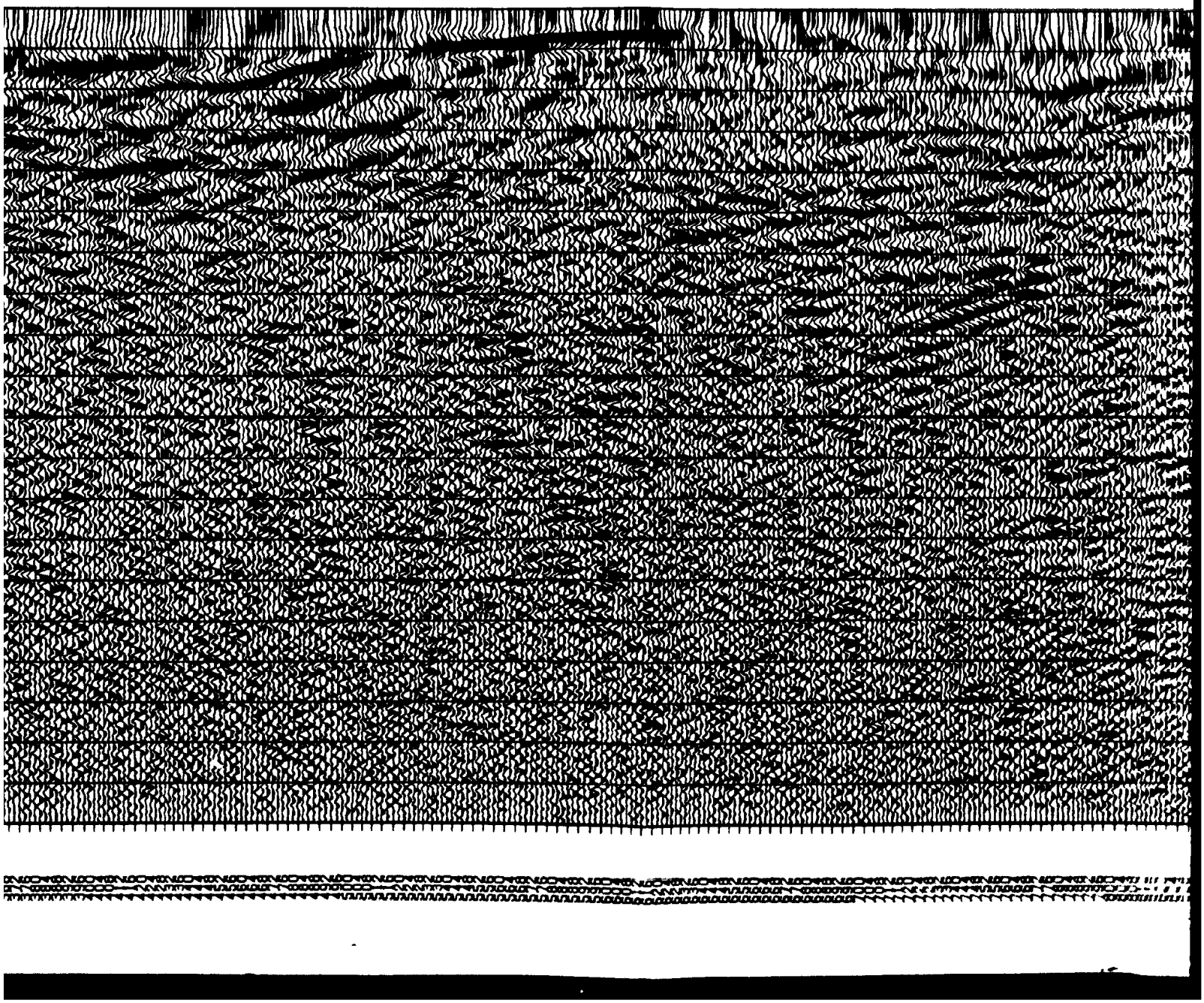

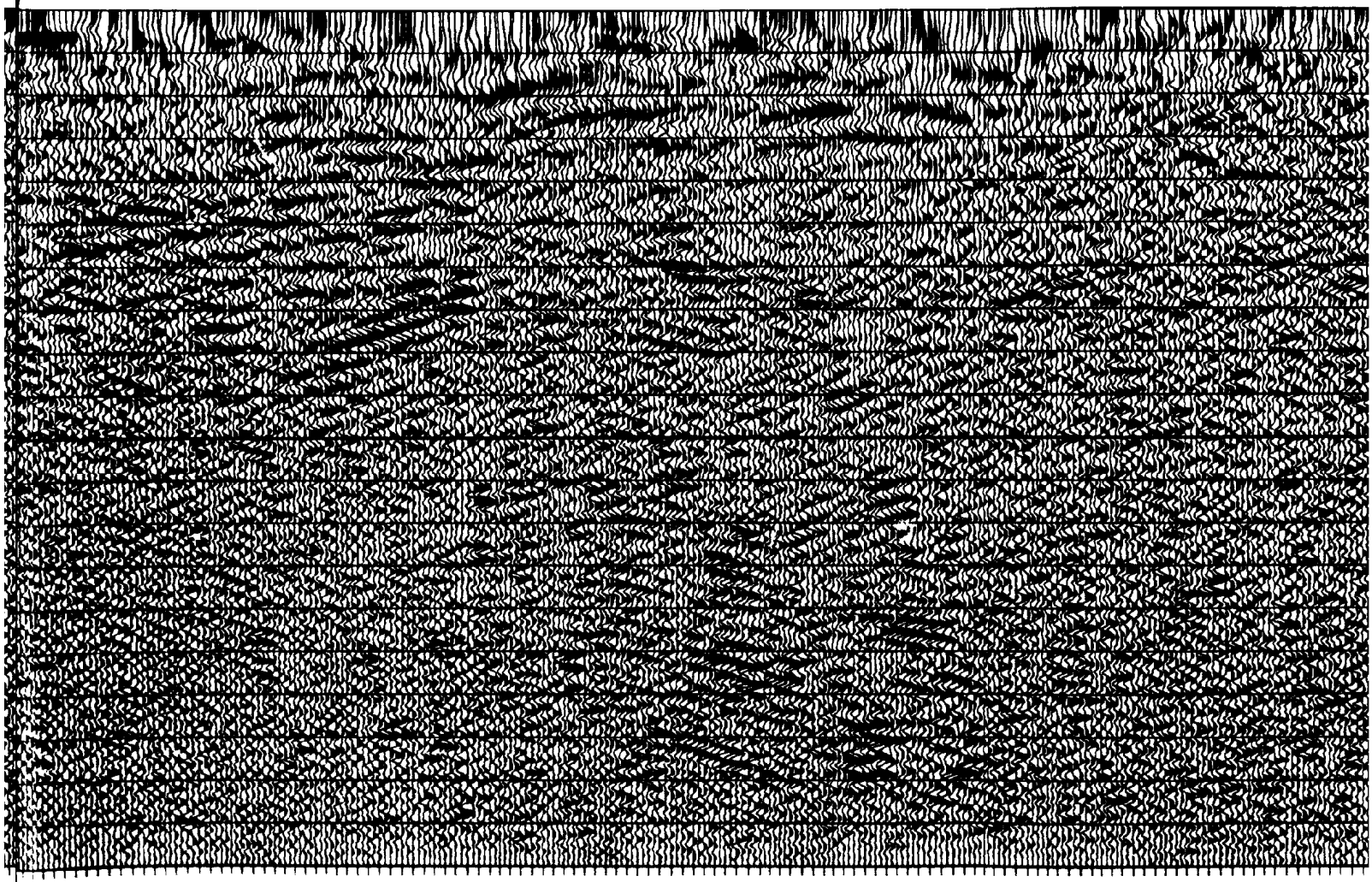

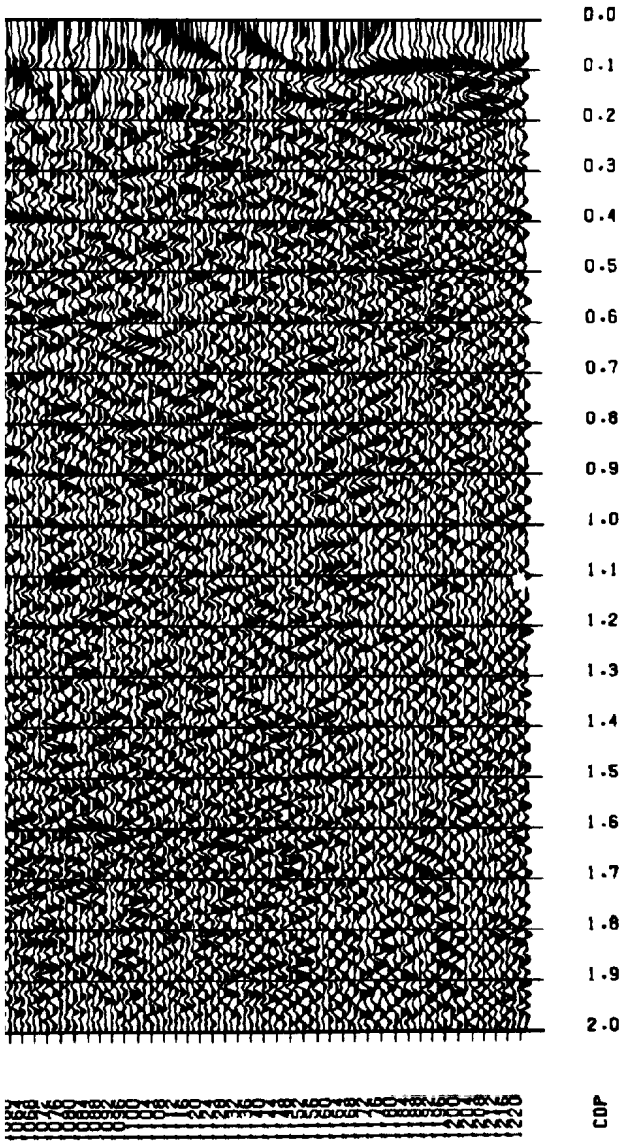
0.0
0.1
0.2
0.3
0.4
0.5
0.6
0.7
0.8
0.9
1.0
1.1
1.2
1.3
1.4
1.5
1.6
1.7
1.8
1.9
2.0
CDP

Figure 3.7 (c). Constant
marks indicate velocity

velocity stack of 2700 m/s, blue
picks.

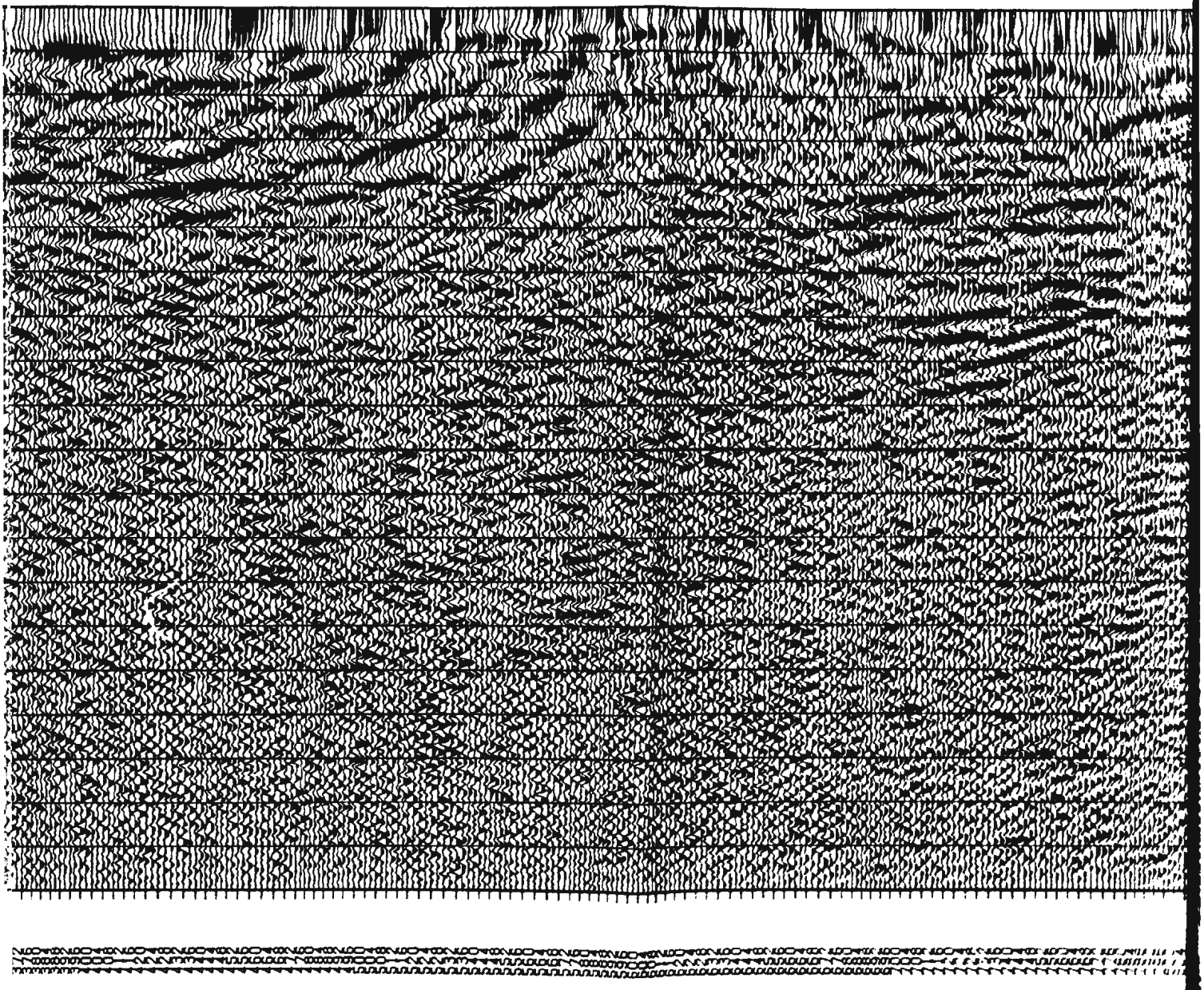

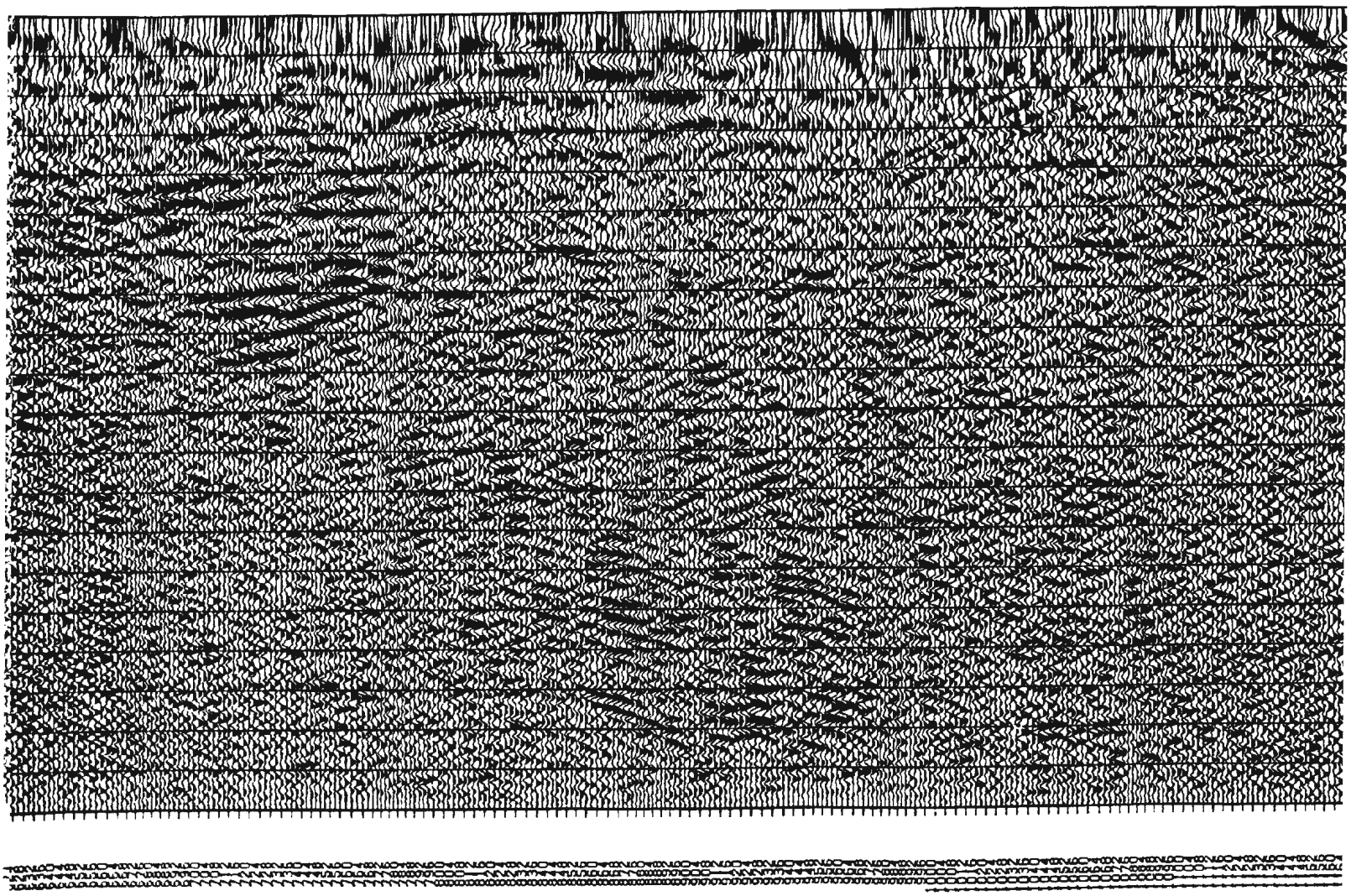

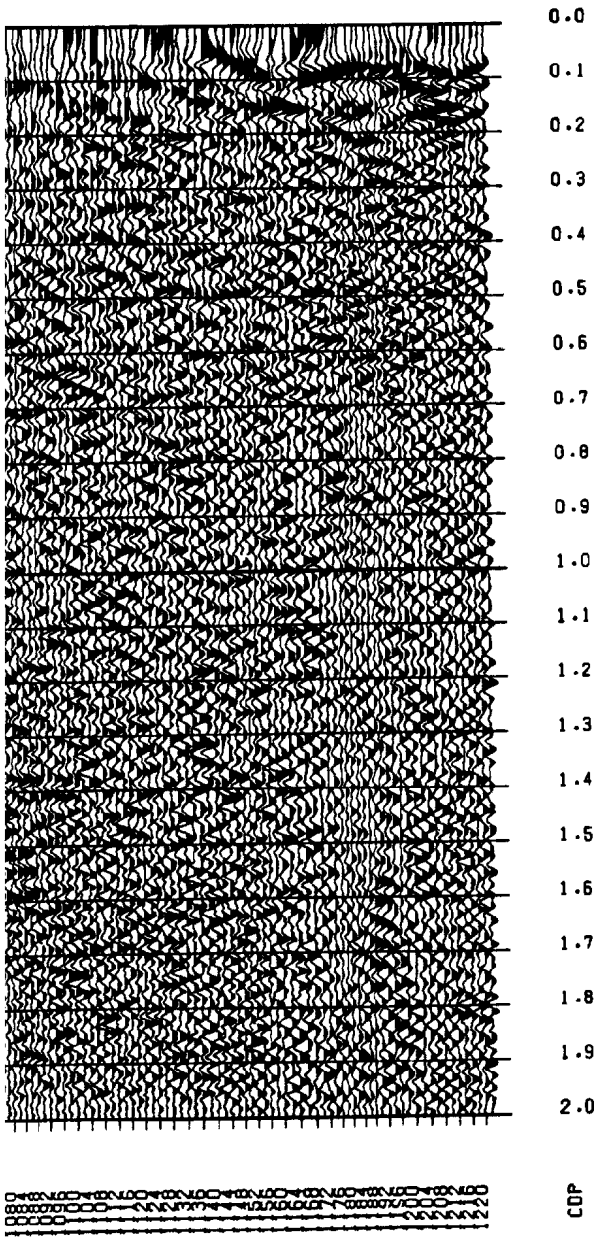
0.0
0.1
0.2
0.3
0.4
0.5
0.6
0.7
0.8
0.9
1.0
1.1
1.2
1.3
1.4
1.5
1.6
1.7
1.8
1.9
2.0
CDP

Figure 3.7 (b). Constant ve
marks indicate velocity pick

b). Constant velocity stack of 2600 m/s, blue
ıte velocity picks.

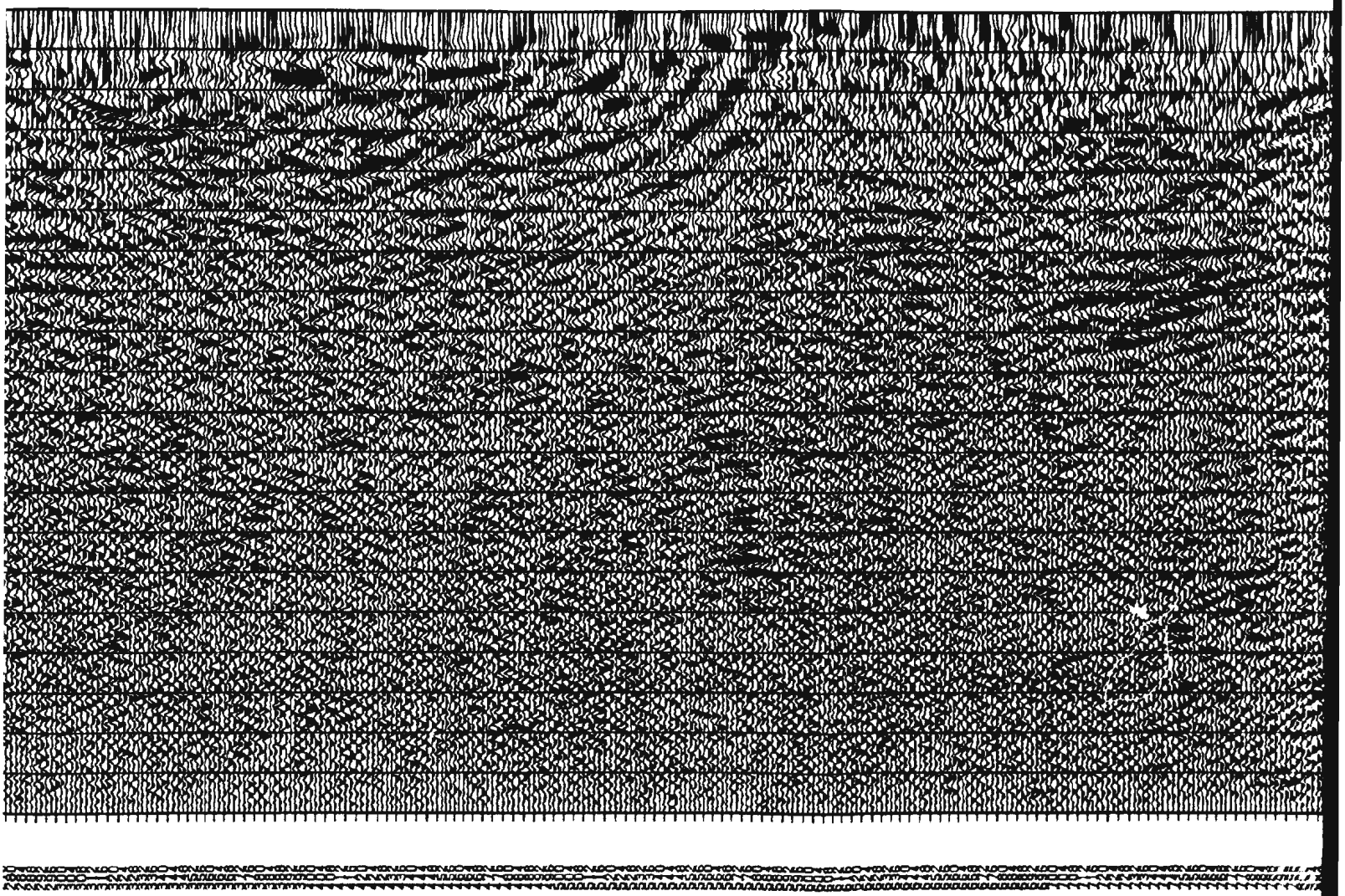

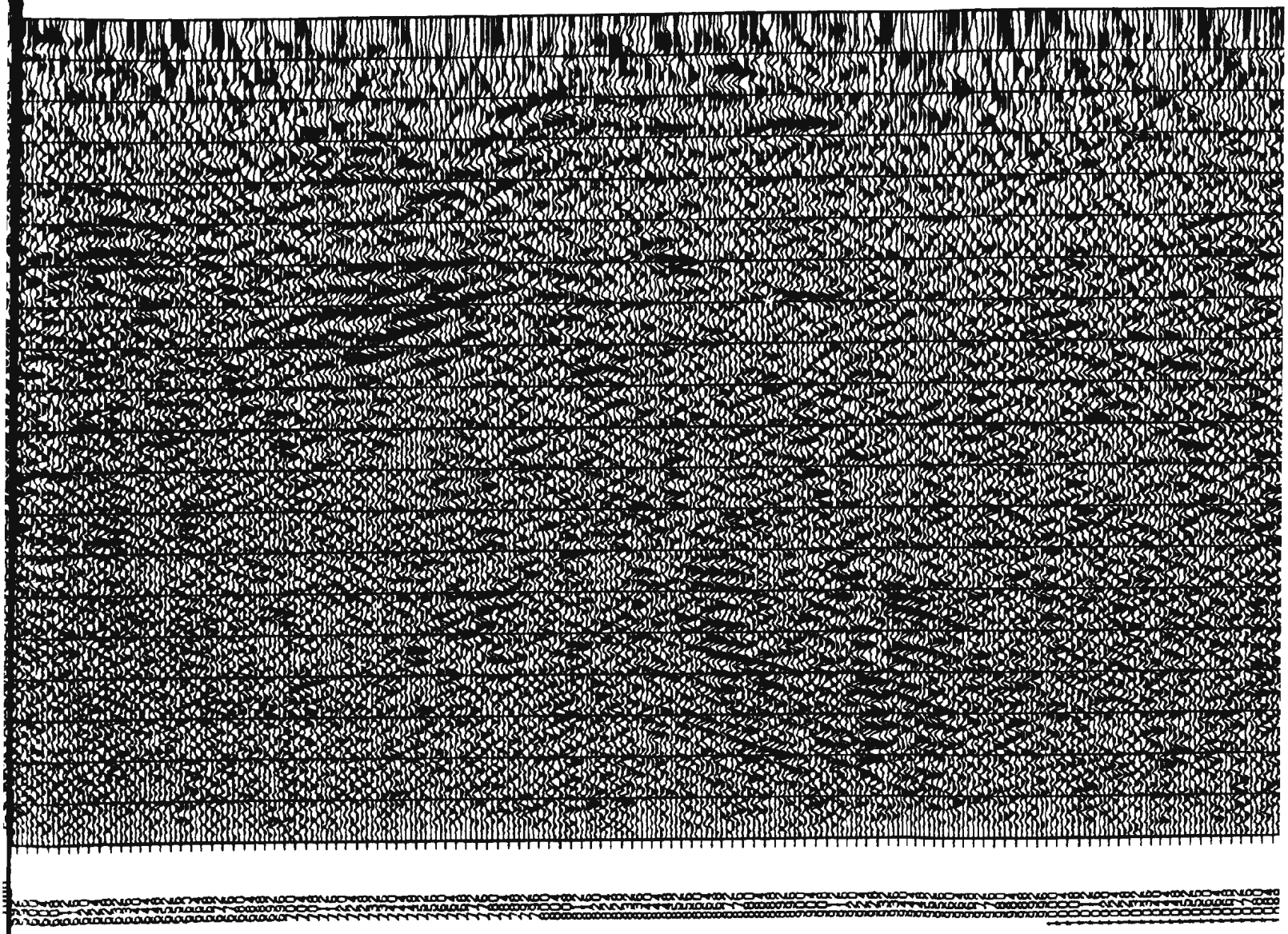

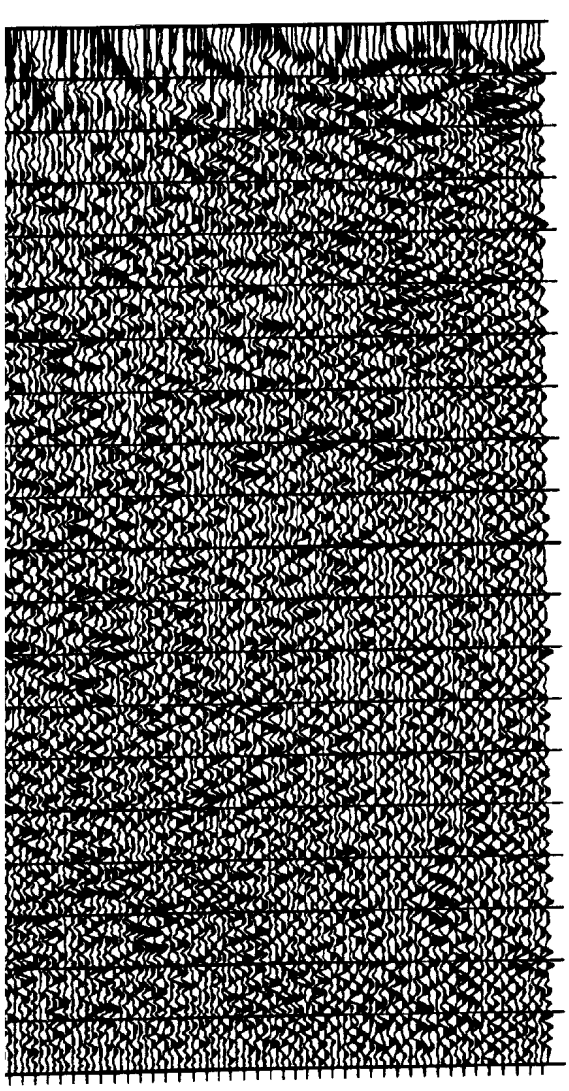
0.0
0.1
0.2
0.3
0.4
0.5
0.6
0.7
0.8
0.9
1.0
1.1
1.2
1.3
1.4
1.5
1.6
1.7
1.8
1.9
2.0
COP

Figure 3.7 (a). Constant velocity s
velocity picks at this velocity.

'elocity stack of 2500 m/s, no
ity.

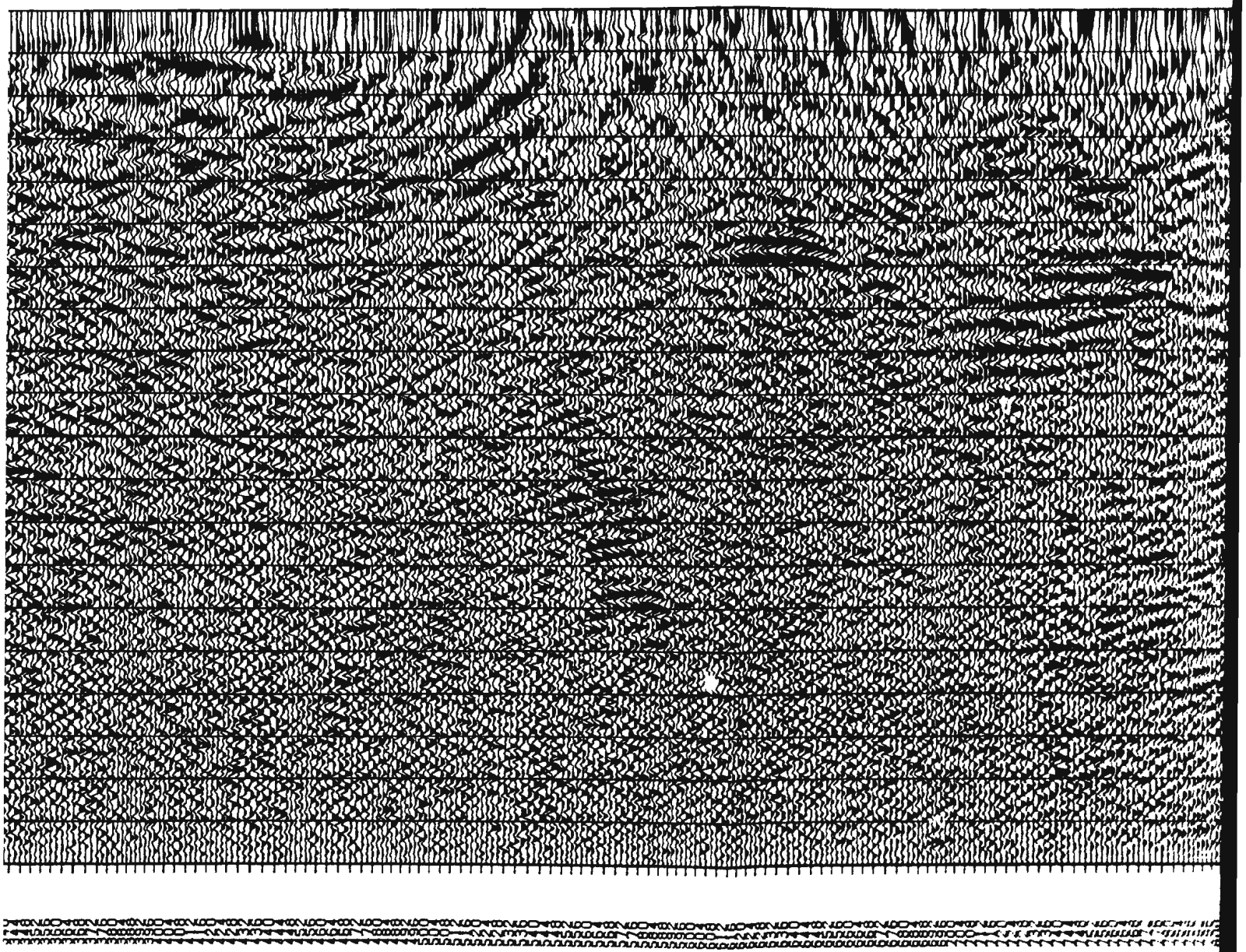

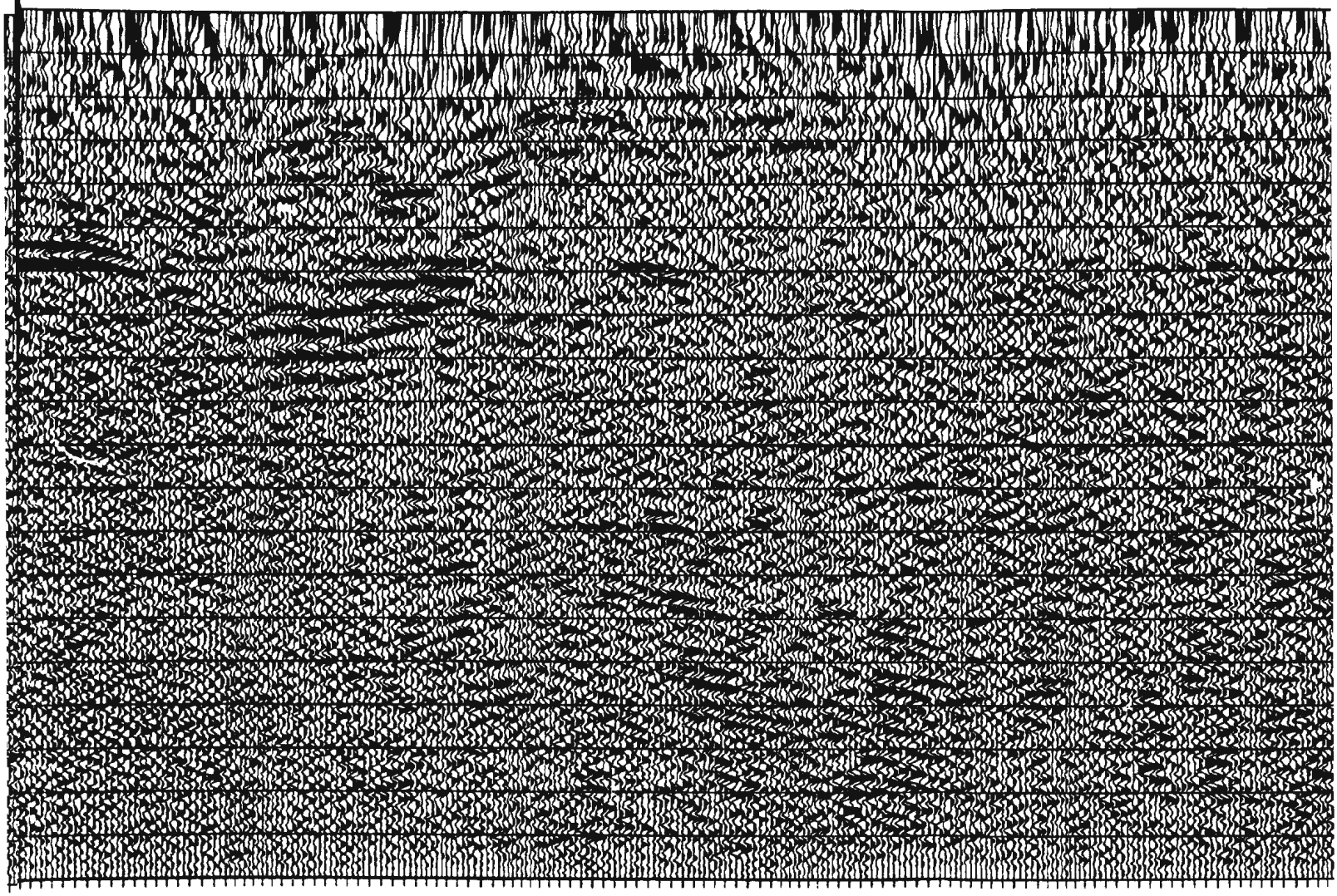

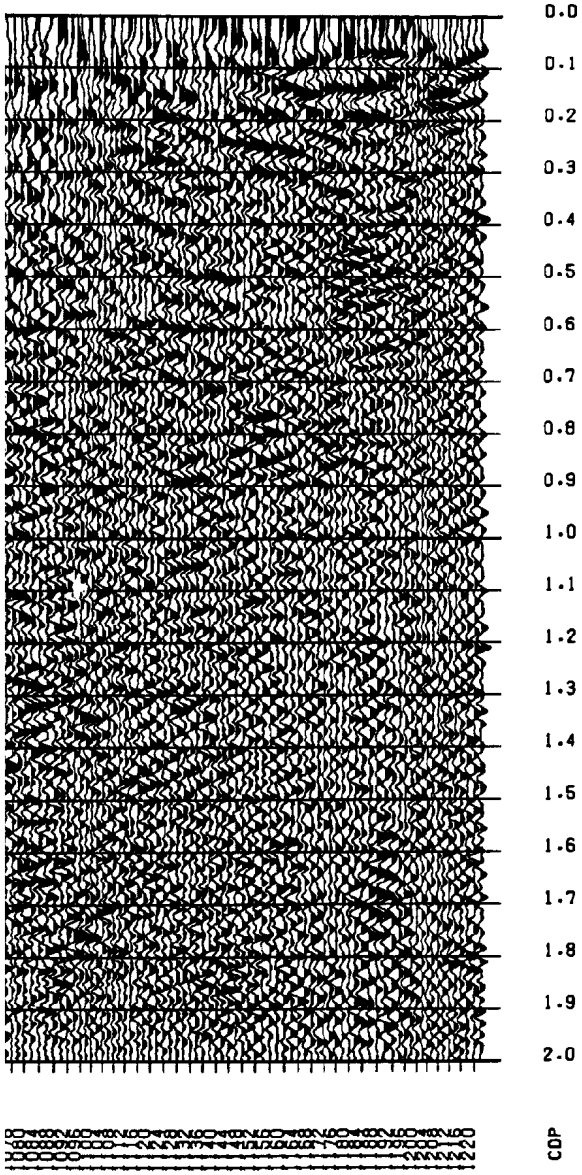
0.0
0.1
0.2
0.3
0.4
0.5
0.6
0.7
0.8
0.9
1.0
1.1
1.2
1.3
1.4
1.5
1.6
1.7
1.8
1.9
2.0
CDP

372000
373000
374000
375000
5348000
5347000
5346000
5345000
BIN 1
10
20
30
40
50
60
70
80
90
100
110
120

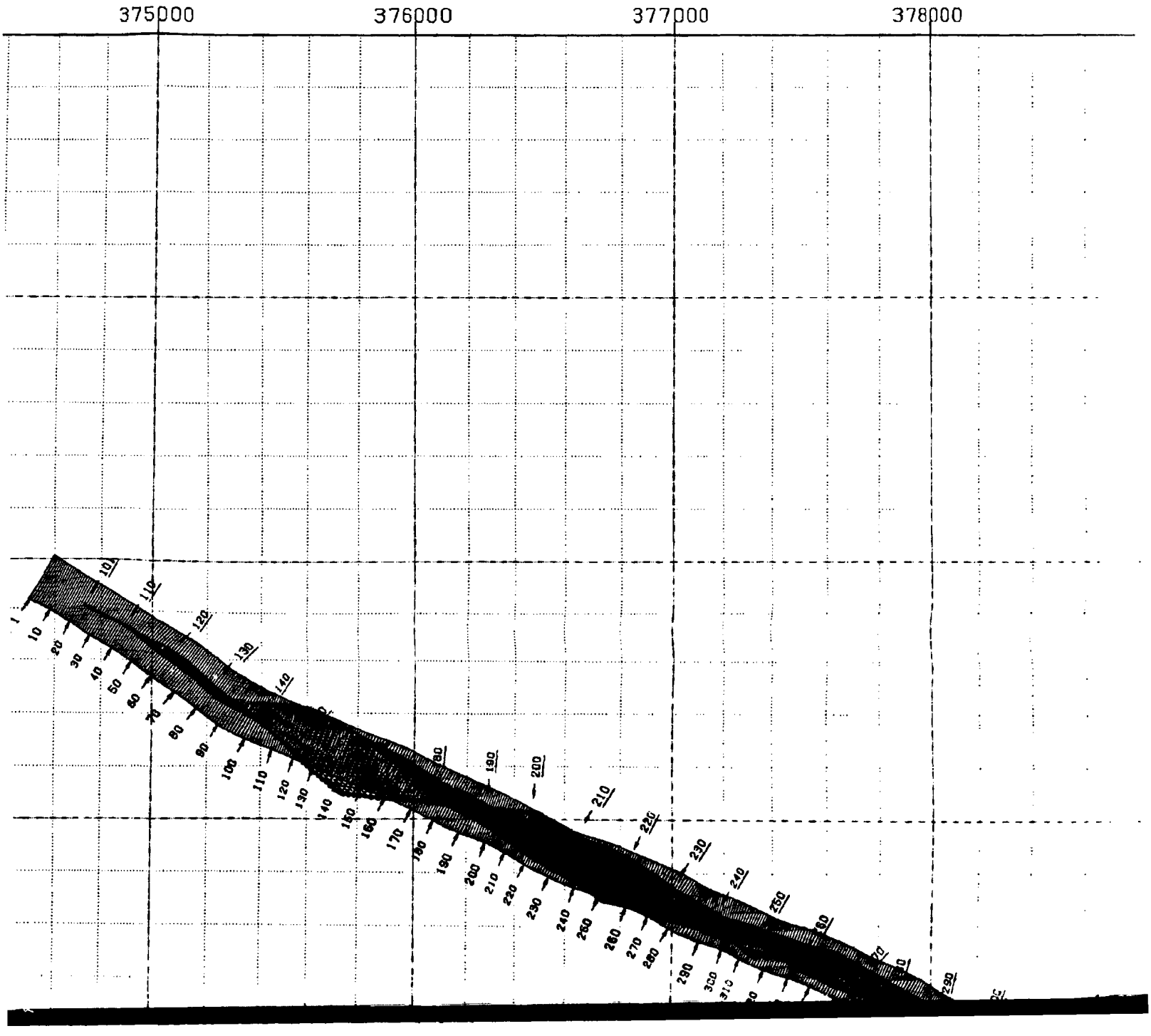
375000
376000
377000
378000

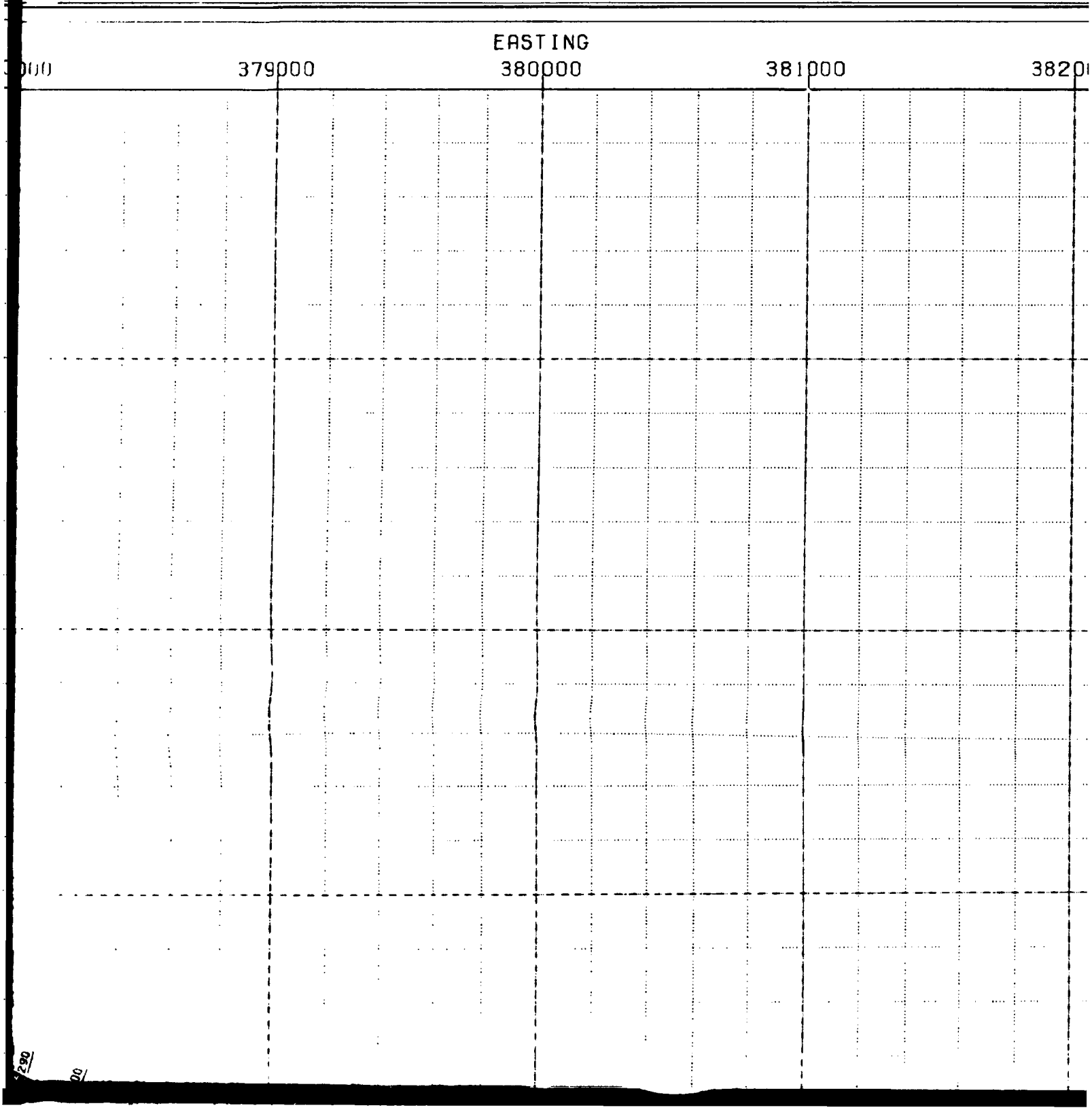
EASTING
379000
380000
381000

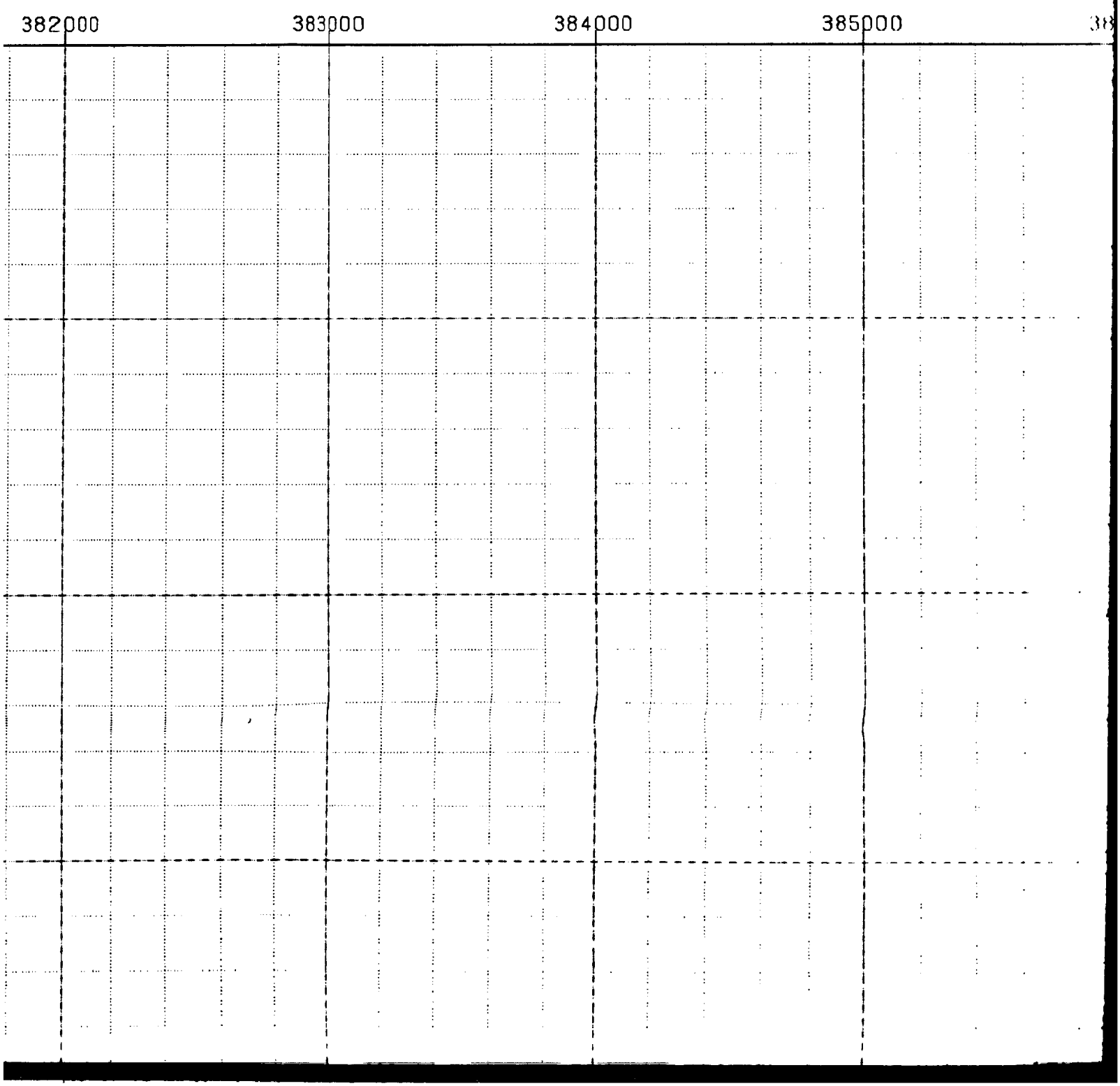
382000
383000
384000
385000

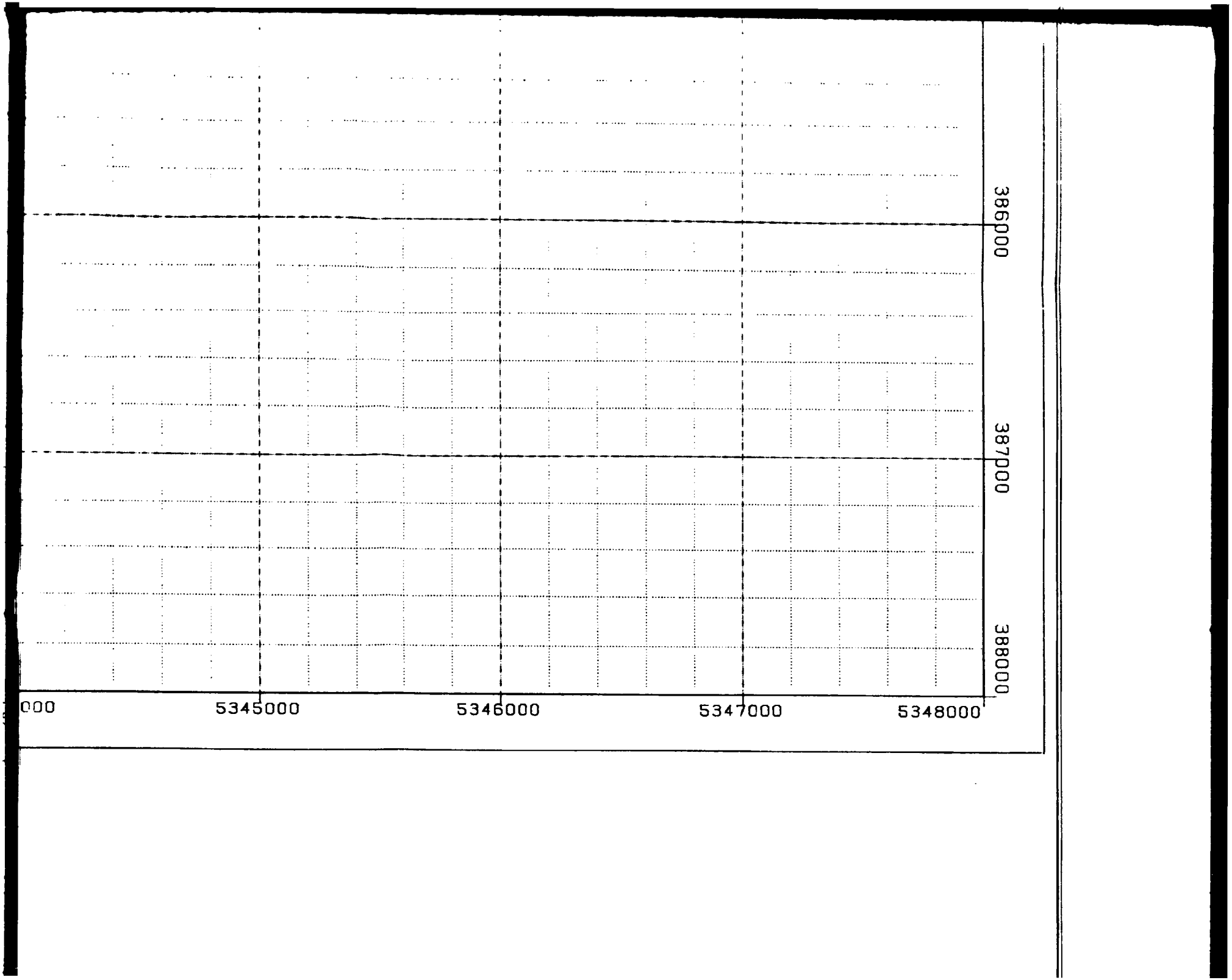
386000
387000
388000
000
5345000
5346000
5347000
5348000

Figure 3.19. Bandpass filter test panels of stacked section from CMP 660 to 700. The numbers at the top of the panels indicate range of frequencies passed, for example, 20TO40 means only frequencies between 20 to 40 Hz inclusive, were passed in the filter. Note how events get out of focus at high frequencies.

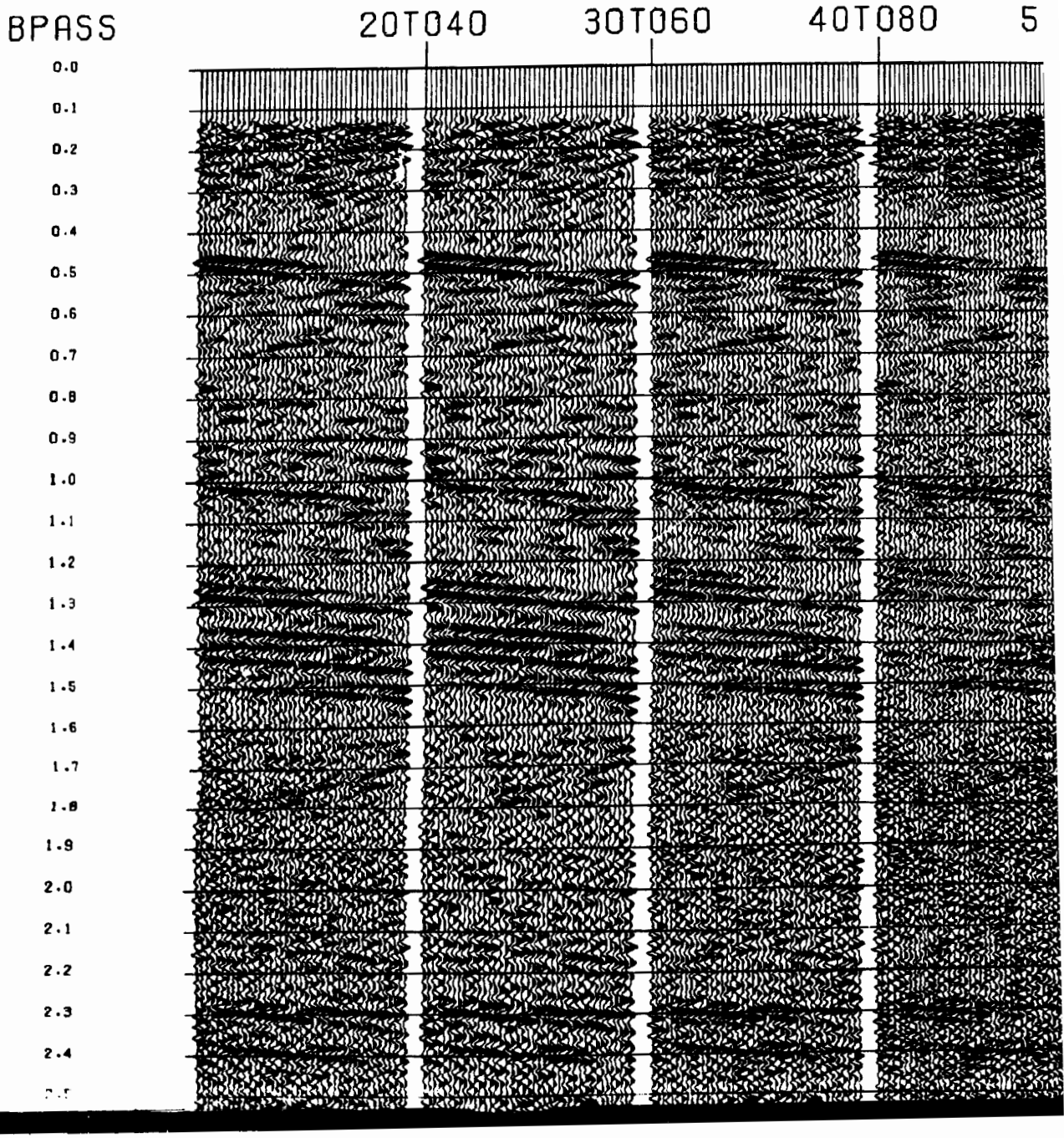

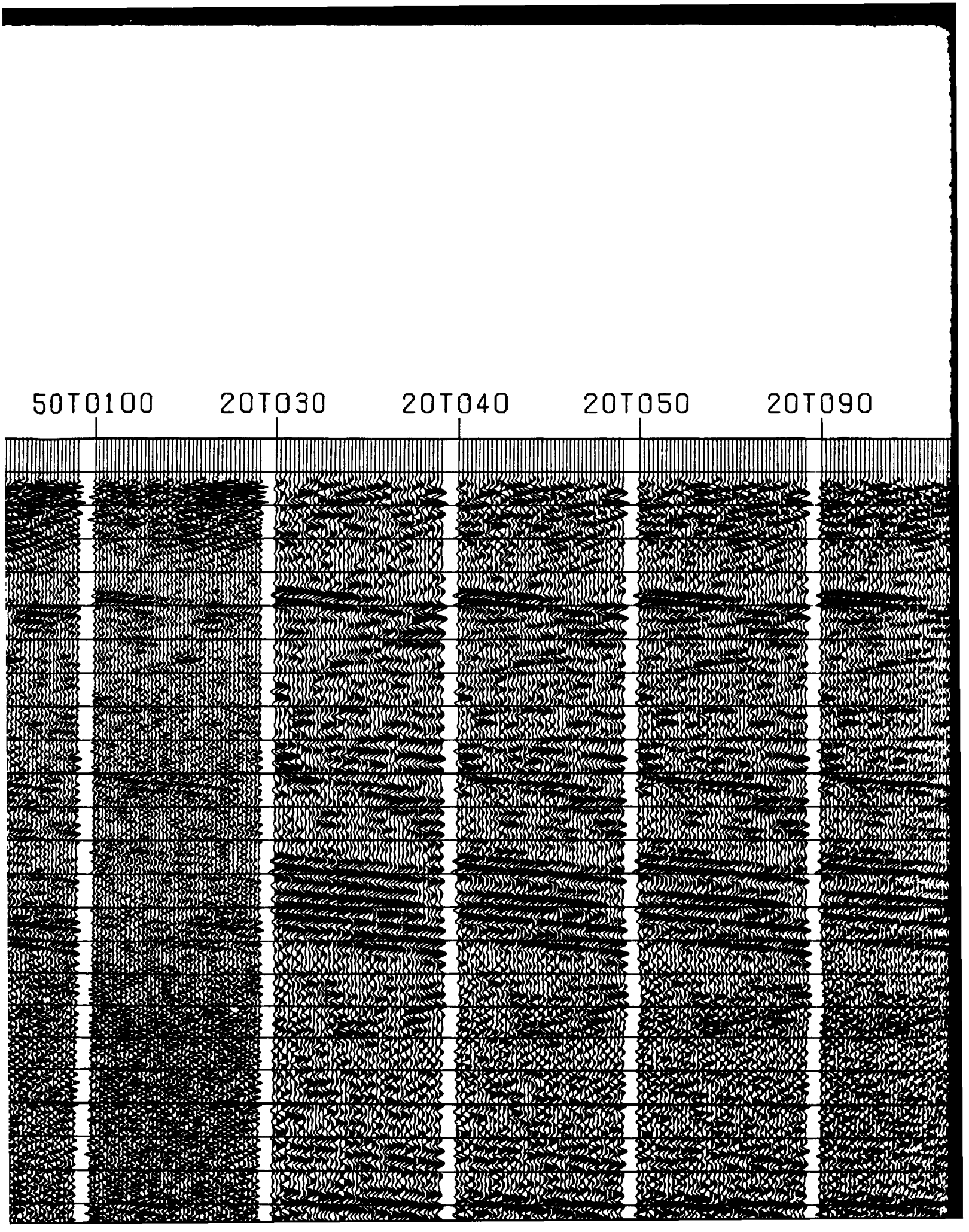
50T0100
20T030
20T040
20T050
20T090

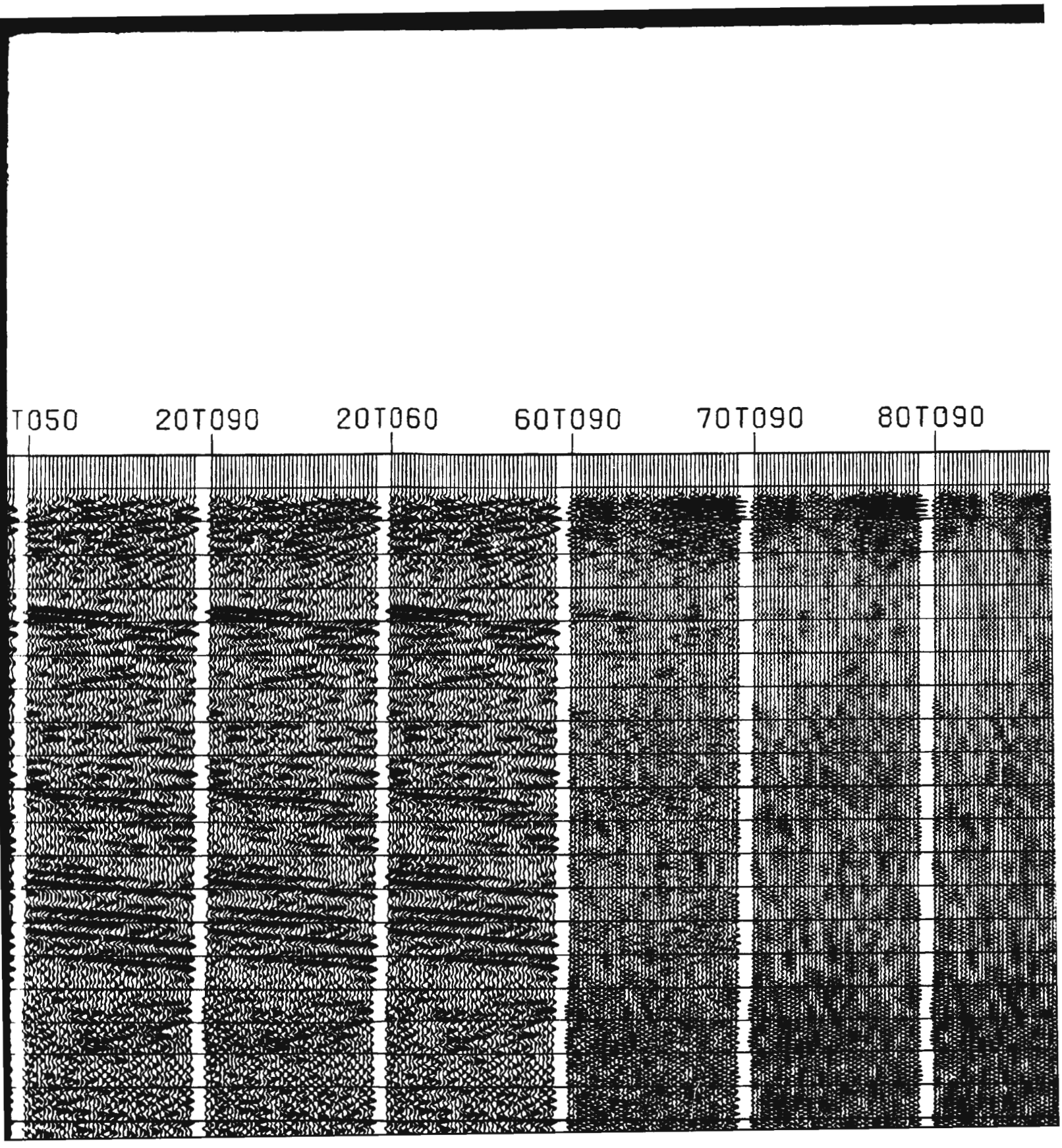
T050
20T090
20T060
60T090
70T090
80T090

)90

BPASS

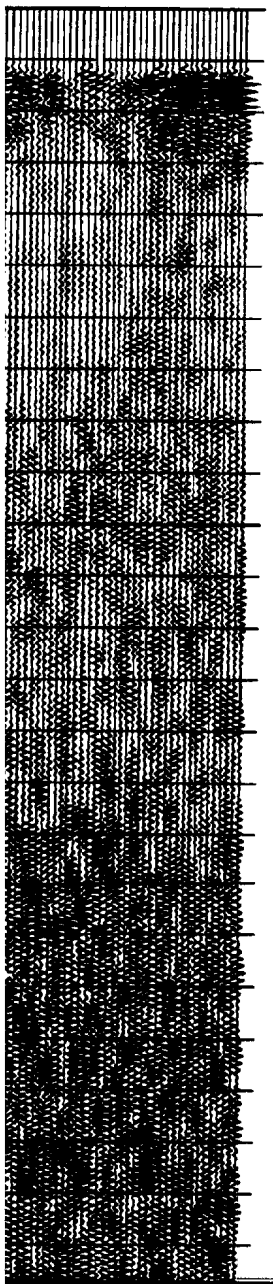

0.0
0.1
0.2
0.3
0.4
0.5
0.6
0.7
0.8
0.9
1.0
1.1
1.2
1.3
1.4
1.5
1.6
1.7
1.8
1.9
2.0
2.1
2.2
2.3
2.4

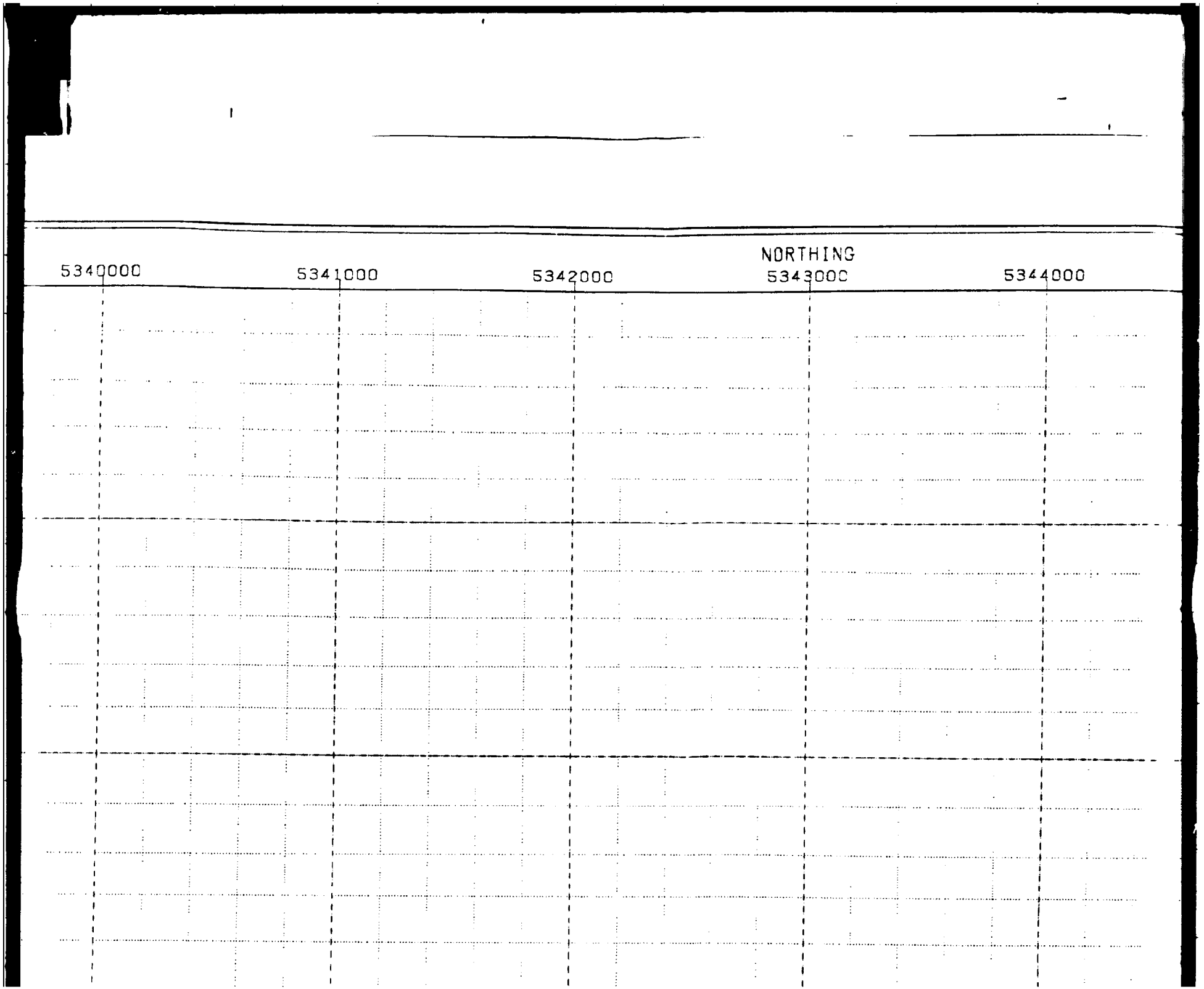
NORTHING
5340000
5341000
5342000
5343000
5344000

270
280
290
300
310
320
330
340
350
360
370
380
390
400
410
420
430
440
450
460
290
300
310

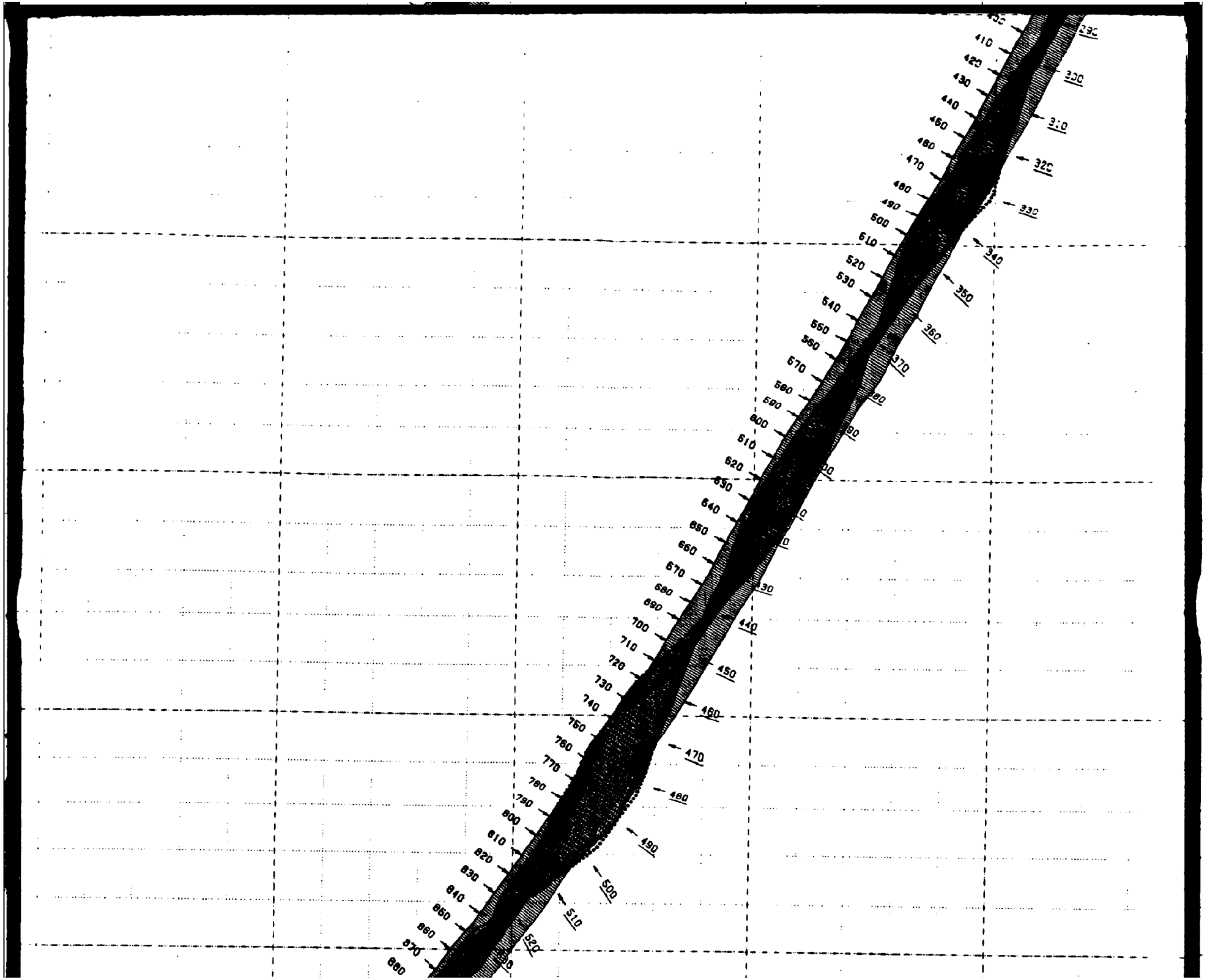

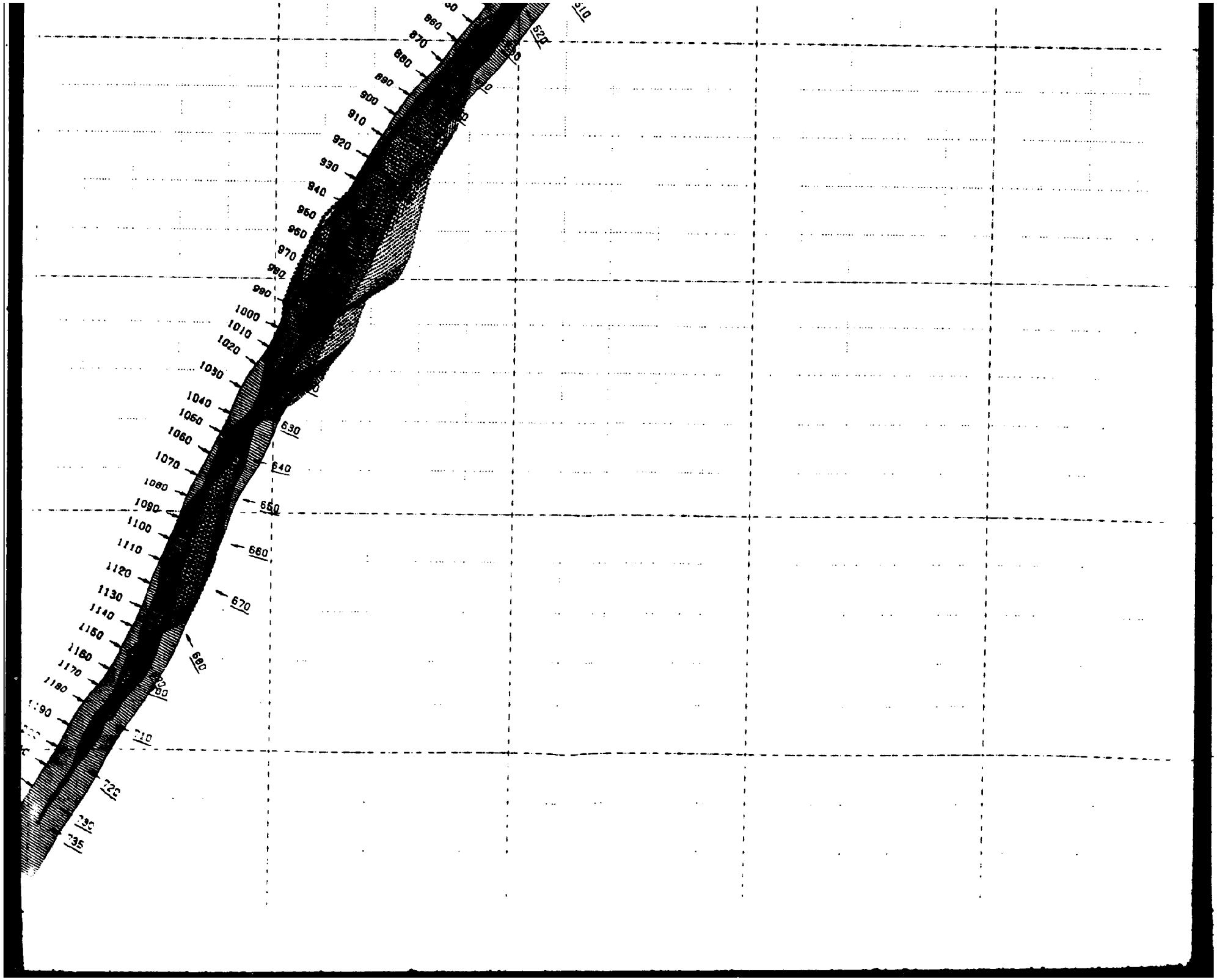
960
970
980
990
1000
1010
1020
1030
1040
1050
1060
1070
1080
1090
1100
1110
1120
1130
1140
1150
1160
1170
1180
630
640
650
660
670
680

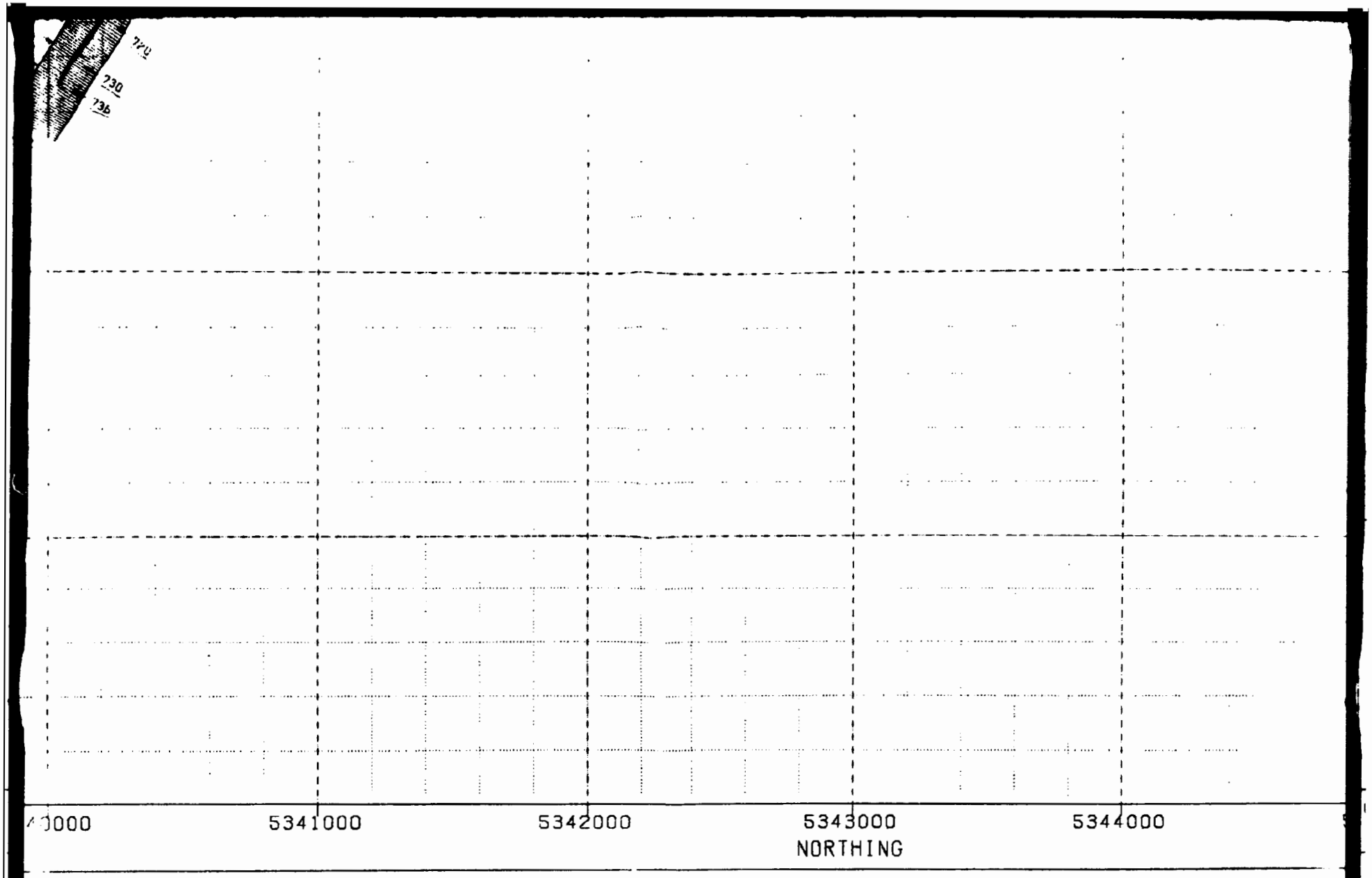

Figure 3.2. Binning strategy chart. The scale is 1:50 and the axes are in UTM zone 21 coordinates.

axes are in UTM zone 21 coordinates.

Post-stack bandpass filter-trial

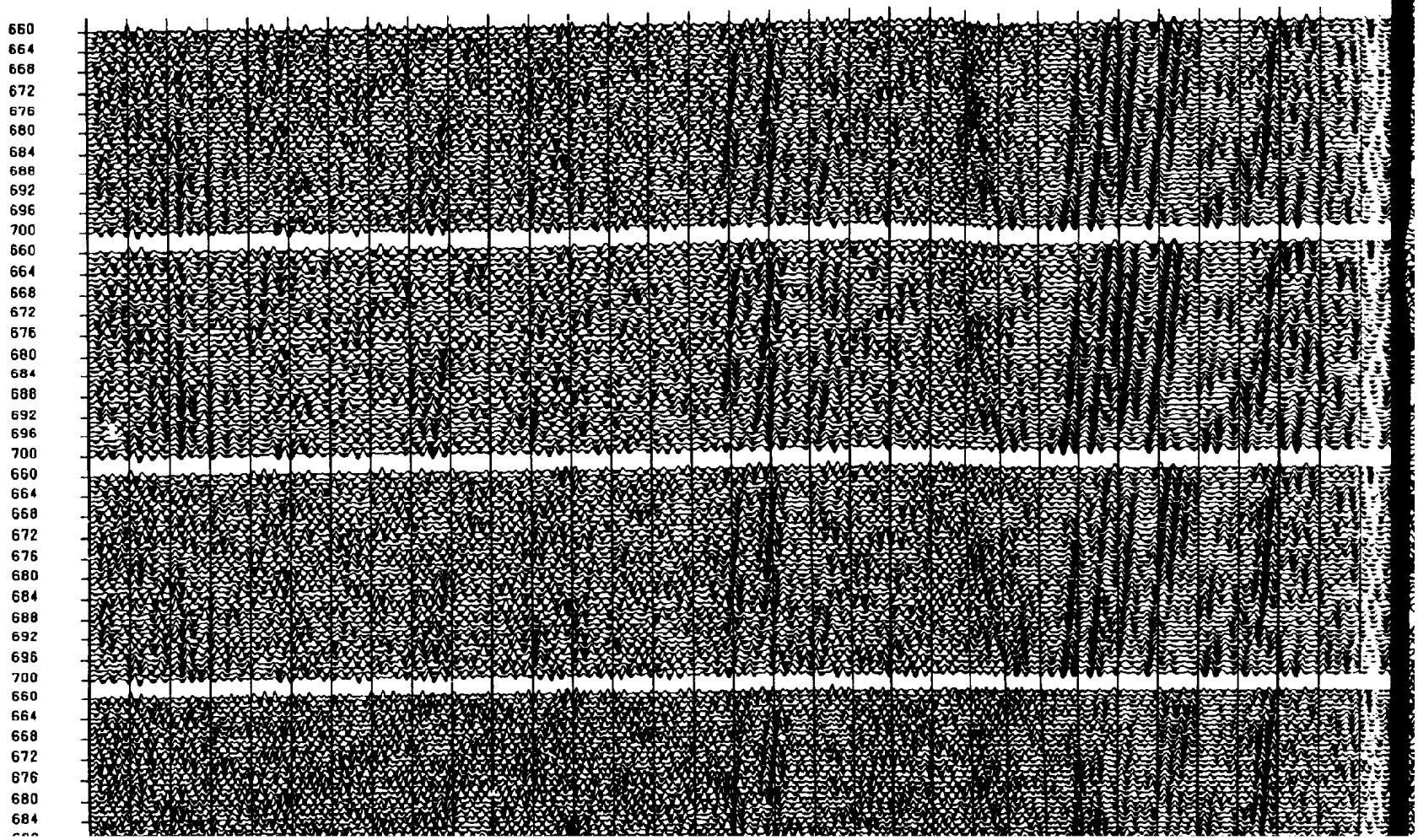

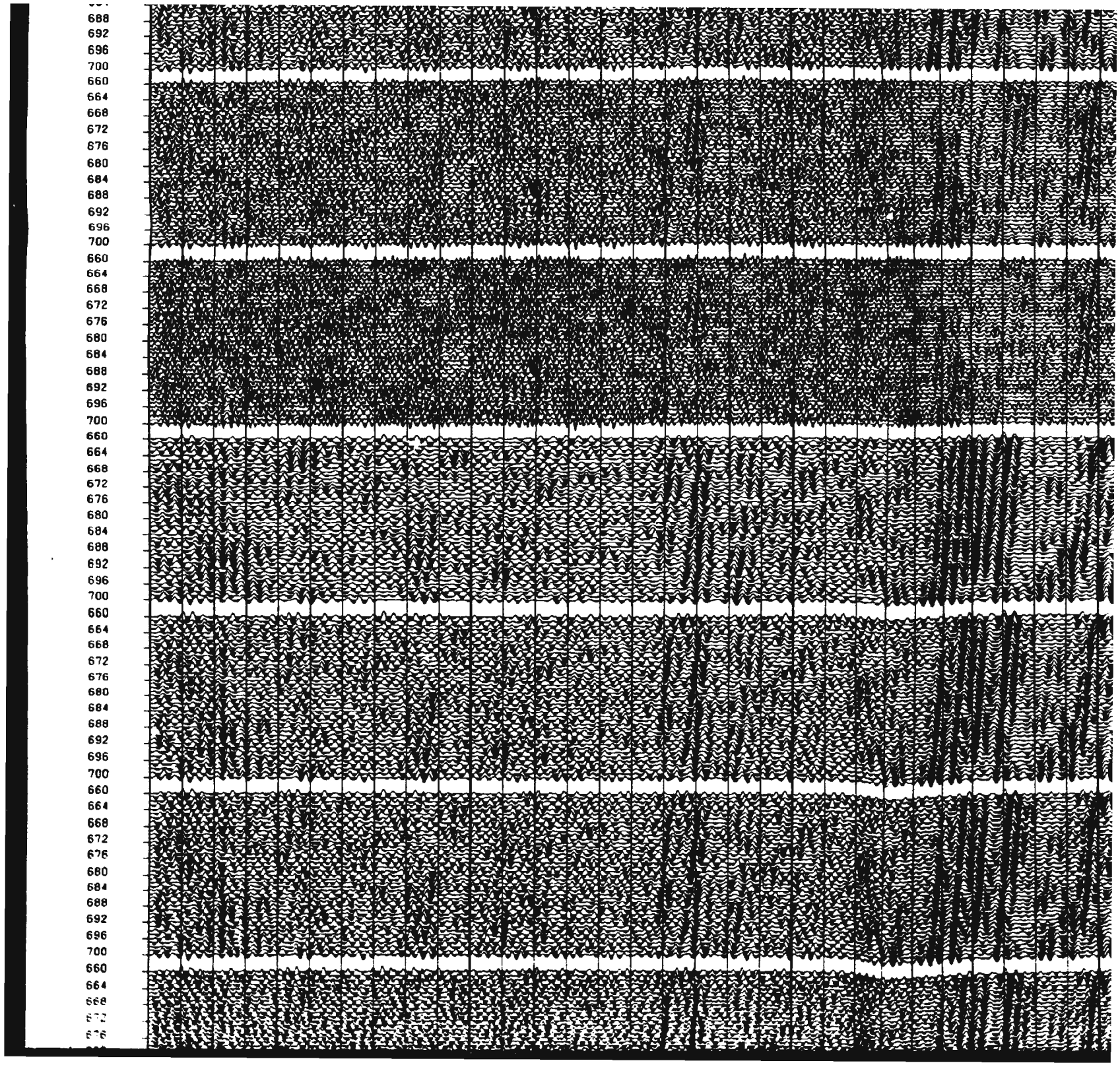
688
692
696
700
660
664
668
672
676
680
684
688
692
696
700
660
664
668
672
676
680
684
688
692
696
700
660
664
668
672
676
680
684
688
692
696
700
660
664
668
672
676
680
684
688
692
696
700
660
664
668
672
676
680
684
688
692
696
700
660
664
668
672
676

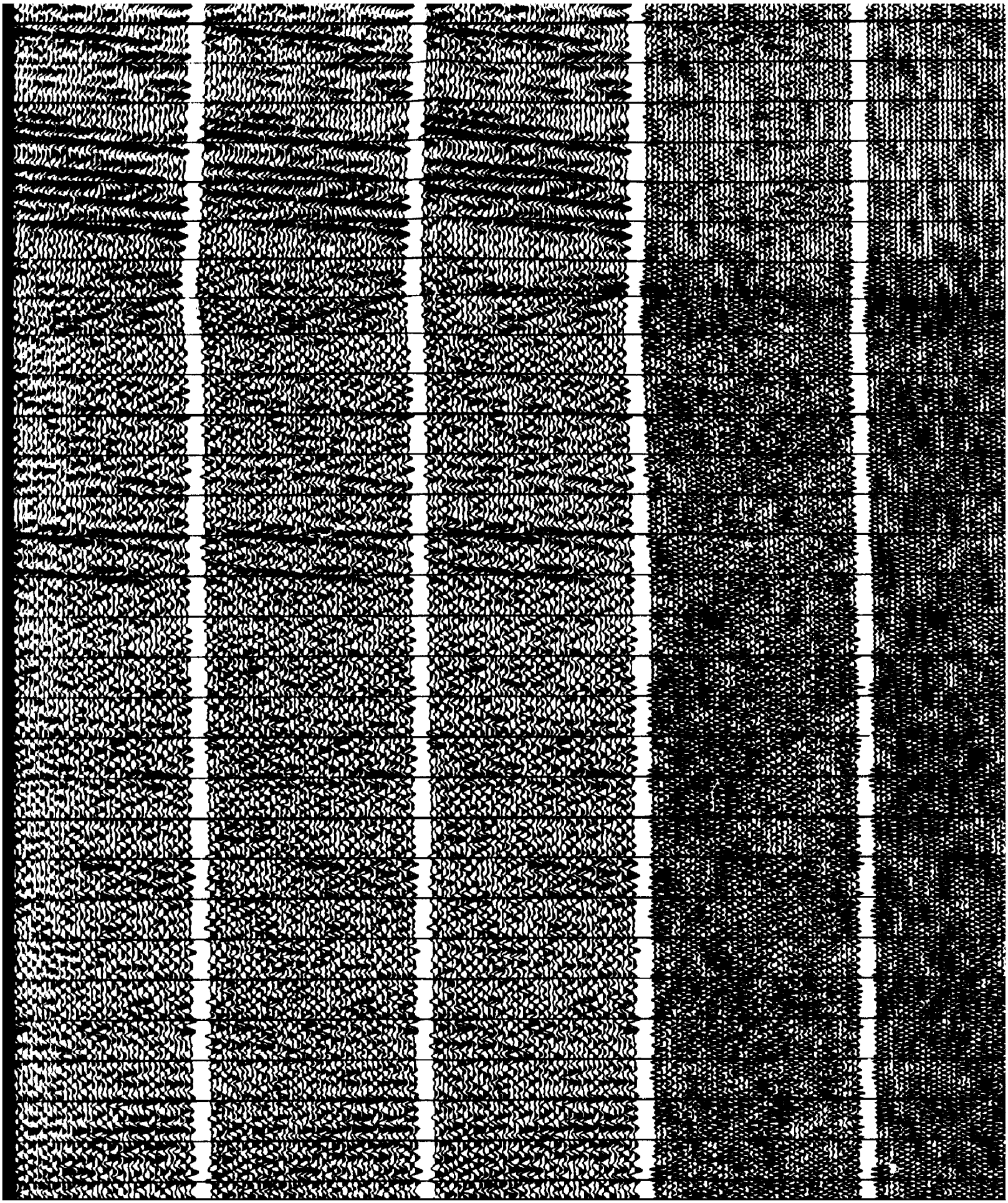

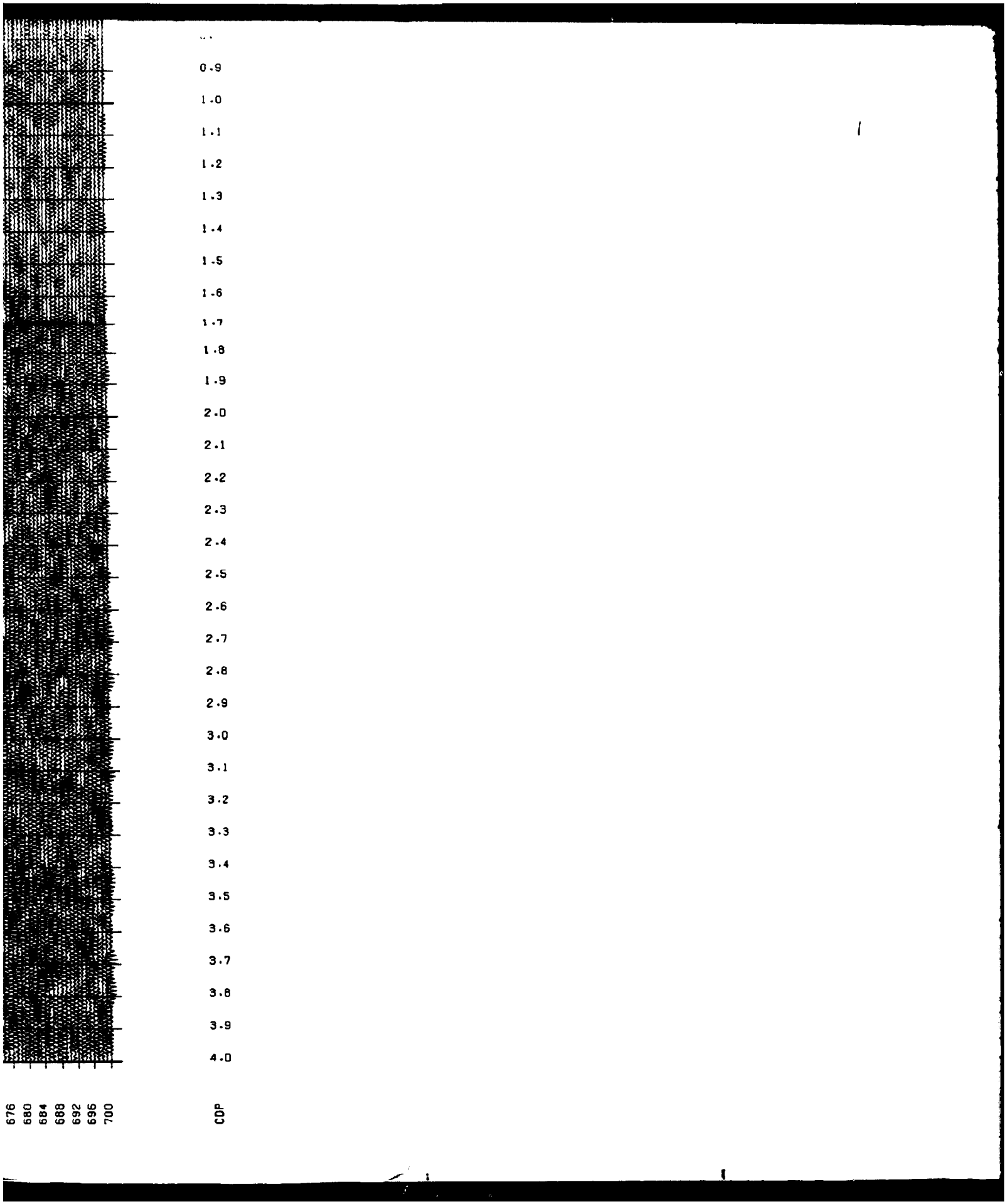
0.9
1.0
1.1
1.2
1.3
1.4
1.5
1.6
1.7
1.8
1.9
2.0
2.1
2.2
2.3
2.4
2.5
2.6
2.7
2.8
2.9
3.0
3.1
3.2
3.3
3.4
3.5
3.6
3.7
3.8
3.9
4.0
676
680
684
688
692
696
700
CDP

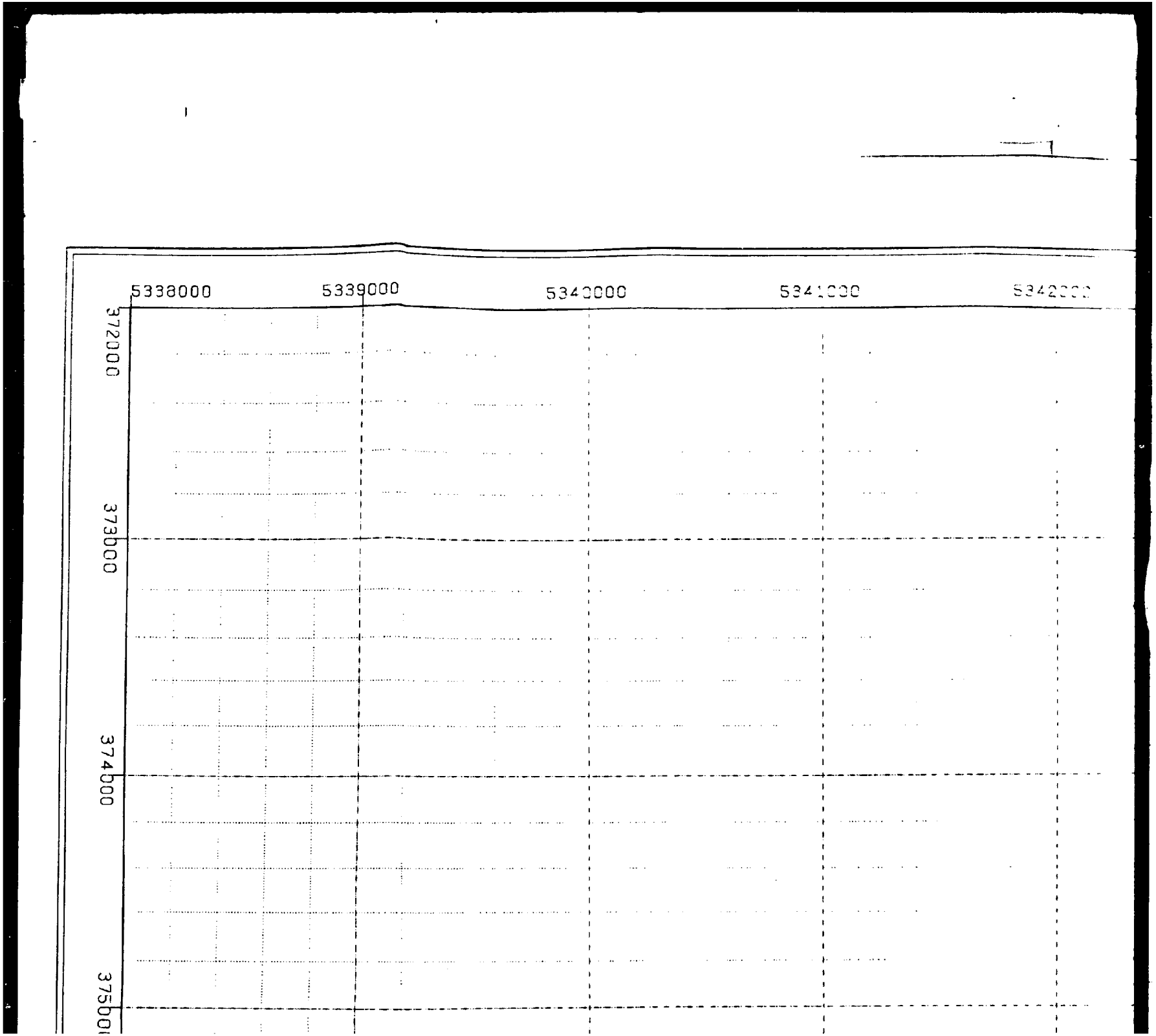
5338000
5339000
5340000
5341000
372000
373000
374000
375000

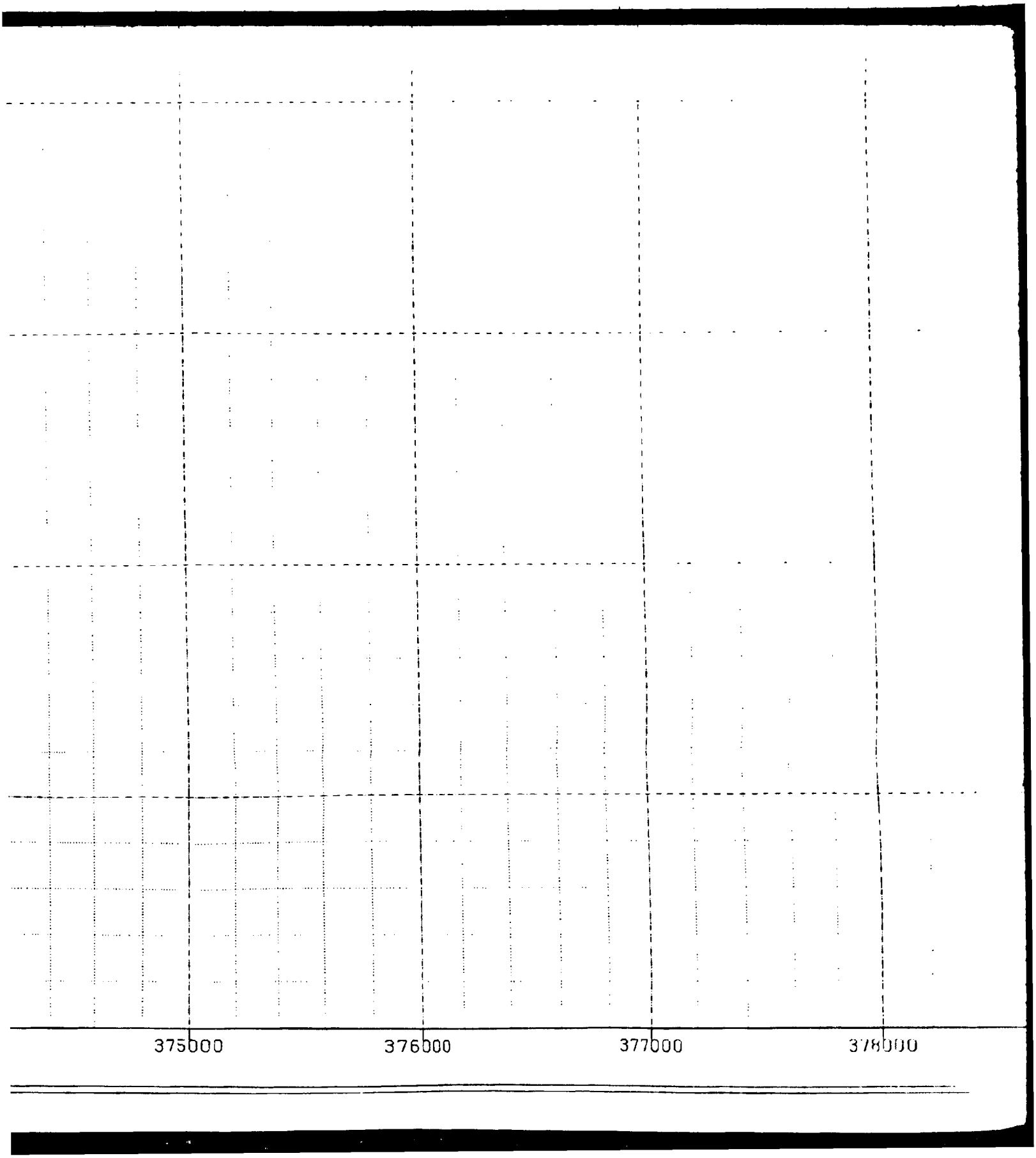
375000
376000
377000
378000

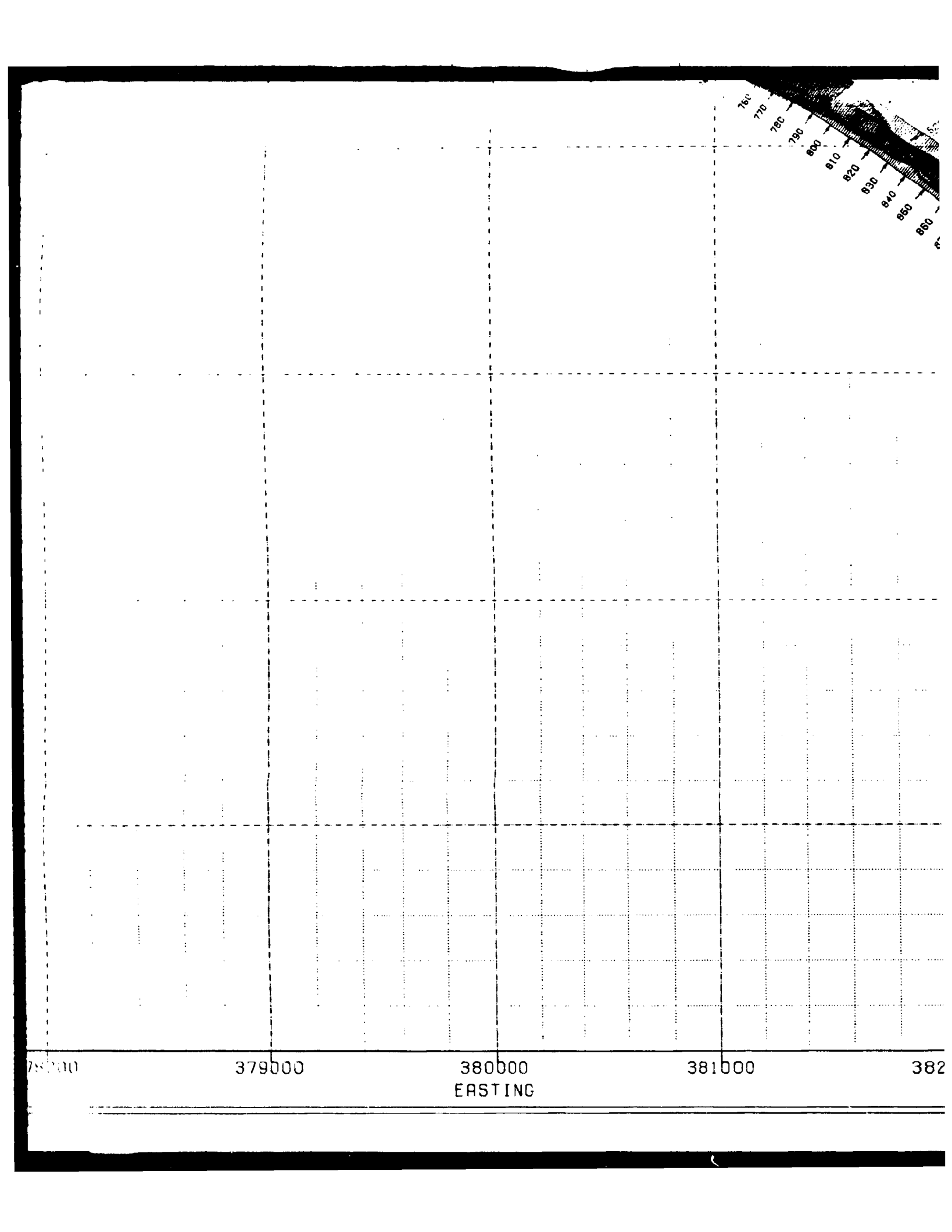
760
770
780
790
800
810
820
830
840
850
860
379000
380000
381000
382
EASTING

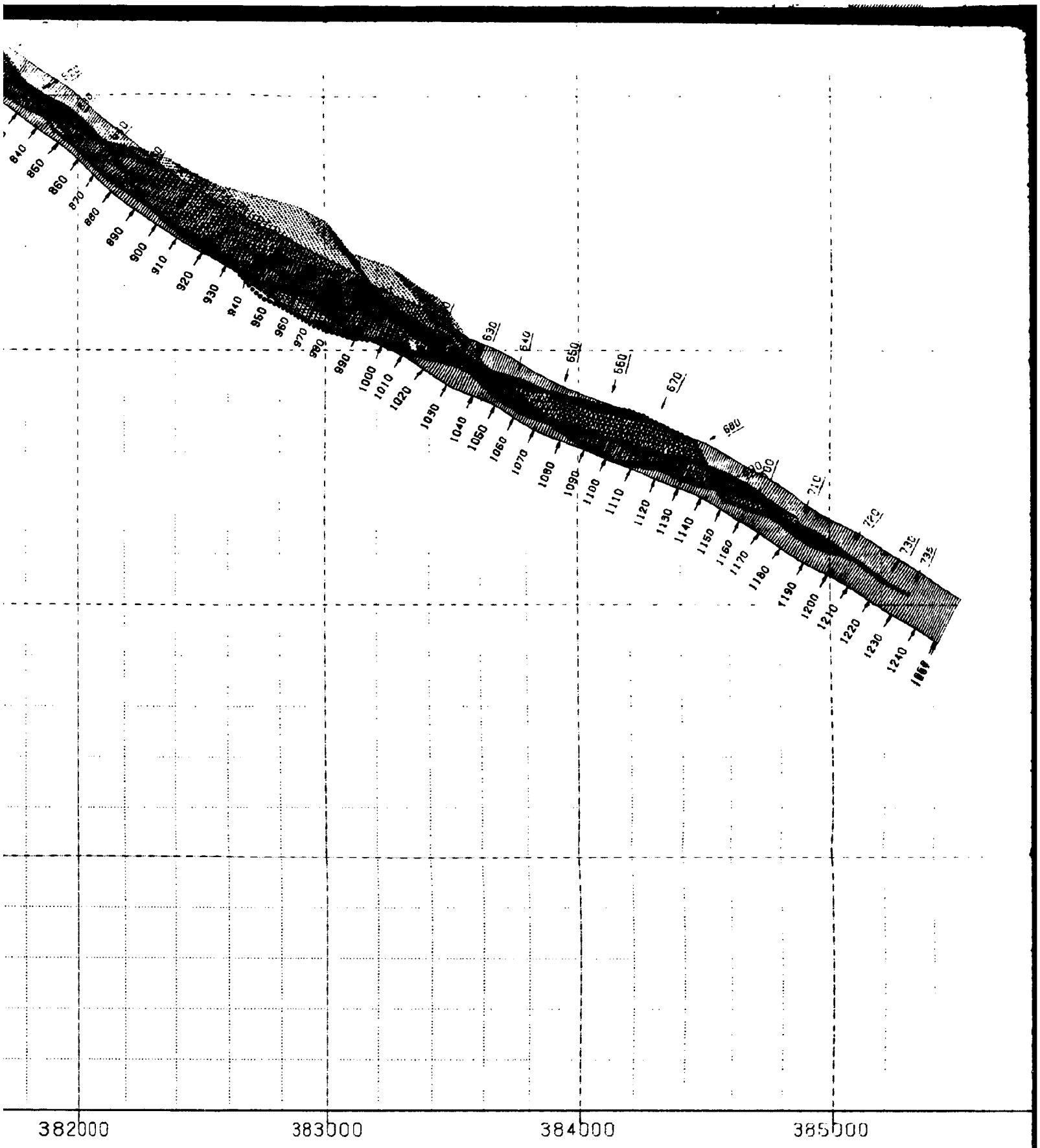
382000
383000
384000
385000

Figure 3.2. Binning strategy chart. The scal
axes are in UTM zone 21 coordinates.

axes are in UTM zone 17 coordinates.

O

IS

IS

9900

0.4

DMETRES

NO 1

BRIVZZ

1
1